Neural Plasticity

Investigating and Modulating Physiological and Pathological Brain Oscillations: The Role of Oscillatory Activity in Neural Plasticity

Lead Guest Editor: Andrea Guerra
Guest Editors: John-Stuart Brittain, Matteo Feurra, and Giovanni Pellegrino

Investigating and Modulating Physiological and Pathological Brain Oscillations: The Role of Oscillatory Activity in Neural Plasticity

Neural Plasticity

Investigating and Modulating Physiological and Pathological Brain Oscillations: The Role of Oscillatory Activity in Neural Plasticity

Lead Guest Editor: Andrea Guerra
Guest Editors: John-Stuart Brittain, Matteo Feurra, and Giovanni Pellegrino

Contents

Hindawi
Neural Plasticity
Volume 2019, Article ID 9403195, 3 pages
https://doi.org/10.1155/2019/9403195

Editorial

Investigating and Modulating Physiological and Pathological Brain Oscillations: The Role of Oscillatory Activity in Neural Plasticity

Andrea Guerra,[1] **Matteo Feurra**,[2,3] **Giovanni Pellegrino**,[4] **and John-Stuart Brittain**[5]

[1]*IRCCS Neuromed, Pozzilli, Italy*
[2]*National Research University, Higher School of Economics, Moscow, Russia*
[3]*Centre for Cognition and Decision-Making, Institute for Cognitive Neuroscience, National Research University, Higher School of Economics, Moscow, Russia*
[4]*Department of Neurology and Neurosurgery, Montreal Neurological Institute and Hospital, McGill University, Montréal, Canada*
[5]*School of Psychology, University of Birmingham, Birmingham, UK*

Correspondence should be addressed to Andrea Guerra; andrea.guerra@uniroma1.it

Received 24 July 2019; Accepted 26 July 2019; Published 26 November 2019

There is accumulating evidence that oscillatory activity plays a significant role in regulating brain function. Rhythmic phenomena are routinely observed during perception, motor, and cognitive tasks and have been implicated in altered functions across a broad range of diseases [1]. Several studies suggest that the alpha rhythm gates information flow, beta inhibits changes in motor activity and is responsible for the maintenance of the current sensorimotor or cognitive state, and gamma reflects intracortical local synchronization [1–3]. However, so far, understanding of the contribution of these rhythms to human behaviour and the manifestation of symptoms in disease states is limited. Moreover, the relationship between brain oscillations and neural plasticity is not clear, although recent evidence supports a link. For instance, it has been demonstrated that resonant rhythms in sensorimotor areas modulate motor learning and enhanced high-gamma activity in the primary motor cortex influences LTP/LTD-like plastic mechanisms [1, 2, 4]. As such we find ourselves in an era where we are rapidly garnering the tools to not only observe brain activity but also alter neural processes in a circumscribed manner. Such causal interactions allow deeper understanding of the role of neural oscillations in everyday life and of how changes in rhythmic activity can lead to altered functions in disease states. Noninvasive electrophysiological techniques such as high-density EEG and magnetoencephalography (MEG), invasive recordings of local field potentials, and advanced neuroimaging techniques able to infer brain oscillatory activity are now increasingly combined with different forms of brain stimulation [5, 6]. Sensory rhythmic stimulation, transcranial magnetic stimulation (TMS), and transcranial alternating current stimulation (tACS), used alone or in combination, allow targeting and causally interacting with rhythmic brain activity [2–4, 7]. Also, EEG activity can be used to guide TMS in a closed-loop configuration so as to induce and/or interfere with specific brain states [8]. These novel approaches provide new opportunities for drawing strong parallels between oscillatory activity and brain functions, including processes of cortical plasticity.

In the current special issue, we present ten articles that contribute to the debate on brain oscillations, plasticity, and behaviour. These articles address many aspects of brain oscillations, ranging from innovative methodologies to the rhythmic modulation of physiological function, the characterization of cortical and subcortical electrophysiological changes in the pathophysiology of neurological and psychiatric disorders, as well as the study of neurophysiological substrates of therapies that reflect neural plastic changes.

Finally, specific patterns of brain oscillations have been proposed as possible biomarkers to drive treatments or predict clinical outcomes in neurological disorders.

At a systems level, S. Glim et al. showed that by adopting a TMS-EEG coregistration technique, single-pulse and repetitive TMS can transiently enhance theta-gamma, alpha-gamma, and beta-gamma phase-amplitude coupling (PAC). The demonstration of the effectiveness of this perturbational approach paves the way for interventions to study and modulate PAC in different physiological and pathological conditions. A. Lehr et al. applied tACS at theta frequency to the left dorsolateral prefrontal cortex in young healthy subjects during a color-word Stroop task in order to investigate cognitive control and conflict detection processes that involve prefrontal brain regions. The study revealed a reduction of the Stroop effect (response time difference between congruent and incongruent trials) and a modulation of adaptive mechanisms of the cognitive control network, providing evidence for a causal role of theta oscillations in cognitive control. The role of brain rhythms on physiological function was also explored by S. Ricci et al. through the use of high-density EEG recordings. In line with previous reports [9], they found that elderly participants and young subjects share similar patterns of cortical oscillations. In particular, the authors demonstrated that the depth of beta modulation in the sensorimotor and frontal regions increases during practice, an expression of cortical plastic mechanisms, and this change occurs regardless of age.

Specific alterations in oscillatory activity occur in pathological conditions. A. Ahnaou et al. demonstrated robust functional changes in the hippocampus of a tau-seeding mouse model in which preformed synthetic tau fibrils were injected into the locus coeruleus. Alterations in the functional properties of the network included impaired coherence and global coherent network efficiency in the ipsilateral hippocampus, deficient propagation directionality of gamma oscillations, and decreased theta-gamma PAC in the hippocampal circuit, suggesting early dysfunctional hippocampal networks and impaired synaptic plasticity in brainstem tau pathology. C. Jiang et al. show that neuropathological mechanisms contributing to cancer-related fatigue include a reduced corticomuscular coherence in alpha and beta frequency bands. Q. Ye et al. examined EEG recordings of spontaneous fluctuations of neuronal oscillations and functional connectivity during resting state in patients with somatoform pain disorder. The enhancement of parietal alpha rhythm, positively correlating with the somatization severity, as well as the increase in alpha frontoparietal connectivity, were suggested as pathophysiological hallmarks of processes underlying somatoform pain.

The study of brain oscillations also guides medical treatments and can even help to identify neural substrates for therapeutic approaches. Indeed, Z. Shen et al. observed that the effects of electroacupuncture in regulating pain memory-related behaviours in rats are paralleled by a downregulation of theta power in the rostral anterior cingulate cortex; these neurophysiological changes are therefore associated with the inhibited retrieval of aversive memories and the alleviation of pain memory-induced aversive behaviours. R. I. Carino-Escobar et al. conducted a longitudinal analysis of changes in brain rhythms by means of EEG recordings in subacute stroke patients during an innovative interventional strategy for hand rehabilitation. Event-related (de-)synchronization (ERD/ERS) in alpha and beta were modified across the intervention sessions, suggesting neural plastic phenomena, with the latter predicting the extent of upper limb motor recovery.

The study of brain oscillations also allows identifying specific and reliable patterns of activity that can be used as biomarkers and then applied in clinical practice. In this regard, the clinical trial from D. Güntensperger et al. conducted in patients suffering from chronic tinnitus took advantage of an adjusted alpha/delta neurofeedback protocol based on the measurement of individual alpha peak frequency, instead of the use of a fixed alpha frequency. This protocol led to a sustained reduction of tinnitus-related distress and to a temporary effect on tinnitus loudness. Finally, F. Zappasodi et al. followed up 120 patients affected by a monohemispheric stroke in the territory of the middle cerebral artery. They demonstrated that, in the acute phase, the bilateral, ipsi-, and contralesional increase in low band activity (i.e., increase in interhemispheric symmetry of the homologous areas' powers) predicted a reduced functional outcome in the subsequent stabilized phase. Interestingly, this biomarker, based on pathological changes in cortical oscillatory activity, could be used for patient selection in designing rehabilitation treatments and/or noninvasive neuromodulation protocols [10].

The achievements of the presented research allow us to confirm that brain oscillations play an important role in driving physiological brain function, as well as dysfunction in pathological conditions. Neural plastic processes appear to be both influenced, and indexed by, changes in power and connectivity. The impressive array of neurophysiological tools now at our disposal (including high-density EEG, MEG, TMS-EEG, and tACS) allow us to study and modulate oscillatory activities in increasingly more prescriptive ways. This level of observation coupled with intervention allow us to draw strong parallels between brain oscillatory function and behaviour, including symptomology. We hope that by continuing to clarify the role of brain rhythms in physiological and pathological conditions, we can facilitate the identification of neurophysiological biomarkers for clinical utility, and that subsequent manipulation of brain state through optimised forms of neural intervention will induce long-term plastic changes capable of maintaining prolonged amelioration of symptoms. We see strong evidence that this approach is not only feasible but also imminently achievable, and we encourage ongoing research in this field.

Conflicts of Interest

A.G., M.F., G.P., and J.S.B. declare that they have no conflicts of interest regarding the publication of this special issue.

Acknowledgments

M.F. declare that the article was prepared within the framework of the Basic Research Program at the National Research

University Higher School of Economics and supported with a subsidy from the Russian Academic Excellence Project "5-100."

Andrea Guerra
Matteo Feurra
Giovanni Pellegrino
John-Stuart Brittain

References

[1] A. Giovanni, F. Capone, L. di Biase et al., "Oscillatory activities in neurological disorders of elderly: biomarkers to target for neuromodulation," *Frontiers in Aging Neuroscience*, vol. 9, p. 189, 2017.

[2] A. Guerra, A. Suppa, M. Bologna et al., "Boosting the LTP-like plasticity effect of intermittent theta-burst stimulation using gamma transcranial alternating current stimulation," *Brain Stimulation*, vol. 11, no. 4, pp. 734–742, 2018.

[3] G. Pellegrino, G. Arcara, G. Di Pino et al., "Transcranial direct current stimulation over the sensory-motor regions inhibits gamma synchrony," *Human Brain Mapping*, vol. 40, no. 9, pp. 2736–2746, 2019.

[4] A. Guerra, A. Suppa, F. Asci et al., "LTD-like plasticity of the human primary motor cortex can be reversed by γ-tACS," *Brain Stimulation*, vol. 12, no. 6, pp. 1490–1499, 2019.

[5] G. Thut, T. O. Bergmann, F. Fröhlich et al., "Guiding transcranial brain stimulation by EEG/MEG to interact with ongoing brain activity and associated functions: a position paper," *Clinical Neurophysiology*, vol. 128, no. 5, pp. 843–857, 2017.

[6] G. Pellegrino, M. Maran, C. Turco et al., "Bilateral transcranial direct current stimulation reshapes resting-state brain networks: a magnetoencephalography assessment," *Neural Plasticity*, vol. 2018, Article ID 2782804, 10 pages, 2018.

[7] A. Shpektor, M. Nazarova, and M. Feurra, "Effects of transcranial alternating current stimulation on the primary motor cortex by online combined approach with transcranial magnetic stimulation," *Journal of Visualized Experiments*, no. 127, article e55839, 2017.

[8] C. Zrenner, P. Belardinelli, F. Müller-Dahlhaus, and U. Ziemann, "Closed-loop neuroscience and non-invasive brain stimulation: a tale of two loops," *Frontiers in Cellular Neuroscience*, vol. 10, p. 92, 2016.

[9] F. Ferreri, F. Vecchio, A. Guerra et al., "Age related differences in functional synchronization of EEG activity as evaluated by means of TMS-EEG coregistrations," *Neuroscience Letters*, vol. 647, pp. 141–146, 2017.

[10] A. Guerra, V. López-Alonso, B. Cheeran, and A. Suppa, "Solutions for managing variability in non-invasive brain stimulation studies," *Neuroscience Letters*, article 133332, 2017.

Hindawi
Neural Plasticity
Volume 2019, Article ID 1971875, 10 pages
https://doi.org/10.1155/2019/1971875

Research Article

Acute Phase Neuronal Activity for the Prognosis of Stroke Recovery

Filippo Zappasodi,[1,2] Patrizio Pasqualetti,[3] Paolo M. Rossini,[4,5] and Franca Tecchio[6]

[1]*Department of Neuroscience, Imaging and Clinical Sciences, "G. d'Annunzio" University of Chieti, Chieti 66100, Italy*
[2]*Institute for Advanced Biomedical Technologies, "G. d'Annunzio" University, Chieti 66100, Italy*
[3]*Medical Statistics and Information Technology, Fatebenefratelli Foundation for Health Research and Education, AFaR Division, Rome 00186, Italy*
[4]*Institute of Neurology, Department of Geriatrics, Neurosciences & Orthopaedics, Catholic University of Sacred Heart, Rome 00168, Italy*
[5]*Policlinic Gemelli Foundation, IRCCS, Rome 00168, Italy*
[6]*Laboratory of Electrophysiology for Translational neuroScience (LET'S)-ISTC-CNR, Rome 00185, Italy*

Correspondence should be addressed to Franca Tecchio; franca.tecchio@cnr.it

Received 24 January 2019; Revised 17 May 2019; Accepted 24 June 2019; Published 8 September 2019

Guest Editor: John-Stuart Brittain

Strokes causing similar lesions and clinical states can be followed by diverse regains of neurological functions, indicating that the clinical recovery can depend on individual modulating factors. A promising line to disclose these factors, to finally open new therapeutic strategies, is to search for individual indices of recovery prognosis. Here, we pursued on strengthening the value of acute phase electrophysiological biomarkers for poststroke functional recovery in a wide group of patients. We enrolled 120 patients affected by a monohemispheric stroke within the middle cerebral artery territory (70 left and 50 right damages) and collected the NIH stroke scale (NIHSS) score in the acute phase (T0, median 4 days) and chronic follow-up (T1, median 6 months). At T0, we executed electrophysiological noninvasive assessment (19-channel electroencephalography (EEG) or 28 channels per side magnetoencephalography (MEG)) of brain activity at rest by means of band powers in the contra- and ipsilesional hemispheres (CLH, ILH) or the homologous area symmetry (HArS). Low-band (2-6 Hz) HArS entered the regression model for predicting the stabilized clinical state ($p < 0.001$), with bilateral impairment correlated with a poor outcome. Present data strengthen the fact that low-band impairment of homologous ipsi- and contralesional hemispheric regions in the acute stroke indicate a negative prognosis of clinical recovery.

1. Introduction

It is a common experience that after stroke the patients' clinical course is largely variable despite a nearly identical early clinical picture and similar size and location of the lesion [1]. In this scenario, we move on searching for individual features with prognostic value about the final outcome, which would help to better elucidate the mechanisms of poststroke functional recovery and to provide prospectively a guide in the selection of personalized rehabilitation treatments. Aware that stroke is a leading cause of disability [2], we searched for changeable factors indicating potential targets of sensorimotor rehabilitation enrichments. Previous studies revealed a clear neurovascular uncoupling in stroke patients [3] with preserved electrophysiological activity even in the presence of impaired hemodynamics [4]. Taking into account that neuronal plasticity definitely supports recovery abilities [5–8], and that it is mediated by changes of the neuronal electric activity, neuronal electric activity features per se are good candidates when searching for prognostic

markers about clinical recovery. Furthermore, the existence of neuromodulation interventions enhancing recovery from stroke (for review, [9–12]) strengthens the relevance of electrophysiological prognostic markers to better tailor such interventions in compensating specific alteration in individual patients. On these bases, while it is crucial to operate the best of knowledge in limiting the lesion dimension by proper interventions in the first hours after the stroke [13], we will devote our investigation on the electrophysiological assessment of neuronal activity after patients' vital parameter stabilization, in the 2-10 days from the symptom onset.

Our aim was to strengthen the value of acute phase electrophysiological biomarkers for poststroke functional recovery in a wide group of patients suffering from a monolateral middle cerebral artery (MCA) stroke. We moved from the knowledge that the balances of EEG rhythm powers between interhemispheric homologous areas [14] and the low-band power of the contralesional hemisphere [15, 16] provide information about the clinical recovery ability after stroke. In diverse clinical conditions, the dynamic interplay between homologous cortical areas was a critical element for a proper functioning of the motor system either during task execution or even at rest. Notably, the behavioral performance associates with the functional connectivity across the nodes of the devoted networks in a resting state [17–19]. Thus, here, we focused on the interhemispheric balance at rest between the neuronal activities of areas supplied by the MCA. Deriving the neuronal activity from noninvasive electrophysiological recordings, i.e., electro- and magnetoencephalography (EEG and MEG), we obtained a normalized index of homologous area balance. We finally considered the hemispheric values to elucidate the local impairments accounting for the occurring imbalances.

2. Materials and Methods

2.1. Subjects. We enrolled 120 patients (mean age 70.6 ± 11.0 years, 75 men and 45 women) admitted to our departments (S. Giovanni Calibita Hospital and Fondazione Policlinico Agostino Gemelli, Rome) for a first-ever monohemispheric and monolesional ischemic stroke in the MCA territory. The inclusion criteria were clinical evidence of sensorymotor deficit of the upper limb and neuroradiological diagnosis of ischemic brain damage in MCA territory. The exclusion criteria were previous stroke on clinical history, neuroradiological evidence of involvement of both hemispheres or of brain hemorrhage, and dementia or aphasia severe enough to impair patients' compliance with the procedures. Patients received the best clinical care according to the Italian stroke guidelines (SPREAD).

Thirty-three healthy volunteers, matched for age and gender with patients, were also enrolled as the control group (mean age 70.0 ± 11.6 years, 20 males, 13 females, independent t-test for age between patients and controls: $p = 0.770$). All subjects of the control group were right-handed, as confirmed by the Edinburgh Manuality test, were not receiving any psychoactive pharmacological treatment at the time of recordings, and resulted normal at both neurological and brain magnetic resonance examinations.

The Ethics Committees of our hospitals approved the experimental protocol (Fatebenefratelli EC 40/2011), and all patients and healthy subjects signed a written informed consent before participating.

2.2. Data Collection. Clinical scores, EEG or MEG recordings, and MRI evaluation were collected in patients during the same day, after stabilization of the vital parameters and always before day 10 from the symptom onset (T0). Clinical scores were also collected in the postacute stabilized phase after 6 months (T1). The neurological assessment of stroke severity was executed by an accredited neurologist via the NIH stroke scale (NIHSS). The same neurologist scored the scale both at T0 and at T1. We decided to assess the clinical state by the NIHSS score even in the stabilized T1 phase to better serve the aim of our study. This choice was done to quantify the recovery processes separating from the stabilized phase clinical conditions the changes with respect to the acute phase state. Thus, we calculated the "effective recovery" (ER) as the percentage of the occurred improvement with respect to the total possible improvement, taking into account that NIHSS = 0 corresponds to the absence of clinical symptoms:

$$\mathrm{ER} = 100 * \frac{\mathrm{NIHSS\ at\ t0} - \mathrm{NIHSS\ at\ t1}}{\mathrm{NIHSS\ at\ t0} - 0}. \quad (1)$$

The brain MRI was carried out at 1.5 T Spin-Echo, Turbo Spin-Echo, using fluid-attenuated inversion recovery sequences. All sequences provided contiguous 5 mm thick slices on sagittal, coronal, and axial planes. The identification of the lesion site was performed on axial slices. Lesions were classified as "cortical" (C), if the cortical grey matter was involved and all subcortical structures were spared; as "subcortical" (S), when the white matter, internal capsule, thalamus, or basal ganglia were affected; and finally, as "cortico-subcortical" (CS), when both the cortical and the subcortical structures were involved.

A five-minute open-eye electroencephalographic (EEG) or magnetoencephalographic (MEG) recording was acquired at rest, while subjects sat on a comfortable armchair or lied on a hospital bed. Eighty patients (mean age 71.2 ± 9.8 years, 29 women) and 20 healthy controls (mean age 71.5 ± 6.4 years, 7 women, independent t-test for age between patients and controls: $p = 0.895$) underwent EEG recording, while 40 patients (mean age 69.4 ± 13.1 years, 16 women) and 13 healthy controls (mean age 67.7 ± 16.8 years, 6 women, independent t-test for age between patients and controls: $p = 0.705$) completed MEG examination.

The EEG activity was recorded by 19 Ag-AgCl cup electrodes positioned according to the 10–20 international EEG system (F1, F7, T3, T5, O1, F3, C3, P3, FZ, CZ, PZ, F2, F8, T4, T6, O2, F4, C4, and P4) in fronto-central reference; an additional electrode pair served for recording electrooculogram to control for eye blinking. Electrocardiogram was monitored by one bipolar channel placed on the chest. EEG data were sampled at 256 Hz (presampling analogical filter 0.1-70 Hz) and collected for offline processing. The MEG activity was recorded by a 28-channel system (16 inner axial

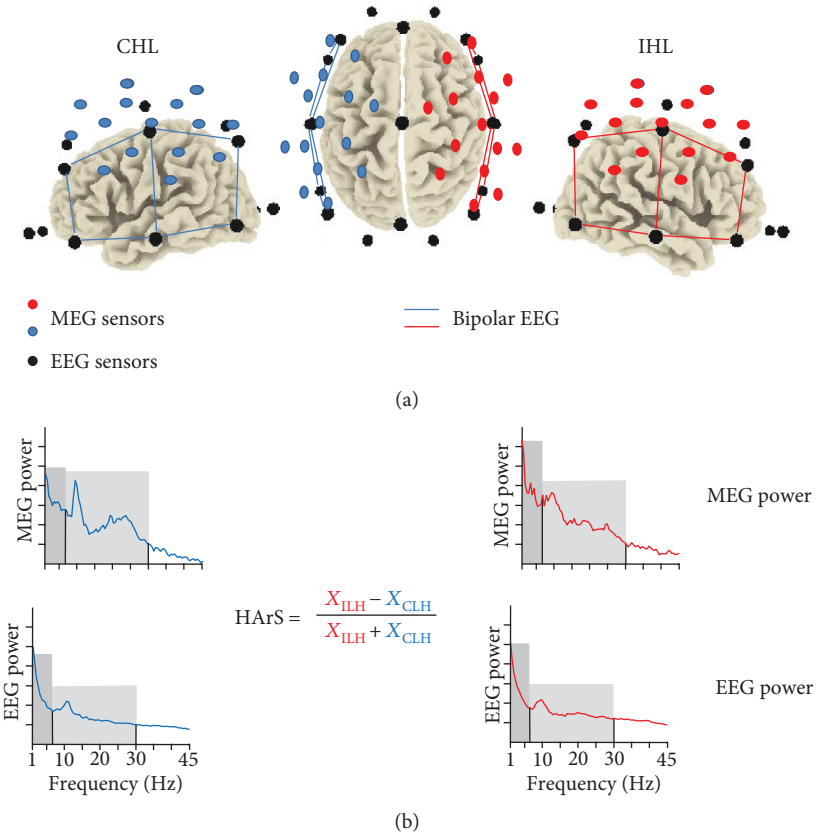

Figure 1: (a) International 10–20 system electrode positions in relation to the cerebral cortex (black circles). In a representative subject with the lesion in the right hemisphere, coloured bars show bipolar derivations overlying the MCA territory, used in our experiment to assess EEG spectral powers (red for the hemisphere ipsilateral to the lesion (ILH) and blue for the hemisphere contralateral to the lesion (CLH)). Red (ILH) and blue (CLH) circles indicate the positions of the 16 gradiometers in each hemisphere used to assess MEG spectral powers. (b) Spectral power densities were separately calculated in the ILH and CLH as the mean of those of bipolar derivations overlying MCA territory (EEG signals) or as the mean of those of gradiometers (MEG signals). Spectral power densities are shown in two exemplificative patients (MEG and EEG signals). We evidenced DeltaTheta (dark grey) and AlphaBeta (light grey) bands. The homologous area symmetry (HArS) index is calculated as shown for band and total powers.

gradiometers, 8 cm baseline and 9 mm pick-up coil diameter; 9 peripheral squared magnetometers, 9 mm pick-up coil edge; and three balancing magnetometers devoted to noise reduction) covering a scalp area of about 180 cm^2, inside a magnetically shielded room (Vacuumschmelze GmbH). We recorded brain magnetic fields from the parietofrontal region of each hemisphere, by centering the sensor array on C3 and C4 of the international 10–20 electroencephalographic system. The system positioning was selected to assess cortical sensorimotor area activity, mostly affected by the lesion [20–23]. MEG data were sampled at 1000 Hz (presampling analogical filter 0.48-250 Hz) and collected for offline processing.

2.3. Data Analysis. A semiautomatic procedure based on Independent Component Analysis [24] was applied to both MEG and EEG data, in order to identify and eliminate artefacts (i.e., eye movements, cardiac activity, and scalp muscle contraction) without epoch exclusion. For EEG data, bipolar derivations between pairs of first-near electrodes in posterior-anterior and mediolateral directions were estimated selecting the sites overlying the MCA territory and maintaining separated the measures in the two hemispheres: F3-F7, C3-F3, F7-T3, C3-T3, C3-P3, T3-T5, and P3-T5 for the left hemisphere and the F4-F8, F4-C4, F8-T4, C4-T4, C4-P4, T4-T6, and P4-T6 for the right (Figure 1).

We estimated the Power Spectral Density (PSD) for each EEG derivation or MEG channel via the Welch procedure, using time windows of 4 s duration (resulting in a frequency resolution of 0.25 Hz), Hanning windowing, 60% overlap, and about 70 artefact-free trials. The PSD was calculated as the mean of the PSDs obtained for the 7 EEG bipolar derivation (EEG data) or by the 16 inner gradiometer channels (MEG data) separately in the hemisphere ipsilateral to the lesion (ILH) and the hemisphere contralateral to the lesion (CLH). The individual alpha frequency (IAF) peak was firstly calculated as the frequency with maximal PSD in the 7-13.5 Hz interval in parietooccipital regions. Then, as slow frequency has been linked to clinical status, lesion side, and recovery [25–28] and 10-20 Hz activity has physiological relevance in sensorimotor areas (mu rhythm [29, 30]), we considered the following frequency bands: DeltaTheta

(from 2 to the minimum between 7.5 Hz and IAF-2 Hz) and AlphaBeta (from IAF-2 Hz to 30 Hz) according to previous stroke studies [31, 32].

The degree of symmetry of homologous MCA areas (HArS), i.e., between ILH and CLH activity, was obtained for the different bands and total power as [14, 33]:

$$\mathrm{HArS} = \frac{X_{\mathrm{IHL}} - X_{\mathrm{CHL}}}{X_{\mathrm{IHL}} + X_{\mathrm{CHL}}}, \quad (2)$$

being X the power in the DeltaTheta band, in the AlphaBeta band, or in the whole spectrum.

2.4. Statistical Analysis. Statistical analyses were performed using SPSS v. 16 statistical software (Chicago, Illinois, USA), and 0.05 was considered as the significance threshold. All values (band and global HArSs and hemispheric powers) were log transformed to better fit a normal distribution for statistical analysis (checked by the Shapiro-Wilk test) when needed. Moreover, they were controlled not to differ between MEG and EEG groups.

The statistical analysis is aimed at testing whether the interhemispheric activity unbalance, measured by the HArS index, provides prognostic information about the clinical recovery from stroke in the stabilized phase, as measured by NIHSSs. We preliminarily selected the HArS variables which add a prognostic information with respect to the clinical state in the acute phase, applying a regression model with NIHSS at T1 as a dependent variable and NIHSS at T0, total and band HArS values as independent variables. After this selection, we better depicted the link between HArS and the clinical state in the stabilized phase (NIHSS at T1) or effective recovery (ER) by means of Spearman's or Pearson's correlation.

To clarify the phenomena behind the interhemispheric unbalances related to clinical recovery with possible dependence on the lesion side, we applied ANOVA for repeated measures on corresponding band powers with *Hemisphere* (left, right) as the within-subjects factor and *Group* (left lesion, right lesion, and healthy control) as the between-subjects factor. Whenever the interaction *Hemisphere*∗ *Group* effect was found, the significance of the post hoc comparisons between the groups for each hemisphere was assessed-corrected by Bonferroni's procedure.

For the correlative analysis, to develop a measure independent of the laboratory, we derived z scores for band and total powers. Specifically, for each hemisphere and separately for MEG and EEG groups, we divided patients' values for the standard deviation of the distribution of healthy controls, after subtracting the mean of the values of healthy controls. We note that in this way the measure is even independent of EEG/MEG investigation, although band and total powers differ depending on the MEG or EEG assessment. To assess the robustness of the results, a percentile-based bootstrap, with 5000 replicate samples, was performed to assess the 95% confidence intervals of correlation coefficients.

3. Results and Discussion

3.1. Patients' Picture. The NIHSS score in the acute phase (T0) was collected at a median of 4 days (between 1 and 10 days) after the stroke onset. NIHSS at T0 ranged from 1 to 22 (median: 5.0; 5-95 percentile: 1-18). As assessed by NIHSS at T1 with respect to T0, all patients showed at least some clinical recovery, with the exception of 3 patients with a cortico-subcortical lesion in the right hemisphere who showed a worsened clinical picture at T1 and 5 patients who did not change clinical status at the two times. Thirty-four patients showed a complete recovery (ER = 1). Right-lesion and left-lesion patients did not differ for NIHSS in the acute phase, for NIHSS in the stabilized phase, for recovery, or for age (Table 1). Moreover, the clinical picture was not different between patients who underwent EEG or MEG (Table 1). According to the ischemic injury localization, 13 patients (11%) were classified as cortical, 39 (33%) as subcortical, and 68 (56%) as cortical-subcortical.

The following risk factor percentage was present in the recruited stroke population: 21% smoking, 23% diabetes, 69% hypertension, 29% cardiopathy (13% atrial fibrillation), 65% hyperlipidaemia, and 10% familiarity.

3.2. Prognostic Analysis: Homologous Area Symmetry (HArS). HArS variability was only marginally accounted for by technique MEG/EEG groups (eta − square = 0.006, $p = 0.413$); therefore, HArSs were studied in the whole group of the 120 patients.

The regression analysis with NIHSS at T1 as a dependent variable included the clinical status in the acute phase and total and band HArS as independent variables. In addition to NIHSS at T0, HArS in DeltaTheta entered the model, as expressed by

$$\begin{aligned}(\text{NIHSS at T1}) = {} & -2.0 + 0.75\,(\text{NIHSS at T0}) \\ & - 25.73\,(\text{DeltaTheta HArS}).\end{aligned} \quad (3)$$

The 73% of the variance of NIHSS at T1 was explained by this model ($F(2{,}117) = 152.608$, $p < 0.001$). The signs of the coefficients tell us that, as expected, a worse clinical status at T0 correlates with a worse clinical status at T1. Furthermore, a smaller DeltaTheta interhemispheric symmetry in the acute phase correlates with a better clinical picture in the stabilized phase.

3.3. Hemispheric ILH and CLH Powers. To understand the origin of higher DeltaTheta asymmetries correlated with better recovery levels, we analysed the subtending hemispheric powers. To discriminate phenomena possibly depending on right vs. left lesions, we executed a repeated measures ANOVA design on DeltaTheta band power with *Hemisphere* (left, right) as a within-subjects factor and *Lesion Side* (lesion in the left hemisphere, lesion in the right hemisphere, no lesion = healthy control) as a between-subjects factor. A clear interaction *Hemisphere*∗ *Lesion Side* was found ($F(1, 78) = 10{,}901$; $p = 0.001$, EEG group; $F(1, 38) = 7{,}160$; $p = 0.011$, MEG group). Post hoc comparisons with respect to controls (Bonferroni-

Table 1: Demographic, clinical, and neuroradiological picture of the 120 monohemispheric MCA stroke patients.

	EEG ($n = 80$)						MEG ($n = 40$)						*Comparison*	
Lesion side	Left			Right			Left			Right			*EEG vs. MEG*	*L vs. R lesion*
Number *(% of EEG/MEG group)*	46 *(58%)*			34 *(42%)*			24 *(60%)*			16 *(40%)*				
Gender	Male		Female	Male		Female	Male		Female	Male		Female	*0.694*	*0.849*
Number (% of lesion side group)	28 *(61%)*		18 *(39%)*	23 *(68%)*		11 *(32%)*	15 *(64%)*		9 *(36%)*	9 *(56%)*		7 *(44%)*		
Age *(mean ± st dev)*	70.0 ± 8.6			72.8 ± 11.2			68.8 ± 12.2			70.3 ± 14.8			*0.389*	*0.239*
Lesion class	*C*	*S*	*CS*	*C*	*S*	*CS*	*C*	*S*	*CS*	*C*	*S*	*CS*	*0.451*	*0.404*
	5	19	22	3	11	20	3	6	15	2	3	11		
Clinical picture														
NIHSS at T0 *Median (5-95 perc.)*	**6** (1–20)			**5** (1–18)			**5** (2–14)			**5** (2–14)			*0.565*	*0.307*
NIHSS at T1 *Median (5-95 perc.)*	**2** (0–18)			**2** (0–11)			**1** (0–8)			**3** (0–10)			*0.474*	*0.785*
Effective recovery *Median (5-95 perc.)*	**70** (9–100)			**73** (30–100)			**83** (1–100)			**67** (-22–100)			*0.500*	*0.855*

In the last 2 columns, p values of the statistical test are shown, which were used to compare EEG vs. MEG groups and patients with the lesion in the left or in the right hemisphere; independent sample t-test (age, ER), chi-square (gender, lesion class), and Mann-Whitney test (NIHSS in acute and stabilized phases).

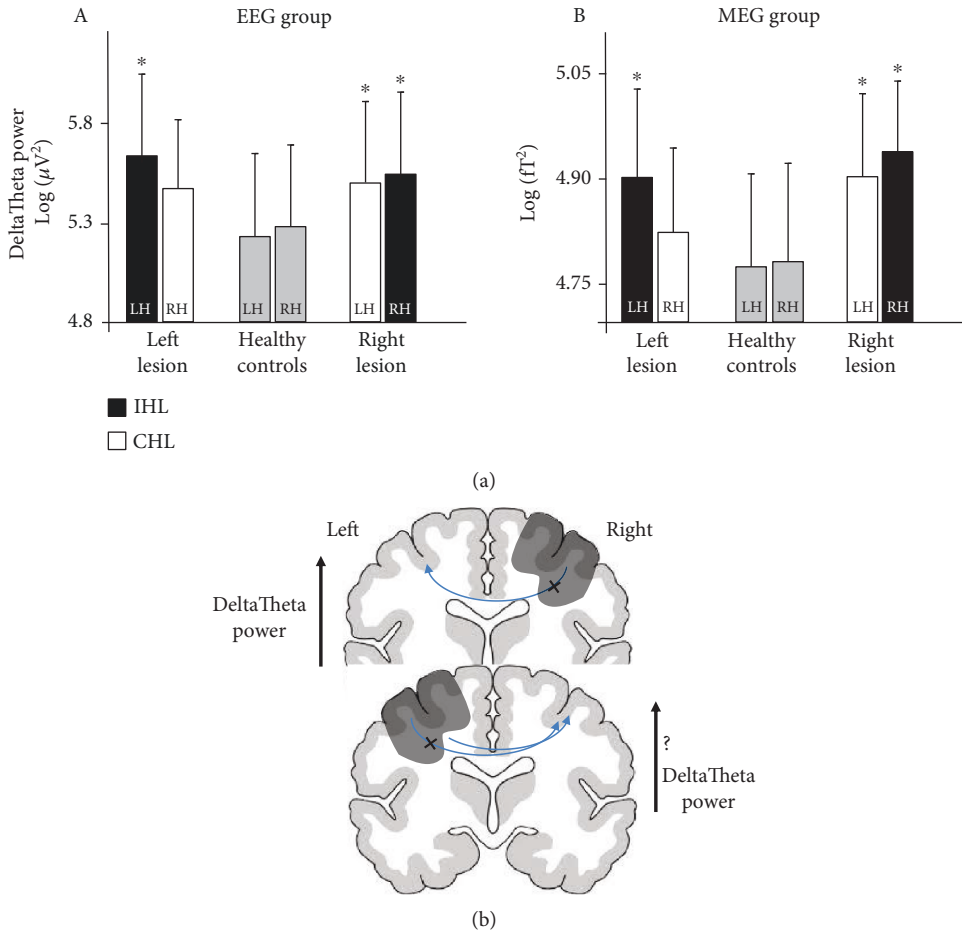

Figure 2: Asymmetric impact of a left or right lesion. (a) For the EEG group (A) and the MEG group (B): mean (standard deviation) of DeltaTheta band powers of left and right hemispheres in patients with the lesion in the left hemisphere, healthy controls, and patients with the lesion in the right hemisphere. For patients, the black bar indicates the hemisphere ipsilateral to the lesion (ILH) and the white bar indicates the hemisphere contralateral to the lesion (CLH). Asterisk indicates that the post hoc independent t-test with respect to the value of the corresponding hemisphere in healthy controls is significant (Bonferroni-corrected). (b) A schematic representation of the functional asymmetry of the right/left interhemispheric projections (see Results and Discussion).

corrected, Figure 2) showed that left-damaged patients had DeltaTheta power increased in the ILH, and right-damaged patients had a bilateral increase (ILH and CLH, Figure 2). We can observe correspondingly that the DeltaTheta symmetry is higher in the right-damaged patient than left-damaged patients (DeltaTheta HArS values: 0.004 ± 0.019 vs. 0.012 ± 0.023, respectively; independent t-test: $t(118) = 2.136$; $p = 0.035$). Notably, after z-transformation (see Materials and Methods), we selected those patients with DeltaTheta CHL power higher than the 97,7% of DeltaTheta of controls (z score $= \pm 2$). They were 18 (15% of the 120 patients) and displayed a higher symmetry with respect to the other 102 patients (DeltaTheta HArS: 0.004 ± 0.020 vs. 0.011 ± 0.020, independent sample t-test: $t(116) = 2.704$; $p = 0.008$). Consistently, they showed a lower clinical recovery at T1 (ER: $40\% \pm 36\%$ vs. $70\% \pm 31\%$, independent t-test: $t(116) = 3.530$; $p = 0.001$). Furthermore, higher CHL DeltaTheta correlated with worse clinical recovery (Table 2). We note that the same relationships on the predictive value of contralesional low-band activity hold for randomly chosen independent groups in the enrolled sample (Table 2).

4. Discussion

The main result of our study is that following a monohemispheric stroke in the middle cerebral artery territory, the bilateral increase of the brain low-band activity expressed in the increase of interhemispheric symmetry of the homologous areas' powers in the acute phase predicts a worse functional outcome in the stabilized phase.

We posed the working hypothesis that the homologous area activity balance was "the best" prognostic indicator, consistent with the clear achievement that the functional interhemispheric balance serves the network functionality. Interhemispheric unbalance has been recently observed in diverse neurological diseases [34–38], and the evidence of its functional role originated from the results of several studies in animal models and humans, in the consequence of an acquired brain lesion. In animal models, a parallel trend

Table 2: Correlations between spectral band powers and clinical variables.

	DeltaTheta		AlphaBeta		Whole band	
	ILH	CLH	ILH	CLH	ILH	ILH
NIHSS at T0	0.416 (0.251, 0.560) <0.001	0.312 (0.134, 0.469) 0.001	n.s.	n.s.	0.181 (-0.010, 0.360) 0.048	0.208 (0.025, 0.376) 0.023
NIHSS at T1	n.s.	**0.285** (0.119, 0.432) 0.002	n.s.	n.s.	n.s.	n.s.
ER	n.s.	**-0.289** (-0.123, -0.431) 0.002	n.s.	n.s.	n.s.	n.s.

Correlation coefficients (confidence limit in the second line, assessed by the bootstrap procedure, and p value in the third line) of z-scored band and total powers in ipsilesional (ILH) and contralesional (CLH) hemispheres with an acute clinical score (NIHSS at T0 and at T1—Spearman rho), clinical score in the stabilized phase (*NIHSS at T1 adjusted for NIHSS at T0), and effective recovery (ER—Pearson r) both adjusted for NIHSS at T0 (*Pearson r). Values in bold are for significance < 0.050.

emerged between interhemispheric connectivity and neurological improvement after cerebral ischemia, longitudinally followed up from acute to chronic stages [39]. In humans, both fMRI and electrophysiological data in acute and chronic stroke patients demonstrated that the balance of these hemispheric areas associates with a better clinical picture [18, 33, 39–41]. Moreover, a functional interhemispheric uncoupling in the acute phase can lead to adverse prognostic consequences [16], and the interhemispheric asymmetry of complexity of the EEG dynamics in the acute phase is paired to a worse clinical status [42]. In this framework, our data express that the interhemispheric symmetry in the acute phase predicts a worse outcome as an expression of the increased contralesional hemispheric low-frequency activity.

We had considered the interhemispheric symmetry index between homologous areas as a good indicator because it is a parameter largely independent of the recording technique and settings. In this direction, we can consider a strength more than a weakness to include both EEG and MEG data, providing a clear consistency of the results independent of the assessing technique. Our work indicated that also hemispheric powers are informative, in particular via z scores which also minimize dependence on specific recoding settings. z scores depend on the quality of the normative population, which can be ameliorated by increasing the samples in the future.

Damaged areas typically generate delta rhythms [26, 28, 43]. This perilesional low-frequency activity is positively correlated with a worse clinical status in the acute phase [15] but does not add prognostic information with respect to the clinical severity. From a prognostic perspective, the most stable achievement from literature is a negative indication associated with a power increase of the low-frequency range of oscillatory neuronal activity from the CLH [31]. Here, we confirmed our findings of the prognostic value of CHL low-frequency activity found in studies involving independent cohorts [15, 16, 44] or by other authors who considered hemispheric phenomena [45, 46]. We documented that when CLH neuronal low-band activity emerges in addition to the typical increase in ILH one, this phenomenon adds prognostic power to the clinical severity in the acute phase indicating a poor functional outcome. Acute phase increase of delta power in CLH is secondary to transcallosal diaschisis, a more or less transient alteration of brain function remote from the lesion, according to von Monakow, who coined the term in a pre-EEG epoch [47]. Signs that the CLH power increase was mediated by an impairment of local contralesion inhibitory networks secondary to a loss of modulatory projections from damaged areas can be traced from the behavior after a right or left damage. In fact, we found that a right lesion typically induces a bilateral power increase, while a left one does it more rarely. Conceivably, this is consistent with the stronger inhibitory projection from the left onto the right hemisphere, which results more resistant to the damage. Conversely, a weaker inhibitory projection of the right onto the dominant left hemisphere corresponds to a right damage impacting more significantly the left dominant region (Figure 2(b)). Accordingly, functional evidence indicates that in rightward subjects, interhemispheric inhibition phenomena are asymmetric [48], with the left sensorimotor regions inhibiting the right more than the other way around (transcranial magnetic stimulation (TMS) studies [49, 50]; functional magnetic resonance imaging (fMRI) studies [51]).

Different from the role on the lesioned hemisphere, we did not investigate deeply the electrophysiological alterations independent on the lesion localization and extension. This is in agreement with the study design depending on the working hypothesis: when searching for individual features revealing prognosis of recovery, we typically expect factors that are independent on the lesion site and dimension. In this respect, we moved according to our focus on tracking measures in the acute phase associated with diverse regains of neurological functions despite similar lesions and clinical states.

Our main perspective scope is to find prognostic measures about recovery ability to use as biomarkers for patient selection in designing rehabilitation treatments and/or non-invasive neuromodulation protocols.

Our study has a number of limitations. First, all our EEG estimates were derived by homologous bipolar derivations. In the future, it can be that by better evaluating homologous

brain neuronal pools via measures derived on the cerebral sources' activities, we will strengthen the relationships with recovery. Supportive of this idea, in chronic stroke patients, we measured the connectivity between lesional and contralesional sensorimotor regions, by either considering the bipolar-EEG activity as in the present investigation or focusing on the cerebral sources in sensorimotor regions devoted to the paretic and the nonparetic hand [36]. Exclusively, the assessment via the source activities revealed the association with robot-aided rehabilitation effects [40]. Furthermore, we evaluated the clinical state through NIHSS, a suitable scoring in the acute state but roughly assessing the finer functionality of the patient in the stabilized condition. Since the present investigation focuses on acute phase markers correlated with the improvement of the clinical state, we preferred to obtain a relative index of the clinical improvement reached by the patient (normalized by the total possible improvement), instead of using scales proper to assess the patient's functional abilities and everyday independence in T1 (Modified Rankin Scale, Bartlett Index, and Fugl-Meyer) which are not collected in the acute phase; thus, they do not allow a differential T1 vs. T0 evaluation.

5. Conclusions

The interhemispheric homologous areas' low-band power symmetry predicted the functional recovery ability in addition to the clinical state at symptoms' onset, reflecting a power increase of the contralesional hemisphere. A more frequent bilateral increase occurred after a right than left damage. The present data strengthen the notion that proper neuromodulations in acute stroke can enhance recovery abilities and provide suggestions on how to personalize the intervention (select people depending on the HArS value, apply bilateral inhibitory NIBS).

Data Availability

EEG raw data, personal and clinical anonymized data will be available upon reasonable request.

Conflicts of Interest

The authors declare that there is no conflict of interest regarding the publication of this paper.

Acknowledgments

The authors would like to thank neurologists Paolo Profice, Giacomo Della Marca, Giuseppe Granata, Nadia Mariagrazia Giannantoni e Francesco Passarelli, and Francesco Tibuzzi for scientific collaboration and patient recruitment; TNFP Matilde Ercolani and Lucia Fraioli for excellent technical support; neuroradiologists Chiara Gaudino and Domenico Lupoi for lesion evaluation; and engineer Alessandro Giordani for database management. The research leading to these results has received funding from (1) the Italian Ministry of Health (GR-2008-1138642) "Promoting recovery from Stroke: Individually enriched therapeutic intervention in Acute phase"; (2) MIUR (Prot. 2010SH7H3F) "Functional connectivity and neuroplasticity in physiological and pathological aging (ConnAge)"; and (3) PNR-CNR (Aging Program 2012-2018).

References

[1] P. W. Duncan, L. B. Goldstein, D. Matchar, G. W. Divine, and J. Feussner, "Measurement of motor recovery after stroke. Outcome assessment and sample size requirements," *Stroke*, vol. 23, no. 8, pp. 1084–1089, 1992.

[2] *SPREAD – stroke prevention and educational awareness diffusion. Ictus cerebrale: Linee guida italiane*http://www.spread.it.

[3] F. Vernieri, G. Assenza, P. Maggio et al., "Cortical neuromodulation modifies cerebral vasomotor reactivity," *Stroke*, vol. 41, no. 9, pp. 2087–2090, 2010.

[4] P. M. Rossini, C. Altamura, A. Ferretti et al., "Does cerebrovascular disease affect the coupling between neuronal activity and local haemodynamics?," *Brain*, vol. 127, no. 1, pp. 99–110, 2004.

[5] F. Tecchio, F. Zappasodi, M. Tombini et al., "Brain plasticity in recovery from stroke: an MEG assessment," *NeuroImage*, vol. 32, no. 3, pp. 1326–1334, 2006.

[6] F. Tecchio, F. Zappasodi, M. Tombini, M. Caulo, F. Vernieri, and P. M. Rossini, "Interhemispheric asymmetry of primary hand representation and recovery after stroke: a MEG study," *NeuroImage*, vol. 36, no. 4, pp. 1057–1064, 2007.

[7] T. H. Murphy and D. Corbett, "Plasticity during stroke recovery: from synapse to behaviour," *Nature Reviews. Neuroscience*, vol. 10, no. 12, pp. 861–872, 2009.

[8] T. A. Jones, "Motor compensation and its effects on neural reorganization after stroke," *Nature Reviews. Neuroscience*, vol. 18, no. 5, pp. 267–280, 2017.

[9] A. Antal, I. Alekseichuk, M. Bikson et al., "Low intensity transcranial electric stimulation: safety, ethical, legal regulatory and application guidelines," *Clinical Neurophysiology*, vol. 128, no. 9, pp. 1774–1809, 2017.

[10] M. F. ALHarbi, S. Armijo-Olivo, and E. S. Kim, "Transcranial direct current stimulation (tDCS) to improve naming ability in post-stroke aphasia: a critical review," *Behavioural Brain Research*, vol. 332, pp. 7–15, 2017.

[11] M. N. McDonnell and C. M. Stinear, "TMS measures of motor cortex function after stroke: a meta-analysis," *Brain Stimulation*, vol. 10, no. 4, pp. 721–734, 2017.

[12] L. J. Boddington and J. N. J. Reynolds, "Targeting interhemispheric inhibition with neuromodulation to enhance stroke rehabilitation," *Brain Stimulation*, vol. 10, no. 2, pp. 214–222, 2017.

[13] *Fifth edition of the National Clinical Guidelines for stroke*http://www.rcplondon.ac.uk/resources/stroke-guidelines. Published October 2016.

[14] M. J. A. M. Van Putten and D. L. J. Tavy, "Continuous quantitative EEG monitoring in hemispheric stroke patients using the brain symmetry index," *Stroke*, vol. 35, no. 11, pp. 2489–2492, 2004.

[15] F. Tecchio, P. Pasqualetti, F. Zappasodi et al., "Outcome prediction in acute monohemispheric stroke via magnetoencephalography," *Journal of Neurology*, vol. 254, no. 3, pp. 296–305, 2007.

[16] G. Assenza, F. Zappasodi, P. Pasqualetti, F. Vernieri, and F. Tecchio, "A contralesional EEG power increase mediated by interhemispheric disconnection provides negative

prognosis in acute stroke," *Restorative Neurology and Neuroscience*, vol. 31, no. 2, pp. 177–188, 2013.

[17] M. A. Dimyan and L. G. Cohen, "Neuroplasticity in the context of motor rehabilitation after stroke," *Nature Reviews. Neuroscience*, vol. 7, no. 2, pp. 76–85, 2011.

[18] A. Baldassarre, L. E. Ramsey, J. S. Siegel, G. L. Shulman, and M. Corbetta, "Brain connectivity and neurological disorders after stroke," *Current Opinion in Neurology*, vol. 29, no. 6, pp. 706–713, 2016.

[19] M. Corbetta, L. Ramsey, A. Callejas et al., "Common Behavioral Clusters and Subcortical Anatomy in Stroke," *Neuron*, vol. 85, no. 5, pp. 927–941, 2015.

[20] P. M. Rossini, F. Tecchio, V. Pizzella et al., "On the reorganization of sensory hand areas after mono-hemispheric lesion: a functional (MEG)/anatomical (MRI) integrative study," *Brain Research*, vol. 782, no. 1-2, pp. 153–166, 1998.

[21] P. M. Rossini, F. Tecchio, V. Pizzella, D. Lupoi, E. Cassetta, and P. Paqualetti, "Interhemispheric Differences of Sensory Hand Areas after Monohemispheric Stroke: MEG/MRI Integrative Study," *NeuroImage*, vol. 14, no. 2, pp. 474–485, 2001.

[22] F. Tecchio, F. Zappasodi, P. Pasqualetti et al., "Rhythmic brain activity at rest from rolandic areas in acute mono-hemispheric stroke: a magnetoencephalographic study," *NeuroImage*, vol. 28, no. 1, pp. 72–83, 2005.

[23] A. Oliviero, F. Tecchio, F. Zappasodi et al., "Brain sensorimotor hand area functionality in acute stroke: insights from magnetoencephalography," *NeuroImage*, vol. 23, no. 2, pp. 542–550, 2004.

[24] G. Barbati, C. Porcaro, F. Zappasodi, P. M. Rossini, and F. Tecchio, "Optimization of an independent component analysis approach for artifact identification and removal in magnetoencephalographic signals," *Clinical Neurophysiology*, vol. 115, no. 5, pp. 1220–1232, 2004.

[25] J. P. Cillessen, A. C. van Huffelen, L. J. Kappelle, A. Algra, and J. van Gijn, "Electroencephalography improves the prediction of functional outcome in the acute stage of cerebral ischemia," *Stroke*, vol. 25, no. 10, pp. 1968–1972, 1994.

[26] E. Faught, "Current role of electroencephalography in cerebral ischemia," *Stroke*, vol. 24, no. 4, pp. 609–613, 1993.

[27] K. Laaksonen, L. Helle, L. Parkkonen et al., "Alterations in spontaneous brain oscillations during stroke recovery," *PLoS One*, vol. 8, no. 4, article e61146, 2013.

[28] E. Niedermeyer, "The clinical relevance of EEG interpretation," *Clinical Electroencephalography*, vol. 34, no. 3, pp. 93–98, 2003.

[29] H. Gastaut, "Etude électrocroticographique de la reativité des rhythmes rolandiques," *Revue Neurologique (Paris)*, vol. 87, pp. 176–182, 1952.

[30] G. Pfurtscheller and F. H. Lopes da Silva, "Event-related EEG/-MEG synchronization and desynchronization: basic principles," *Clinical Neurophysiology*, vol. 110, no. 11, pp. 1842–1857, 1999.

[31] S. Finnigan and M. J. A. M. van Putten, "EEG in ischaemic stroke: Quantitative EEG can uniquely inform (sub-)acute prognoses and clinical management," *Clinical Neurophysiology*, vol. 124, no. 1, pp. 10–19, 2013.

[32] R. V. A. Sheorajpanday, G. Nagels, A. J. T. M. Weeren, M. J. A. M. van Putten, and P. P. De Deyn, "Quantitative EEG in ischemic stroke: Correlation with functional status after 6months," *Clinical Neurophysiology*, vol. 122, no. 5, pp. 874–883, 2011.

[33] S. Graziadio, L. Tomasevic, G. Assenza, F. Tecchio, and J. A. Eyre, "The myth of the 'unaffected' side after unilateral stroke: Is reorganisation of the non-infarcted corticospinal system to re-establish balance the price for recovery?," *Experimental Neurology*, vol. 238, no. 2, pp. 168–175, 2012.

[34] M. Oliveri, P. M. Rossini, P. Pasqualetti et al., "Interhemispheric asymmetries in the perception of unimanual and bimanual cutaneous stimuli," *Brain*, vol. 122, 9 pages, 1999.

[35] C. Codecà, F. Mori, H. Kusayanagi et al., "Differential patterns of interhemispheric functional disconnection in mild and advanced multiple sclerosis," *Multiple Sclerosis*, vol. 16, no. 11, pp. 1308–1316, 2010.

[36] I. Cogliati Dezza, G. Zito, L. Tomasevic et al., "Functional and structural balances of homologous sensorimotor regions in multiple sclerosis fatigue," *Journal of Neurology*, vol. 262, no. 3, pp. 614–622, 2015.

[37] K. S. Cover, H. Vrenken, J. J. G. Geurts et al., "Multiple sclerosis patients show a highly significant decrease in alpha band interhemispheric synchronization measured using MEG," *NeuroImage*, vol. 29, no. 3, pp. 783–788, 2006.

[38] C. J. Stam, B. F. Jones, I. Manshanden et al., "Magnetoencephalographic evaluation of resting-state functional connectivity in Alzheimer's disease," *NeuroImage*, vol. 32, no. 3, pp. 1335–1344, 2006.

[39] M. P. van Meer, K. van der Marel, K. Wang et al., "Recovery of sensorimotor function after experimental stroke correlates with restoration of resting-state interhemispheric functional connectivity," *The Journal of Neuroscience*, vol. 30, no. 11, pp. 3964–3972, 2010.

[40] G. Pellegrino, L. Tomasevic, M. Tombini et al., "Inter-hemispheric coupling changes associate with motor improvements after robotic stroke rehabilitation," *Restorative Neurology and Neuroscience*, vol. 30, no. 6, pp. 497–510, 2012.

[41] A. R. Carter, S. V. Astafiev, C. E. Lang et al., "Resting interhemispheric functional magnetic resonance imaging connectivity predicts performance after stroke," *Annals of neurology*, vol. 67, no. 3, pp. 365–375, 2010.

[42] F. Zappasodi, E. Olejarczyk, L. Marzetti, G. Assenza, V. Pizzella, and F. Tecchio, "Fractal dimension of EEG activity senses neuronal impairment in acute stroke," *PLoS One*, vol. 9, no. 6, article e100199, 2014.

[43] C. Fanciullacci, F. Bertolucci, G. Lamola et al., "Delta power is higher and more symmetrical in ischemic stroke patients with cortical involvement," *Frontiers in Human Neuroscience*, vol. 11, p. 385, 2017.

[44] F. Zappasodi, M. Tombini, D. Milazzo, P. M. Rossini, and F. Tecchio, "Delta dipole density and strength in acute monohemispheric stroke," *Neuroscience Letters*, vol. 416, no. 3, pp. 310–314, 2007.

[45] S. P. Finnigan, S. E. Rose, and J. B. Chalk, "Contralateral hemisphere delta EEG in acute stroke precedes worsening of symptoms and death," *Clinical Neurophysiology*, vol. 119, no. 7, pp. 1690–1694, 2008.

[46] R. C. Van Kaam, M. J. A. M. van Putten, S. E. Vermeer, and J. Hofmeijer, "Contralesional brain activity in acute ischemic stroke," *Cerebrovascular Diseases*, vol. 45, no. 1-2, pp. 85–92, 2018.

[47] C. Monakow, "Experimentelle und pathologisch-anatomische Untersuchungen über die Haubenregion, den Sehhügel und die Regio subthalamica, nebst Beiträgen zur Kenntniss früh

erworbener Gross- und Kleinhirn-defecte," *Archiv für Psychiatrie und Nervenkrankheiten*, vol. 27, no. 1, pp. 1–128, 1895.

[48] G. Koch, M. Cercignani, S. Bonni et al., "Asymmetry of parietal interhemispheric connections in humans," *The Journal of Neuroscience*, vol. 31, no. 24, pp. 8967–8975, 2011.

[49] J. Netz, "Asymmetry in transcallosal inhibition," *Electroencephalography and Clinical Neurophysiology. Supplement*, vol. 51, pp. 137–144, 1999.

[50] F. E. van den Berg, S. P. Swinnen, and N. Wenderoth, "Excitability of the motor cortex ipsilateral to the moving body side depends on spatio-temporal task complexity and hemispheric specialization," *PLoS One*, vol. 6, no. 3, p. e17742, 2011.

[51] N. Tzourio-Mazoyer, L. Petit, L. Zago et al., "Between-hand difference in ipsilateral deactivation is associated with hand lateralization: fMRI mapping of 284 volunteers balanced for handedness," *Frontiers in Human Neuroscience*, vol. 9, 2015.

Hindawi
Neural Plasticity
Volume 2019, Article ID 2687150, 10 pages
https://doi.org/10.1155/2019/2687150

Research Article

Hyperexcitability of Cortical Oscillations in Patients with Somatoform Pain Disorder: A Resting-State EEG Study

Qian Ye,[1,2] **Dong Yan**,[3,4] **Manlin Yao**,[1,2] **Wutao Lou**,[5] **and Weiwei Peng**[1,2]

[1]*School of Psychology, Shenzhen University, Shenzhen, China*
[2]*Shenzhen Key Laboratory of Affective and Social Cognitive Science, Shenzhen University, Shenzhen, China*
[3]*Department of Pain Medicine and Shenzhen Municipal Key Laboratory for Pain Medicine, Shenzhen Nanshan People's Hospital of Shenzhen University Health Science Center, Shenzhen, China*
[4]*School of Traditional Chinese Medicine, Southern Medical University, Guangzhou, China*
[5]*Department of Medicine and Therapeutics, The Chinese University of Hong Kong, Hong Kong*

Correspondence should be addressed to Wutao Lou; louwutao@gmail.com and Weiwei Peng; ww.peng0923@gmail.com

Received 18 November 2018; Revised 16 April 2019; Accepted 15 May 2019; Published 9 July 2019

Guest Editor: Matteo Feurra

Patients with somatoform pain disorder (SPD) suffer from somatic pain that cannot be fully explained by specific somatic pathology. While the pain experience requires the integration of sensory and contextual processes, the cortical oscillations have been suggested to play a crucial role in pain processing and integration. The present study is aimed at identifying the abnormalities of spontaneous cortical oscillations among patients with SPD, thus for a better understanding of the ongoing brain states in these patients. Spontaneous electroencephalography data during a resting state with eyes open were recorded from SPD patients and healthy controls, and their cortical oscillations as well as functional connectivity were compared using both electrode-level and source-level analysis. Compared with healthy controls, SPD patients exhibited greater resting-state alpha oscillations (8.5-12.5 Hz) at the parietal region, as reflected by both electrode-level spectral power density and exact low-resolution brain electromagnetic tomography (eLORETA) cortical current density. A significant correlation between parietal alpha oscillation and somatization severity was observed in SPD patients, after accounting for the influence of anxiety and depression. Functional connectivity analysis further revealed a greater frontoparietal connectivity of the resting-state alpha oscillations in SPD patients, which was indexed by the coherence between pairs of electrodes and the linear connectivity between pairs of eLORETA cortical sources. The enhanced resting-state alpha oscillation in SPD patients could be relevant with attenuated sensory information gating and excessive integration of pain-related information, while the enhanced frontoparietal connectivity could be reflecting their sustained attention to bodily sensations and hypervigilance to somatic sensations.

1. Introduction

Patients with somatoform pain disorder (SPD) suffer from somatic pain (widespread pain or localized head, back, and abdominal pain) that cannot be fully explained by a specific somatic pathology [1]. Besides pain in different locations, functional complaints such as fatigue and dizziness, as well as complaints of comorbid depressive or anxiety disorders, are also common among these patients [2]. Somatosensory amplification is considered to play a crucial role in somatization [3], manifested as exaggerated and sustained attention to bodily sensations or symptoms,as well as hypervigilance to somatic sensations with excessive affect and cognitions, which intensifies these patients more distressing and alarming. Somatoform patients with greater somatization severity tend to have less behavioral activities (e.g., shopping, watching TV) requiring attention distracted from pain bodily symptoms [4, 5]. Functional neuroimaging studies revealed that patients with somatoform pain had enhanced cerebral processing of experimental nociceptive stimuli than healthy controls [6], including greater cortical activations of brain regions of pain neuromatrix (e.g., primary and secondary somatosensory cortex, amygdala, anterior insula, and inferior parietal cortex). The hyperactivations to noxious stimuli

within the pain-related brain regions supported the involvement of somatosensory amplification (heightened salience to noxious percepts) in somatoform patients.

The investigation of spontaneous fluctuations of neural activities during a resting state could help identify the representation of ongoing brain state in somatoform patients. The resting-state large-scale reorganization of functional network has ever been identified among patients with SPD [7], manifested as a decreased functional connectivity between default-mode network and executive network and an increased functional connectivity between sensorimotor and frontoparietal network. Beyond the spatially extended functional network connectivity, the dynamic functional state of the brain can also be well represented by the spontaneous cortical oscillations in multiple frequency bands [8] that can be effectively measured by electroencephalography (EEG) or magnetoencephalography (MEG). It has been proposed that cortical oscillations and synchronization serve the flexible routing of information flow within the brain [9], e.g., gamma (30-100 Hz) and alpha (8-13 Hz) oscillations, respectively, relevant with feedforward and feedback information processing within the brain. While the pain experience requires the integration of sensory and contextual processes, cortical oscillations have been suggested to play a crucial role in pain processing and integration. For example, the suppression of alpha oscillation induced by the nociceptive stimulation is regarded to reflect the cortical excitability within the somatosensory system [10, 11], and the prestimulus alpha oscillation is involved in the top-down controlled gating mechanism that modulates the subsequent pain perception [12, 13]. The gamma oscillation has been considered to be particularly relevant with the encoding of pain perception, i.e., pain-induced enhancement of gamma oscillation over primary somatosensory cortex could represent the subjective perception of pain stimuli [14, 15].

To investigate the abnormalities of ongoing brain states in chronic pain patients, the analysis of cortical oscillations is also conceptually promising and methodologically well suited. While alterations of resting-state cortical oscillations have been reported for many types of chronic pain patients, the obtained results were not fully consistent. The increased resting-state alpha oscillation in patients with multiple sclerosis has been associated with attention deficit and attenuated sensory gating [16, 17], the enhanced alpha oscillation in patients with neuropathic pain has been interpreted as cognitive dysfunction [18, 19], and the positive correlation between pain duration and alpha oscillation power among patients with chronic back pain led to the speculation for the role of alpha oscillations in pain chronification [20]. In contrast, some studies also reported the decrease of alpha oscillation power among patients with chronic low back pain [21] and patients with chronic pain after spinal cord injury [22], which has been interpreted as a dysfunction of cortical inhibition and the functional comorbidity of drowsiness among these patients. The alterations of cortical oscillations in other frequency bands were also reported for chronic pain patients. Fibromyalgia patients showed general increases in theta oscillation power at the left dorsolateral prefrontal and orbitofrontal cortex, as well as increases of beta and gamma power at insular and sensorimotor cortices [23], and these alterations were suggested to be functionally relevant with their abnormalities in the cognitive and emotional modulation of pain. Among chronic low back pain patients, a positive association between ongoing pain intensity and prefrontal beta and gamma oscillations has been reported [24], indicating the relevance of chronic low back pain with the altered gamma oscillation.

While resting-state cortical oscillations might offer diagnostic and therapeutic benefits, the alterations of resting-state EEG oscillations in patients with SPD still remained unclear. For a better understanding of ongoing brain states among the patients with SPD, the present study is aimed at identifying their abnormalities of EEG oscillations during a resting state. Resting-state EEG data with eyes open were recorded from both SPD patients and healthy controls, then their spectral power density and functional connectivity were compared using both electrode-level and source-level analysis.

2. Materials and Methods

2.1. Participants. Seventeen patients (right-handed, 5 females, 35.77 ± 1.75 years, in the range of 25 and 55 years) with SPD were recruited from the Shenzhen Municipal Sixth People's Hospital (Shenzhen, China). Inclusion criteria for patients included (1) diagnosis of SPD according to the International Classification of Diseases (ICD-10) criteria; (2) over 18 and below 60 years old; (3) right-handed; (4) Han Chinese ethnics; and (5) duration of clinical pain for at least 6 months. Seventeen age- and sex-matched healthy controls (right-handed, 8 females, 33.06 ± 1.63 years, in the range of 19 and 46 years) were recruited via advertisements posted in nearby communities. The healthy controls had no chronic/ongoing pain and did not meet the ICD-10 criteria for psychiatric diagnosis. Exclusion criteria for all participants included (1) presence of pain symptoms due to severe somatic diseases; (2) presence of major psychiatric illness, including depression, anxiety, obsessive compulsive disorder, and posttraumatic stress disorder; and (3) existence of neurological diseases such as congestive heart failure, hypertension, and cerebrovascular disease. All participants gave their written informed consent after the experimental procedure had been carefully explained. The research was approved by the local research ethics committee.

2.2. Questionnaires. The subjective and multidimensional experience of pain in SPD patients was quantitatively measured using the Short-Form McGill Pain Questionnaire [25]. It comprises three subscales: a pain rating index (PRI) describing the qualities of pain, a 10 cm visual analogue scale (VAS) describing the intensity of averaged daily pain during the past 2 weeks, and a present pain intensity (PPI) index describing the intensity of current pain. Both SPD patients and healthy controls were instructed to fill in (1) the somatization subscale of Symptom Check List 90-Revised Version (SCL-90-R) that measures the level of somatization severity [26]; (2) Beck Depression Inventory (BDI) that measures cognitive and endogenous aspects of

Table 1: Definitions of electrode-level and source-level regions of interests (ROIs).

	Electrode-level (electrodes)	Source-level (Brodmann areas)
Frontal	Fz, F1, F2, F3, F4, F5, F6, F7, F8	8, 9, 10, 11, 44, 45, 46, 47
Central	Cz, C1, C2, C3, C4, C5, C6	1, 2, 3, 4, 6
Parietal	Pz, P1, P2, P3, P4, P5, P6	5, 7, 30 39, 40 43
Occipital	Oz, O1, O2	17, 18, 19
Temporal	T7, T8, FT7, FT8, TP7, TP8	20 21, 22, 37, 38, 41, 42

depression [27]; and (3) State-Trait Anxiety Inventory (STAI) that measures transitory or situational level of anxiety symptoms [28].

2.3. EEG Recording. Participants were seated in a comfortable chair in a silent and temperature-controlled room. They were instructed to keep eyes open and view a fixation cross in the center of a computer screen, throughout the experiment. Five minutes of continuous EEG data were recorded using 64 Ag-AgCl scalp electrodes placed according to the International 10-20 system (Brain Products GmbH; Munich, Germany; band pass: 0.01–100 Hz; sampling rate: 1000 Hz), using the FCz as recording reference. Electrode impedances were kept below 10 kΩ. Electrooculographic (EOG) signals were simultaneously recorded using two surface electrodes to monitor ocular movements and eyeblinks, one placed ~10 mm below the left eye and the other placed ~10 mm from the outer canthus of the left eye.

2.4. EEG Data Preprocessing. EEG data were preprocessed using EEGLAB, an open source toolbox running under the MATLAB environment (The MathWorks Inc., Natick, Massachusetts, United States). Electrodes located on the neck/face were removed, and the bad electrodes with huge jumps or completely flat were interpolated using a spherical spline method. Continuous EEG data were band-pass filtered (1-45 Hz) using a Hamming finite impulse response filter (filter order: 3300; transition band width: 1 Hz; cutoff frequencies: 0.5-45.5 Hz). Then, the continuous EEG data were segmented into consecutive 2-second epochs, and epochs with the amplitude values exceeding ± 80 μV at any electrode were further rejected. The resulting number of EEG epochs was not different between patients and controls (130.12 ± 1.89 s vs. 127.15 ± 1.15 s, $p = 0.20$, $t = 1.29$). Epochs contaminated by eyeblinks and movements were corrected using an independent component analysis algorithm [28]. In all datasets, independent components with a large electrooculogram (EOG) contribution and a frontal scalp distribution were removed [28]. Finally, the artifact-free resting-state EEG were rereferenced to the common average for further processing, to harmonize the resting-state EEG data collected with different reference electrodes and make our results more comparable with other studies [16, 22, 29, 30].

2.5. Estimation of Resting-State EEG Oscillations. Preprocessed EEG signals were transformed to the frequency domain using a Fast Fourier Transform (FFT, Welch algorithm, Hanning window, no phase shift, 0.5 Hz frequency resolution), yielding an EEG spectrum ranging from 1 to 45 Hz. For each participant, the spectra of each electrode were averaged across epochs. To identify the frequency intervals within which spectral power showed significantly different between healthy controls and SPD patients, we adopted point-by-point statistical analyses (e.g., for each frequency point) combined with nonparametric permutation approach [31]. The spectral power density, measured at parietal electrodes (Pz, P1, P2, P3, P4, P5, and P6) exhibiting the most prominent oscillation during wakeful rest [32, 33], was compared between healthy controls and SPD patients on each frequency point, thus yielding a map of t values for each frequency point. To account for the multiple comparison problem in the point-by-point analysis, a cluster-level nonparametrical permutation testing was performed [31]. Specifically, significant frequency points ($p < 0.05$) were categorized in clusters based on their frequency adjacency (cluster-level statistical analysis). Only the cluster with the largest number of significant frequency points was selected to control for false-positive observations. We performed 5000 random permutations, thus generating the cluster-level permutation t statistics. The cluster-level statistics were defined by calculating the sum of the t values of all frequency points within the cluster, and the two-tailed p values were derived by locating the observed cluster-level t statistics under the estimated permutation distribution. In order to confirm the identified frequency interval, a region of interest- (ROI-) based statistical analyses were further performed. Within this frequency interval, the average spectral power density within the frontal, central, parietal, occipital, and temporal electrode ROIs (the electrodes for each ROI are summarized in Table 1) was computed for each participant. Electrode-level spectral power density within the alpha frequency band was compared between patients and controls, using mixed-design repeated measures analysis of variance (ANOVA) with factors of "group" (patients and controls) and "ROI" (frontal, central, parietal, occipital, and temporal ROIs).

To further localize the cortical current density of the atypical EEG oscillations in patients, we used the freeware called exact low-resolution brain electromagnetic tomography, eLORETA [34], which represents the improved version of the previous pieces of software called LORETA [35] and standardized LORETA [36]. It used a head volume conductor model composed of the scalp, skull, and brain and solved the so-called EEG inverse problem estimating "neural" current density values at any cortical voxel of the head volume conductor model. The brain model was based on a realistic cerebral shape taken from a template of the Montreal

Table 2: Psychometric variables for patients with SPD and healthy controls.

	Patients	Controls	Statistics
Pain rating index (PRI)	10.82 ± 1.49	—	—
Visual analogue scale (VAS)	47.65 ± 4.37	—	—
Present pain intensity (PPI)	1.71 ± 0.28	—	—
Somatization score (SCL-90-R)	1.62 ± 0.21	0.51 ± 0.10	$p < 0.001$, $t = 4.70$
Depression (BDI)	8.18 ± 1.07	2.88 ± 0.84	$p < 0.001$, $t = 3.89$
State-anxiety (STAI-S)	42.88 ± 2.51	31.71 ± 2.13	$p < 0.001$, $t = 3.40$
Trait-anxiety (STAI-T)	52.24 ± 2.69	34.53 ± 2.60	$p < 0.001$, $t = 4.74$

Neurological Institute average MRI brain map (MNI152) [37]. The input for source estimation was the EEG spectral power density computed at scalp electrode level, and the output was the electrical brain source space formed by 6239 voxels at $5 \times 5 \times 5$ mm spatial resolution, restricted to the cortical grey matter. The current source density of the eLORETA cortical functioning image was calculated for each patient and healthy control, within the identified frequency interval. Further, eLORETA cortical current source density between patients and controls was compared in different brain regions. Consistent with electrode-level ROIs, we defined source-level ROIs including the frontal, central, parietal, occipital, and temporal regions. The respective Brodmann areas of each source-level ROI are summarized in Table 1. Source-level eLORETA cortical current density of resting-state alpha oscillations was compared between patients and controls, using mixed-design repeated measures ANOVA with factors of "group" (patients and controls) and "ROI" (frontal, central, parietal, occipital, and temporal ROIs).

2.6. Estimation of Resting-State EEG Functional Connectivity. The functional connectivity of the identified brain region showing significant between-group difference of cortical oscillations was further investigated on both electrode- and source-level. Specifically, the electrode-level functional connectivity of the averaged alpha oscillation in the parietal ROI with other electrode ROIs was assessed using coherence which estimates the linear time-invariant relationship between time series [38]. The coherence was computed as the squared cross-spectrum of two time series, divided by the power spectra of both time series [38], yielding a value between 0 (indicating no linear relationship) and 1 (indicating perfect linear relationship). The source-level functional connectivity between pairs of cortical ROIs was estimated using lagged linear connectivity (LLC) as implemented in the eLORETA statistical package [39]. The LLC estimation provides linear measurements of statistical interdependence between pairs of eLORETA cortical activations [39]. Notably, the LLC estimation depicts the connectivity of two signals after excluding zero-lag instantaneous artifacts that are not often associated with the true physiological interactions, and has been showed to be resistant to nonphysiological artifacts' particularly low spatial resolution and volume conduction [40, 41]. The resulting functional connectivity measures (both coherence and LLC) between the parietal and other brain regions were converted to z values using the Fisher's r-to-z transformation and were separately compared using mixed-design repeated measures ANOVA with factors of "group" (patients and controls) and "ROI" (frontal, central, occipital, and temporal ROIs).

3. Results

3.1. Psychometric Results. As summarized in Table 2, SPD patients were suffering from moderate pain and had significantly greater somatization ($p < 0.001$), state-anxiety ($p < 0.001$), trait-anxiety ($p < 0.001$), and depression scores ($p < 0.001$). Correlation analysis across all SPD patients revealed that the pain severity was significantly and positively correlated with somatization ($r = 0.66$, $p = 0.004$) and depression ($r = 0.64$, $p = 0.006$). It indicates that SPD patients suffering from greater pain tend to have greater somatization severity and depression symptoms.

3.2. Resting-State EEG Oscillations. Point-by-point statistical analysis combined with nonparametrical permutation testing (5,000 times) indicated that patients had significantly greater resting-state EEG spectral power density within the 8.5-12.5 Hz (i.e., alpha) frequency interval ($p_{perm} = 0.018$, Figure 1). The topographies of spectral power density for alpha oscillations were maximal over parietal electrodes for both patients and controls (Figure 2(a)). The average values of alpha power density at different regions were summarized in Figure 2(c). The ANOVA revealed a main effect of "group" ($F = 4.29$, $p = 0.047$, $\eta_p^2 = 0.12$) where patients showed greater alpha oscillatory power and a main effect of "ROI" ($F = 61.31$, $p < 0.001$, $\eta_p^2 = 0.66$) where alpha oscillatory power at parietal and occipital electrodes was greater. The interaction between factors of "group" and "ROI" was not significant ($F = 1.80$, $p = 0.17$, $\eta_p^2 = 0.055$). Independent-sample t-test revealed that the EEG alpha oscillations in patients were in greater power than healthy controls at frontal, parietal, and occipital electrodes ($p = 0.036$, $p = 0.022$, and $p = 0.044$, respectively, Figure 2(c)) but not significantly different at central and temporal electrodes ($p = 0.13$ and $p = 0.077$, respectively).

The source-level eLORETA cortical current density for resting-state alpha oscillation also showed maximal distribution over the parietal lobe for both patients and controls (Figure 2(b)). The average values of eLORETA current

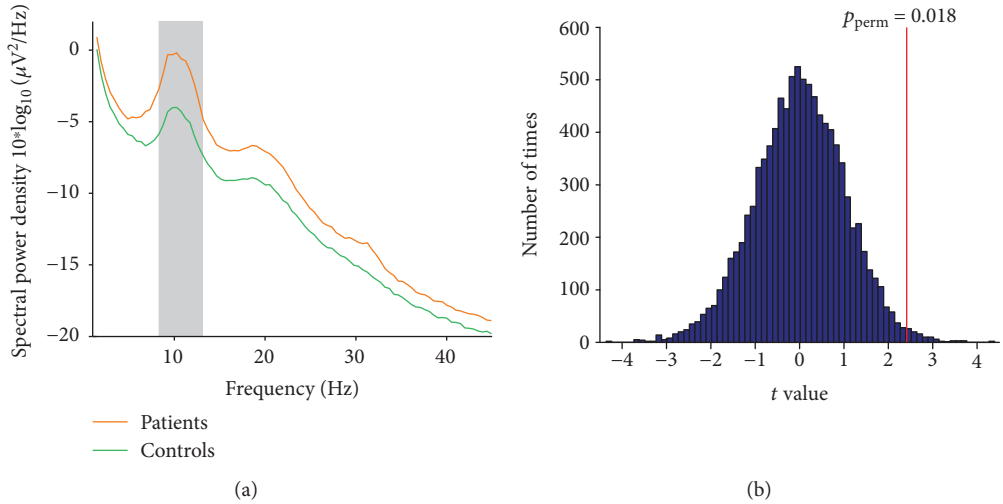

Figure 1: Comparisons of resting-state EEG oscillations for patients and controls. Grand average resting-state spectral power density (measured at parietal electrodes (a)) in the frequency range of 1-45 Hz for SPD patients (orange line) and healthy controls (green line). Within the frequency interval 8.5-12.5 Hz (marked using a grey rectangle), patients exhibited significantly greater spectral power density than healthy controls (t value, vertical red line (b); $p = 0.018$; 5,000 permutations).

density (log transformed) at different cortical regions were summarized in Figure 2(d) and were compared using ANOVA with factors of "ROI" and "group." It revealed a main effect of "ROI" ($F = 50.31$, $p < 0.001$, $\eta_p^2 = 0.62$) where alpha oscillatory power at the parietal and occipital lobes were greater, but the main effect of "group" was marginally significant ($F = 2.93$, $p = 0.097$, $\eta_p^2 = 0.086$) suggesting that patients tend to exhibit greater alpha oscillation power. The interaction between factors of "group" and "ROI" was not significant ($F = 1.67$, $p = 0.19$, $\eta_p^2 = 0.051$). Independent-sample t-test revealed that the eLORETA current source density of patients was significantly greater at the parietal lobe ($p = 0.039$, Figure 2(d)), but not at the frontal, central, occipital, and temporal lobes ($p = 0.24$, $p = 0.23$, $p = 0.09$, and $p = 0.22$, respectively), as compared to controls. This result further confirmed the atypical resting-state alpha oscillations at the parietal region in patients, which has been identified by electrode-level spectral analysis.

After accounting for the influence of anxiety and depression on somatization severity and resting-state alpha oscillation, the residual somatization severity and parietal alpha oscillation (electrode-level spectral power density and eLORETA cortical current density) were obtained using linear regression analysis. Across all the patients, the residual somatization severity was significantly and positively correlated with the alpha oscillation power density at parietal electrodes ($r = 0.58$, $p = 0.015$, Figure 3) and marginally correlated with the eLORETA cortical current density at the parietal lobe ($r = 0.47$, $p = 0.056$, Figure 3). It suggests that SPD patients with greater somatization severity tend to have a greater resting-state alpha oscillation.

3.3. Resting-State EEG Functional Connectivity. We further assessed the functional connectivity of the parietal region using coherence between pairs of electrode ROIs and LLC between pairs of cortical ROIs, within the alpha frequency band. Mixed-design ANOVA on coherence measures revealed a significant interaction between factors of "group" and "ROI" ($F = 4.25$, $p = 0.018$, $\eta_p^2 = 0.12$). Post hoc independent-sample t-test showed that SPD patients had greater functional connectivity between the parietal and frontal regions ($p = 0.018$) than healthy controls, while the functional connectivity of the parietal region with the central, temporal, and occipital regions was not different between patients and controls ($p > 0.05$ for all comparisons, Figure 4(a)). Mixed-design ANOVA on LLC measures revealed a significant main effect of "group" ($F = 6.52$, $p = 0.016$, $\eta_p^2 = 0.17$) indicating that patients had greater functional connectivity than healthy controls. As summarized Figure 4(b), compared with healthy controls, the parietal functional connectivity was greater with the frontal ($p = 0.021$), central ($p = 0.042$), and temporal lobes ($p = 0.038$) for patients with SPD, but not with the occipital lobe ($p = 0.13$).

4. Discussion

The present study recorded EEG data from SPD patients and healthy controls during a resting state with eyes open, and their cortical oscillations, as well as functional connectivity, were compared based on electrode-level and source-level analysis. We have obtained two main findings. First, compared with controls, patients with SPD exhibited greater alpha oscillations (8.5-12.5 Hz) at the parietal region, as confirmed by both electrode-level spectral power density and source-level eLORETA cortical current density. Second, patients showed greater frontoparietal connectivity for the resting-state alpha oscillatory signals, as confirmed by the coherence between pairs of electrodes and the LLC between pairs of eLORETA cortical sources. These alterations demonstrated the frequency-dependent hyperactivation of resting-state EEG oscillations among the SPD patients, which could

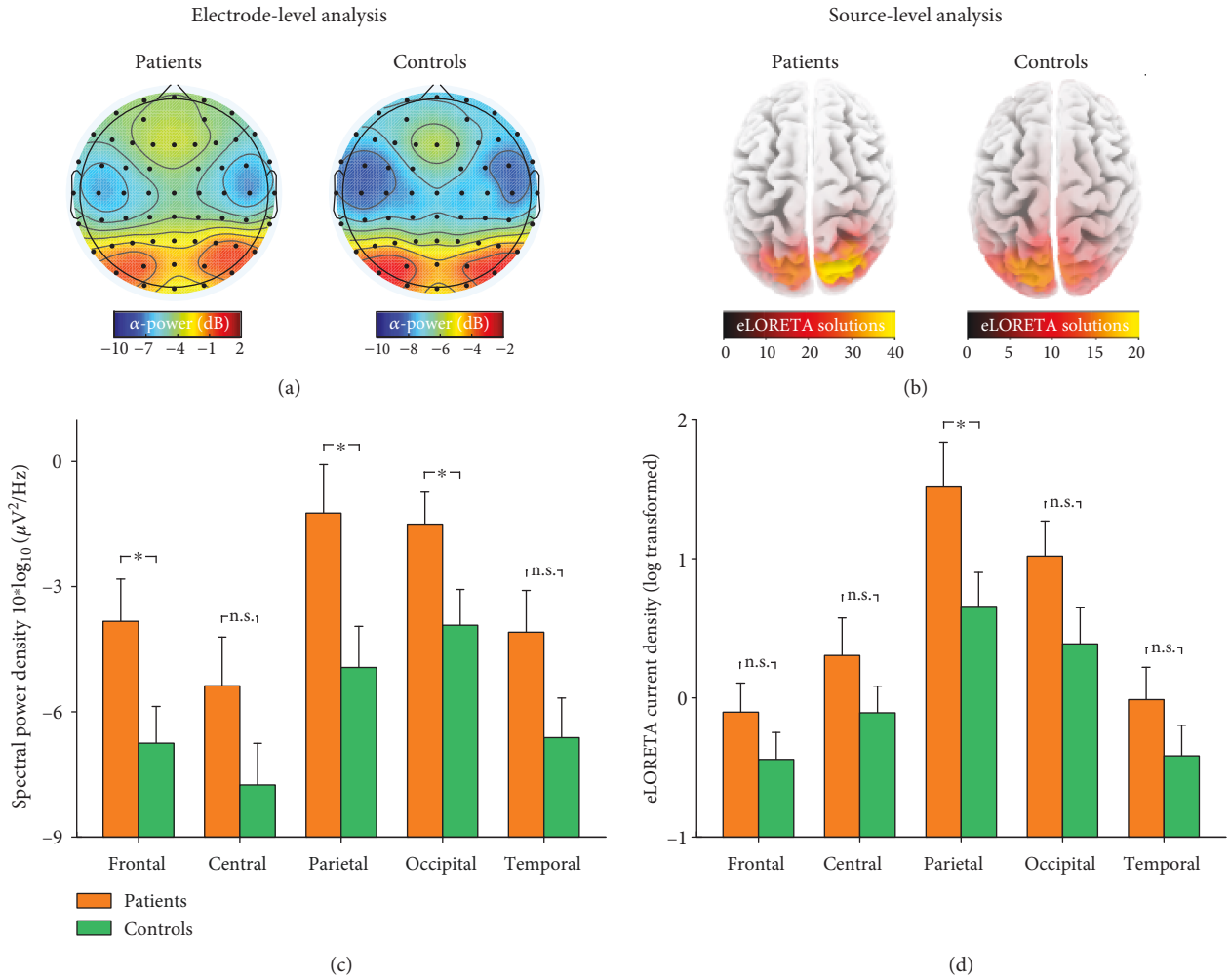

Figure 2: Resting-state EEG alpha oscillations for patients and controls. Group averages of electrode-level spectral power density (a, c) and eLORETA cortical current density (b, d) for resting-state EEG alpha oscillations. The scalp topographies of resting-state alpha oscillations were maximal at the parietal region for both SPD patients and healthy controls, as confirmed by electrode-level and source-level spatial distributions. For a displaying purpose, the color map limits were adjusted for each group. Data are expressed using Mean ± SEM. $^{*}p < 0.05$; n.s.: $p > 0.05$, independent-sample t-test.

implicate the hypersensitive bodily attention and somatosensory amplification in these patients. This understanding might offer diagnostic and therapeutic benefits for the sustained somatoform pain.

The experience of pain has been associated with cortical oscillations in different frequency bands that could represent the dynamic interactions between sensory and contextual processes [9]. Alterations of cortical oscillations have been linked with the pathological abnormalities of chronic pain patients [42], but the results are not fully consistent. The most-noticed abnormality is the increase of theta oscillation in chronic pain patients such as neurogenic pain [18, 43], which has been proposed to be relevant with thalamocortical dysrhythmia [44]. However, we also did not observe abnormalities in theta oscillations in patients with somatoform pain, which is similar with results from chronic pain patients with spinal cord injury [22] or chronic back pain [20]. This inconsistence could be arising from the different types of chronic pain patients involved in these clinical studies and the different EEG recording paradigms (eyes-close or eyes-open state with different durations), as well as the different pain comorbidities such as anxiety, depression, and sleeping disorders which could also influence the resting-state cortical oscillations [45–47].

An increase of the oscillation at alpha band frequency has ever been reported in chronic pain patients [17, 43]. For example, among patients with multiple sclerosis, Kim et al. observed an increase of alpha oscillation power within several nodes of the salience network and ascending nociceptive pathway [17], which was interpreted as a result of overflowing sensory information due to a reduced sensory gating. The increased alpha oscillation has also been identified among migraine patients, suggesting an overintegration of sensory information in these patients [48]. The increase of alpha oscillation in chronic pain patients is in line with the findings from animal models of acute, inflammatory, and neuropathic pain, which exhibited increased cortical oscillation within broad frequency band (3-30 Hz) over the primary somatosensory cortex and the prefrontal cortex [49, 50]. Well consistent with these results, SPD

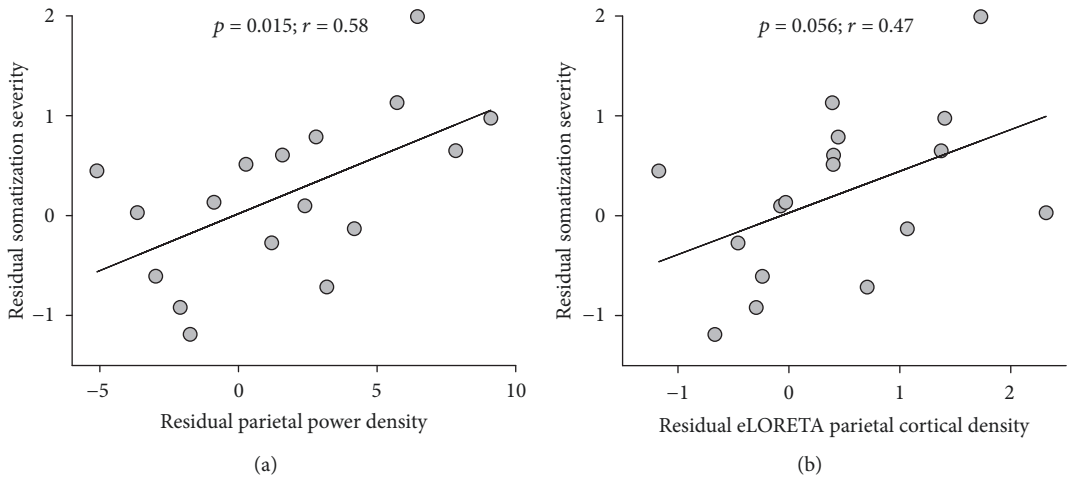

Figure 3: Relationship between somatization severity and resting-state alpha oscillation in SPD patients. After accounting for the influence of anxiety and depression, the residual somatization severity was significantly correlated with residual alpha oscillation power density at parietal electrodes and marginally significantly correlated with the residual eLORETA cortical current density at the parietal lobe. Each grey dot represents values from a single SPD patient, and black lines represent the best linear fit.

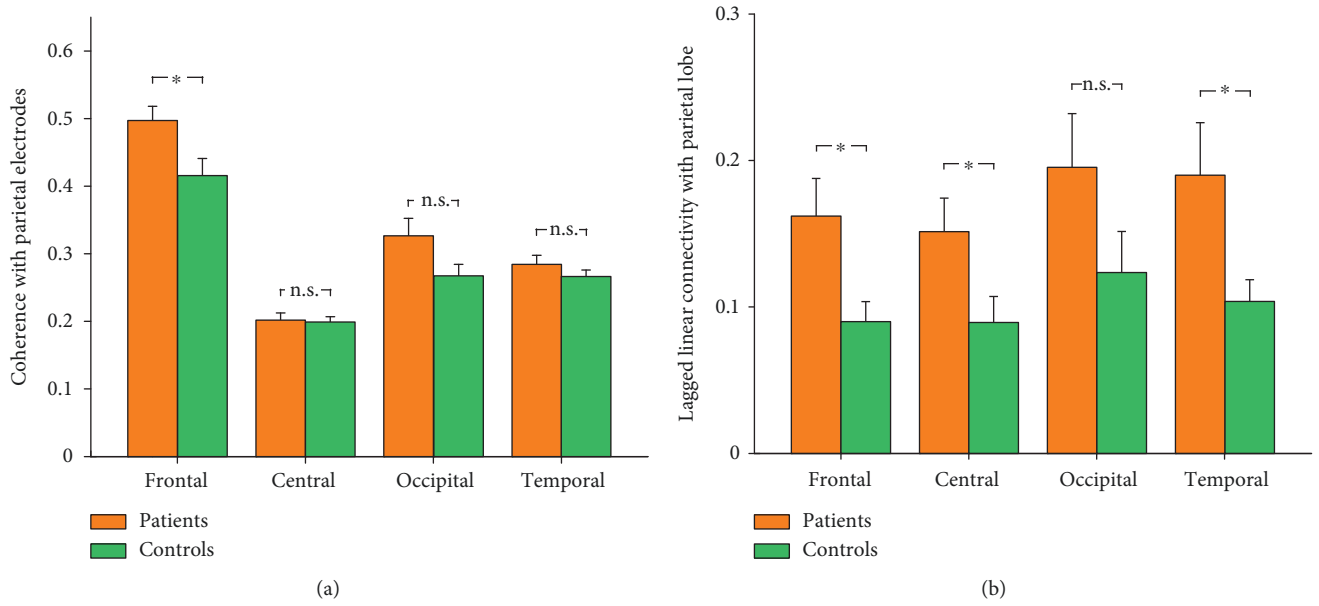

Figure 4: Functional connectivity with the parietal region for resting-state alpha oscillations between patients and controls. The functional connectivity for resting-state alpha oscillatory activity was assessed using coherence between pairs of electrodes (a) and using lagged linear connectivity between pairs of cortical regions (b). Data are expressed using Mean ± SEM. $^{*}p < 0.05$; n.s.: $p > 0.05$, independent-sample t-test.

patients had increased alpha oscillations with maximal distribution over the parietal region, as confirmed by both electrode-level spectral power density and source-level eLORETA cortical current density. Considering the functional role of alpha oscillations in local inhibition and sensory gating [17, 51, 52], the increased alpha oscillations in SPD patients could be reflecting the attenuated sensory information gating and excessive integration of pain-related information, thus appeared as somatosensory amplification in these patients. This hypothesis was further supported by the positive correlation between resting-state alpha oscillation power and somatization severity across the SPD patients, where somatization severity and somatosensory amplification are closely linked [53, 54]. Although the observed increased alpha oscillation among SPD patients was consistent with findings from many chronic pain studies [17, 19, 43, 55], it was in contrast with experimental pain studies [12, 13, 56] showing the negative correlation between prestimulus alpha oscillation and subsequent pain perception. This could be arising from the differences between experimental pain (well controlled with limited duration and specified location) and clinical pain (long lasting and widespread, with pain interference such as sleep interference), particularly considering the absence of organic pathology involved in the maintenance of chronic pain suffered by SPD patients.

After identifying the enhanced alpha oscillations at the parietal region among the SPD patients, we further investigated the parietal functional connectivity for the resting-state alpha oscillatory signals. Compared with healthy controls, patients with SPD also exhibited greater frontoparietal connectivity, as confirmed by (1) coherence for the alpha oscillatory signals measured at parietal and frontal electrodes and (2) LLC estimations for the alpha oscillatory eLORETA solutions estimated at the parietal and frontal lobes. Human frontoparietal functional connectivity has long been implicated in allocating attention resources to perceptual or internal representations, such that attention can adaptively be directed towards external stimuli as well as internal representations [57]. The frontoparietal functional connectivity showed to be correlated with expectancy-induced pain modulation [58], thus suggesting the association between frontoparietal connectivity and endogenous pain modulation. Combining the understanding that somatoform patients typically exhibit excessive attention to their bodily sensations and intensify them as more alerting and distressing [53, 59], the observed enhanced frontoparietal connectivity might represent the sustained bodily attention, hypervigilance to somatic sensations, and/or the dysfunction of pain modulation systems among the SPD patients. Indeed, our result was in line with the enhanced medial prefrontal cortex functional connectivity with the posterior cingulate cortex and precuneus among patients with idiopathic temporomandibular disorder, which was linked with pain rumination across the chronic pain patients [60].

Several limitations should be noted in the present study. First, while EEG data were recorded from the patients and controls during a resting state with eyes open, we could not completely rule out the possibility that the identified abnormalities of resting-state cortical oscillations were relevant with their drowsiness or eyes closing. Second, the sample size of patients is limited, and the relationship between somatoform pain and resting-state cortical oscillations should be further investigated based on a large sample of patients. Third, while we have identified the alterations of resting-state alpha oscillations among SPD patients, the exact role of the altered alpha oscillation in the maintenance of somatoform pain is still unclear. This deserves to be further investigated using simultaneous electrophysiological recordings combined with pharmacological interventions.

In summary, this study provides evidence for enhanced resting-state alpha oscillations and frontoparietal connectivity among patients with SPD, which could be functionally relevant with the sustained attention to bodily sensations and hypervigilance to somatic sensations in these patients. Further studies are needed to validate these findings in a larger cohort of patients and to identify the exact role of the atypical oscillations in the maintenance of somatoform pain.

Data Availability

The datasets used to support the findings of this study are available from the corresponding author on reasonable request.

Conflicts of Interest

All authors declare no conflicts of interest.

Authors' Contributions

Qian Ye and Dong Yan contributed equally.

Acknowledgments

This study was funded by the National Natural Science Foundation of China (31871127), the Shenzhen Basic Research Project (JCYJ20170818093231953), and the Shenzhen University Natural Science Research Fund (2017073).

References

[1] N. Egloff, R. J. A. Cámara, R. von Känel, N. Klingler, E. Marti, and M. L. G. Ferrari, "Hypersensitivity and hyperalgesia in somatoform pain disorders," *General Hospital Psychiatry*, vol. 36, no. 3, pp. 284–290, 2014.

[2] S. Reid, S. Wessely, T. Crayford, and M. Hotopf, "Medically unexplained symptoms in frequent attenders of secondary health care: retrospective cohort study," *BMJ*, vol. 322, no. 7289, p. 767, 2001.

[3] A. J. Barsky, J. D. Goodson, R. S. Lane, and P. D. Cleary, "The amplification of somatic symptoms," *Psychosomatic Medicine*, vol. 50, no. 5, pp. 510–519, 1988.

[4] N. M. Hall, R. Kuzminskyte, A. D. Pedersen, E. Ornbol, and P. Fink, "The relationship between cognitive functions, somatization and behavioural coping in patients with multiple functional somatic symptoms," *Nordic Journal of Psychiatry*, vol. 65, no. 3, pp. 216–224, 2011.

[5] M. P. Jensen and P. Karoly, "Control beliefs, coping efforts, and adjustment to chronic pain," *Journal of Consulting and Clinical Psychology*, vol. 59, no. 3, pp. 431–438, 1991.

[6] H. Gündel, M. Valet, C. Sorg et al., "Altered cerebral response to noxious heat stimulation in patients with somatoform pain disorder," *Pain*, vol. 137, no. 2, pp. 413–421, 2008.

[7] Z. Zhao, T. Huang, C. Tang et al., "Altered resting-state intra- and inter- network functional connectivity in patients with persistent somatoform pain disorder," *PLoS One*, vol. 12, no. 4, p. e0176494, 2017.

[8] A. Schnitzler and J. Gross, "Normal and pathological oscillatory communication in the brain," *Nature Reviews Neuroscience*, vol. 6, no. 4, pp. 285–296, 2005.

[9] M. Ploner, C. Sorg, and J. Gross, "Brain rhythms of pain," *Trends in Cognitive Sciences*, vol. 21, no. 2, pp. 100–110, 2017.

[10] L. Hu, W. Peng, E. Valentini, Z. Zhang, and Y. Hu, "Functional features of nociceptive-induced suppression of alpha band electroencephalographic oscillations," *The Journal of Pain*, vol. 14, no. 1, pp. 89–99, 2013.

[11] M. Ploner, J. Gross, L. Timmermann, B. Pollok, and A. Schnitzler, "Pain suppresses spontaneous brain rhythms," *Cerebral Cortex*, vol. 16, no. 4, pp. 537–540, 2006.

[12] C. Babiloni, A. Brancucci, C. D. Percio et al., "Anticipatory electroencephalography alpha rhythm predicts subjective perception of pain intensity," *The Journal of Pain*, vol. 7, no. 10, pp. 709–717, 2006.

[13] Y. Tu, Z. Zhang, A. Tan et al., "Alpha and gamma oscillation amplitudes synergistically predict the perception of

forthcoming nociceptive stimuli," *Human Brain Mapping*, vol. 37, no. 2, pp. 501–514, 2016.

[14] J. Gross, A. Schnitzler, L. Timmermann, and M. Ploner, "Gamma oscillations in human primary somatosensory cortex reflect pain perception," *PLoS Biology*, vol. 5, no. 5, article e133, 2007.

[15] Z. G. Zhang, L. Hu, Y. S. Hung, A. Mouraux, and G. D. Iannetti, "Gamma-band oscillations in the primary somatosensory cortex–a direct and obligatory correlate of subjective pain intensity," *The Journal of Neuroscience*, vol. 32, no. 22, pp. 7429–7438, 2012.

[16] P. M. Keune, S. Hansen, E. Weber et al., "Exploring resting-state EEG brain oscillatory activity in relation to cognitive functioning in multiple sclerosis," *Clinical Neurophysiology*, vol. 128, no. 9, pp. 1746–1754, 2017.

[17] J. A. Kim, R. L. Bosma, K. S. Hemington et al., "Neuropathic pain and pain interference are linked to alpha-band slowing and reduced beta-band magnetoencephalography activity within the dynamic pain connectome in patients with multiple sclerosis," *Pain*, vol. 160, no. 1, pp. 187–197, 2019.

[18] J. Sarnthein, J. Stern, C. Aufenberg, V. Rousson, and D. Jeanmonod, "Increased EEG power and slowed dominant frequency in patients with neurogenic pain," *Brain*, vol. 129, no. 1, pp. 55–64, 2006.

[19] A. Vuckovic, M. A. Hasan, M. Fraser, B. A. Conway, B. Nasseroleslami, and D. B. Allan, "Dynamic oscillatory signatures of central neuropathic pain in spinal cord injury," *The Journal of Pain*, vol. 15, no. 6, pp. 645–655, 2014.

[20] S. Schmidt, J. R. Naranjo, C. Brenneisen et al., "Pain ratings, psychological functioning and quantitative EEG in a controlled study of chronic back pain patients," *PLoS One*, vol. 7, no. 3, article e31138, 2012.

[21] S. Ahn, J. H. Prim, M. L. Alexander, K. L. McCulloch, and F. Fröhlich, "Identifying and engaging neuronal oscillations by transcranial alternating current stimulation in patients with chronic low back pain: a randomized, crossover, double-blind, sham-controlled pilot study," *The Journal of Pain*, vol. 20, no. 3, pp. 277.e1–277.e11, 2019.

[22] M. P. Jensen, L. H. Sherlin, K. J. Gertz et al., "Brain EEG activity correlates of chronic pain in persons with spinal cord injury: clinical implications," *Spinal Cord*, vol. 51, no. 1, pp. 55–58, 2013.

[23] M. Lim, J. S. Kim, D. J. Kim, and C. K. Chung, "Increased low- and high-frequency oscillatory activity in the prefrontal cortex of fibromyalgia patients," *Frontiers in Human Neuroscience*, vol. 10, 2016.

[24] E. S. May, M. M. Nickel, S. Ta Dinh et al., "Prefrontal gamma oscillations reflect ongoing pain intensity in chronic back pain patients," *Human Brain Mapping*, vol. 40, no. 1, pp. 293–305, 2019.

[25] R. H. Dworkin, D. C. Turk, D. A. Revicki et al., "Development and initial validation of an expanded and revised version of the Short-form McGill Pain Questionnaire (SF-MPQ-2)," *Pain*, vol. 144, no. 1, pp. 35–42, 2009.

[26] L. R. Derogatis and P. A. Cleary, "Factorial invariance across gender for the primary symptom dimensions of the SCL-90," *The British Journal of Social and Clinical Psychology*, vol. 16, no. 4, pp. 347–356, 1977.

[27] A. T. Beck, C. H. Ward, M. Mendelson, J. Mock, and J. Erbaugh, "An inventory for measuring depression," *Archives of General Psychiatry*, vol. 4, no. 6, pp. 561–571, 1961.

[28] A. Delorme and S. Makeig, "EEGLAB: an open source toolbox for analysis of single-trial EEG dynamics including independent component analysis," *Journal of Neuroscience Methods*, vol. 134, no. 1, pp. 9–21, 2004.

[29] A. M. González-Roldán, I. Cifre, C. Sitges, and P. Montoya, "Altered dynamic of EEG oscillations in fibromyalgia patients at rest," *Pain Medicine*, vol. 17, no. 6, pp. 1058–1068, 2016.

[30] S. Vanneste, J. Ost, T. Van Havenbergh, and D. De Ridder, "Resting state electrical brain activity and connectivity in fibromyalgia," *PLoS One*, vol. 12, no. 6, article e0178516, 2017.

[31] E. Maris and R. Oostenveld, "Nonparametric statistical testing of EEG- and MEG-data," *Journal of Neuroscience Methods*, vol. 164, no. 1, pp. 177–190, 2007.

[32] R. Hari, R. Salmelin, J. P. Makela, S. Salenius, and M. Helle, "Magnetoencephalographic cortical rhythms," *International Journal of Psychophysiology*, vol. 26, no. 1-3, pp. 51–62, 1997.

[33] V. Romei, J. Gross, and G. Thut, "On the role of prestimulus alpha rhythms over occipito-parietal areas in visual input regulation: correlation or causation?," *The Journal of Neuroscience*, vol. 30, no. 25, pp. 8692–8697, 2010.

[34] R. D. Pascual-Marqui, "Discrete, 3D distributed, linear imaging methods of electric neuronal activity. Part 1: exact, zero error localization," 2007, http://arxiv.org/abs/0710.3341.

[35] R. D. Pascual-Marqui, C. M. Michel, and D. Lehmann, "Low resolution electromagnetic tomography: a new method for localizing electrical activity in the brain," *International Journal of Psychophysiology*, vol. 18, no. 1, pp. 49–65, 1994.

[36] R. D. Pascual-Marqui, M. Esslen, K. Kochi, and D. Lehmann, "Functional imaging with low-resolution brain electromagnetic tomography (LORETA): a review," *Methods and Findings in Experimental and Clinical Pharmacology*, vol. 24, Supplement C, pp. 91–95, 2002.

[37] J. Mazziotta, A. Toga, A. Evans et al., "A probabilistic atlas and reference system for the human brain: International Consortium for Brain Mapping (ICBM)," *Philosophical Transactions of the Royal Society of London. Series B, Biological Sciences*, vol. 356, no. 1412, pp. 1293–1322, 2001.

[38] J. Gross, J. Kujala, M. Hamalainen, L. Timmermann, A. Schnitzler, and R. Salmelin, "Dynamic imaging of coherent sources: studying neural interactions in the human brain," *Proceedings of the National Academy of Sciences of the United States of America*, vol. 98, no. 2, pp. 694–699, 2001.

[39] R. D. Pascual-Marqui, D. Lehmann, M. Koukkou et al., "Assessing interactions in the brain with exact low-resolution electromagnetic tomography," *Philosophical Transactions. Series A, Mathematical, Physical, and Engineering Sciences*, vol. 369, no. 1952, pp. 3768–3784, 2011.

[40] R. D. Pascual-Marqui, "Coherence and phase synchronization: generalization to pairs of multivariate time series, and removal of zero-lag contributions," 2007, http://arxiv.org/abs/0706.1776.

[41] R. D. Pascual-Marqui, "Instantaneous and lagged measurements of linear and nonlinear dependence between groups of multivariate time series: frequency decomposition," 2007, http://arxiv.org/abs/0711.1455.

[42] E. S. dos Santos Pinheiro, F. C. d. Queirós, P. Montoya et al., "Electroencephalographic patterns in chronic pain: a systematic review of the literature," *PLoS One*, vol. 11, no. 2, p. e0149085, 2016.

[43] J. Stern, D. Jeanmonod, and J. Sarnthein, "Persistent EEG overactivation in the cortical pain matrix of neurogenic pain patients," *NeuroImage*, vol. 31, no. 2, pp. 721–731, 2006.

[44] R. R. Llinás, U. Ribary, D. Jeanmonod, E. Kronberg, and P. P. Mitra, "Thalamocortical dysrhythmia: a neurological and neuropsychiatric syndrome characterized by magnetoencephalography," *Proceedings of the National Academy of Sciences*, vol. 96, no. 26, pp. 15222–15227, 1999.

[45] J. L. Cantero, M. Atienza, and R. M. Salas, "Human alpha oscillations in wakefulness, drowsiness period, and REM sleep: different electroencephalographic phenomena within the alpha band," *Neurophysiologie Clinique/Clinical Neurophysiology*, vol. 32, no. 1, pp. 54–71, 2002.

[46] G. G. Knyazev, A. N. Savostyanov, and E. A. Levin, "Alpha oscillations as a correlate of trait anxiety," *International Journal of Psychophysiology*, vol. 53, no. 2, pp. 147–160, 2004.

[47] A. F. Leuchter, I. A. Cook, Y. Jin, and B. Phillips, "The relationship between brain oscillatory activity and therapeutic effectiveness of transcranial magnetic stimulation in the treatment of major depressive disorder," *Frontiers in Human Neuroscience*, vol. 7, 2013.

[48] L. O'Hare, F. Menchinelli, and S. J. Durrant, "Resting-state alpha-band oscillations in migraine," *Perception*, vol. 47, no. 4, pp. 379–396, 2018.

[49] B. W. LeBlanc, P. M. Bowary, Y.-C. Chao, T. R. Lii, and C. Y. Saab, "Electroencephalographic signatures of pain and analgesia in rats," *Pain*, vol. 157, no. 10, pp. 2330–2340, 2016.

[50] B. W. LeBlanc, T. R. Lii, J. J. Huang et al., "T-type calcium channel blocker Z944 restores cortical synchrony and thalamocortical connectivity in a rat model of neuropathic pain," *Pain*, vol. 157, no. 1, pp. 255–263, 2016.

[51] O. Jensen and A. Mazaheri, "Shaping functional architecture by oscillatory alpha activity: gating by inhibition," *Frontiers in Human Neuroscience*, vol. 4, 2010.

[52] W. Klimesch, P. Sauseng, and S. Hanslmayr, "EEG alpha oscillations: the inhibition-timing hypothesis," *Brain Research Reviews*, vol. 53, no. 1, pp. 63–88, 2007.

[53] K. Muramatsu, H. Miyaoka, Y. Muramatsu et al., "The amplification of somatic symptoms in upper respiratory tract infections," *General Hospital Psychiatry*, vol. 24, no. 3, pp. 172–175, 2002.

[54] M. Nakao and A. J. Barsky, "Clinical application of somatosensory amplification in psychosomatic medicine," *BioPsychoSocial Medicine*, vol. 1, no. 1, p. 17, 2007.

[55] E. N. Van den Broeke, O. H. G. Wilder-Smith, H. van Goor, K. C. P. Vissers, and C. M. van Rijn, "Patients with persistent pain after breast cancer treatment show enhanced alpha activity in spontaneous EEG," *Pain Medicine*, vol. 14, no. 12, pp. 1893–1899, 2013.

[56] W. Peng, C. Babiloni, Y. Mao, and Y. Hu, "Subjective pain perception mediated by alpha rhythms," *Biological Psychology*, vol. 109, pp. 141–150, 2015.

[57] H. C. Lückmann, H. I. L. Jacobs, and A. T. Sack, "The cross-functional role of frontoparietal regions in cognition: internal attention as the overarching mechanism," *Progress in Neurobiology*, vol. 116, pp. 66–86, 2014.

[58] J. Kong, K. Jensen, R. Loiotile et al., "Functional connectivity of the frontoparietal network predicts cognitive modulation of pain," *Pain*, vol. 154, no. 3, pp. 459–467, 2013.

[59] A. J. Barsky, "Amplification, somatization, and the somatoform disorders," *Psychosomatics*, vol. 33, no. 1, pp. 28–34, 1992.

[60] A. Kucyi, M. Moayedi, I. Weissman-Fogel et al., "Enhanced medial prefrontal-default mode network functional connectivity in chronic pain and its association with pain rumination," *The Journal of Neuroscience*, vol. 34, no. 11, pp. 3969–3975, 2014.

Hindawi
Neural Plasticity
Volume 2019, Article ID 6747049, 13 pages
https://doi.org/10.1155/2019/6747049

Research Article

Modulation of Conflict Processing by Theta-Range tACS over the Dorsolateral Prefrontal Cortex

Albert Lehr, Niklas Henneberg, Tarana Nigam, Walter Paulus, and Andrea Antal

Department of Clinical Neurophysiology, University Medical Center Göttingen, Göttingen 37073, Germany

Correspondence should be addressed to Albert Lehr; alehrresearch@gmail.com

Received 13 February 2019; Revised 16 May 2019; Accepted 15 June 2019; Published 8 July 2019

Guest Editor: Andrea Guerra

Behavioral response conflict arises in the color-word Stroop task and triggers the cognitive control network. Midfrontal theta-band oscillations correlate with adaptive control mechanisms during and after conflict resolution. In order to prove causality, in two experiments, we applied transcranial alternating current stimulation (tACS) at 6 Hz to the dorsolateral prefrontal cortex (DLPFC) during Stroop task performance. Sham stimulation served as a control in both experiments; 9.7 Hz tACS served as a nonharmonic alpha band control in the second experiment. We employed generalized linear mixed models for analysis of behavioral data. Accuracy remained unchanged by any type of active stimulation. Over both experiments, the Stroop effect (response time difference between congruent and incongruent trials) was reduced by 6 Hz stimulation as compared to sham, mainly in trials without prior conflict adaptation. Alpha tACS did not modify the Stroop effect. Theta tACS can both reduce the Stroop effect and modulate adaptive mechanisms of the cognitive control network, suggesting midfrontal theta oscillations as causally involved in cognitive control.

1. Introduction

In the face of conflicting information, human beings are capable of adjusting their executive control to resolve conflict and perform the appropriate behavior.

During this process, the cognitive control network first detects conflict, then selects and monitors behaviors for attaining a goal. Multiple brain regions jointly exercise inhibitory control when task demands are high to override stimulus-driven behavior. Generally, cognitive control is measured by performance in conflict tasks, like the Stroop task, in which conflicting task-irrelevant information has to be suppressed for responding correctly [1, 2].

In the Stroop color-word task (SCWT), participants indicate the ink color of a color-word while not responding to its semantic meaning. Responses are faster when the semantic meaning and ink color match (congruent, low-conflict, e.g., "Blue" in blue ink) compared to a mismatch (incongruent, high-conflict, e.g., "Blue" in red ink). This response time difference is a function of the congruence and named after its discoverer *Stroop* [3].

Previous electroencephalography (EEG) and functional magnetic resonance imaging (fMRI) studies found that several brain regions are activated during the Stroop task, including the dorsal Anterior Cingulate Cortex (dACC), the dorsolateral prefrontal cortex (DLPFC), and the posterior parietal cortex (PPC) [4–7]. Neuroimaging studies suggest that the left DLPFC is active (300 ms–440 ms) before the dACC (520 ms–680 ms), indicating the left DLPFC as the source of cognitive control implemented for Stroop task performance [4, 6]. Contrarily, the dACC has also been hypothesized to detect conflict at an earlier point in time (220–340 ms) and to engage the DLPFC that then implements cognitive control and resolves the conflict [6, 8]. This apparent contradiction resolves as cognitive control is exerted strongly in trials following an incongruent trial.

Responses in incongruent trials, which are preceded by incongruent trials (iI), are faster than in incongruent trials, which are preceded by congruent trials (cI). Conversely, responses in cI are slower than in cC [5]. This congruency sequence effect (CSE) in trials preceded by incongruent trials is known as the Gratton effect [9]. A conflict in the previous

trial recruits greater cognitive control that modulates response times in the subsequent trial. This behavioral adjustment is predicted by the conflict adaptation hypothesis [10–12]. The dACC activity increases in conflict trials [12]. It precedes behavioral adaptations promoted by increased DLPFC activity. Thus, this theory postulates that the interplay of conflict-detecting dACC and allocation of control by the DLPFC is responsible for adaptation of the congruency effect. As conflict trials activate the dACC, engagement of DLPFC reduces both the Stroop effect and the dACC activity in trials after a conflict [5]. If the DLPFC activity is high after engagement, it abolishes the Stroop effect independent of the dACC activation level [6]. Only when the DLPFC activity is low (no earlier engagement by dACC) will the dACC activity correlate with the size of the Stroop effect and negatively with error rates [6]. Therefore, it is conceivable that constant high activation of the DLPFC throughout the Stroop task leads to the abolishment of the Stroop effect. In this study, we aim to increase DLPFC activity exogenously to test this hypothesis.

Transcranial alternating current stimulation (tACS) allows us to causally infer function of oscillatory networks [13]. Through the injection of alternating current into the cortex, membrane potentials of many neurons are rhythmically and simultaneously shifted [14]. This effectively entrains networks exogenously [15]. By controlling the rhythmic brain activity, resulting changes in cognitive functions can be causally attributed to the brain oscillation.

In this study, we have chosen tACS with a frequency of 6 Hz based on previous electrophysiological results. Generally, these electrophysiological studies are in line with and corroborate the findings of neuroimaging studies in the Stroop task. The dACC has been shown to be the generator of mediofrontal negativity in the theta (4–8 Hz) range marked by a stronger negative potential around 450 ms in the incongruent condition [16–18]. This midfrontal theta-band (4–8 Hz) oscillatory activity supposedly reflects neural mechanisms of conflict detection [19].

Furthermore, dACC and left DLPFC couple in the theta phase between conflict detection and resolution [20]. In this phase, dACC activity predicts DLPFC activity, establishing dACC as the driving brain region [21]. This intra-areal theta connectivity is prolonged in incongruent compared with congruent trials [20]. Similar to the Gratton effect for response times, oscillatory power in narrow-band theta (6 Hz–7 Hz) in the left-frontal region is significantly higher in iC trials compared to cC trials, while it is slightly lower in iI trials compared to cI trials [22]. Additionally, non-phase-locked theta power correlates with response times [23]. Thus, the evidence suggests that theta power in the left-frontal region and response times are both influenced by conflict in preceding trials. Natural increase in frontocentral theta power and phase-coupling between dACC and left DLPFC in conflict mediate the increased conflict adaption in the next trial. In the Simon task, the congruency effect was reduced during theta-range tACS directed medially towards the dACC because response times slowed in congruent trials [24]. However, in the color-word Stroop task, the evidence for the importance of dACC and DLPFC interaction for the successful resolution of conflict remains correlational. By stimulating the DLPFC, we aim to illuminate the role of the DLPFC in the cognitive control network during the performance of the Stroop task.

Similarly to our approach, a previous work has also targeted the left DLPFC with a theta-range tACS during decision-making requiring cognitive control [25]. Stimulation increased riskier decision, which confirms the DLFPC as a key region for adaptation of decision strategies. Likewise, theta-range tACS to the left DLPFC increased performance in the easy items of a problem solving test by changing attentional components [26]. The stimulation did however not improve performance in a visual-spatial reasoning task. These results indicate DLPFC specifically as a promising target for low-frequency tACS during cognition, while numerous studies have shown transcranial electrical stimulation to modulate cognitive processes in general [27].

To investigate the efficacy of tACS on conflict processing, we have used the drift diffusion model for conflict tasks (DMC). The DMC is a newly developed extension of the classical drift diffusion model (DDM) [28, 29].

Generally, cognitive processing in conflict tasks is studied by behavioral measures like response time and accuracy, which are influenced by a trade-off between speed and accuracy of response. Cognitive models allow decomposing the response time and accuracy into several parameters underlying the decision process. The DDM models the cognitive processes underlying two-alternative forced choice tasks by assuming that participants start to accumulate for either alternative over the time of the trial. The accumulation of evidence begins at the start of the trial, and as soon as it reaches a certain threshold for one alternative, a decision is being made. Due to noisy sensory input, the accumulation is a stochastic process which occasionally results in error trials. Aside from the decision process, the time needed for nondecisional processes is also accounted for.

In DMC, evidence accumulation is the sum of a controlled process (naming of color) and another, automatic process (recognition of semantic meaning). These processes are summed, either leading to (slower) faster responses in (in)congruent trials. The distribution in time of the automatic process is a gamma density function, peaking early during the trial and decaying afterwards. Therefore, the DMC is well suited as it accounts for both the RT distributions and accuracies of conflict tasks as Stroop, Simon, or Eriksen flanker task [30, 31].

We aimed to externally modulate theta power in the left DLPFC and to thereby causally change the function of the cognitive control network. We employed tACS in the theta range (6 Hz) with a high-definition (HD) electrode montage over the left DLPFC in two experiments, in order to entrain the cortical control network [32, 33]. While both experiment stimulations were compared to sham, the second experiment additionally used tACS in the alpha range (9.7 Hz) as a control. This serves as an active control for the possible frequency-unspecific effects of stimulation.

As mentioned above, we employed GLMM and the newly developed DMC to analyse the effects of tACS on response times and accuracy and also the interaction with the congruency effect [29].

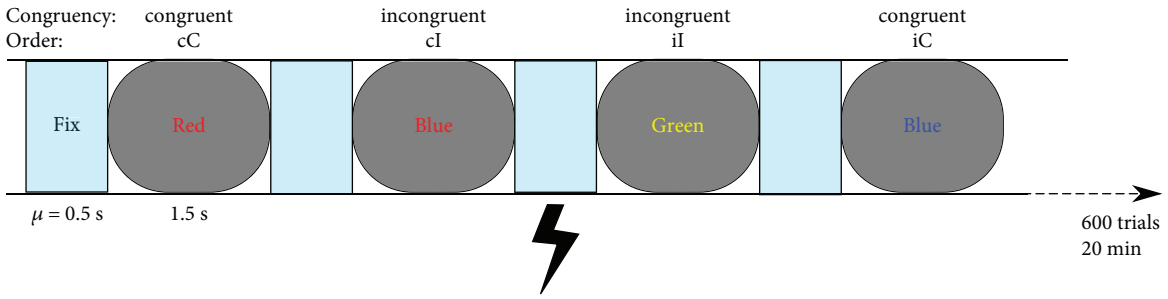

Figure 1: The color-word Stroop task. After practice trials, the participants performed 600 trials within one session while being stimulated by tACS. They responded as quickly and accurately as possible during the 1.5 s of a single trial. Congruent and incongruent trials appeared equally often and were subcategorized depending on the preceding trial.

We hypothesized that the cortical control network can be exogenously entrained (via the left DLFPC) by theta tACS. This would result in increased theta power during and after conflict resolution. With longer phase-coupling between the dACC and the left DLPFC, all trials would show activation patterns similar to those in the incongruent trial. This would induce higher cognitive control for the next trial, comparable to the iC or iI conditions of the Gratton effect. Therefore, we predicted a reduced Stroop effect in the active condition compared to the controls. We expected trials which are preceded by a congruent trial to be more strongly affected by stimulation (reduced Stroop effect) as normally they show no conflict adaptation mediated by theta phase-coupling. Consequently, in DMC, the influence of the automatic process on the decision-making should be reduced.

2. Methods

2.1. Participants. The participants consisted of 22 healthy, right-handed, and native German-speaking adult volunteers, who have normal or corrected-to-normal vision and gave their written informed consent to join the study. They were measured in two experimental groups. The first group consisted of 10 participants (8 females, mean age: 24.4 ± 3.8 years); the second group consisted of 12 participants (8 females, mean age: 25 ± 3.7 years). None of the participants reported neurological or psychiatric disorders and drug-dependency or were taking medication acting on the central nervous system prior to or during the experimental sessions. They were informed about the exclusion criteria and possible adverse effects of tACS. The Ethics Committee of the University Medical Center of Göttingen, Germany, approved the study, which was conducted according to the regulations of the 1964 Declaration of Helsinki.

2.2. Experimental Protocol. The experiments were double-blinded, placebo-controlled, and executed in a within-subject design. Experiment 1 ($n = 10$) consisted of an active 6 Hz tACS and a sham stimulation session. Experiment 2 ($n = 12$) had an additional active control condition (alpha tACS). Subjects participated in all sessions of a given experiment. The condition order was counterbalanced across participants to minimize learning effects. Between experimental sessions, a duration of at least 48 hours was maintained to diminish possible carry-over effects of stimulation. Before and after each session, participants reported their level of arousal and indicated their subjective experience of the stimulation after the session. The dependent variables in this study were accuracy and response times (RTs). Additionally, the arousal and sleep quality were also reported.

2.3. Task. Participants performed a Stroop color-word task (SCWT) [2], which was designed using the PsychoPy toolbox [34]. In the SCWT, the participants have to indicate the color of the font. The stimuli were four German capitalized color-words (Green, Red, Yellow, and Blue) presented with matching or different font colors. The task was designed as a two-alternative forced choice task, meaning that two colors (Green and Red) mapped onto the same one of the two response buttons that the participant had to press manually. Responses were collected by a dedicated response pad (RB-740; Cedrus Corporation, San Pedro, USA) with a time resolution of 2 ms to 3 ms according to the manufacturer. The congruent condition consisted of the matching color-word and font color (e.g., RED written in red). In the incongruent condition, the color-word and the font color were different but also mapped onto different buttons (e.g., RED in yellow). The CIE Lightness Chroma hue device-independent colorimetric space (Commission Internationale de l'éclairage, 1976) was applied. Red (hue = 30), Blue (hue = 280), Green (hue = 140), and Yellow (hue = 100) had the same lightness ($L = 51$) and chroma level (CL = 55%). The gray fixation cross had the same lightness.

Each session started with a minimum of 50 practice trials (termination rule: 18 of the last 20 trials correct), and the following main phase consisted of 300 congruent and incongruent trials in a randomized order. The length of a trial was 1.5 s; the mean interstimulus interval lasted 0.5 s (Chi-squared distribution, range 0.3 s–0.7 s) during which a gray fixation cross (hue) was shown. The participants were instructed to respond as quickly and accurately as possible. The SCWT lasted for 20 minutes (Figure 1).

2.4. Transcranial Alternating Current Stimulation. Stimulation was delivered by a CE-certified neuroConn multichannel stimulator (neuroConn GmbH, Ilmenau, Germany) throughout the main experimental phase [13].

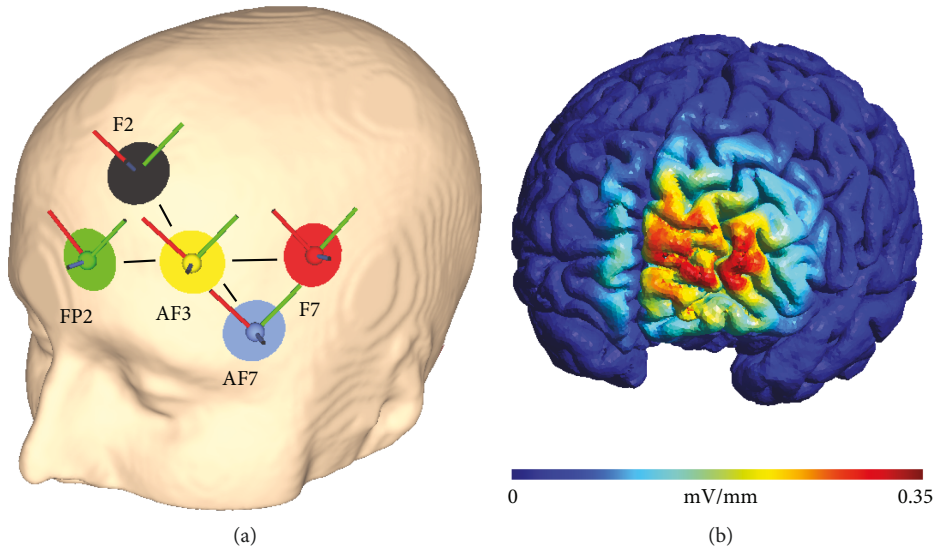

Figure 2: The HD tACS montage for stimulation of the left dorsolateral prefrontal cortex and the modelled electric field strength. (a) The central electrode of the HD montage is centered over AF3. Two pairs of return electrodes form equilateral triangles of 6 cm side length with the central electrode. The distance between both pairs is 10 cm. The return electrodes are located over F5, Fp2, F2, and AF7. (b) The electric field strength is maximal (0.35 mV/mm) over the left prefrontal cortex including the DLPFC. The graphics and electric field strength modelling are derived from SimNIBS 2.0.1.

The high-definition (HD) montage centered over AF3 according to the international 10-10 EEG system with four return electrodes. The return electrodes were positioned over F5, F2, Fp2, and AF7 as in earlier studies targeting the DLPFC [35]. In previous studies, this electrode positioning was used to modulate the activity of the DLPFC. Following the recommendation of previously published modelling studies, the orientation of the plugs and cables was kept constant (facing away perpendicular to the medial line) [36]. Round rubber electrodes of 1 cm radius were fixed on the scalp of participants with the conductive Ten20 paste. This placement leads to left hemispheric frontal stimulation with peak field intensities of 0.3 V/m (Figure 2) according to simulations with the SimNIBS standardized head model [37].

Sinusoidal tACS of 1 mA (peak-to-baseline) intensity and 6 Hz frequency was applied throughout the 20 min duration of the WCST in the active stimulation condition (including 10 s ramp-up and ramp-down periods). Similarly, 9.7 Hz was used as an active control stimulation in the alpha range in the second experiment. Sham stimulation was limited to 30 s (including 10 s ramp-up and ramp-down periods) during the beginning and the end of the SCWT in order to blind the participants while not influencing task performance. The impedances were kept below 15 kΩ. The current density at the main electrode was 0.159 mA/cm^2.

2.5. Analysis. The DMC fitting and the organization of behavioral datasets were done in Python. All statistical testing were conducted in R [38].

2.5.1. Generalized Linear Mixed Models. Generalized linear mixed models (GLMMs) are increasingly utilized to analyse complex research designs [39, 40]. They are mainly used for correlated data, e.g., data in which many data points per individual participant exist [41]. This hierarchical structure is analysed without using mean data averaged across the participants' responses. Response time distributions are normally right-skewed, but GLMM does not assume data to be normally distributed [42]. Overall, GLMM allows data to be analysed without reducing it first to mean values [42].

Parsimonious GLMMs were run on nontransformed RTs of correctly answered trials using an identity-linked Inverse Gaussian distribution as recommended by Lo and Andrews [42]. Similarly, for error rates, the GLMM was run including incorrectly answered trials using an identity-linked binomial distribution. We fitted with the packages RePsychLing 0.0.4 [43] and lme4 1.1–15 [44] following recommendations for nongeneralized models [45]. Maximum likelihood was used to fit the GLMM.

The random effects in the final parsimonious model included intercepts for participants and word-color, with slopes of current trial congruency for word-color and within-participant slopes of current trial congruency and stimulation. The random effects account for variance in the data which arises as, for instance, every participant balances the speed-accuracy trade-off differently, which leads to individual response time and accuracy distributions. The categorical two-level fixed effects stimulation (sham, 6 Hz), congruencies of current and preceding trials (both: congruent, incongruent), was sum-coded numerically for the first experiment. In the second experiment, the stimulation (sham, 6 Hz, 9.7 Hz) was also sum-coded numerically, allowing the effect of the active stimulations to be individually compared to sham. Additionally, we could analyse the interaction of the stimulation with the current trial congruency (Stroop effect) and with the current and preceding trial congruencies (Gratton effect). These factorial predictors were

contrast-coded to extract their main effects and their interactions on the grand means of reaction time and accuracy. We report the Z values and p values of the effects via Welch-Satterthwaite's approximation method [46]. All data points are plotted with 95% prediction interval, which marks the range within which the data points would be with a probability of 95% upon resampling.

2.5.2. Fitting Drift Diffusion Models for Conflict Tasks. DMC assumes that the total response time is the sum of the duration of the decision process (D) and the residual time (R), which includes the sensory processing of stimulus and response execution [29]. Additionally, it assumes that the congruency effect occurs only in the decision process. DMC decomposes the D underlying a two-alternative forced choice into several parameters by accounting for the RTs and accuracy of both congruent and incongruent trials. The boundary (a) is the threshold which has to be crossed by the evidence accumulation to elicit a decision. The nondecision (Ter) and the variability of the nondecision time (sr) characterize R. A controlled process operates on task-relevant information and an automatic process on task-irrelevant information. The controlled process has a constant drift rate (μ_c), whereas the drift rate of the automatic process is changing over time best described by a gamma density function. It decays over time after an early maximum. The amplitude (ζ), shape parameter (α), and scaling parameter (τ) underlie the gamma function [29].

Model fitting was done on individual participants per session (and individual "original" datasets in the recovery study) as described in [29] following these steps:

(1) Plausible starting values from the pilot study were drawn for all parameters from a uniform distribution

(2) Minimization of G^2 statistic as a goodness of fit of parameters to the RT distribution and accuracy was done by the Nelder-Mead simplex method [47]. The maximum number of iterations was 250, each with a sample size of 50,000 observations per congruency condition. The integration constant (delta $t = 1$ ms) and diffusion coefficient (sigma = 4) were as in [29]

(3) The first two steps were repeated 30 times. Computations were done in parallel with the Göttingen Campus High-Performance Computing Centre as each repetition had a run time of around 30 h

We further analysed the parameters which best fit the data as indicated by the G^2 statistic. Parameters were statistically compared to infer which parameters had been influenced by the stimulation using permutation tests. The above-mentioned DMC parameters were the dependent variables with the stimulation condition being the independent variable. However, due to poor recovery, the shape and the time characteristic of the automatic process gamma function were excluded from this analysis (see supplementary Figure S1). Permutation tests are nonparametric tests. In the first experiment with its two stimulation conditions, approximative Monte Carlo Fisher-Pitman permutation tests were run for each analysed DMC parameter. As the second experiment included three stimulation conditions, we performed approximative multivariate Kruskal-Wallis tests. In both tests, 10,000 iterations were used [48, 49]. We adopted the hypothesis testing threshold according to the Bonferroni-Holm method for multiple testing.

2.5.3. Arousal and Sleep. Arousal levels in the Stroop task correlate with better performance in congruent trials and worse performance in incongruent trials [50]. For the control, participants self-reported their arousal level before and after performing the Stroop task on a scale from 1 (very tired) to 10 (totally awake). Sleep deprivation increases response times in the Stroop task but leaves interference and accuracy unchanged [51]. Participants self-reported quality from 1 (miserable) to 5 (excellent) and duration (in hours) of their previous night's sleep. All indicators of each session were analysed across stimulation conditions using the two-sided nonparametric paired sample Wilcoxon signed rank test in Experiment 1 and the two-sided nonparametric paired sample Kruskal-Wallis test in Experiment 2.

3. Results

3.1. First Experiment. Overall accuracy was 94.9% (SD 2.3%), and mean RTs were 624.3 ms (SD 54 ms). Within sham stimulation, accuracy was lower and mean RTs prolonged for incongruent trials (94.6%, SD 2.4%; 652.3 ms, SD 59.1 ms) compared to congruent trials (95.9%, SD 2.8%; 604.2 ms, SD 50.6 ms). Equally, in the active stimulation condition, incongruent trials (93.7%, 2.7%; 638.8 ms, 61.9 ms) were more erroneous and slower than congruent ones (95.3%, SD 2.9%; 602.2 ms, 59.1 ms) (see Table 1).

To assess the effect of the stimulation condition, we were interested in the main effect of the stimulation, its interaction with the congruency of the current trial and its effect on the Gratton effect (i.e., the interaction between congruency of the current and the previous trials). Additionally, we expected an interaction between congruency of the current trial and the stimulation conditions when the preceding trial was either congruent or incongruent. Two generalized linear mixed models were conducted: one for error rates including all trials and the other for the nontransformed response times excluding all error and posterror trials (10.4% of all trials; see Table 2).

For accuracy, significant main effects exist for the congruency (congruent, incongruent) of the current trial (CCT; $Z = 2.801$, $p < 0.01$) but not for stimulation ($Z = 1.875$, $p = 0.06$) or the congruency of the preceding trial (CPT; $Z = 1.491$, $p = 0.13$). Overall, participants were less accurate during incongruent trials ($M = 93.8\%$, SE = 0.7%) than during congruent trials ($M = 95.3\%$, SE = 1.0%, $p < 0.001$). No effects were found for any higher-order interactions, including the interaction factors CCT *x stimulation* ($Z = 0.139$, $p = 0.88$) or *CCT x CPT x stimulation* ($Z = 0.87$, $p = 0.38$). The accuracy is only influenced by the CCT but not by stimulation or CPT.

The analysis of the response times revealed significant main effects for CCT ($Z = 4.37$, $p < 0.001$) but neither

Table 1: Descriptive statistics of both experiments. For both experiments, the difference in behavior between congruent and incongruent trials is broken down per stimulation condition. Mean values are reported with their respective standard deviation.

	Accuracy (%)	Response times (ms)
Experiment 1	94.9 ± 2.3	624.3 ± 54
Sham		
Congruent	95.9 ± 2.8	604.2 ± 50.6
Incongruent	94.6 ± 2.4	652.3 ± 59.1
6 Hz		
Congruent	95.3 ± 2.9	602.2 ± 59.1
Incongruent	93.7 ± 2.7	638.8 ± 61.9
Experiment 2	97.6 ± 2.1	578.1 ± 57
Sham		
Congruent	98.2 ± 1.7	583.4 ± 68.6
Incongruent	97.8 ± 1.5	604.5 ± 84.9
6 Hz tACS		
Congruent	97.6 ± 2.5	554.9 ± 60.5
Incongruent	96.9 ± 3.4	583.4 ± 68.6
9.7 Hz tACS		
Congruent	98.1 ± 1.9	560.3 ± 49.2
Incongruent	97.0 ± 2.3	595.5 ± 69

for CPT ($Z = 1.06$, $p = 0.28$) nor for stimulation ($Z = 0.49$, $p = 0.61$). For CCT, the response times were faster for congruent trials ($M = 600$ ms, SE = 16.1 ms) compared to incongruent ($M = 639.9$ ms, SE = 17.6 ms) trials (Stroop effect). The significant interaction CCT x CPT ($Z = 3.026$, $p < 0.01$) constitutes the Gratton effect, in which the size of the Stroop effect depends on whether the CCT is preceded by a congruent ($M = 47.9$ ms, SE = 7.1 ms) or an incongruent ($M = 30.9$ ms, SE = 4.1 ms) trial. The interaction CCT x stimulation showed a trend ($Z = 1.847$, $p = 0.06$) towards reduced Stroop effect under stimulation ($M = 33.8$ ms, SE = 3.7 ms) compared to sham ($M = 46.2$ ms, SE = 7.1 ms; see Figure 3). The triple interaction CCT x stimulation x CPT narrowly missed the significance criterion ($Z = 1.828$, $p = 0.06$). Further exploration by dividing the dataset according to the congruency of the previous trial revealed a significant interaction CCT x stimulation for trials preceded by a congruent trial ($Z = 2.87$, $p < 0.01$) but no interaction if preceded by an incongruent one ($Z = 0.01$, $p = 0.98$; see Figure 3). Thus, in trials preceded by congruent trials, the stimulation reduces the Stroop effect ($M = 35.8$ ms, SE = 6.1 ms) compared to sham ($M = 60.2$ ms, SE = 11.1 ms).

3.2. Second Experiment. Overall accuracy was 97.6% (SD 2.1%), and mean RTs were 578.1 ms (SD 57 ms).

In sham stimulation, accuracy was lower and mean RTs prolonged for incongruent trials (97.8%, SD 1.5%; 604.5 ms, SD 84.9 ms) compared to congruent trials (98.2%, SD 1.7%; 569.5 ms, SD 68.1 ms). Equally, in the 6 Hz condition, incongruent values are 96.9%, SD 3.4%; 583.4 ms, SD 68.6 ms and congruent values are 97.6%, SD 2.5%; 554.9 ms, SD 60.5 ms,

Table 2: Statistical analysis of the first experiment. The results of the GLMMs are shown for both accuracy and response time data of the first experiment. Additionally, the response times were divided according to the congruency of the previous trial in additional model runs. For every factor, the mean values and standard errors of each factor level are reported. The results of the statistical testing of the difference between these mean values are also reported as Z and p values.

	Estimate (mean ± SE)	Z value	p value
Accuracy (%)			
CCT	Δ1.5	2.801	<0.01
Congruent	95.3 ± 1.0		
Incongruent	93.8 ± 0.7		
CPT	Δ0.6	1.491	0.13
Congruent	93.4 ± 1.2		
Incongruent	94.0 ± 1.0		
Stimulation	Δ0.9	1.875	0.06
Sham	94.2 ± 1.1		
6 Hz	93.3 ± 1.1		
Response times (ms)			
CCT (Stroop effect)	Δ39.9	4.37	<0.001
Congruent	600 ± 16.1		
Incongruent	639.9 ± 17.6		
CPT	Δ3.2	1.06	0.28
Congruent	624.3 ± 22.9		
Incongruent	627.5 ± 22.9		
Stimulation	Δ6	0.49	0.61
Sham	628.9 ± 22.7		
6 Hz	622.9 ± 24.4		
CCT x stimulation	Δ12.4	1.847	0.06
Stroop effect (sham)	46.2 ± 7.1		
Stroop effect (6 Hz)	33.8 ± 3.7		
CCT x CPT	Δ17	3.026	<0.01
Stroop effect (CPT: congruent)	47.9 ± 7.1		
Stroop effect (CPT: incongruent)	30.9 ± 4.1		
CCT x CPT x stimulation	Δ23.1	1.828	0.06
Response times (ms)–data divided according to congruency of previous trial (CPT)			
CPT = congruent			
CCT x stimulation	Δ24.4	2.87	<0.01
Stroop effect (sham)	60.2 ± 11.1		
Stroop effect (6 Hz)	35.8 ± 6.1		
CPT = incongruent			
CCT x stimulation	Δ1.3	0.01	0.98
Stroop effect (sham)	30.9 ± 5.9		
Stroop effect (6 Hz)	32.2 ± 6.3		

SE: standard error.

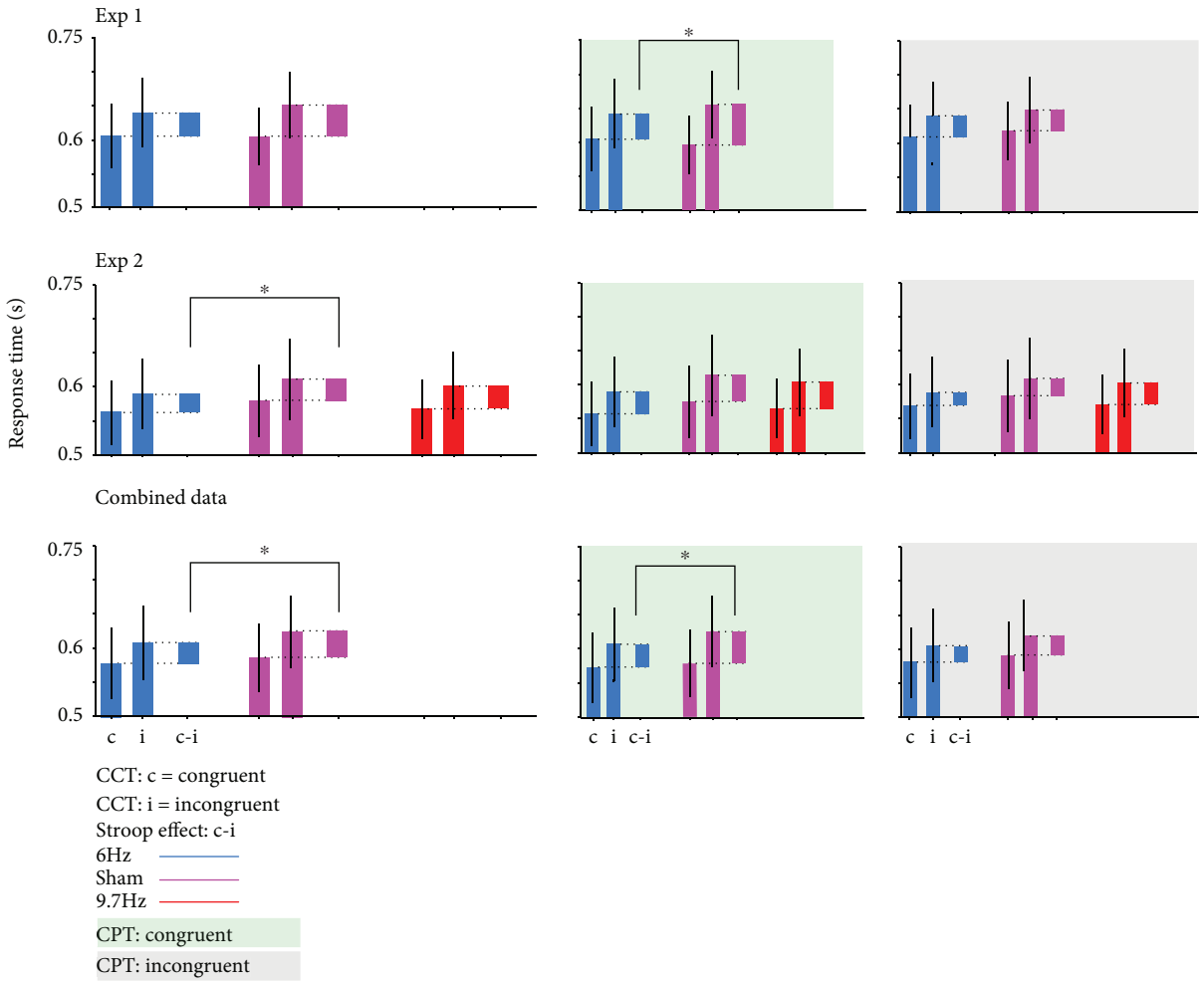

Figure 3: Effect of stimulation on response time. The response times for congruent and incongruent trials and the time difference between these (Stroop effect) are plotted for each stimulation condition individually for all trials in the left panels. In the middle panels, only data of trials which were preceded by a congruent trial are displayed; in the right panels, only for trials preceded by an incongruent trial. Experiment 1 (first row): CCT (size of Stroop effect) and stimulation interact significantly in trials preceded by congruent trials. Experiment 2 (middle row): the interaction CCT x stimulation is significant for all trials but not for the data subsets differentiated by the preceding trial. The active control stimulation in the alpha range did not change the interaction between stimulation and CCT. Combined dataset of both experiments (last row): the interaction between stimulation and CCT is significant across all trials. The significant interaction for trials preceded by congruent trials underlies the effect across all trials. All data is plotted including the 95% confidence interval.

and in the active control condition, incongruent values are 97.0%, SD 2.3%; 595.9 ms, SD 69.0 ms and congruent values are 98.1%, SD 1.9%; 560.3 ms, SD 49.2 ms (see Table 1).

To assess the effect of the stimulation condition, we were interested in the main effects of the two active conditions (stimulation: 6 Hz; control: 9.7 Hz). The two interactions were individually compared to sham stimulation. We further investigated their interaction with the congruency of the current trial and their effect on the Gratton effect (i.e., the interaction between congruency of the current and the previous trials). Additionally, we expected a change in their interaction between congruency of the current trial and the stimulation conditions when the preceding trial was either congruent or incongruent. Two generalized linear mixed models were conducted: one for error rates including all trials and the other for the nontransformed response times excluding all error and posterror trials (4.7% of all trials; see Table 3).

For accuracy, significant main effects existed for CCT ($Z = 2.952$, $p < 0.01$) but not for CPT ($Z = 0.441$, $p = 0.65$). Neither the stimulation ($Z = 0.579$, $p = 0.56$) nor the control ($Z = 0.43$, $p = 0.66$) was significantly different from sham. Overall, participants committed more errors during incongruent trials ($M = 97.1\%$, SE = 0.6%) than during congruent trials ($M = 98.0\%$, SE = 0.5%). For stimulation compared to sham, no effects were found for any higher-order interactions, including the interaction factors CCT *x stimulation* ($Z = 0.380$, $p = 0.703$) and *CCT x CPT x stimulation* ($Z = 0.876$, $p = 0.38$). For the control compared to sham, no effects were found for any higher-order interactions, including the interaction factors CCT *x stimulation* ($Z = 1.305$, $p = 0.191$) and *CCT x CPT x stimulation* ($Z = 1.572$, $p = 0.11$). As in the first experiment, the accuracy is only influenced by the CCT but not by stimulation or CPT.

Table 3: Statistical analysis of Experiment 2. The results of the GLMMs are shown for both accuracy and response time data of the second experiment. For every factor, the mean values and standard errors of each factor level are reported. The results of the statistical testing of the difference between these mean values are also reported as Z and p values.

	Estimate (mean ± SE)	Z value	p value
Accuracy (%)			
CCT	Δ0.9	2.952	<0.01
Congruent	98.0 ± 0.5		
Incongruent	97.1 ± 0.6		
CPT	Δ0.1	0.441	0.65
Congruent	98.6 ± 0.6		
Incongruent	98.7 ± 0.4		
Stimulation			
Sham	98.5 ± 0.3		
6 Hz (vs. sham)	Δ0.2	0.579	0.56
6 Hz	98.3 ± 0.5		
9.7 Hz (vs. sham)	Δ0	0.43	0.66
9.7 Hz	98.5 ± 0.4		
Response times (ms)			
CCT (Stroop effect)	Δ31.3	3.12	0.001
Congruent	561.1 ± 15.0		
Incongruent	592.4 ± 18.4		
CPT	Δ7.2	2.28	0.02
Congruent	573.1 ± 16.5		
Incongruent	580.3 ± 16.6		
Stimulation			
Sham	585.1 ± 24.1		
6 Hz (vs. sham)	Δ4.6	0.78	0.43
6 Hz	580.5 ± 21.8		
9.7 Hz (vs. sham)	Δ2	0.06	0.95
9.7 Hz	584.9 ± 27.5		
CCT x stimulation			
Stroop effect (sham)	32.9 ± 7.2		
Stroop effect (6 Hz vs. sham)	Δ6.9	2.11	0.03
Stroop effect (6 Hz)	26.0 ± 5.0		
Stroop effect (9.7 Hz vs. sham)	Δ2.1	1.44	0.14
Stroop effect (9.7 Hz)	35.0 ± 8.4		
CCT x CPT	Δ11.8	3.48	<0.001
Stroop effect (CPT: congruent)	36.7 ± 7.6		
Stroop effect (CPT: incongruent)	24.9 ± 5.0		
CCT x CPT x stimulation			
CCT x CPT (6 Hz vs. sham)	Δ0.7	0.35	0.72
CCT x CPT (9.7 Hz vs. sham)	Δ1.8	0.87	0.38

SE: standard error.

The analysis of the response times revealed significant main effects for CCT ($Z = 3.12$, $p = 0.001$) and for CPT ($Z = 2.28$, $p = 0.02$). Compared to sham, neither the stimulation ($Z = 0.78$, $p = 0.43$) nor the control ($Z = 0.06$, $p = 0.95$) had an effect on the response times. For CCT, the response times were faster for congruent ($M = 561.1$ ms, SE = 15.0 ms) compared to incongruent ($M = 592.4$ ms, SE = 18.4 ms) trials (Stroop effect). For CPT, the response times were faster when trials were preceded by congruent ($M = 573.1$ ms, SE = 16.5 ms) compared to incongruent ($M = 580.3$ ms, SE = 16.6 ms) trials. The significant interaction CCT x CPT ($Z = 3.48$, $p < 0.001$) constitutes the Gratton effect, in which the size of the Stroop effect depends on whether the CCT is preceded by a congruent (Stroop effect: $M = 36.7$ ms, SE = 7.6 ms) or an incongruent (Stroop effect: $M = 24.9$ ms, SE = 5.0 ms) trial. The active stimulation significantly interacted with CCT ($Z = 2.11$, $p = 0.03$) but not with the interaction CCT x CPT ($Z = 0.35$, $p = 0.72$; see Figure 3).

The size of the Stroop effect depends on whether participants were stimulated with 6 Hz tACS (Stroop effect: $M = 26.0$ ms, SE = 5.0 ms) and the control stimulation (Stroop effect: $M = 35.0$ ms, SE = 8.4 ms) or only sham-stimulated (Stroop effect: $M = 32.9$ ms, SE = 7.2 ms).

The active control did not significantly interact with either CCT ($Z = 1.44$, $p = 0.14$) or interaction CCT x CPT ($Z = 0.87$, $p = 0.38$).

3.3. Joint Analysis of Both Datasets. The response time datasets of Experiments 1 and 2 were combined post hoc and reanalysed to increase statistical power (see Table 4). The control condition of Experiment 2 was excluded from further analysis, but the session order was included as a random factor in order to account for increased training effects not balanced out. The analysis of the response times revealed significant main effects for CCT ($Z = 3.98$, $p < 0.001$) but neither for stimulation ($Z = 1.25$, $p = 0.20$) nor for CPT ($Z = 1.17$, $p = 0.23$). For CCT, the response times were faster for congruent ($M = 579.2$ ms, SE = 12.0 ms) compared to incongruent ($M = 613.3$ ms, SE = 14.0 ms) trials (Stroop effect). The significant interaction CCT x CPT ($Z = 4.40$, $p < 0.001$) constitutes the Gratton effect, in which the size of the Stroop effect depends on whether the CCT is preceded by a congruent (Stroop effect: $M = 41.1$ ms, SE = 5.0 ms) or an incongruent (Stroop effect: $M = 26.3$ ms, SE = 3.5 ms) trial. The interaction CCT x stimulation met the significance criterion ($Z = 2.37$, $p = 0.01$), but the triple interaction CCT x stimulation x CPT did not meet the criterion ($Z = 1.37$, $p = 0.17$; see Figure 3). The size of the Stroop effect depended on whether the participants are really stimulated (Stroop effect: $M = 29.5$ ms, SE = 3.2 ms) or sham-stimulated (Stroop effect: $M = 38.9$ ms, SE = 5.1 ms). Further exploration by dividing the dataset according to the congruency of the previous trial revealed a significant interaction CCT x stimulation for trials preceded by a congruent trial ($Z = 2.65$, $p < 0.01$) but no interaction if preceded by an incongruent one ($Z = 0.71$, $p = 0.47$; see Figure 3). Thus, in trials preceded by congruent trials, the stimulation reduces the Stroop effect ($M = 33.3$ ms, SE = 4.3 ms) compared to sham ($M = 48.9$ ms, SE = 7.0 ms).

Table 4: Statistical analysis of combined dataset. The results of the GLMMs are shown for both accuracy and response time data of the combined dataset of both experiments. Additionally, the response times were divided according to the congruency of the previous trial in additional model runs. For every factor, the mean values and standard errors of each factor level are reported. The results of the statistical testing of the difference between these mean values are also reported as Z and p values.

	Estimate (mean ± SE)	Z value	p value
Response times (ms)			
CCT (Stroop effect)	Δ34.1	3.98	<0.001
Congruent	579.2 ± 12.0		
Incongruent	613.3 ± 14.0		
CPT	Δ3.7	1.17	0.23
Congruent	595.1 ± 25.5		
Incongruent	598.8 ± 25.5		
Stimulation	Δ12.3	1.25	0.20
Sham	603.1 ± 20.3		
6 Hz	590.8 ± 19.3		
CCT x stimulation	Δ9.4	2.37	0.01
Stroop effect (sham)	38.9 ± 5.1		
Stroop effect (6 Hz)	29.5 ± 3.2		
CCT x CPT	Δ14.8	4.40	<0.001
Stroop effect (CPT: congruent)	41.1 ± 5.0		
Stroop effect (CPT: incongruent)	26.3 ± 3.5		
CCT x CPT x stimulation	Δ13.3	*1.37*	*0.17*
Response times (ms)—data divided according to congruency of previous trial (CPT)			
CPT = congruent			
CCT x stimulation	Δ15.6	2.65	<0.01
Stroop effect (sham)	48.9 ± 7.0		
Stroop effect (6 Hz)	33.3 ± 4.3		
CPT = incongruent			
CCT x stimulation	Δ2.3	0.71	0.47
Stroop effect (sham)	27.9 ± 5.7		
Stroop effect (6 Hz)	25.6 ± 3.9		

SE: standard error.

3.4. Diffusion Drift Model for Conflict Task. In Experiment 1, Fisher-Pitman permutation tests investigated statistical differences in the DMC parameter (a, Ter, sr, μ_c, ζ, t_{max}, and t_{90th}) samples recovered for either stimulation conditions. After correcting for multiple comparisons, no statistically significant difference was found for the parameters a ($Z = 0.02$, $p = 1$), μ_c ($Z = 0.51$, $p = 1$), Ter ($Z = 0.22$, $p = 1$), s_t ($Z = 1.94$, $p = 0.33$), ζ ($Z = 0.07$, $p = 1$), t_{90} ($Z = -0.38$, $p = 0.71$), and t_{max} ($Z = -0.12$, $p = 1$). In Experiment 2, we employed Kruskal-Wallis tests to conduct statistical hypothesis testing on the DMC parameters recovered for all three stimulation conditions. No post hoc tests were performed as there was no statistically significant difference for all parameters after correcting for multiple comparisons: a (maxT = 0.41, $p = 1$), μ_c (maxT = 0.99, $p = 1$), Ter (maxT = 0.38, $p = 1$), s_t (maxT = 1.39, $p = 1$), ζ (maxT = 0.93, $p = 1$), t_{90} (maxT = 1.07, $p = 0.71$), and t_{max} (maxT = 1.18, $p = 1$).

3.5. Arousal and Sleep. In the first experiment, the Wilcoxon signed rank test indicated no significant differences between stimulation conditions in mean arousal ($p = 0.878$), sleep quality ($p = 0.999$), and sleep duration ($p = 0.439$). Similarly, neither the Kruskal-Wallis test indicated significant differences between stimulation conditions in mean arousal ($p = 0.777$), sleep quality ($p = 0.5278$), and sleep duration ($p = 0.935$). No subsequent pairwise comparisons were performed. Table S2 summarizes the descriptive and inferential statistics.

4. Discussion

Response conflict increases midfrontal theta dynamics between dACC and the DLPFC [20, 21]. We entrained the cortical control network exogenously by theta tACS during the Stroop task in order to support a causal role of this theta rhythm. For the combined data of both experiments, applying 6 Hz theta tACS reduced the Stroop effect significantly. This effect was driven as expected by reduction in Stroop effect only in trials preceded by congruent trials. The DMC parameters being unchanged did not allow for a more specific characterization.

This is in line with a reduction of congruency effect in the Simon task by theta tACS targeted towards the dACC [24]. This was driven by prolonged response times in congruent trials preceded by congruent trials (cC). Our results and this study provide common evidence for a causal role of mediofrontal theta dynamics in cognitive control.

4.1. Electrophysiology of the Stroop Task. EEG recordings in healthy subjects and intracranial recording in epilepsy patients suggest a causal role for the neural oscillatory connection between dACC and DLPFC [20, 21]. The power of theta oscillations is suggested to increase in proportion to the amount of response conflict [20]. Independent of this theta power increase, the phase-coupling in theta range between left DLPFC and dACC changes depending on the congruency of the trial. Specifically, it persists longer and is stronger in incongruent trials [20]. Additionally, DLPFC activity during the Stroop task is associated with activity increase in gamma frequency range (30 Hz–100 Hz), and electrical stimulation in this frequency band led to causal changes in performance [52]. Intracranial EEG recordings revealed for the DLPFC a preparatory period directly after stimulus offset in which theta power increases and gamma oscillations are coupled to theta oscillations [21]. This cross-frequency coupling correlates with accuracy. The detection of conflict at around ~290 ms leads to increases in theta power in dACC, which drives the phase-coupling in theta range with the DLPFC and cross-frequency coupling

between DLPFC gamma activity and the phase of the theta activity in dACC. Also, the theta power in dACC between conflict detection and resolution correlates positively with response time. The dACC modulates the DLPFC activity before conflict resolution, whereas the DLPFC modulates the dACC after conflict resolution. The modulation occurs via theta phase synchronization. The gamma power in DLPFC after a response correlates negatively with response times for the next incongruent trial reflecting a preparatory mechanism, and the increased theta phase synchronization is a mechanism for the DLPFC to influence the dACC theta activity. Thus, the directionality of information transfer from DLPFC to dACC via theta phase synchronization and gamma activity cross-frequency coupling (CFC) might implement a different response strategy, which does not require the dACC to be active [21].

We chose the DLPFC as a target since its location at the brain surface allows a more reliable stimulation. Stimulation of the dACC, in which due to its deep location is a more difficult target, has been done however [24, 53, 54]. Active conflict detection and resolution are attributed to dACC activity, whereas the adaptation after response is attributed to DLPFC activity [21]. Increased DLPFC activity after incongruent trials leads to less dACC activity following conflict trials and to reduced congruency effects [6]. Exogenously increased DLPFC activity would reduce dACC activity similarly. Since we targeted the DLPFC with tACS, we hypothesized that the DLPFC-dACC circuitry might have been preferentially influenced when DLPFC was active in adaptation of cognitive control for the next trial. Event-related tACS only during the conflict detection and resolution phase in which the dACC is driving the interaction or only during the adaptation phase could lead to different behavioral outcomes as the latter might have a higher efficacy in manipulating the circuitry's activity. It remains an open question if the DLPFC-dACC circuitry can only be modulated intermittently when stimulating the DLPFC constantly.

It has to be noted that in the first experiment the reduced congruency effect was clearly driven by trials which were preceded by congruent trials. It fits very well in our second hypothesis that stronger cognitive control is exerted when tACS increases the normally low DLPFC activity. However, the Stroop effect was reduced for all trials in the second experiment, not only those preceded by congruent trials. Therefore, the first hypothesis that theta-range tACS reduces the Stroop effect is fulfilled. While 6 Hz tACS reduced the Stroop effect in both experiments, it is a partial replication as different subsets of data are affected. In the combined dataset of the studies, both effects survive the joint analysis, showing a general effect of DLPFC on Stroop effect across all participants. Both experiments were designed equally except for the active control condition. Participants acted as their own control by participating in all sessions of an experiment, which cancels out possible difference in performance between the experiments. Therefore, the pooling of the data of both experiments is statistically valid and allows the interpretation of trends underlying both datasets. Inconsistent effects of tACS have been reported before in internal replications [55], but the results of both experiments in this study causally corroborate the importance of DLPFC activity during the Stroop task.

We confirmed the validity of the used DMC by recovering simulated data (see Supplementary Material), replicating an earlier study [56]. We hypothesized the DMC parameters to reflect increased conflict adaptation and therefore a decreased influence of the automatic process on the stochastic decision process. This would entail a combination of reduced amplitude and reduced t_{90} or t_{max} of the automatic process (word reading), which we did not find when estimating the parameters [29]. Therefore, the DMC models indicate for both experiments that the influence of the automatic process remained the same for sham and active stimulation. In the first experiment, 6 Hz stimulation reduced the Stroop effect for all trials by 12.4 ms (38.8%) compared to sham; in the second experiment, by 6.9 ms (22.0%). The breakdown of the behavioral data of each participant and session into 7 underlying DMC parameters reduced the statistical power of the subsequent analysis. Therefore, the DMC was insufficient to detect small absolute changes in both response times and accuracy in this study.

The stimulation frequency of 6 Hz chosen as oscillatory power in narrow-band theta (6 Hz–7 Hz) in the left-frontal region correlates with reaction time in conflict adaptation [22]. While most studies documenting the increased phase-coupling between DLPFC and dACC do not further delimit the frequency beyond being in the theta range, it has been suggested that dACC theta phase at 5 Hz modulates gamma activity in the DLPFC [21]. As the frequency of 6 Hz is at the center of the range of individualized theta frequencies in a study employing a Simon task, we are confident that 6 Hz stimulation was an appropriate choice [24]. In particular, in the context of theta-gamma coupling, the option of superimposing more gamma cycles on a longer theta wave may provide better effects in future experiments. Further studies might obtain stronger abolishments of the Stroop effect when stimulating at the individuals' theta peak frequencies [57].

Our choice of active control frequency in the second experiment fell on a nonharmonic frequency in the alpha range. In previous studies, alpha power decreased after conflict trials as it marks higher arousal [22, 58] but has no indicated role in conflict detection or resolution.

Alpha tACS showed a trend towards a reduced congruency effect during the Simon task in an earlier study [24]. Our results do not show this trend, and therefore, the effect of theta tACS on the conflict processing cannot be attributed to unspecific stimulation effects.

4.2. Outlook and Clinical Relevance. For future studies, the stimulation of the DLPFC in a broad gamma range would be a promising target as DLPFC gamma power after response predicted response times in subsequent trials. Also, theta-gamma cross-frequency stimulation paradigms promise stronger abolishment of the Stroop effect as they effectively change functionality of distant brain regions which exhibited this type of cross-frequency behavior [57].

It is of note that the theta stimulation to the DLPFC could be equally effective if limited to the time after response.

Therefore, the effect of stimulation on adaptation could be isolated while not interfering with conflict detection and resolution. A transfer of the stimulation paradigm to different conflict tasks could show causally if the cognitive control network's physiology is equal in all these tasks.

The Stroop task is a frequently applied neurophysiological test to study neural mechanisms of inhibitory control and its dysfunction [59]. Clinically diverse disorders as chronic alcoholism, schizophrenia, and age-related memory impairment are associated with increased interference in the Stroop task [60–62], which is a biomarker for the inability to correctly inhibit automatic responses and to maintain goal-directed behavior [59]. Both these executive functions are essential to living a well-adapted life, and their restoration is desirable [63].

5. Conclusion

This is the first study stimulating the DLPFC by theta tACS. We demonstrate that the cognitive control network can also be influenced by stimulation targeting the DLPFC. We were able to reduce the Stroop effect in a subset of trials over both experiments. The equalization of response times in congruent and incongruent trials suggests that postconflict adaptation was changed. We propose the hypothesis that theta stimulation of the DLPFC is effective in changing preparatory mechanisms after conflict resolution. The key questions to be clarified are whether (a) gamma tACS leads to more reduction of the Stroop effect, (b) theta stimulation applied only after a conflict resolution is equally effective, and (c) the results are generalizable to other conflict tasks.

Data Availability

The behavioral data used to support the findings of this study are available from the corresponding author upon request.

Disclosure

The funders had no role in study design, collection and analysis of data, decision to publish, or drafting the manuscript.

Conflicts of Interest

The authors declare that there is no conflict of interest regarding the publication of this paper.

Acknowledgments

We acknowledge support by the German Research Foundation and the Open Access Publication Funds of the Göttingen University. The study was funded by the University Medical Center Göttingen, Göttingen, Germany.

Supplementary Materials

The supplementary material is a recovery study for one of the used models, which shows that the model works and can be applied to the data. Additionally, it includes one table specifying the age and gender of the participants and one table showing the quality of sleep and the arousal parameters. *(Supplementary Materials)*

References

[1] M. W. Cole and W. Schneider, "The cognitive control network: integrated cortical regions with dissociable functions," *NeuroImage*, vol. 37, no. 1, pp. 343–360, 2007.

[2] J. R. Stroop, "Studies of interference in serial verbal reactions," *Journal of Experimental Psychology*, vol. 18, no. 6, pp. 643–662, 1935.

[3] C. MacLeod, "The Stroop task in cognitive research," in *Cognitive methods and their application to clinical research*, American Psychological Association, 2005.

[4] M. T. Banich, M. P. Milham, R. A. Atchley et al., "Prefrontal regions play a predominant role in imposing an attentional 'set': evidence from fMRI," *Cognitive Brain Research*, vol. 10, no. 1-2, pp. 1–9, 2000.

[5] J. G. Kerns, J. D. Cohen, A. W. MacDonald, R. Y. Cho, V. A. Stenger, and C. S. Carter, "Anterior cingulate conflict monitoring and adjustments in control," *Science*, vol. 303, no. 5660, pp. 1023–1026, 2004.

[6] R. L. Silton, W. Heller, D. N. Towers et al., "The time course of activity in dorsolateral prefrontal cortex and anterior cingulate cortex during top-down attentional control," *NeuroImage*, vol. 50, no. 3, pp. 1292–1302, 2010.

[7] J. Derrfuss, M. Brass, J. Neumann, and D. Y. von Cramon, "Involvement of the inferior frontal junction in cognitive control: meta-analyses of switching and Stroop studies," *Human Brain Mapping*, vol. 25, no. 1, pp. 22–34, 2005.

[8] C. S. Carter and V. van Veen, "Anterior cingulate cortex and conflict detection: an update of theory and data," *Cognitive, Affective, & Behavioral Neuroscience*, vol. 7, no. 4, pp. 367–379, 2007.

[9] G. Gratton, M. G. H. Coles, and E. Donchin, "Optimizing the use of information: strategic control of activation of responses," *Journal of Experimental Psychology: General*, vol. 121, no. 4, pp. 480–506, 1992.

[10] C. S. Carter, T. S. Braver, D. M. Barch, M. M. Botvinick, D. Noll, and J. D. Cohen, "Anterior cingulate cortex, error detection, and the online monitoring of performance," *Science*, vol. 280, no. 5364, pp. 747–749, 1998.

[11] M. M. Botvinick, T. S. Braver, D. M. Barch, C. S. Carter, and J. D. Cohen, "Conflict monitoring and cognitive control," *Psychological Review*, vol. 108, no. 3, pp. 624–652, 2001.

[12] M. M. Botvinick, J. D. Cohen, and C. S. Carter, "Conflict monitoring and anterior cingulate cortex: an update," *Trends in Cognitive Sciences*, vol. 8, no. 12, pp. 539–546, 2004.

[13] A. Antal, K. Boros, C. Poreisz, L. Chaieb, D. Terney, and W. Paulus, "Comparatively weak after-effects of transcranial alternating current stimulation (tACS) on cortical excitability in humans," *Brain Stimulation*, vol. 1, no. 2, pp. 97–105, 2008.

[14] M. M. Ali, K. K. Sellers, and F. Frohlich, "Transcranial alternating current stimulation modulates large-scale cortical network activity by network resonance," *The Journal of Neuroscience*, vol. 33, no. 27, pp. 11262–11275, 2013.

[15] R. F. Helfrich, T. R. Schneider, S. Rach, S. A. Trautmann-Lengsfeld, A. K. Engel, and C. S. Herrmann, "Entrainment of brain oscillations by transcranial alternating current stimulation," *Current Biology*, vol. 24, no. 3, pp. 333–339, 2014.

[16] R. West and C. Alain, "Event-related neural activity associated with the Stroop task," *Cognitive Brain Research*, vol. 8, no. 2, pp. 157–164, 1999.

[17] M. Liotti, M. G. Woldorff, R. Perez III, and H. S. Mayberg, "An ERP study of the temporal course of the Stroop color-word interference effect," *Neuropsychologia*, vol. 38, no. 5, pp. 701–711, 2000.

[18] R. West, K. Jakubek, N. Wymbs, M. Perry, and K. Moore, "Neural correlates of conflict processing," *Experimental Brain Research*, vol. 167, no. 1, pp. 38–48, 2005.

[19] J. F. Cavanagh and M. J. Frank, "Frontal theta as a mechanism for cognitive control," *Trends in Cognitive Sciences*, vol. 18, no. 8, pp. 414–421, 2014.

[20] S. Hanslmayr, B. Pastötter, K.-H. Bäuml, S. Gruber, M. Wimber, and W. Klimesch, "The electrophysiological dynamics of interference during the Stroop task," *Journal of Cognitive Neuroscience*, vol. 20, no. 2, pp. 215–225, 2008.

[21] C. R. Oehrn, S. Hanslmayr, J. Fell et al., "Neural communication patterns underlying conflict detection, resolution, and adaptation," *The Journal of Neuroscience*, vol. 34, no. 31, pp. 10438–10452, 2014.

[22] D. Tang, L. Hu, and A. Chen, "The neural oscillations of conflict adaptation in the human frontal region," *Biological Psychology*, vol. 93, no. 3, pp. 364–372, 2013.

[23] M. X. Cohen and T. H. Donner, "Midfrontal conflict-related theta-band power reflects neural oscillations that predict behavior," *Journal of Neurophysiology*, vol. 110, no. 12, pp. 2752–2763, 2013.

[24] J. van Driel, I. G. Sligte, J. Linders, D. Elport, and M. X. Cohen, "Frequency band-specific electrical brain stimulation modulates cognitive control processes," *PLoS One*, vol. 10, no. 9, article e0138984, 2015.

[25] T. Sela, A. Kilim, and M. Lavidor, "Transcranial alternating current stimulation increases risk-taking behavior in the balloon analog risk task," *Frontiers in Neuroscience*, vol. 6, p. 22, 2012.

[26] A. Pahor and N. Jaušovec, "The effects of theta transcranial alternating current stimulation (tACS) on fluid intelligence," *International Journal of Psychophysiology*, vol. 93, no. 3, pp. 322–331, 2014.

[27] M.-F. Kuo and M. A. Nitsche, "Effects of transcranial electrical stimulation on cognition," *Clinical EEG and Neuroscience*, vol. 43, no. 3, pp. 192–199, 2012.

[28] R. Ratcliff, "A theory of memory retrieval," *Psychological Review*, vol. 85, no. 2, pp. 59–108, 1978.

[29] R. Ulrich, H. Schröter, H. Leuthold, and T. Birngruber, "Automatic and controlled stimulus processing in conflict tasks: superimposed diffusion processes and delta functions," *Cognitive Psychology*, vol. 78, pp. 148–174, 2015.

[30] J. R. Simon and A. P. Rudell, "Auditory S-R compatibility: the effect of an irrelevant cue on information processing," *The Journal of Applied Psychology*, vol. 51, no. 3, pp. 300–304, 1967.

[31] B. A. Eriksen and C. W. Eriksen, "Effects of noise letters upon the identification of a target letter in a nonsearch task," *Perception & Psychophysics*, vol. 16, no. 1, pp. 143–149, 1974.

[32] D. Edwards, M. Cortes, A. Datta, P. Minhas, E. M. Wassermann, and M. Bikson, "Physiological and modeling evidence for focal transcranial electrical brain stimulation in humans: a basis for high-definition tDCS," *NeuroImage*, vol. 74, pp. 266–275, 2013.

[33] M. F. Villamar, M. S. Volz, M. Bikson, A. Datta, A. F. Dasilva, and F. Fregni, "Technique and considerations in the use of 4x1 ring high-definition transcranial direct current stimulation (HD-tDCS)," *Journal of Visualized Experiments*, vol. 77, no. 77, p. e50309, 2013.

[34] J. W. Peirce, "PsychoPy—Psychophysics software in Python," *Journal of Neuroscience Methods*, vol. 162, no. 1–2, pp. 8–13, 2007.

[35] G. A. de Lara, P. N. Knechtges, W. Paulus, and A. Antal, "Anodal tDCS over the left DLPFC did not affect the encoding and retrieval of verbal declarative information," *Frontiers in Neuroscience*, vol. 11, p. 452, 2017.

[36] G. B. Saturnino, A. Antunes, and A. Thielscher, "On the importance of electrode parameters for shaping electric field patterns generated by tDCS," *NeuroImage*, vol. 120, pp. 25–35, 2015.

[37] A. Thielscher, A. Antunes, and G. B. Saturnino, "Field modeling for transcranial magnetic stimulation: a useful tool to understand the physiological effects of TMS?," in *2015 37th Annual International Conference of the IEEE Engineering in Medicine and Biology Society (EMBC)*, pp. 222–225, Milan, Italy, August 2015.

[38] R. Core Team, *R: A Language and Environment for Statistical Computing*, R Foundation for Statistical Computing, Vienna, Austria, 2018.

[39] N. E. Breslow and D. G. Clayton, "Approximate inference in generalized linear mixed models," *Journal of the American Statistical Association*, vol. 88, no. 421, p. 9, 1993.

[40] B. M. Bolker, M. E. Brooks, C. J. Clark et al., "Generalized linear mixed models: a practical guide for ecology and evolution," *Trends in Ecology & Evolution*, vol. 24, no. 3, pp. 127–135, 2009.

[41] C. E. McCulloch, "Chapter 4: Generalized linear mixed models (GLMMs)," in *Generalized Linear Mixed Models, Vol. Volume 7*, pp. 28–33, Institute of Mathematical Statistics and American Statistical Association, Beechwood OH, USA and Alexandria VA, USA, 2003.

[42] S. Lo and S. Andrews, "To transform or not to transform: using generalized linear mixed models to analyse reaction time data," *Frontiers in Psychology*, vol. 6, article 1171, 2015.

[43] H. Baayen, D. Bates, R. Kliegl, and S. Vasishth, "RePsychLing: Data sets from psychology and linguistics experiments [Computer software manual]," 2015, Retrieved from https://github.com/dmbates/RePsychLing (R package version 0.0.4).

[44] D. Bates, M. Mächler, B. Bolker, and S. Walker, "Fitting linear mixed-effects models using lme4," 2014, http://arxiv.org/abs/1406.5823.

[45] D. Bates, R. Kliegl, S. Vasishth, and H. Baayen, "Parsimonious mixed models," 2015, http://arxiv.org/abs/1506.04967.

[46] A. Kuznetsova, P. B. Brockhoff, and R. H. B. Christensen, "lmerTest package: tests in linear mixed effects models," *Journal of Statistical Software*, vol. 82, no. 13, pp. 1–26, 2017.

[47] J. A. Nelder and R. Mead, "A simplex method for function minimization," *The Computer Journal*, vol. 7, no. 4, pp. 308–313, 1965.

[48] T. Hothorn, K. Hornik, M. A. van de Wiel, and A. Zeileis, "A Lego system for conditional inference," *The American Statistician*, vol. 60, no. 3, pp. 257–263, 2006.

[49] T. Hothorn, K. Hornik, M. A. Wiel, and A. Zeileis, "Implementing a class of permutation tests: the coin package,"

Journal of Statistical Software, vol. 28, no. 8, pp. 1–23, 2008.

[50] M. S. Pallak, T. S. Pittman, J. F. Heller, and P. Munson, "The effect of arousal on Stroop color-word task performance," *Bulletin of the Psychonomic Society*, vol. 6, no. 3, pp. 248–250, 1975.

[51] S. W. Cain, E. J. Silva, A.-M. Chang, J. M. Ronda, and J. F. Duffy, "One night of sleep deprivation affects reaction time, but not interference or facilitation in a Stroop task," *Brain and Cognition*, vol. 76, no. 1, pp. 37–42, 2011.

[52] S. Koga, R. Rothermel, C. Juhász, T. Nagasawa, S. Sood, and E. Asano, "Electrocorticographic correlates of cognitive control in a Stroop task-intracranial recording in epileptic patients," *Human Brain Mapping*, vol. 32, no. 10, pp. 1580–1591, 2011.

[53] K. Onoda, T. Kawagoe, H. Zheng, and S. Yamaguchi, "Theta band transcranial alternating current stimulations modulates network behavior of dorsal anterior cingulate cortex," *Scientific Reports*, vol. 7, no. 1, p. 3607, 2017.

[54] W. T. To, J. Eroh, J. Hart, and S. Vanneste, "Exploring the effects of anodal and cathodal high definition transcranial direct current stimulation targeting the dorsal anterior cingulate cortex," *Scientific Reports*, vol. 8, no. 1, p. 4454, 2018.

[55] D. Veniero, C. S. Y. Benwell, M. M. Ahrens, and G. Thut, "Inconsistent effects of parietal α-tACS on pseudoneglect across two experiments: a failed internal replication," *Frontiers in Psychology*, vol. 8, p. 952, 2017.

[56] C. N. White, M. Servant, and G. D. Logan, "Testing the validity of conflict drift-diffusion models for use in estimating cognitive processes: a parameter-recovery study," *Psychonomic Bulletin & Review*, vol. 25, no. 1, pp. 286–301, 2018.

[57] I. Alekseichuk, Z. Turi, G. Amador de Lara, A. Antal, and W. Paulus, "Spatial working memory in humans depends on theta and high gamma synchronization in the prefrontal cortex," *Current Biology*, vol. 26, no. 12, pp. 1513–1521, 2016.

[58] J. Carp and R. J. Compton, "Alpha power is influenced by performance errors," *Psychophysiology*, vol. 46, no. 2, pp. 336–343, 2009.

[59] E. Strauss, E. M. S. Sherman, O. Spreen, and O. Spreen, *A Compendium of Neuropsychological Tests : Administration, Norms, and Commentary*, Oxford University Press, 2006.

[60] M. H. Dao-Castellana, Y. Samson, F. Legault et al., "Frontal dysfunction in neurologically normal chronic alcoholic subjects: metabolic and neuropsychological findings," *Psychological Medicine*, vol. 28, no. 5, pp. 1039–1048, 1998.

[61] K. R. Hanes, D. G. Andrewes, D. J. Smith, and C. Pantelis, "A brief assessment of executive control dysfunction: discriminant validity and homogeneity of planning, set shift, and fluency measures," *Archives of Clinical Neuropsychology*, vol. 11, no. 3, pp. 185–191, 1996.

[62] T. Hanninen, M. Hallikainen, K. Koivisto et al., "Decline of frontal lobe functions in subjects with age-associated memory impairment," *Neurology*, vol. 48, no. 1, pp. 148–153, 1997.

[63] A. Diamond, "Executive functions," *Annual Review of Psychology*, vol. 64, no. 1, pp. 135–168, 2013.

Hindawi
Neural Plasticity
Volume 2019, Article ID 2490750, 11 pages
https://doi.org/10.1155/2019/2490750

Research Article

Functional Corticomuscular Signal Coupling Is Weakened during Voluntary Motor Action in Cancer-Related Fatigue

Changhao Jiang,[1] **Qi Yang**,[2] **Tingting Chen**,[3] **Vlodek Siemionow**,[2] **Vinoth K. Ranganathan**,[2] **Alice F. Yan**,[4] **and Guang H. Yue**[2,5,6]

[1]*Beijing Key Lab of Physical Fitness Evaluation and Tech Analysis, Capital University of Physical Education and Sports, Beijing, China*
[2]*Department of Biomedical Engineering, The Cleveland Clinic, Cleveland, OH 44195, USA*
[3]*Beijing Key Laboratory of Learning and Cognition & School of Psychology, Capital Normal University, Beijing, China*
[4]*School of Public Health, University of Wisconsin Milwaukee, Milwaukee, WI 53201, USA*
[5]*Human Performance and Engineering Research, Kessler Foundation, West Orange, NJ 07052, USA*
[6]*Department of Physical Medicine and Rehabilitation, Rutgers New Jersey Medical School, Rutgers University, Newark, NJ 07103, USA*

Correspondence should be addressed to Guang H. Yue; gyue@kesslerfoundation.org

Received 28 November 2018; Revised 8 April 2019; Accepted 30 April 2019; Published 26 June 2019

Guest Editor: Matteo Feurra

Background and Purpose. Cancer-related fatigue (CRF) is widely recognized as one of the most common symptoms and side effects of cancer and/or its treatment. However, neuropathological mechanisms contributing to CRF are largely unknown, and the lack of knowledge makes CRF difficult to treat. Recent research has shown dissociation between changes in the brain and muscle signals during voluntary motor performance in cancer survivors with CRF, and this dissociation may be caused by an interruption in functional coupling (FC) of the two signals. The goal of this study was to assess the FC between EEG (cortical signal) and EMG (muscular signal) in individuals with CRF and compare the FC with that of healthy controls during a motor task that led to progressive muscle fatigue. *Method*. Eight cancer survivors with CRF and nine healthy participants sustained an isometric elbow flexion contraction (at 30% maximal level) until self-perceived exhaustion. The entire duration of the EEG and EMG recordings was divided into the first-half (less-fatigue stage) and second-half (more-fatigue stage) artifact-free epochs without overlapping. The EEG-EMG coupling (measured by coherence of the two signals) in each group and stage was computed. Coherence values at different frequencies were statistically analyzed using a repeated-measure general linear model. *Results*. The results demonstrated that compared to healthy controls, CRF participants sustained the contraction for a significantly shorter time and exhibited robust and significantly lower EEG-EMG coherence at the alpha (8~14 Hz) and beta (15~35 Hz) frequency bands. Both the CRF and healthy control groups exhibited significantly decreased EEG-EMG coherence from the less-fatigue to more-fatigue stages at the alpha and beta frequency bands, indicating fatigue-induced weakening of functional corticomuscular coupling. *Conclusion*. Impaired functional coupling between the brain and muscle signals could be a consequence of cancer and/or its treatment, and it may be one of the contributing factors to the abnormal feeling of fatigue that caused the early failure of sustaining a prolonged motor task.

1. Introduction

Different from the typical feeling of fatigue in everyday life in healthy people, cancer-related fatigue (CRF) experienced by cancer survivors usually during cancer treatment is a persistent subjective sense of tiredness that is not relieved by rest or sleep and may continue for months or even years after treatment is complete. CRF is widely recognized as one of the most common symptoms and side effects of cancer and/or its treatment that occurs in 25% to 99% of people with cancer, particularly in individuals actively undergoing treatment [1–7], while the understanding of its etiology

and pathophysiology is very limited. Because of the lack of knowledge of the underlying mechanisms, treatment options for CRF are scarce. CRF has been reported to worsen during motor task exertion and interfere with daily activities [8]. Indeed, cancer survivors with CRF experience muscle weakness and loss of motor endurance that prevent them from performing prolonged motor activities as well as healthy individuals [9].

In a particular study, the authors [9] found that although participants with CRF felt exhausted at the time of failing a sustained muscle contraction, their muscle involved in performing the motor task was not severely fatigued as assessed by physiological measurements. This observation suggests a dissociation between fatigue levels at central (brain) and peripheral (muscle) locations in CRF. Indeed, this dissociation at muscular and supraspinal levels during muscle fatigue is seen even in healthy populations [10–14], but it is significantly exaggerated in individuals with CRF [15–17]. The dissociation between the central and muscular signals with muscle fatigue in healthy and CRF populations seems to suggest an impairment in functional coupling or connectivity between the two signals, and it is interesting to learn if the impairment is more significant in CRF than in the healthy population since CRF patients experience significantly more central than muscle fatigue compared with healthy participants [9]. Distinguishing between the cortical muscular functional coupling pattern in CRF patients with that in healthy controls would help better understand the CRF mechanisms from the neuromuscular perspective and develop effective therapies.

Both cortical and muscular oscillatory activities have been known as common physiological observations. Their coupling of rhythmic oscillations calculated by corticomuscular signal coherence has recently been used to understand cortical control of movement since Conway et al.'s first systematic study based on magnetoencephalography (MEG) and surface electromyography (EMG) signals [18]. There is a general agreement that corticomuscular signal coherence reflects communication between the brain and muscle, which is considered to be related to the control of force and fatigue [19–22] and possibly mediated by the direct corticospinal pathway [23]. Significant correlation between signals of the brain and muscle in the alpha band (8-14 Hz) and beta band (15 to 35 Hz) during voluntary motor actions has been reported in healthy subjects, either in EEG-EMG coherence [24] or MEG-EMG coherence studies [18, 21]. The abnormal features of corticomuscular coherence were also identified in populations with motor disorders, such as stroke [25, 26], tremor [27, 28], and Parkinson's disease [29].

The present study aimed at assessing muscle fatigue-related alterations in functional corticomuscular coupling by measuring EEG-EMG coherence during a sustained submaximal contraction of the elbow flexor muscles in cancer survivors with CRF and compare the outcome with that of healthy controls. It was hypothesized that the functional coupling would be weakened in CRF than in healthy controls due to possible pathophysiological impairment in the central and peripheral nervous systems caused by cancer and/or its treatment [30], and the abnormal corticomuscular signal coupling, among other factors, may worsen fatigue in cancer survivors with CRF.

2. Methods

2.1. Subjects. Eight right-handed cancer survivors with advanced solid cancer (lung, breast, and gastrointestinal cancer) and CRF (62.9 ± 12.3 years old, 5 men) and 9 right-handed healthy subjects (48.2 ± 14.8 years old, 3 men) participated in the study. The age difference between the two groups was not significant ($P > 0.05$). Among the 8 patients, one (male) had stage 4 breast cancer; two (males), stage 4 colon cancer; one (male), stage 4 kidney cancer; three (two females (both stage 3) and one male (stage 4)), lung cancer; and one (female), stage 4 stomach cancer. Although detailed treatment information of these patients was not clear at the time of the study, it was assured, however, that no patient received chemotherapy or radiation therapy within four weeks prior to the participation in the study and all were postoperative for at least 4 weeks. Eligible patients had a hemoglobin concentration > 10 g/dl and no clinical evidence of polyneuropathy, amyotrophy, or a myasthenic syndrome, by history and physical examination. Significant pulmonary compromise as determined by oxygen dependence was an exclusion criterion for both groups. Patients with weight loss greater than 10% of preillness body weight were excluded. Depressed individuals were identified with a single screening question of "Are you depressed?," and those with a positive response were excluded from the study [9]. The study was approved by the local Institutional Review Board. All subjects gave informed consent prior to their participation. All subjects were screened by the Brief Fatigue Inventory (BFI) [31] and performed a sustained contraction (SC) of the right-arm elbow flexion at 30% maximal level until self-perceived exhaustion. Elbow flexion force, surface EMG, and high-density EEG were simultaneously recorded during the SC.

2.2. Data Recording

2.2.1. Sustained Contraction (SC) to Induce Fatigue. An isometric SC was performed to fatigue the elbow flexor muscles. A target force of 30% maximal voluntary contraction (MVC) force was displayed on an oscilloscope using a horizontal cursor. (The maximal force was measured at the beginning of the experiment.) Participants matched the target with the exerted elbow flexion force in a sitting position with the elbow joint at ~100° and maintained the exerted force on the target until they felt exhausted and were no longer able to continue the contraction. Although motivation for performing the SC was not specifically measured, all participants were verbally vigorously encouraged to continue the SC for as long as possible. The SC was terminated if the exerted force dropped 10% or more for more than 3 s. The forces (maximal and SC) were sensed by a force transducer (JR3 Universal Force-Moment Sensor System, Woodland, CA), acquired by a Spike2 data-acquisition system (1401 Plus, Cambridge Electronic Design Ltd., Cambridge, UK),

digitized at 100 samples/s, and stored on the hard disk of a personal computer (PC).

2.2.2. Electromyogram (EMG) Measurements. Bipolar surface EMG was recorded from the belly of the biceps brachii (BB), brachioradialis (BR), and triceps brachii (TB) muscles using Ag-AgCl electrodes (In Vivo Metric, Healdsburg, CA). The recording diameter of each electrode was 8 mm, and center-to-center interelectrode distance was ~3 cm. A reference electrode was placed on the skin overlying the lateral epicondyle near the elbow joint. The EMG signals were amplified (×1000), band-pass filtered (3 Hz–1 KHz), digitized (2000 samples/s), acquired by the Spike2 system, and stored on the hard disk of the PC.

2.2.3. High-Density EEG Measurements. Scalp EEG signals were recorded continuously during the SC using a 128-channel EEG data acquisition system (Electrical Geodesics Inc., Eugene, OR, USA.). All channels of the signals were amplified (×75,000), band-pass filtered (0.1-100 Hz), digitized (250 sample/s), and recorded on the hard disk of a dedicated PC connected to the EEG acquisition hardware and installed with the acquisition and analysis software.

2.3. Data Processing and Analysis. The EMG signals were resampled (250 Hz), high-pass filtered at 10 Hz, and rectified. EEG signals were high-pass filtered at 3 Hz. All the EEG data were inspected visually. Recordings with artifacts caused by events such as eye blinks or head movements were excluded, and the corresponding EMG signals were discarded. The entire duration of the EEG and EMG recordings was then divided into the first half (less-fatigue stage) and second half (more-fatigue stage), and subsequently, the signals in each stage were segmented into artifact-free epochs of 256 samples without overlapping (mean = 98.5 epochs, ranged from 44 to 153 for CRF, and mean = 148.5 epochs, ranged from 56 to 264 for controls).

In each stage, a multivariate autoregressive (MVAR) model was applied to each matched epoch of EEG and EMG signals and the coefficients were derived by ARfit MATLAB software [32]. An order of 6 was chosen for the MVAR model based on Schwarz's Bayesian Criterion [33]. Autospectrum and cross-spectrum of the EEG and EMG were calculated from the MVAR coefficients, and the coherence of the two signals was obtained from normalization of the cross-spectrum: $C_{xy}^2(f) = |S_{xy}(f)|^2 / S_{xx}(f) * S_{yy}(f)$, where $S_{xx}(f)$ and $S_{yy}(f)$ are the cross-trial smoothed autospectrum of the EEG and EMG signals, x and y, for a given frequency f, and the $S_{xy}(f)$ is the cross-trial smoothed cross-spectrum. The frequency resolution was set as 1 Hz. A bootstrap 95% significance level was calculated for every paired EEG-EMG signal at each stage from 100 randomly resampling paired trials [34].

Due to the volume of information, especially the large number of EEG channels, the coherence values of the 128 EEG channels with each of the three muscles (BB, BR, or TB) were grouped into five scalp areas for statistical comparisons: left, right, frontal, central, and parietal [25, 35]. Because no significant EEG-EMG coherence was detected either in the nonfatigue or the fatigue stage at other frequencies, crossing-stage comparisons were limited at the alpha (8-14 Hz) and beta (15-35 Hz) frequency bands. The calculated coherence was normalized by the arc hyperbolic tangent transformation to stabilize the standard deviation [36].

2.4. Statistical Analysis. A repeated-measure general linear model was used to statistically compare the coherence between the CRF and control groups at each frequency band by SPSS 12.0 (SPSS Inc., Chicago, IL, USA). The between-subject factor was group and the within-subject factors were fatigue stage, muscle, and scalp area. Additionally, the peak coherence values were also subject to statistical analysis. EMG amplitude of two groups were also compared using a repeated-measure general linear model. Statistical significance level was set at $P \leq 0.05$. Multiple comparisons were corrected with the Bonferroni method.

3. Results

Brief Fatigue Inventory (BFI) scores were higher ($P < 0.01$) in the CRF than in the healthy control group. The mean (±standard deviation) BFI score of the nine questions was 5.2 ± 0.17 for patients and 0.08 ± 0.09 for the controls. Force was well maintained at about 30% of the MVC level, and there was no significant difference of force between stage 1 and stage 2 in both the patient and the control group. However, CRF participants sustained the contraction for a significantly shorter time (335 ± 129 s in CRF vs. 554 ± 140 s in controls, $P < 0.01$), and their MVC elbow flexion force measured before the sustained contraction was significantly lower (187 ± 66 N in CRF vs. 261 ± 75 N, $P < 0.01$) (this means the CRF group sustained a lower absolute force for a shorter time as the target force (30% MVC) was calculated based on the MVC force).

Figure 1 shows the EMG results in the two stages of the sustained elbow flexion of the two groups. The amplitude of surface EMG signals from the elbow flexor muscles (BB, TB) increased significantly ($P < 0.01$) within both groups. No significant differences were found either between groups or different muscles. The increase of the EMG signal of the involved elbow flexor muscles in stage 2 indicated that subjects had to increase their effort to maintain the same force level (by recruiting additional muscle fibers/motor units and/or their activation level) to compensate for the loss of force-generating capability of the fatigued motor units/muscle fibers, which was an indication of muscle fatigue.

EEG-EMG coherence averaged across subjects and electrodes within the cortical area was significantly lower in patients than in controls (Figure 2), especially at the upper beta band (~30 Hz). Control subjects had the first peak coherence value at the upper alpha band (~12 Hz) in both stages of the fatigue process and the second peak value around the upper beta band almost in each muscle and cortical area combination. But CRF patients usually only had the peak coherence value at the upper alpha, and there was an obvious reduction in the value of coherence in the upper beta band in both stages compared to controls. A

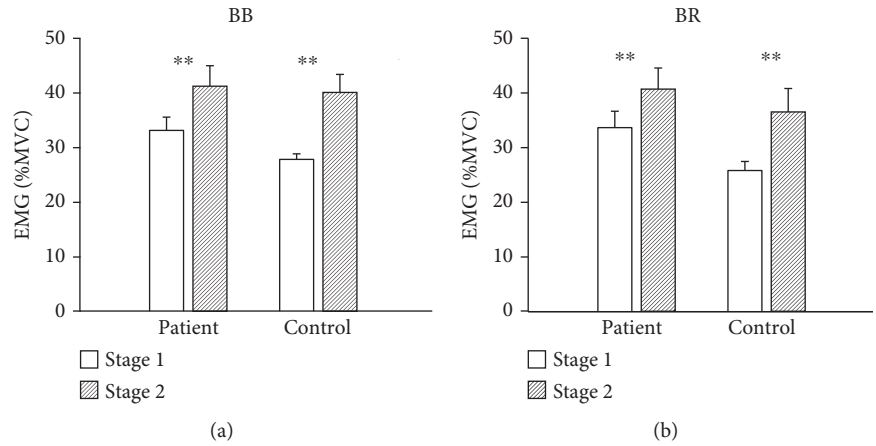

Figure 1: The EMG amplitude of patients and controls in the two stages of the sustained elbow flexion for each agonist muscle. BB: biceps brachii; BR: brachioradialis.

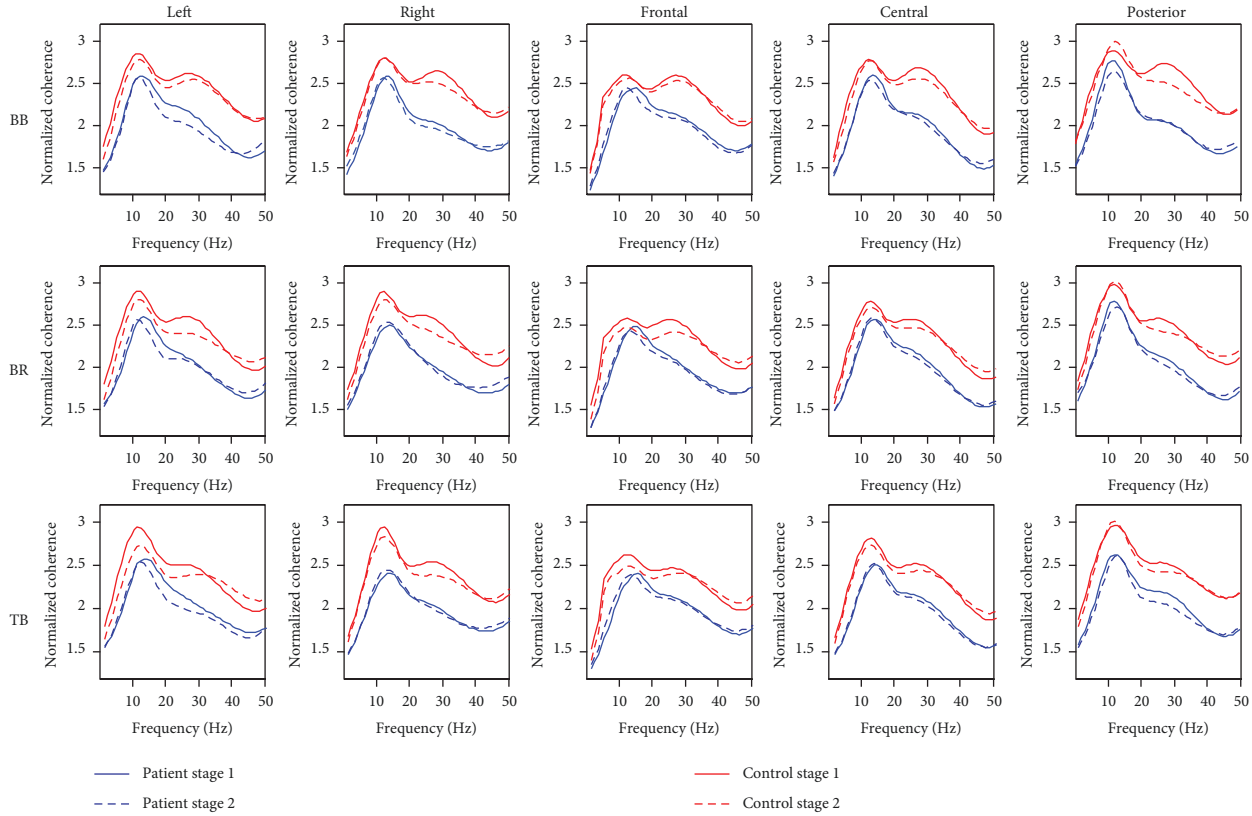

Figure 2: Averaged EEG-EMG coherence spectra related to three muscles in five cortical areas for both patients and controls. BB: biceps brachii; BR: brachioradialis; TB: triceps brachii.

typical example of EEG and EMG power spectra, EEG-EMG coherence spectra, for one CRF subject is shown in Figure 3.

Figure 4 displays coherence maps (average of the 8 CRF patients and 9 healthy controls) based on the 128 EEG channels with EMG of the three muscles (BB, BR, and TR) for stage 1 (columns 1 (patients) and 3 (controls)) and stage 2 (columns 2 (patients) and 4 (controls)) at the beta band (15-35 Hz). The color bar indicates color-coded Z-transformed coherence values (red color indicates higher coherence value and blue color lower coherence value). The figure shows clearly that (i) the level of coherence declined substantially in stage 2 (more-fatigued condition) compared to stage 1 (less-fatigued condition) in both groups, (ii) the coherence level was higher in the control than in the patient group especially in the baseline stage (stage 1), and (iii) the patterns of the coherence maps between the two groups based on the 128 EEG electrodes and three muscles were dramatically different. Because the EEG sources were not

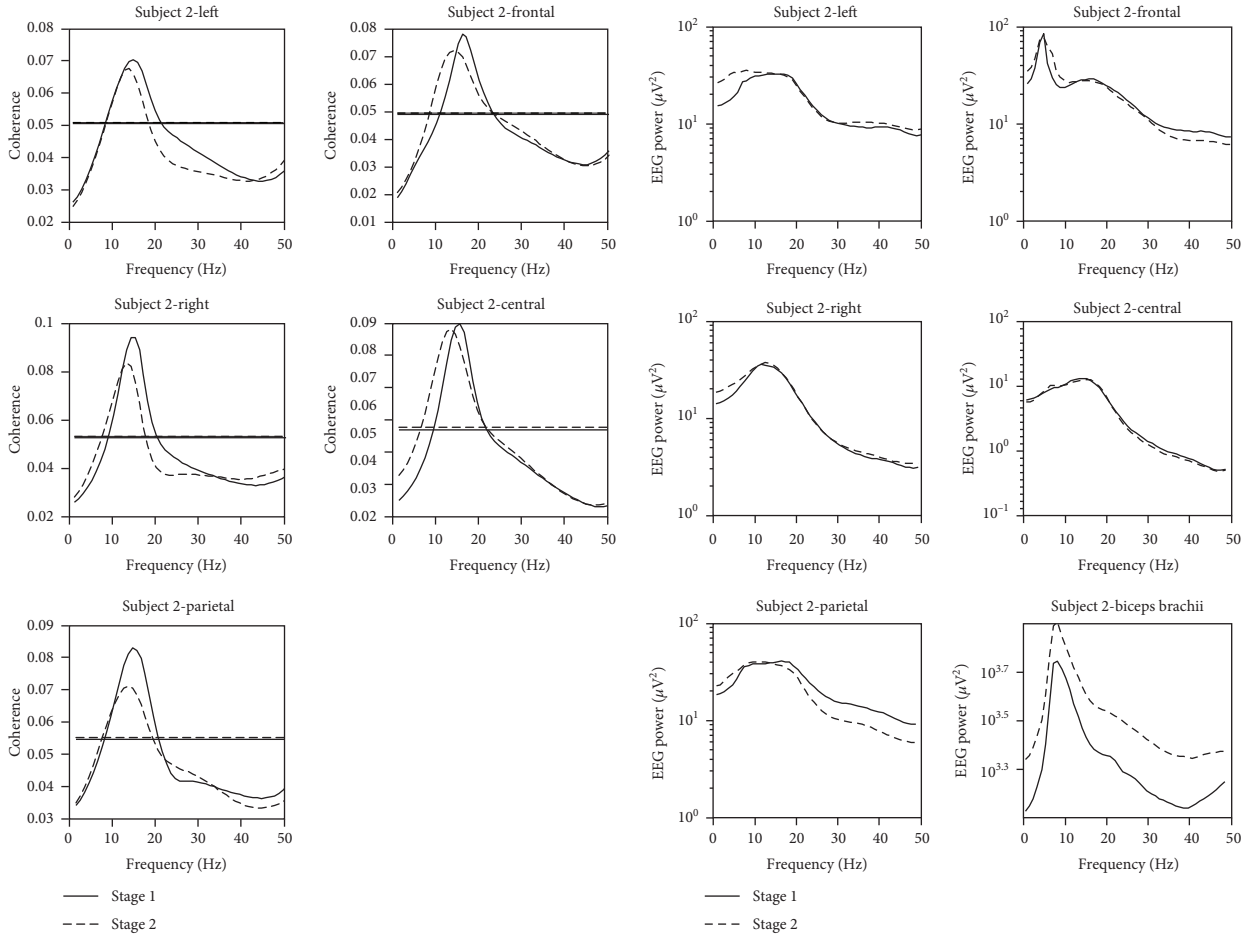

Figure 3: EEG-EMG coherence spectra (a) related to the biceps brachii muscle in five cortical areas and corresponding EEG and EMG power spectra (b) of a typical patient subject data.

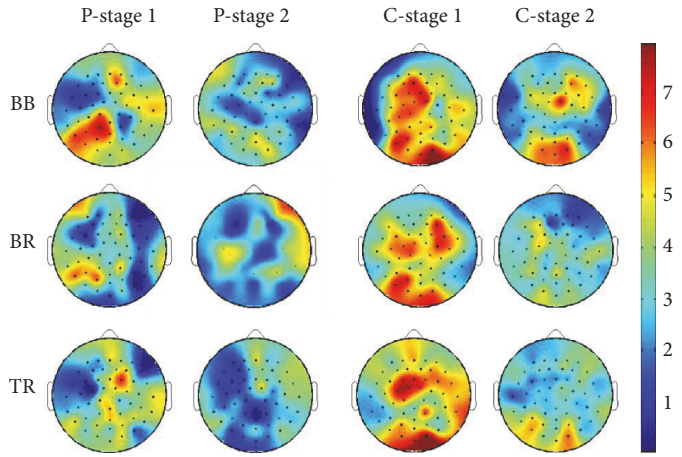

Figure 4: Mapping EEG-EMG coherence based on significant coherence values of the selected 128 EEG channels with EMG of the three muscles at the beta (15-35 Hz) band in CRF patients (left two columns) and healthy subjects (right two columns). The color bar indicates Z-transformed coherence values (red means higher and blue lower coherence). The level of coherence declined substantially in stage 2 (fatigue condition, 2nd, and 4th columns) compared with stage 1 (1st and 3rd columns). The coherence values in CRF patients were remarkably lower compared to those in the controls especially in stage 1. BB: biceps brachii; BR: brachioradialis; TB: triceps brachii; P: patients; C: controls.

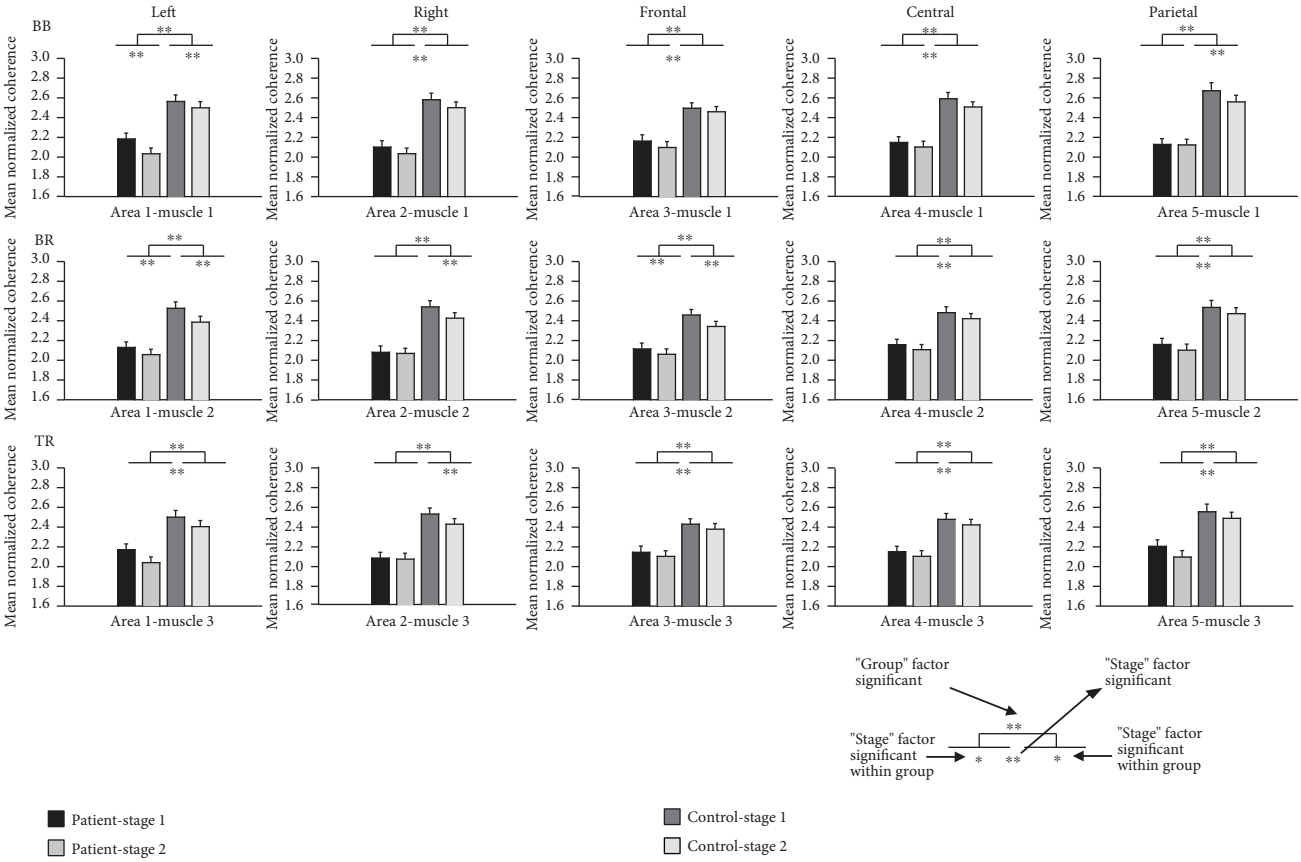

Figure 5: Normalized coherence of all cortical area and muscle combinations in the beta band. The mean coherence was averaged across subjects and electrodes within the cortical area. BB: biceps brachii; BR: brachioradialis; TB: triceps brachii; Left: left cortical area; Right: right cortical area; Frontal: frontal cortical area; Central: central cortical area; Parietal: parietal cortical area. $^{**}P < 0.01$ and $^{*}P < 0.05$.

estimated, we could not pinpoint cortical locations whose signal coherence with the EMG was affected by CRF or fatigue. However, by examining the maps in Figure 4, coherence decreased most significantly in the central middle of the frontal lobe and the central posterior areas of the parietal lobe in CRF vs. those in control subjects in stage 1 (compare columns 1 and 3 from left in Figure 4). The fatigue effect on the coherence was most prominent on the left hemisphere in CRF (compare two columns on the left in Figure 4) but almost evenly distrusted on the entire head/brain surface in controls (the two columns on right side of Figure 4).

The statistical analysis of coherence values by the general linear model of repeated measures showed significantly lower corticomuscular coherence for the CRF group compared with that for the healthy controls at both the alpha and beta bands (beta band: $P < 0.01$, alpha band: $P < 0.05$). The within-subject factor "stage" was significant in both the beta and alpha bands ($P < 0.01$). That means the coherence value decreased significantly in stage 2 compared to stage 1 of the sustained elbow flexion for both the CRF and control groups. The within-subject factor "muscle" was significant in the beta band only ($P < 0.01$). And the within-subject factor "area" was significant in the alpha band only ($P < 0.01$). Since the interactions of the factors were significant at both the alpha and beta bands, further analysis of coherence in each cortical area and muscle combination was necessary. The column chart of normalized coherence of all cortical area and muscle combinations are shown in Figures 5 and 6. At the beta band (Figure 5), the coherence values between the right scalp area (area 2) EEG and EMG of the BR and TB muscles, and the parietal area (area 5) EEG and EMG of the BB muscle were not significantly different between stages 1 and 2 of the motor task in the CRF group, while the differences were significant in the control group. At the alpha band (Figure 6), the difference in the coherence between the two stages in the CRF group was smaller compared to the control group in most of the areas except the parietal cortical area (area 5).

4. Discussion

This study, for the first time, showed that functional corticomuscular coupling measured by EEG-EMG coherence was significantly weaker in individuals with CRF compared to healthy controls. And the coupling significantly weakened from less-fatigue to more-fatigue conditions during the sustained elbow flexion contraction in a number of brain areas indicated by signals from multiple EEG electrodes distributed on a large scalp area in both the CRF and control groups.

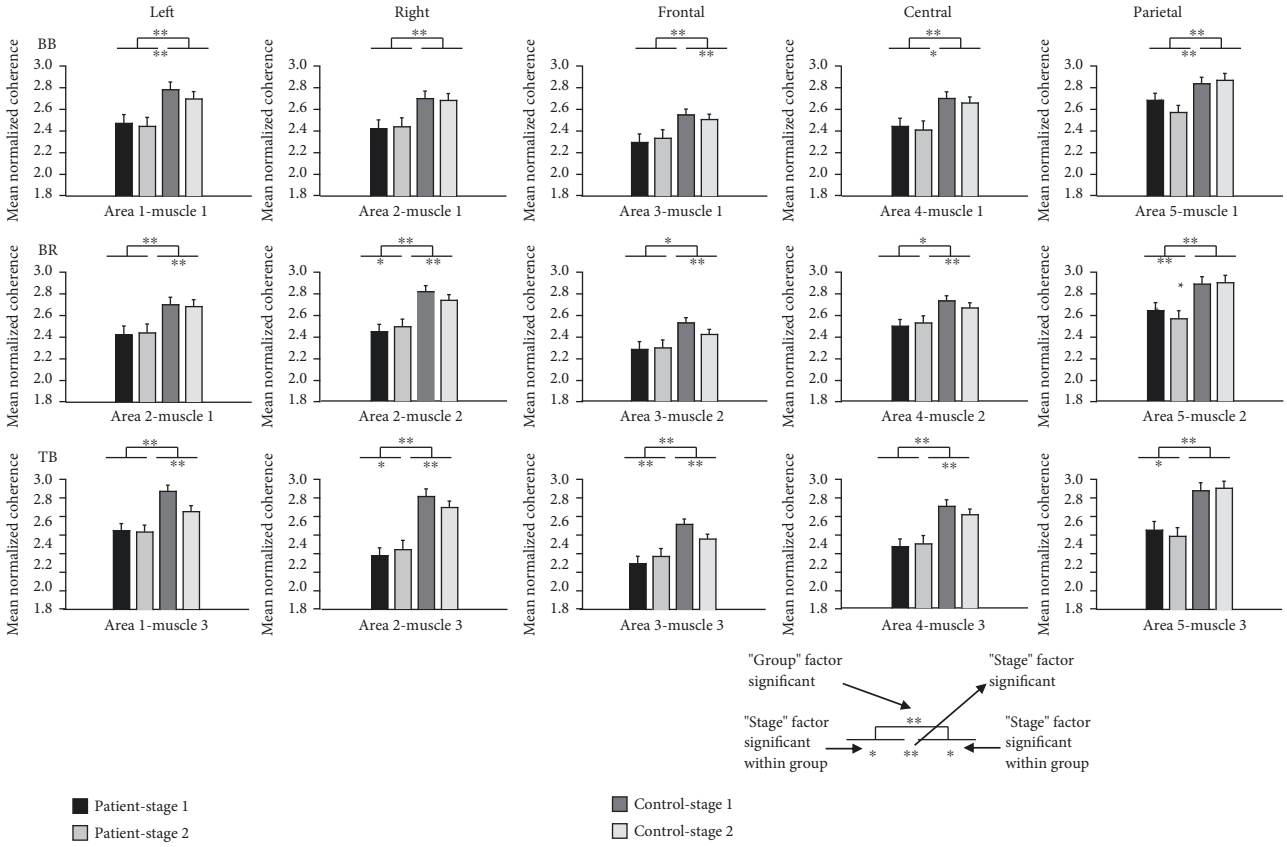

Figure 6: Normalized coherence of all cortical area and muscle combinations in the alpha band. The mean coherence was averaged across subjects and electrodes within the cortical area. BB: biceps brachii; BR: brachioradialis; TB: triceps brachii; Left: left cortical area; Right: right cortical area; Frontal: frontal cortical area; Central: central cortical area; Parietal: parietal cortical area. $^{**}P < 0.01$, $^{*}P < 0.05$.

The novel finding that EEG-EMG coherence was significantly and robustly lower in cancer survivors with CRF suggests significantly impaired functional coupling between the brain and muscular signals in performing a sustained voluntary motor task in individuals with CRF. A voluntary muscle contraction activity is accomplished through generation of a motor command in the brain and transmitting the command signal via the descending pathways to the motor neuron pool in the spinal cord projecting to the target muscle across the neuromuscular junction (NMJ). Since EEG-EMG coherence value reflects the degree of the oscillatory activity "binding" between the central nervous system (CNS) and the muscle [21], any impairment in each component or any block in the pathway during the whole process would increase the dissociation of brain and muscle system signal changes, thus decreasing the corresponding EEG-EMG coherence. Several factors or mechanisms could contribute to the decreased EEG-EMG coherence. One likely candidate is impairment in NMJ transmission. If the central signals cannot be smoothly and efficiently transmitted across the NMJ, the muscle would not be fully recruited into the contraction, which would possibly prevent normal muscle activation and weaken functional coupling between the central and muscular signals. Indeed, a remarkable reduction (~50%) in the NMJ transmission (measured by compound muscle action potential or M-wave elicited by electrically stimulating the motor nerve (pre-NMJ) and recorded on the muscle (post-MNJ)) in cancer survivors with CRF has been reported [9, 37]. Similarly, NMJ propagation efficiency decreased and fatigue increased in prostate cancer patients undergoing radiation therapy, and these symptoms improved 5 to 6 weeks after completion of the radiation intervention [38].

Another factor that could potentially weaken functional corticomuscular coupling during voluntary muscle activation is the diminished central drive from the brain to the muscle. Our previous study has suggested CRF is more centrally mediated fatigue. This was supported by the facts that individuals with CRF exhibited greater subjective fatigue (higher perceived fatigue scores and feeling exhaustion sooner during a prolonged muscle contraction), but physiological indices revealed they experienced less muscle fatigue (compared to healthy controls) at the end of the motor task even though they felt exhausted at the time [15–17]. Voluntary EMG signals at the end the motor task (when participants felt exhausted) suggested diminished central drive to maintain the muscle contraction in CRF participants compared to healthy controls [9, 17], which could be a reason for weakened functional corticomuscular coupling in CRF. With all other factors unchanged, diminished central drive can result in a reduction in the amplitude of muscle force/EMG and perhaps alters frequency content

of EEG and EMG signals. These changes could lead to a decrease in the level of corticomuscular coupling or EEG-EMG coherence. Although previous research has indicated that the level of corticomuscular coupling is associated with the magnitude of voluntary force output [21] or central drive, the current study observed an increase in EMG (representing central drive) but a decrease in EEG-EMG coherence in stage 2 of the SC. This observation was contradictory to the positive relationship between voluntary muscle force/EMG and EEG-EMG coherence [39]. Our explanation is that the positive relationship may only hold under nonfatigue conditions. With muscle fatigue in our study, the positive influence of increased central drive on the coherence might have been overridden by effects of fatigue-induced other changes such as frequency content in the EEG and/or EMG signals on the coherence. For example, a frequency band of one signal (e.g., EMG) may have been diminished in stage 2 compared to the other signal (e.g., EEG).

The robust pathophysiological changes in the EEG-EMG coherence in CRF participants observed by the current study may also explain other corticomuscular abnormalities, such as cytokine and neuroendocrine changes in cancer survivors with CRF [6]. Among these changes, the increased proinflammatory cytokines in CRF patients may indicate the switching-on of the immune process by cancer or cancer treatment, which can signal the brain, leading to a variety of effects including fatigue [40]. But exactly how and where these factors take effect are still unknown.

Central and peripheral neuropathy in cancer survivors is well known and thought to contribute to many symptoms such as neuropathic pain, cognitive function impairment, weakness, and fatigue [15, 37, 41, 42]. Both animal and human studies have shown consistent findings of white matter damage in the brain by chemotherapy [43–45]. Numerous studies have also reported peripheral neuropathy caused by chemo drugs [30, 46]. Either the central or the peripheral neuropathy or both are expected to affect generation and conduction of the signals, and communication of the information between the central and peripheral systems. Logically, damage made by chemo or radiation treatment on the central and peripheral systems and its detrimental influence on physiological roles of the systems should interfere with the normal corticomuscular signal coupling for voluntary motor activities.

The significant decrease in EEG-EMG coherence from the less-fatigued to the more-fatigued stage in individuals with CRF was in general consistent with the coherence changes in healthy controls doing the same motor task. This decrease may be due to the inadequate or inhibited drive from various sources that act upon the output neurons [47, 48]. Inhibitory feedback mediated by group III and IV muscle afferents increased along with a decrease in muscle spindle facilitation in progressive muscle fatigue [49–52] or neuromuscular junction propagation changes [53–55]. All these changes are physiologically induced by fatigue motor task, which can be recovered by enough rest or sleep, while those changes that contribute to the lower coherence value in CRF patients compared to the controls in both stages of fatigue motor task may be mainly due to the pathophysiological reasons induced by cancer or cancer treatment, which cannot be recovered just by rest [6, 56]. One interesting observation is that it seems that the coherence value reduction from the less-fatigue to the more-fatigue stage was smaller in CRF than in healthy participants. As can be seen from Figures 5 and 6, in the beta band, the coherence related to the right scalp area EEG and muscle of BR and TB was not significantly different between two stages of the fatigue motor task in the patient group, while it was significant in the control group. And in the alpha band, the difference of two stages' coherence in the CRF group was also smaller compared to that in the control group in most of the areas except the parietal cortical area. An explanation for smaller fatigue-induced EEG-EMG coherence reduction in CRF participants could be that their muscular system was not as fatigued as in the control group [9, 15–17] and perhaps experienced less influence on the coupling of the two signals due to the lower level of muscle fatigue.

Our results suggest that the EEG-EMG coherence of both the CRF patient group and the control group in the beta band was not area dependent (within-subject factor "area" was not significant) but muscular dependent (within-subject factor "muscle" was significant with the P value less than 0.01). However, in the alpha band, the coherence in both groups was area dependent ($P < 0.01$) and not muscular dependent. Also, the spatial distribution of the beta band coherence was different from the spatial distribution of the alpha band coherence in patients. The beta band coherence had obvious focus localized around the sensorimotor area while the alpha band coherence had higher value in the parietal cortex. These differences may imply that the mechanisms contributing to the coherence in the alpha and the beta band are at least partially different. It is more likely that the coherence in the beta band is mainly related to the motor control [19–22], while the coherence in the alpha band is more associated with the cognitive component of the motor control [57, 58] besides motor functioning [18, 20]. Cancer survivors with CRF usually also experience cognition-related symptoms, more or less, such as depression [59]. Although we excluded the severely depressed patients in this study by a simple question, cognitive function changes in the participating patients cannot be ruled out.

The study has a number of limitations. First, the sample size was small, which limits our ability to generalize our findings. The major reason for the small sample size was that the study was primarily supported by a small institutional grant with the goal of generating pilot data for future larger-scale studies. Second, the cancer survivors were not limited to a single type of cancer, which made it difficult to explain if a particular cancer contributed more or less to the observed outcomes. Third, although all the participants were verbally encouraged to maintain the sustained contraction for as long as possible, the level of motivation for performing the task was not specifically measured, and therefore, it was possible that one group of participants may have had higher or lower motivation to perform the task than the other, and the difference in motivation might have influenced the motor performance (length of the contraction) as well as the level of corticomuscular coupling. However, given the

pilot nature of the study and the robust and significant difference in functional corticomuscular signal coupling during a prolonged voluntary muscle contraction between cancer survivors with CRF and healthy controls, these limitations do not seem to have a significant effect on the major finding of the study.

In conclusion, this study quantified EEG-EMG coherence to evaluate functional corticomuscular coupling in cancer survivors with CRF and healthy controls during a sustained voluntary motor task that led to fatigue. The results indicated significant and robust weakening of corticomuscular signal coupling in CRF compared to healthy controls, which may be caused by central and peripheral neuropathies resulting in cancer treatment and/or the disease itself. Furthermore, both the CRF and healthy participants exhibited decreased functional corticomuscular coupling under muscle fatigue condition with less such decrease in CRF, which is considered to be due to fatigue-induced physiological changes in the sensorimotor system.

Data Availability

The data used to support the findings of this study are available from the corresponding author upon request.

Conflicts of Interest

All authors declare that there are no conflicts of interest in this study.

Authors' Contributions

Changhao Jiang and Qi Yang contributed equally to the paper.

Acknowledgments

We would like to thank Drs. Mellar Davis and Declan Walsh for their valuable help in recruiting cancer patients in the Taussig Cancer Center at the Cleveland Clinic, Cleveland, OH. The data presented in this paper are part of those in a doctoral thesis collected by one of the co-first authors (QY) at the Cleveland State University, Cleveland, Ohio, USA [60]. This work was supported in part by a Cleveland Clinic Research Program Council grant (RPC6700), NIH grants (R01NS037400 and R01CA189665), and a Department of Defense grant (DAMD17-01-1-0665) to GHY and by grants from the National Natural Science Foundation of China (31771244), State General Administration for Sports Scientific Research (2015B040), and Open Research Fund of the State Key Laboratory of Cognitive Neuroscience and Learning to CJ.

References

[1] D. Cella, J. S. Lai, C. H. Chang, A. Peterman, and M. Slavin, "Fatigue in cancer patients compared with fatigue in the general United States population," *Cancer*, vol. 94, no. 2, pp. 528–538, 2002.

[2] S. Donnelly and D. Walsh, "The symptoms of advanced cancer," *Seminars in Oncology*, vol. 22, 2 Suppl 3, pp. 67–72, 1995.

[3] D. M. Irvine, L. Vincent, N. Bubela, L. Thompson, and J. Graydon, "A critical appraisal of the research literature investigating fatigue in the individual with cancer," *Cancer Nursing*, vol. 14, no. 4, pp. 188–199, 1991.

[4] G. R. Morrow, A. R. Shelke, J. A. Roscoe, J. T. Hickok, and K. Mustian, "Management of cancer-related fatigue," *Cancer Investigation*, vol. 23, no. 3, pp. 229–239, 2005.

[5] P. Servaes, C. Verhagen, and G. Bleijenberg, "Fatigue in cancer patients during and after treatment: prevalence, correlates and interventions," *European Journal of Cancer*, vol. 38, no. 1, pp. 27–43, 2002.

[6] A. Sood and T. J. Moynihan, "Cancer-related fatigue: an update," *Current Oncology Reports*, vol. 7, no. 4, pp. 277–282, 2005.

[7] D. Walsh, S. Donnelly, and L. Rybicki, "The symptoms of advanced cancer: relationship to age, gender, and performance status in 1,000 patients," *Support Care Cancer*, vol. 8, no. 3, pp. 175–179, 2000.

[8] V. Mock, A. Atkinson, A. Barsevick et al., "National Comprehensive Cancer Network: NCCN practice guidelines for cancer-related fatigue," *Oncology (Williston Park) NY*, vol. 14, no. 11A, pp. 151–161, 2000.

[9] T. Yavuzsen, M. P. Davis, V. K. Ranganathan et al., "Cancer related fatigue, central or peripheral?," *Journal of Pain and Symptom Management*, vol. 38, no. 4, pp. 587–596, 2009.

[10] J. E. Butler, J. L. Taylor, and S. C. Gandevia, "Responses of human motoneurons to corticospinal stimulation during maximal voluntary contractions and ischemia," *The Journal of Neuroscience*, vol. 23, no. 32, pp. 10224–10230, 2003.

[11] S. C. Gandevia, G. M. Allen, J. E. Butler, and J. L. Taylor, "Supraspinal factors in human muscle fatigue: evidence for suboptimal output from the motor cortex," *The Journal of Physiology*, vol. 490, no. 2, pp. 529–536, 1996.

[12] J. Z. Liu, Z. Y. Shan, L. D. Zhang, V. Sahgal, R. W. Brown, and G. H. Yue, "Human brain activation during sustained and intermittent submaximal fatigue muscle contractions: an FMRI study," *Journal of Neurophysiology*, vol. 90, no. 1, pp. 300–312, 2003.

[13] J. Z. Liu, B. Yao, V. Siemionow et al., "Fatigue induces greater brain signal reduction during sustained than preparation phase of maximal voluntary contraction," *Brain Research*, vol. 1057, no. 1-2, pp. 113–126, 2005.

[14] J. Z. Liu, L. Zhang, B. Yao, V. Sahgal, and G. H. Yue, "Fatigue induced by intermittent maximal voluntary contractions is associated with significant losses in muscle output but limited reductions in functional MRI-measured brain activation level," *Brain Research*, vol. 1040, no. 1-2, pp. 44–54, 2005.

[15] B. Cai, D. Allexandre, V. Rajagopalan et al., "Evidence of significant central fatigue in patients with cancer-related fatigue during repetitive elbow flexions till perceived exhaustion," *PLoS One*, vol. 9, no. 12, article e115370, 2014.

[16] K. Kisiel-Sajewicz, M. P. Davis, V. Siemionow et al., "Lack of Muscle Contractile Property Changes at the Time of Perceived Physical Exhaustion Suggests Central Mechanisms Contributing to Early Motor Task Failure in Patients With Cancer-Related Fatigue," *Journal of Pain and Symptom Management*, vol. 44, no. 3, pp. 351–361, 2012.

[17] K. Kisiel-Sajewicz, V. Siemionow, D. Seyidova-Khoshknabi et al., "Myoelectrical manifestation of fatigue less prominent

in patients with cancer related fatigue," *PLoS One*, vol. 8, no. 12, article e83636, 2013.

[18] B. A. Conway, D. M. Halliday, S. F. Farmer et al., "Synchronization between motor cortex and spinal motoneuronal pool during the performance of a maintained motor task in man," *The Journal of Physiology*, vol. 489, no. 3, pp. 917–924, 1995, Pt 3.

[19] B. Feige, A. Aertsen, and R. Kristeva-Feige, "Dynamic synchronization between multiple cortical motor areas and muscle activity in phasic voluntary movements," *Journal of Neurophysiology*, vol. 84, no. 5, pp. 2622–2629, 2000.

[20] J. M. Kilner, S. N. Baker, S. Salenius, V. Jousmäki, R. Hari, and R. N. Lemon, "Task-dependent modulation of 15-30 Hz coherence between rectified EMGs from human hand and forearm muscles," *The Journal of Physiology*, vol. 516, no. 2, pp. 559–570, 1999.

[21] J. M. Kilner, S. N. Baker, S. Salenius, R. Hari, and R. N. Lemon, "Human cortical muscle coherence is directly related to specific motor parameters," *The Journal of Neuroscience*, vol. 20, no. 23, pp. 8838–8845, 2000.

[22] J. F. Marsden, K. J. Werhahn, P. Ashby, J. Rothwell, S. Noachtar, and P. Brown, "Organization of cortical activities related to movement in humans," *The Journal of Neuroscience*, vol. 20, no. 6, pp. 2307–2314, 2000.

[23] T. Mima and M. Hallett, "Corticomuscular coherence: a review," *Journal of Clinical Neurophysiology*, vol. 16, no. 6, pp. 501–511, 1999.

[24] R. Kristeva, L. Patino, and W. Omlor, "Beta-range cortical motor spectral power and corticomuscular coherence as a mechanism for effective corticospinal interaction during steady-state motor output," *NeuroImage*, vol. 36, no. 3, pp. 785–792, 2007.

[25] Y. Fang, J. J. Daly, J. Sun et al., "Functional corticomuscular connection during reaching is weakened following stroke," *Clinical Neurophysiology*, vol. 120, no. 5, pp. 994–1002, 2009.

[26] T. Mima, K. Toma, B. Koshy, and M. Hallett, "Coherence between cortical and muscular activities after subcortical stroke," *Stroke*, vol. 32, no. 11, pp. 2597–2601, 2001.

[27] B. Hellwig, S. Häussler, M. Lauk et al., "Tremor-correlated cortical activity detected by electroencephalography," *Clinical Neurophysiology*, vol. 111, no. 5, pp. 806–809, 2000.

[28] J. Volkmann, M. Joliot, A. Mogilner et al., "Central motor loop oscillations in parkinsonian resting tremor revealed by magnetoencephalography," *Neurology*, vol. 46, no. 5, pp. 1359–1370, 1996.

[29] P. Brown, D. M. Corcos, and J. C. Rothwell, "Does parkinsonian action tremor contribute to muscle weakness in Parkinson's disease?," *Brain*, vol. 120, no. 3, pp. 401–408, 1997.

[30] R. J. Freilich, C. Balmaceda, A. D. Seidman, M. Rubin, and L. M. DeAngelis, "Motor neuropathy due to docetaxel and paclitaxel," *Neurology*, vol. 47, no. 1, pp. 115–118, 1996.

[31] T. R. Mendoza, X. S. Wang, C. S. Cleeland et al., "The rapid assessment of fatigue severity in cancer patients: use of the Brief Fatigue Inventory," *Cancer*, vol. 85, no. 5, pp. 1186–1196, 1999.

[32] A. Neumaier and T. Schneider, "Estimation of parameters and eigenmodes of multivariate autoregressive models," *ACM Transactions on Mathematical Software*, vol. 27, no. 1, pp. 27–57, 2001.

[33] G. Schwarz, "Estimating the dimension of a model," *The Annals of Statistics*, vol. 6, no. 2, pp. 461–464, 1978.

[34] B. Efron, *The jackknife, the bootstrap and other resampling plans*, Society for Industrial and Applied Mathematics, Philadelphia, 1982.

[35] Q. Yang, Y. Fang, C.-K. Sun et al., "Weakening of functional corticomuscular coupling during muscle fatigue," *Brain Research*, vol. 1250, pp. 101–112, 2009.

[36] J. R. Rosenberg, A. M. Amjad, P. Breeze, D. R. Brillinger, and D. M. Halliday, "The Fourier approach to the identification of functional coupling between neuronal spike trains," *Progress in Biophysics and Molecular Biology*, vol. 53, no. 1, pp. 1–31, 1989.

[37] D. S. Khoshknabi, M. P. Davis, V. K. Ranganathan et al., "Combining objective and subjective outcomes in cancer related fatigue: illustrations from a single case report," *Journal of Palliative Medicine*, vol. 11, no. 6, pp. 829–833, 2008.

[38] U. Monga, M. Jaweed, A. J. Kerrigan et al., "Neuromuscular fatigue in prostate cancer patients undergoing radiation therapy," *Archives of Physical Medicine and Rehabilitation*, vol. 78, no. 9, pp. 961–966, 1997.

[39] M. B. Bayram, V. Siemionow, and G. H. Yue, "Weakening of corticomuscular signal coupling during voluntary motor action in aging," *The Journals of Gerontology Series A: Biological Sciences and Medical Sciences*, vol. 70, no. 8, pp. 1037–1043, 2015.

[40] J. E. Bower, "Management of cancer-related fatigue," *Clinical Advances in Hematology & Oncology*, vol. 4, no. 11, pp. 828-829, 2006.

[41] R. Hung, P. Krebs, E. J. Coups et al., "Fatigue and functional impairment in early-stage non-small cell lung cancer survivors," *Journal of Pain and Symptom Management*, vol. 41, no. 2, pp. 426–435, 2011.

[42] T. J. Iwashyna, E. W. Ely, D. M. Smith, and K. M. Langa, "Long-term cognitive impairment and functional disability among survivors of severe sepsis," *JAMA*, vol. 304, no. 16, pp. 1787–1794, 2010.

[43] S. Deprez, F. Amant, A. Smeets et al., "Longitudinal assessment of chemotherapy-induced structural changes in cerebral white matter and its correlation with impaired cognitive functioning," *Journal of Clinical Oncology*, vol. 30, no. 3, pp. 274–281, 2012.

[44] V. Koppelmans, M. de Groot, M. B. de Ruiter et al., "Global and focal white matter integrity in breast cancer survivors 20 years after adjuvant chemotherapy," *Human Brain Mapping*, vol. 35, no. 3, pp. 889–899, 2014.

[45] S. Morioka, M. Morimoto, K. Yamada et al., "Effects of chemotherapy on the brain in childhood: diffusion tensor imaging of subtle white matter damage," *Neuroradiology*, vol. 55, no. 10, pp. 1251–1257, 2013.

[46] P. H. E. Hilkens, J. Verweij, G. Stoter, C. J. Vecht, W. L. J. van Putten, and M. J. van den Bent, "Peripheral neurotoxicity induced by docetaxel," *Neurology*, vol. 46, no. 1, pp. 104–108, 1996.

[47] K. Søgaard, S. C. Gandevia, G. Todd, N. T. Petersen, and J. L. Taylor, "The effect of sustained low-intensity contractions on supraspinal fatigue in human elbow flexor muscles," *The Journal of Physiology*, vol. 573, no. 2, pp. 511–523, 2006.

[48] J. L. Taylor and S. C. Gandevia, "Transcranial magnetic stimulation and human muscle fatigue," *Muscle & Nerve*, vol. 24, no. 1, pp. 18–29, 2001.

[49] A. Belhaj-Saif, A. Fourment, and B. Maton, "Adaptation of the precentral cortical command to elbow muscle fatigue," *Experimental Brain Research*, vol. 111, no. 3, pp. 405–416, 1996.

[50] B. Bigland-Ritchie, "EMG/force relations and fatigue of human voluntary contractions," *Exercise and Sport Sciences Reviews*, vol. 9, pp. 75–117, 1981.

[51] C. T. Leonard, J. Kane, J. Perdaems, C. Frank, D. G. Graetzer, and T. Moritani, "Neural modulation of muscle contractile properties during fatigue: afferent feedback dependence," *Electroencephalography and Clinical Neurophysiology*, vol. 93, no. 3, pp. 209–217, 1994.

[52] J. L. Taylor, G. Todd, and S. C. Gandevia, "Evidence for a supraspinal contribution to human muscle fatigue," *Clinical and Experimental Pharmacology & Physiology*, vol. 33, no. 4, pp. 400–405, 2006.

[53] F. Bellemare and N. Garzaniti, "Failure of neuromuscular propagation during human maximal voluntary contraction," *Journal of Applied Physiology*, vol. 64, no. 3, pp. 1084–1093, 1988.

[54] A. J. Fuglevand, M. Bilodeau, and R. M. Enoka, "Short-term immobilization has a minimal effect on the strength and fatigability of a human hand muscle," *Journal of Applied Physiology*, vol. 78, no. 3, pp. 847–855, 1995.

[55] A. J. Fuglevand, K. M. Zackowski, K. A. Huey, and R. M. Enoka, "Impairment of neuromuscular propagation during human fatiguing contractions at submaximal forces," *The Journal of Physiology*, vol. 460, no. 1, pp. 549–572, 1993.

[56] A. Chaudhuri and P. O. Behan, "Fatigue in neurological disorders," *Lancet*, vol. 363, no. 9413, pp. 978–988, 2004.

[57] N. M. Safri, N. Murayama, T. Igasaki, and Y. Hayashida, "Effects of visual stimulation on cortico-spinal coherence during isometric hand contraction in humans," *International Journal of Psychophysiology*, vol. 61, no. 2, pp. 288–293, 2006.

[58] L. L. Zheng, Z. Y. Jiang, and E. Y. Yu, "Alpha spectral power and coherence in the patients with mild cognitive impairment during a three-level working memory task," *Journal of Zhejiang University. Science. B*, vol. 8, no. 8, pp. 584–592, 2007.

[59] B. N. Lee, R. Dantzer, K. E. Langley et al., "A cytokine-based neuroimmunologic mechanism of cancer-related symptoms," *Neuroimmunomodulation*, vol. 11, no. 5, pp. 279–292, 2004.

[60] Q. Yang, *Bio-signal analysis in fatigue and cancer related fatigue; weakening of corticomuscular functional coupling*, ETD Archive. Paper 313, 2008.

Hindawi
Neural Plasticity
Volume 2019, Article ID 6981268, 23 pages
https://doi.org/10.1155/2019/6981268

Research Article

Early Electrophysiological Disintegration of Hippocampal Neural Networks in a Novel Locus Coeruleus Tau-Seeding Mouse Model of Alzheimer's Disease

A. Ahnaou, C. Walsh, N. V. Manyakov, S. A. Youssef, and W. H. Drinkenburg

Department of Neuroscience Discovery, Janssen Research & Development, Janssen Pharmaceutica NV, Turnhoutseweg 30, B-2340 Beerse, Belgium

Correspondence should be addressed to A. Ahnaou; aahnaou@its.jnj.com

Received 1 February 2019; Revised 19 April 2019; Accepted 30 April 2019; Published 12 June 2019

Guest Editor: Andrea Guerra

Alzheimer's disease (AD) is a progressive, neurodegenerative disease characterized by loss of synapses and disrupted functional connectivity (FC) across different brain regions. Early in AD progression, tau pathology is found in the locus coeruleus (LC) prior to amyloid-induced exacerbation of clinical symptoms. Here, a tau-seeding model in which preformed synthetic tau fibrils (K18) were unilaterally injected into the LC of P301L mice, equipped with multichannel electrodes for recording EEG in frontal cortical and CA1-CA3 hippocampal areas, was used to longitudinally quantify over 20 weeks of functional network dynamics in (1) power spectra; (2) FC using intra- and intersite phase-amplitude theta-gamma coupling (PAC); (3) coherence, partial coherence, and global coherent network efficiency (Eglob) estimates; and (4) the directionality of functional connectivity using extended partial direct coherence (PDC). A sustained leftward shift in the theta peak frequency was found early in the power spectra of hippocampal CA1 networks ipsilateral to the injection site. Strikingly, hippocampal CA1 coherence and Eglob measures were impaired in K18-treated animals. Estimation of instantaneous EEG amplitudes revealed deficiency in the propagation directionality of gamma oscillations in the CA1 circuit. Impaired PAC strength evidenced by decreased modulation of the theta frequency phase on gamma frequency amplitude further confirms impairments of the neural CA1 network. The present results demonstrate early dysfunctional hippocampal networks, despite no spreading tau pathology to the hippocampus and frontal cortex. The ability of the K18 seed in the brainstem LC to elicit such robust functional alterations in distant hippocampal structures in the absence of pathology challenges the classic view that tau pathology spread to an area is necessary to elicit functional impairments in that area.

1. Introduction

Alzheimer's disease (AD) is the most common cause of dementia, characterized by a progressive loss of cognitive function and, eventually, in the late stages of the disease, loss of basic motor functions such as swallowing [1, 2]. Currently, the only treatments available for AD are aimed at reducing the severity of cognitive impairments; there are no available treatments which halt, or even slow, the progression of the disease. This may soon result in an unmanageable public health disaster with an even heavier socioeconomic burden [3]. The main pathological hallmarks of AD are the formation of two types of lesions in the brain, extracellular plaques of amyloid beta (Aβ), and intracellular neurofibrillary tangles (NFT) of tau protein, leading to widespread neurodegeneration and atrophy of the brain [4, 5]. Until relatively recently, pharma drug discovery in the field of AD has been focused on therapies that reduce the levels of soluble or insoluble Aβ in the brain; however, numerous high-profile late-stage failures in clinical trials have resulted in a shift in focus to reducing the levels of tau in the brain far earlier in the presymptomatic stage of the disease [6]. A great deal of work is currently going on to investigate biomarkers of deteriorating brain function that could aid early diagnosis and act as indicators of therapeutic efficacy [7–11]. The back translational value of using functional biomarkers in preclinical

AD drug discovery could be extremely high; the ability to predict whether an experimental therapeutic compound will have a functional benefit in humans before costly clinical testing would save the pharmaceutical industry time and money and allow discovery scientists to better identify the best compounds to take to the next stage [11].

Another obstacle that AD drug discovery must overcome is the lack of suitable AD animal models available for preclinical research. Recent high-profile failures of late-stage AD compounds have led many in the field to critically analyze the translatability of currently available AD mouse models and focus on earlier disease interventions, prior to the onset of symptoms. To date, there have been no mutations found in the tau gene that cause spontaneous AD; however, several proaggregation tau mutations have been discovered for another tauopathy, frontotemporal dementia with parkinsonism linked to chromosome 17 (FTDP-17), and many of these have been used to create tau transgenic mice [12]. Two of the most common tau mutations used in Alzheimer's mouse models are the P301L and P301S mutations. Both P301L and P301S mutations affect only 4 repeat tau isoforms as they occur within exon 10 of the tau sequence [13, 14]. Depending on the gene promoter under which these transgenes are expressed, tau pathology in the brains of these animals can develop primarily in the hindbrain or the forebrain. JNPL3 and rTg4510 mice both express the P301L mutation, but while JNPL3 mice express the transgene under a mouse prion promoter and have primarily hindbrain pathology [15], rTg4510 mice express it under a CaMK-II promoter, resulting in a predominantly forebrain expression [16]. It is for this reason that severe motor impairments are present in JNPL3 mice, yet absent in rTg4510 mice [15, 17]. The spatiotemporal progression of tau pathology in Alzheimer's disease was shown by [18] to vary very little between individuals, and unlike amyloid pathology which develops diffusely throughout the neocortex [19], tau pathology has been shown to develop in specific, anatomically connected regions of the brain [20]. This exact neuropathological staging has not been replicated in any mouse models, and without understanding the exact cause of the development of tau pathology in these areas, it will not be possible to perfectly model AD in mice. It has also recently been hypothesized that in AD, pathological tau proteins spread from affected regions like infectious proteins called prions and it is this spread of tau pathology to an area of the brain that results in the functional changes seen in this newly affected area [21].

An alternative novel disease model of AD in animals involves a seeding approach, which templates and spreads the pathology following the injection of aggregates of Aβ or tau protein into an area of the animal's brain [22]. In the case of tau, this pathology has been shown to spread to anatomically connected areas, similar to the pathological spread of tau in AD [23], and seeding tau aggregation in the CA1 hippocampal area impaired neuronal network dynamics in the seeded area [24]. It was recently discovered that the tau pathology in AD may in fact begin far earlier than expected, during adolescence, in the brainstem locus coeruleus (LC), before any clinical symptoms or concomitant cerebral amyloid pathology was evident [25, 26]. This led to the novel hypothesis that the pathologic process of AD is initiated by tau pathology in the LC, which is then transported via anatomically connected neurons to the medial temporal lobe to trigger subsequent neuropathologic changes associated with amyloid deposition before any clinical symptoms, or concomitant cerebral amyloid pathology was observed [27]. The LC complex is a group of small nuclei located deep in the pons and is the sole source of noradrenaline to most brain regions. Noradrenaline facilitates the interactions between networks, and the LC plays an important role in cognitive functions, including memory consolidation and retrieval [28]. Structural imaging studies have investigated changes within the LC with aging and AD. Neuronal loss and atrophy of the LC occur during aging and are early events in AD and correlate with cognitive performance [29]. Subsequently, K18 tau aggregates have been unilaterally injected into the LC of PS19 tau transgenic mice [30], which present with the P301S mutation [31], effectively seeding pathology, which spreads to anatomically connected areas similarly to what is seen in AD, and resulted in cell loss in the injected LC [30]. This seeding model seems to currently be the most effective animal model for the earliest stages of AD, as tau pathology initiates solely in the locus coeruleus, instead of diffusely within the hindbrain as is seen in the JNPL3 mouse [15]. One caveat to this is that surprisingly, there was no tau pathology spread to either the entorhinal cortex or the hippocampus, two regions affected early in AD [18]. The authors could not explain this discrepancy but suggest the possibility that development of tau pathology in these regions may be independent of tau pathology developing in the brainstem [30].

Both Aβ and tau protein have been shown to cause electrophysiological alterations in the brain prior to neurodegeneration [32, 33], and unlike many modern in vivo animal brain imaging techniques, pharmaco-EEG techniques are widely available and well validated for use in rodents [34]. Several hallmark EEG alterations have been demonstrated in AD and in some AD mouse models including the following: a shift from high-frequency oscillations to low-frequency oscillations, resulting in a "slowing," altered coherence between various brain regions and reductions in theta-gamma phase-amplitude coupling (PAC) [9, 24, 35–39]. Many of these alterations have been shown to correlate with the severity of AD symptoms [40].

We therefore have used a seeding approach at the LC nuclei of the tau transgenic mouse strain, tauP301L, chronically equipped with depth multichannel LFP/EEG recording electrodes in key brain locations, to investigate functional network dynamics in relatively distant areas from the seeding location [41]. The tauP301L mouse model was chosen for this study due to its reasonably slow pathology: neurofibrillary tangles are seen from around 4.5 months of age, while neurodegeneration and astrogliosis occur from around 10 months of age [15]. This large window of opportunity allowed us to study any possible functional changes, in the relative absence of severe endogenous tau pathology and neurodegeneration. A recent study, by [30], used a similar approach, using PS19 mice, another tau line with reasonably slow pathology, in order to disentangle endogenous and exogenous tau pathologies. In addition, we investigated

whether the lack of tau pathology in the entorhinal cortex and the hippocampus seen in the previously mentioned LC seeding model [30] was associated with alterations in functional connectivity measures to support or challenge the view that pathology spread to an area is necessary to elicit functional impairments in that area.

2. Materials and Methods

2.1. Animals and Surgical Procedures. All experiments were conducted in strict accordance with the guidelines of the Association for Assessment and Accreditation of Laboratory Animal Care International (AAALAC) and with the European Council Directive of 24 November 1986 (86/609/EEC). All protocols were approved by the local Institutional Animal Care and Use Committee. For this study, 16 male transgenic tauP301L mice, expressing the longest human tau isoform, were used for surgery at the age of 3 months [42]. All mice were implanted with a chip for identification using the Animal Inventory and Weighing (AIW) system. For this study, all animals were housed in full-view Plexiglas® cages (25 cm × 33 cm × 18 cm), in IVC (individually ventilated cage) racks, within a sound-attenuated chamber with controlled environmental conditions: 22 ± 2°C ambient temperature, 60% relative humidity; 12 : 12 light-dark cycle (lights on at 1900 hours, lights off at 0700 hours), light intensity ~100 lux, and food and water available ad libitum.

2.2. Histology Evaluating the Accuracy of the LC Injection Site using Evans Blue Dye. Adult male C57/BL6 mice were deeply anesthetized with isoflurane during the surgical procedures, confirmed by observation of breathing frequency and responsiveness to toe pinching. Anesthesia was induced with 5% isoflurane and maintained with 2% isoflurane while body temperature was maintained at 37°C with a heating pad. To verify correct targeting of the LC site, immunohistochemistry (IHC) technique was performed using Evans blue dye. The LC was stereotaxically (David Kopf Instruments) injected with 1% Toluidine blue solved in distillated water, and a Hamilton syringe of 10 microliters connected to a syringe pump was used to inject a volume of 5 microliters/10 minutes at the stereotaxic mouse brain atlas coordinates of AP: -5.4 mm from the bregma, ML: +1.3 mm, and DV: -3.6 mm [43]. Afterwards, the brains were removed and trimmed after fixation with a mouse brain trimmer. Trimmed specimens were processed, sectioned in serial sequential levels, stained, and examined.

2.3. Tau-Seeding Procedure. At 3 months of age, animals underwent surgery for tau seeding and implantation of electrodes for local field recordings. Animals were anaesthetized with isoflurane, mounted in a stereotaxic frame, with the incisor bar 5 mm beneath the center of the ear bar. Following this, the animals were unilaterally injected with either preformed synthetic tau K18 fibrils ($n = 8$) or buffer ($n = 8$) into the right-side LC [16, 30, 40]. 25 μg of K18, in a volume of 5 μL, or 5 μL of buffer was injected at a rate of 1 μL/min, using a 5 μL Hamilton syringe (Hamilton Company), after which the needle was left in place for 5 minutes before being gently withdrawn. Afterwards, animals were stereotaxically equipped with 6 stainless steel recording electrodes (Figure 1(a)) in the frontal cortex (FC) (AP + 2 mm, L ± 1.4 mm), CA1 (AP − 1.7 mm, L ± 1.5 mm, and ventral ± 1.8 mm), and CA3 (AP − 2.8 mm, L ± 3.2 mm, and ventral ± 3.5 mm) [24]. All electrodes were referenced to a ground screw electrode, placed above the midline of the cerebellum. Electrodes were connected to a pin (Future Electronics: 0672-2-15-15-30-27-10-0) with a small insert (track pins; DataFlex: TRP-1558-0000) and were inserted into a 10-hole connector, which was carefully fixed to the skull with dental cement.

2.4. Experimental Design, Recording, and Analysis. After the one-week recovery period, animals were allowed another week to adaptation to the recording conditions. Body weight was measured prior to surgery and prior to each recording session, in order to monitor for rapid, pathological weight loss and to allow investigation into potential differences in weight gain between the two treatment groups. Due to variability in body weight prior to surgery, data were analyzed as the percentage of body weight change from baseline (presurgery). Core body temperature was taken on one occasion, using a rectal temperature probe to determine whether there were any deviations in this measure between buffer- and K18-injected animals. EEG recordings were taken for 3 hours, once a week, for 20 consecutive weeks. EEG recordings were performed during the dark phase of the circadian cycle, under vigilance-controlled wake, as described elsewhere [7]. Recordings were taken in the animal's home cages, fitted with a removable insert, and placed inside environmentally controlled, sound-attenuated Faraday cages. Motor activity was measured by a pair of passive infrared (PIR) detectors located above every recording cage. Motion levels were analyzed from the envelope of activity from both PIR detectors. Only continuous, waking, artefact-free epochs were used in the analysis. A notch finite impulse response (FIR) filter at 50 Hz was used to filter out possible noise caused by the main power line interference. EEGs were recorded at a sampling rate of 512 Hz using a BioSemi ActiveTwo system (BioSemi, Amsterdam, Netherlands), digitized with a resolution of 24 bits.

2.5. EEG Spectra. Analysis was performed using MATLAB analysis modules. Spectral power density was calculated using Welch's method with the Hanning window function and a block size of 512 data points, giving a resolution of 1.0 Hz. Power was expressed as relative power for each frequency over 1-256 Hz. Average relative power in each frequency bin of each location was averaged across animals for the buffer- and K18-injected groups to obtain the spectrum relative to the total power spectrum. For the sake of clarity in presenting this spectral data, graphs only show the frequency range between 1 and 20 Hz and inset plots from 20 to 100 Hz.

2.6. Phase-Amplitude Cross-Frequency Coupling. To estimate whether high-frequency EEG amplitudes are modulated by

low-frequency phase variations for the same (intrasite electrode) or different (intersite electrode) signals, phase-amplitude coupling (PAC) was calculated using the algorithm based on the modulation index (MI) [24, 44, 45]. MI is estimated as a mean (along time t) absolute value of the signal $z(t) = A_H(t) \times \exp(i \times \varphi_L(t))$, $i = \sqrt{-1}$, using the instantaneous phase $\varphi_L(t)$ derived via the Hilbert transform from the narrow bandpass-filtered signal around the low frequency f_L, and instantaneous amplitude envelope $A_H(t)$ derived via the Hilbert transform from the narrow bandpass-filtered signal around the high frequency f_H. For PAC estimation, f_L was varied in a 2-12 Hz interval with a step of 2 Hz and f_H taken from a 10-200 Hz interval with a step of 5 Hz was considered.

Modulation of $A_H(t)$ in relation to phases $\varphi_L(t)$ could also be represented graphically, if one plots for every phase $\varphi \in [-2\pi, 2\pi)$ of the narrow bandpass-filtered signal around the low frequency f_L an averaged amplitude value A (taken for time points, when the correspondent phase is equal to φ) from the narrow bandpass-filtered signal around the high frequency f_H. Larger variations in amplitude of the obtained near "sinusoidal" curve correspond to higher values of MI. In addition, it becomes possible to estimate the *phase shift* for the obtained curve. This phase shift value could be further used for comparison between groups or experimental conditions.

2.7. Coherence. In order to describe interconnectivity between pairs of EEG electrodes, coherence index was measured, which describes the level of connectivity as a value in interval [0, 1] (where 1 corresponds to complete perfect relation) for each frequency band f. *Coherence* is estimated as $\mathrm{Coh}(f) = |S_{AB}(f)|^2/(S_{AA}(f)S_{BB}(f))$, where S_{AB} is the cross-spectrum between signals A and B from two different electrodes, S_{AA} is the autospectrum of signal A, and S_{BB} is the autospectrum of signal B. Such a pairwise estimation of coherence between all electrodes leads to a network, which could be represented as a graph with electrodes as nodes and coherence values as distances between nodes (weights of edges). To estimate the level of interaction in such a brain network, the global efficiency index (Eglob) was estimated as a mean of inverse shortest distances along all pairs of electrodes [46]. Eglob could be estimated either for a particular frequency f or for a frequency band. In the latter case, mean (along all frequencies in a band) coherence values between pairs of electrodes were used as distances between nodes.

Coherence analysis allows assessment of pairwise synchronization of LFP/EEG signals to shed more light onto the interaction between different brain networks. Highly coherent oscillations between two structures can occur because they are functionally connected or because they share a common input. To exclude indirect relation though other areas where we have recording from, the measure of *partial coherence* was used [47]. Partial coherence between signals A and B is estimated as $M_{AB}/\sqrt{M_{AA}M_{BB}}$, where M_{AB} is a minor of a spectral matrix (matrix of spectra and cross-spectra between all pairs of electrodes) with the A-th row and B-th column removed.

To further add to the assessment of the information flow in a brain network, *extended partial directed coherence* was used [48]. It provides strength of causal *directional* coupling between pairs of electrodes, excluding relations due to the paths through other areas where we have recordings from.

3. Statistical Analysis

Results for described EEG metrics and for groups of buffer- and K18-injected animals are presented as mean values with 95% confidence intervals (CI). Between-group difference in means was assessed using the two-sample t-test, and in case of significance, it is indicated by asterisks on box plots ($^*p$ value < 0.05, $^{**}p$ value < 0.01). For phase shift data (see Figure 2(b)), which are circular in nature, differences in means were tested using the Watson-Williams test. In case of significance, asterisks provide a level of significance ($^*p$ value < 0.05, $^{**}p$ value < 0.01). Difference in means between groups was considered significant, if the p value is below 0.05.

4. Results

4.1. Accuracy of LC Injection Sites. The results shown in Figure 3 indicate that the Evans blue dye was successfully injected into the LC area. Coronal histological images from mouse brains show that the blue dye was present exactly in the neurons of LC (Figures 3(a) and 3(b)) and in the Purkinje/molecular layer neurons around the LC (Figures 3(c) and 3(d)), which may suggest that the fast-blue ink may have been washed out from LC neurons.

4.2. No Changes in Mean Locomotor Activity, Body Weight, Body Temperature, and Food Intake Were Observed between K18- and Buffer-Injected Mice. The body weight and locomotor activity were longitudinally monitored throughout the study. There were no significant differences (two-sample t-test) in average activity levels and body weight between K18- and buffer-treated mice (Figures 4(a) and 4(b)). Body temperature and food intake were assessed in the same group of animals, and both measures remain similar between the study groups at the measurement time points (Figures 4(c) and 4(d)).

4.3. Tau-Seeded Animals Demonstrate Progressive Shift in Theta Relative Power Spectra in the CA1 Region of the Hippocampus Ipsilateral and Contralateral to the Injection Site. We present the effects of tau seeding in the LC on the oscillatory activity of the ipsilateral and contralateral hippocampal CA1 regions as shown by a relative power spectral density of over 1-20 Hz (plots in Figure 1(b)) and 20-100 Hz (plots in Figure 1(c)). Seeding of K18 aggregates in the LC (Figure 1(a)) was shown to cause a significant leftward shift in the theta frequency activity in the contralateral and ipsilateral CA1L/R regions at recording weeks 1, 10, and 20 as compared to buffer-injected animals ($p < 0.05$, the two-sample t-test for the center of mass in the theta band; large plots in Figure 1(b)), while the relative theta power did not change (Figure 1(b), insets with bar plots). At recording week 1, this progresses, with an additional reduction

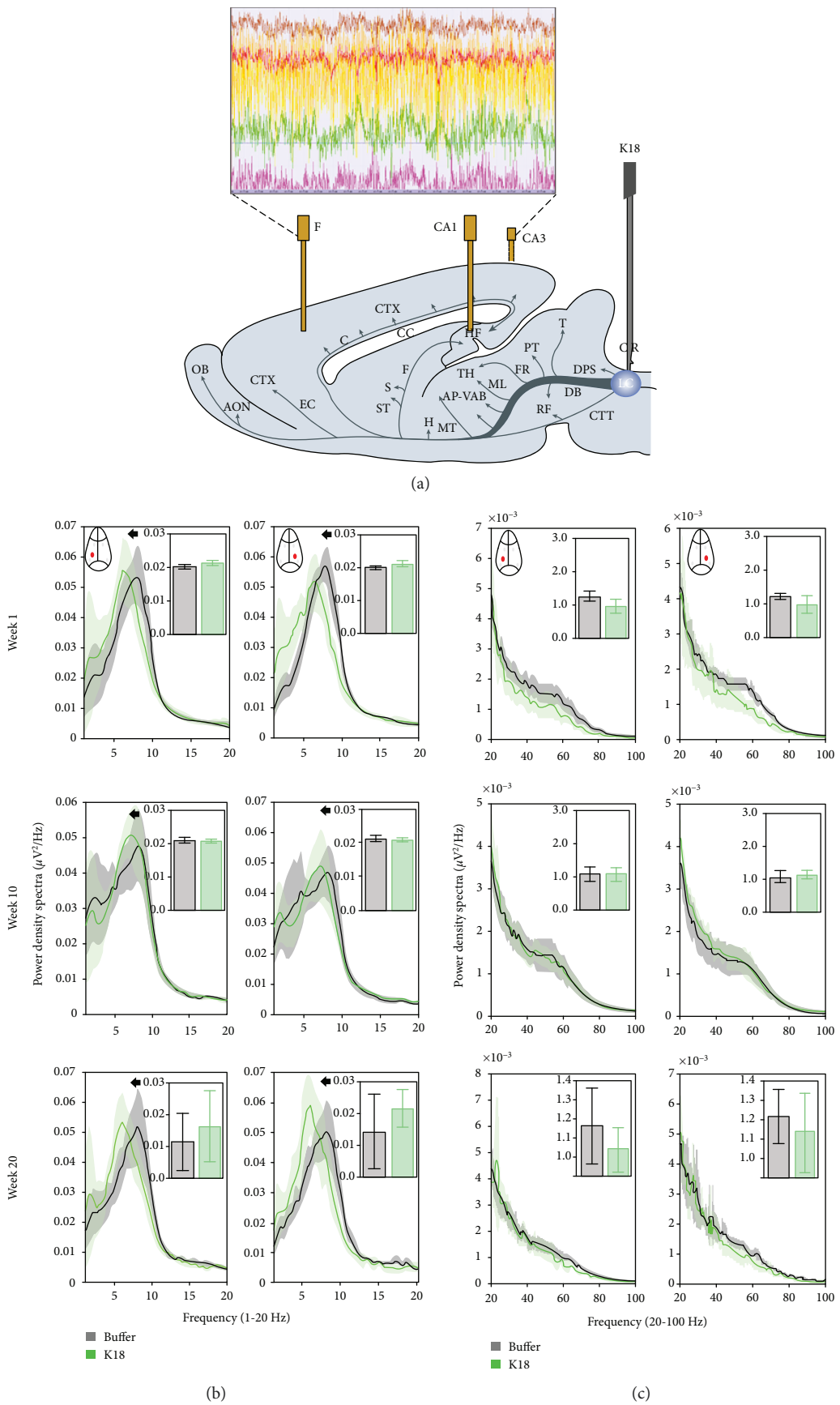

Figure 1: Continued.

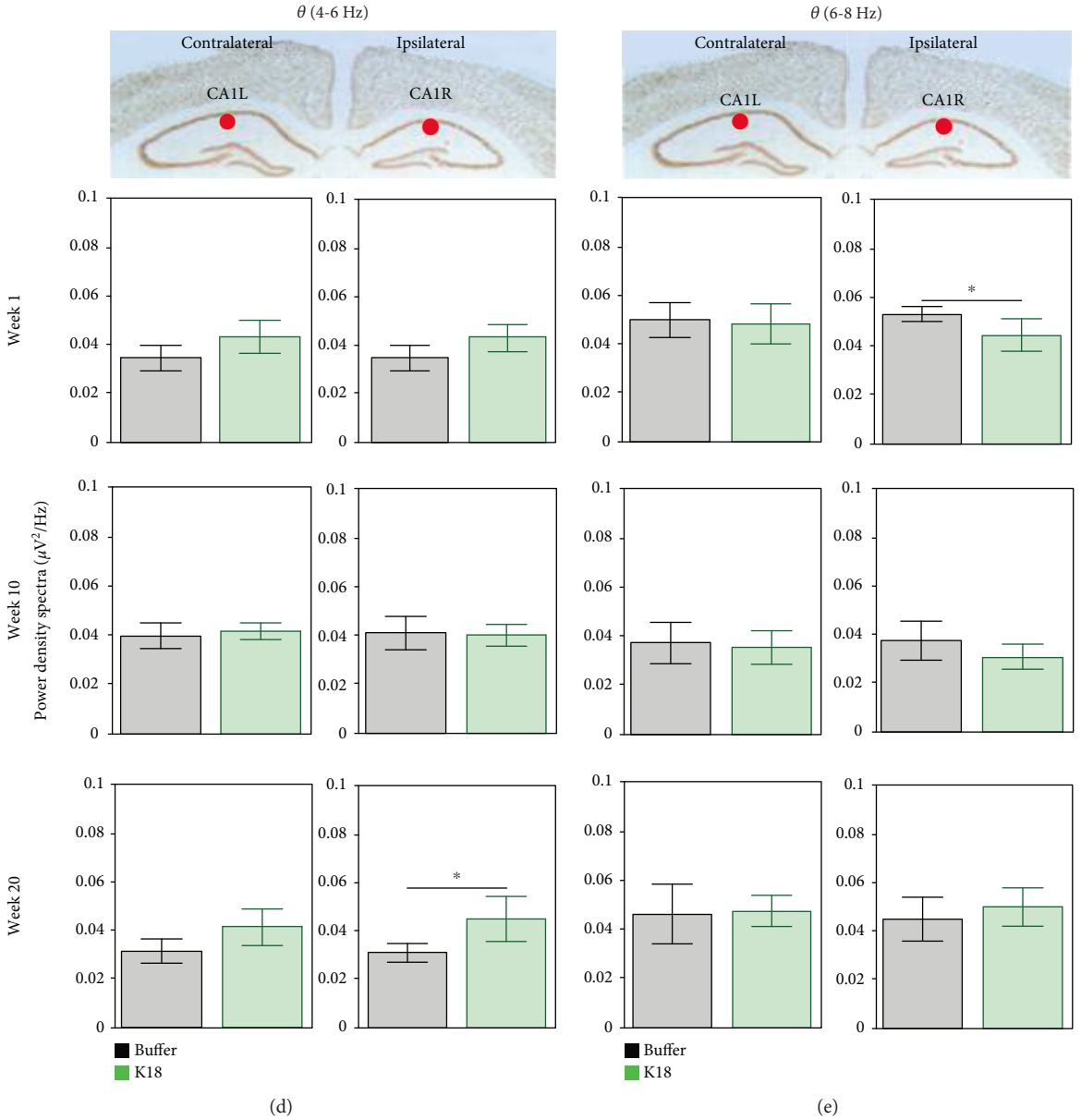

Figure 1: (a) Scheme showing the placement of recording electrodes and a cannula for injection of K18 in the locus coeruleus. (b, c) Relative power spectra in frequency (1-20 Hz (b) and 20-100 Hz (c)) for the CA1R and CA1L electrodes for buffer- (black, $n = 7$) and K18- (green, $n = 8$) injected mice, at recording weeks 1, 10, and 20. Insets indicate total relative power with no significance between group differences (two-sample t-test) at 1-20 Hz and 20-100 Hz in b1 and b2, respectively. (d, e) Relative power spectra in CA1R and CA1L in low (4-6 Hz (d)) and high (6-8 Hz (e)) theta oscillations at recording weeks 1, 10, and 20. Data are presented as mean (across animals) values (and 95% CI). Horizontal lines above bar plots with asterisks indicate the presence of significant difference between buffer- and K18-injected animals (two-sample t-test; $^*p$ value < 0.05).

($p < 0.05$, two-sample t-test) in the high gamma oscillations ($\gamma 1$ 50-80 Hz) (Figure 1(c)). Quantification of the relative power of over 1-20 Hz did not reveal a major difference between groups (Figures 1(d) and 1(e), inset bars), whereas a significant ($p < 0.05$, two-sample t-test) increase in slow theta (4-6 Hz) was observed in the final recording week 20.

4.4. Tau-Seeded Animals Present with Early, Severe Reductions in Intra-Theta-Gamma Phase-Amplitude Coupling in the CA1 Region Ipsilateral to the Injection Site. Recent evidence highlights the functional relevance of temporal relationships between superimposed network oscillations during information processing in the brain [49–51]. We therefore estimated the strength of cross-frequency coupling between the phase of slow and the amplitude of fast oscillations in different recording sites. Mean (across animals) PAC values at the contralateral CA1L and ipsilateral CA1R regions are qualitatively shown in the form of comodulation heat maps for buffer- and K18-injected mice (Figure 2(a), heat maps), at recording weeks 1, 10, and 20. Of note, we show figures of these 3 weeks as a similar pattern was observed throughout the recording weeks. As shown in

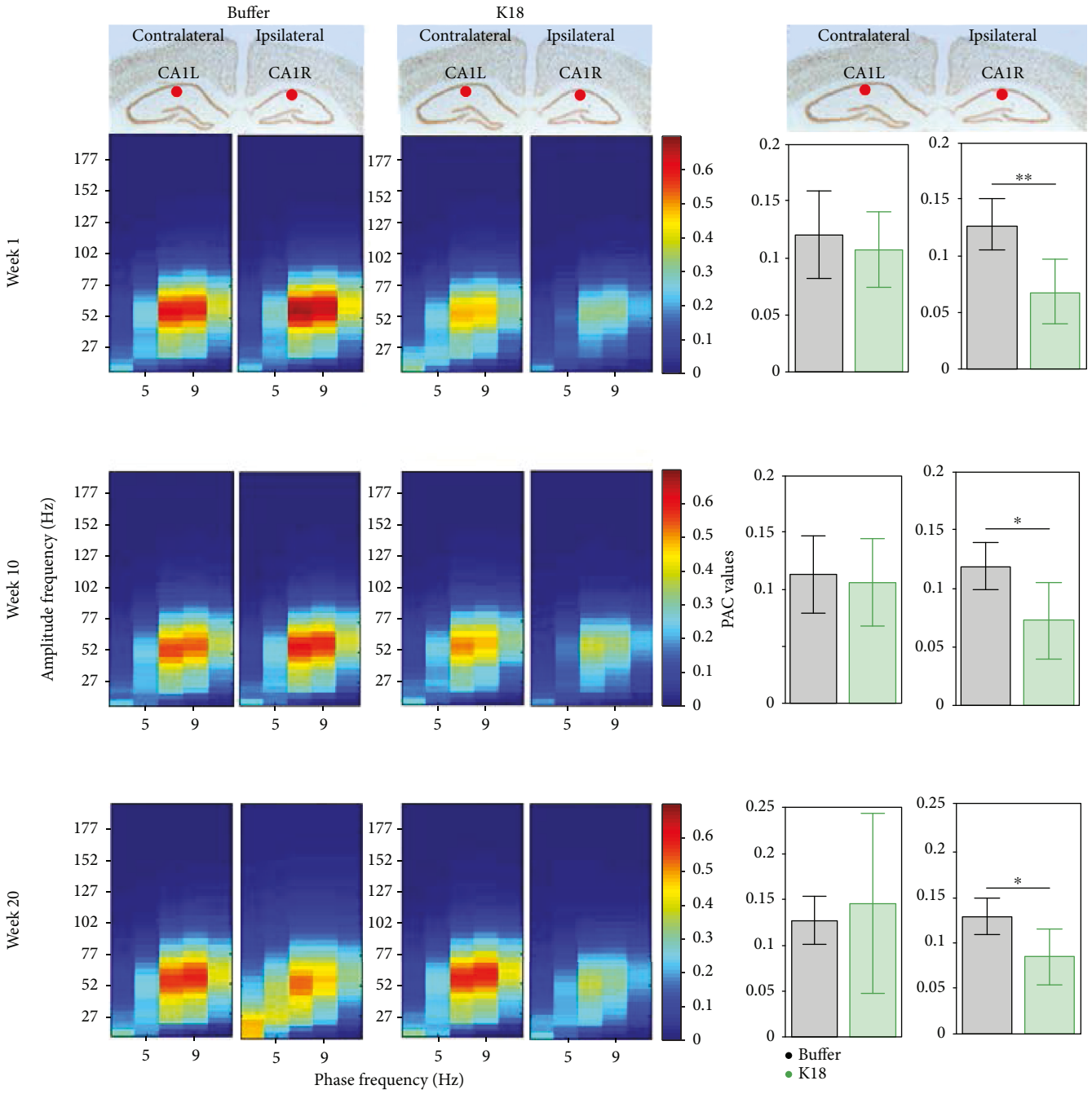

(a)

Figure 2: Continued.

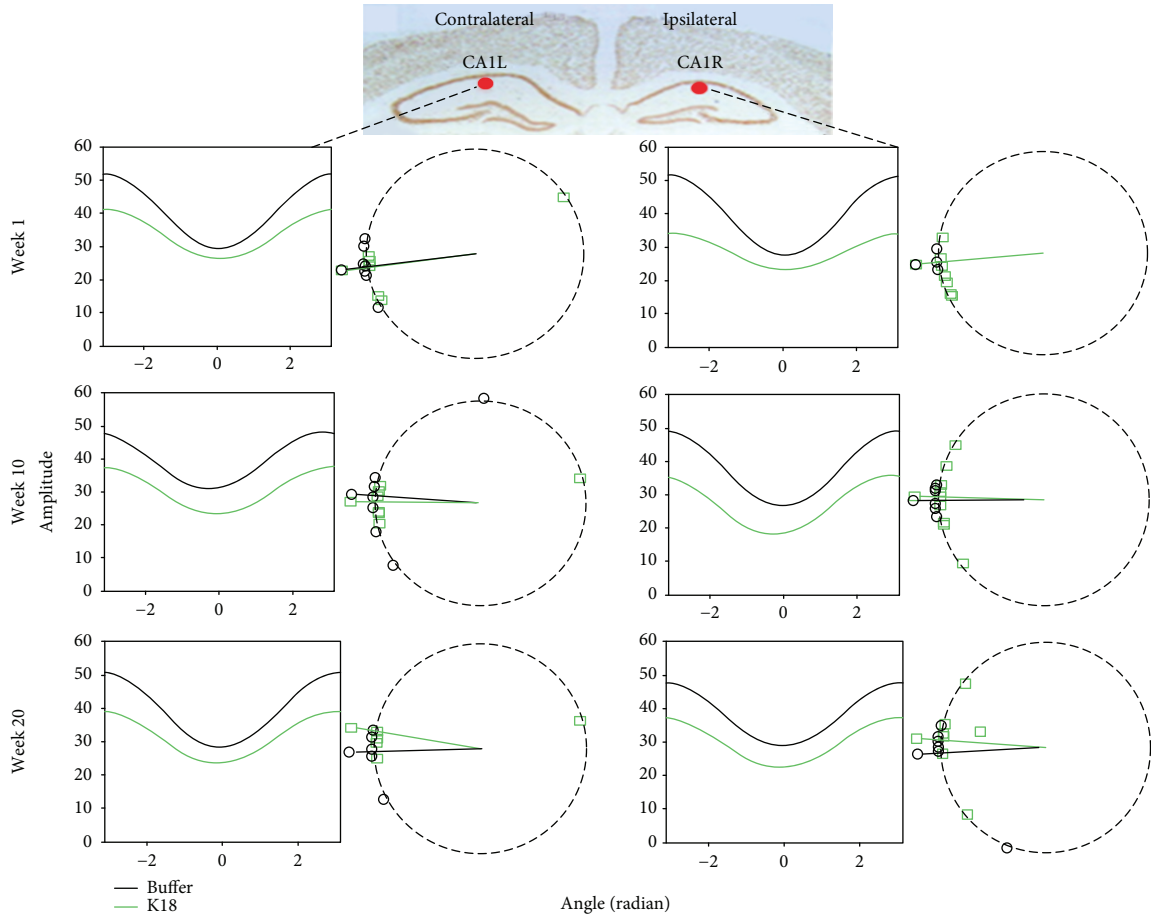

(b)

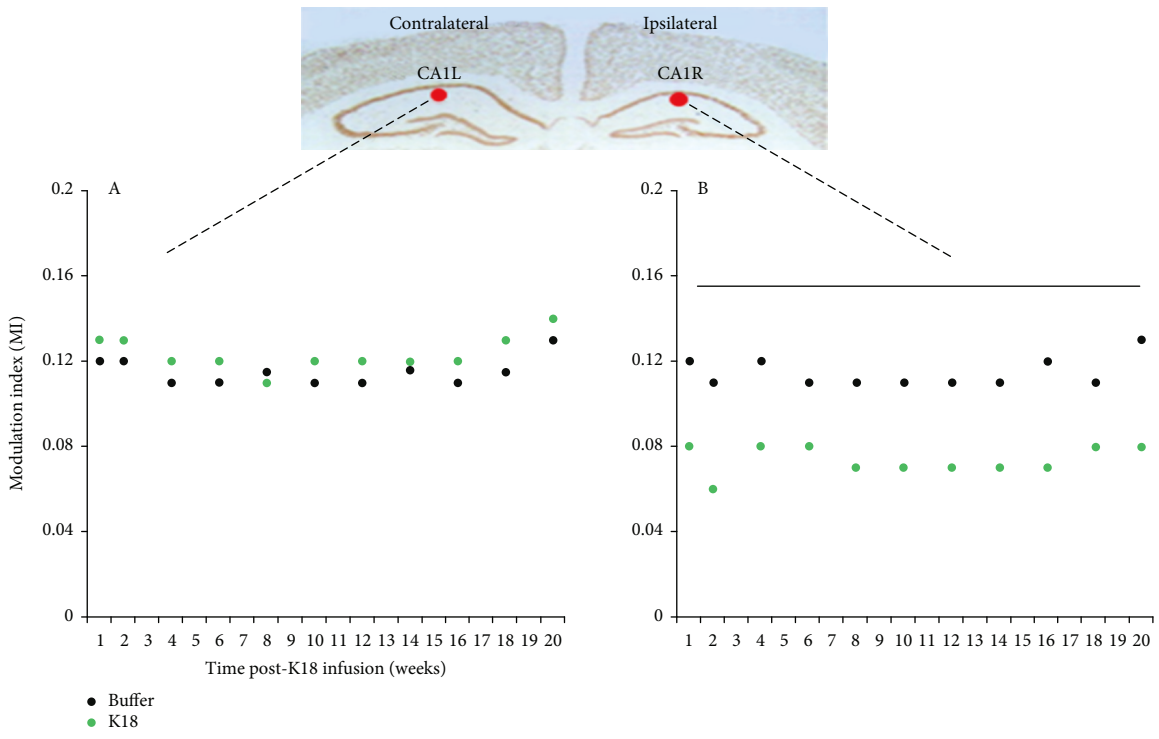

(c)

Figure 2: Continued.

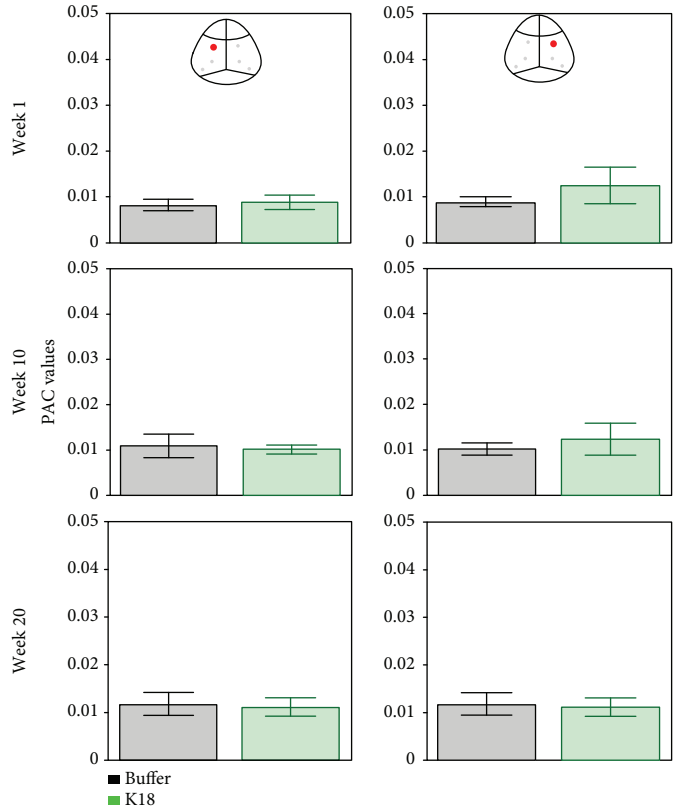

Figure 2: (a) Heat maps showing the mean phase-amplitude coupling (PAC) modulation index at the CA1L and CA1R electrodes for buffer- (black, $n = 7$) and K18- (green, $n = 8$) injected mice, at recording weeks 1, 10, and 20. As shown by the color scale, "hotter" colors indicate high coupling values while "colder" colors indicate low or no coupling. Bar graphs showing the mean (across animals) theta-gamma PAC (with 95% CI) at the CA1L and CA1R electrodes for buffer- (black, $n = 7$) and K18- (green, $n = 8$) injected mice, at recording weeks 1, 10, and 20. These means along animals' PAC values are calculated as the average PAC for the window of phase frequency: 3.5–12.5 Hz, and amplitude frequency: 32–100 Hz, to focus on theta-gamma PAC. Horizontal lines above the bar plots with asterisks indicate the presence of significant difference between buffer- and K18-injected animals (two-sample t-test; $^{*}p$ value < 0.05 and $^{**}p$ value < 0.01). (b) Averaged across animals' variations in gamma amplitude (vertical axes) as a function of theta phases (horizontal axes) obtained from the electrodes implanted in CA1L and CA1R for the weeks 1, 10, and 20 postadministration of the buffer and K18. Right plots show estimated phase shifts in obtained oscillations for each animal (shown as dots) and condition (buffer (black) and K18 (green) injected). Radii show circular mean values for buffer- and K18-injected groups of animals. No significant difference in means between groups across all time points was found with the Watson-Williams test. (c) Scatter graphs show mean theta-gamma PAC at the contralateral (CA1L) and ipsilateral (CA1R) CA1 regions of the K18 injection site, for all recording weeks, demonstrating changes in PAC over time, for the buffer-injected (black) and K18-injected (green) groups. Time intervals with significant differences ($p < 0.05$, two-sample t-test) between buffer-injected and K18-injected animals are shown by a horizontal line. (d) Bar charts quantifying the mean PAC in frontal electrodes for buffer- (black) and K18- (green) injected animals. Note that no significant difference (two-sample t-test) was observed between the study groups. Data are presented as mean values (with 95% CI).

Figure 2(a), left bar plots, buffer-injected animals demonstrate equivalently (no statistical difference, two-sample test) high phase-amplitude coupling in both ipsilateral CA1R and contralateral CA1L regions, at recording weeks 1, 10, and 20. This high coupling peaks around a phase frequency of 7.5 Hz and amplitude frequency of around 52 Hz, in the theta-gamma range (see Figure 2(a), left comodulation heat maps).

Conversely, Figure 2(a), right comodulation heat maps, demonstrates reduced PAC in the ipsilateral CA1R of K18-injected animals at recording week 1, which seems to worsen at recording week 10 and persists during recording sessions up to week 20. PAC comodulation heat maps in the contralateral CA1L of K18-injected animals also seem to be slightly impaired, but to a much lesser extent (Figure 2(a)). Quantification in the form of bar charts at recording weeks 1, 10, and 20 showed a significantly ($p < 0.05$, two-sample t-test) reduced mean theta-gamma PAC in the ipsilateral CA1R region in the K18-injected group as compared to the buffer-injected group (Figure 2(a), right bar plots).

To further investigate whether the pattern of phase-amplitude coupling is different between groups of animals, we sorted the gamma amplitudes by the theta phases and computed the mean gamma amplitude for each radian wide bin (Figure 2(b)) at weeks 1, 10, and 20 postadministration of the buffer and K18. Our results confirm what we already

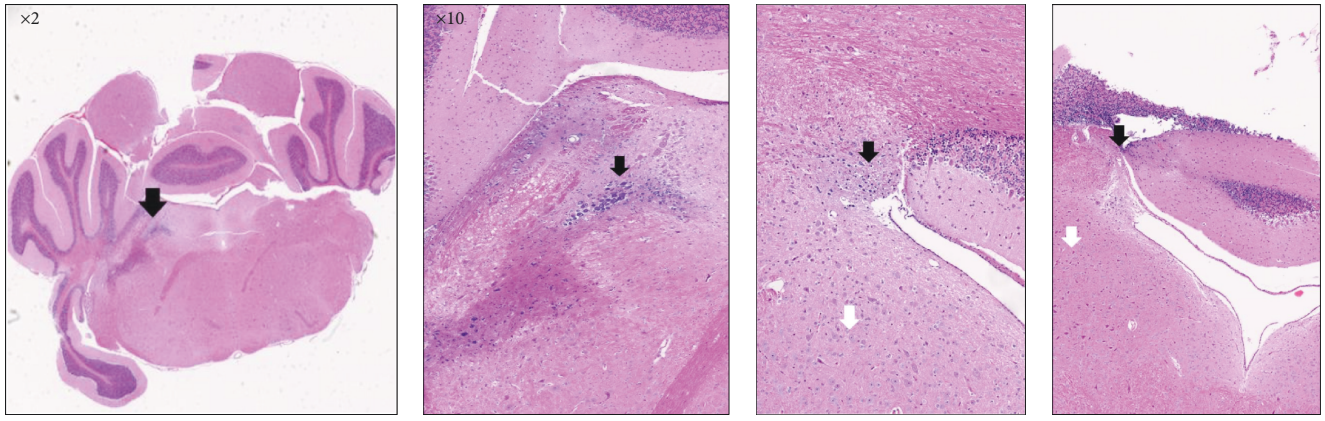

Figure 3: The image in (a) is an image from the mouse brain atlas depicted with black arrows in the LC region from a sagittal view. Areas of interest: microscopic images of coronal views of the neurons of the LC (a, b) and the Purkinje/molecular layer neurons around the LC (c, d).

saw using PAC, i.e., that gamma band activity could be modulated by the phase of theta activity. At the same time, no phase shift was revealed in all comparisons (Watson-Williams test, Figure 2(b), right plots). However, the averaged amplitude of gamma oscillation for all phases of theta oscillation was reduced in K18-treated animals throughout the recording session (Figure 2(b)).

4.5. Theta-Gamma PAC Steadily Deteriorates in the CA1 Region of the Hippocampus Ipsilateral to the Injection Site throughout the 20-Week Recording Period. Figure 2(c) displays the mean theta-gamma PAC at the ipsilateral and contralateral CA1 for all recording weeks, from 1 to 20, to show changes in the trajectory of the PAC strength over time in the buffer-injected and K18-injected groups (Figure 2(c), A and B, respectively). In the buffer-injected group, the mean theta-gamma PAC is almost the same as those in both the ipsilateral CA1R and contralateral CA1L regions from recording week 1 to recording week 20 (no significant difference, two-sample t-test applied for each week of data separately) and stays at a high mean value of around 0.12. However, in the K18-injected group, the mean theta-gamma PAC was greatly reduced throughout the study at the ipsilateral CA1R region ($p < 0.05$, two-sample t-test applied for each week data separately), staying at a mean value of around 0.07 (Figure 2(c), B). There were no major changes (no significant group difference, two-sample t-test) in the PAC strength in cortical regions between the study groups, through the recording sessions (Figure 2(d))

4.6. Intersite PAC Indices between Electrodes Demonstrate Significant Reductions in Phase-Amplitude Coupling between Contralateral and Ipsilateral CA1 Theta-Gamma Oscillations, in Tau-Seeded Animals. Theta-gamma PAC not only is an important mechanism underlying synaptic plasticity in one region of the brain but can also facilitate communication and functional connectivity between distant brain regions. Unlike the previously mentioned intrasite PAC, intersite PAC analyses characterize coupling of oscillations in one brain region with oscillations in another brain region, which gives hints into the directionality of these interactions. Therefore, we questioned how the phase of theta oscillations in one brain region may modulate the amplitude of gamma oscillations in a different region. We investigated theta-gamma PAC between contralateral CA1L and ipsilateral CA1R electrodes, as shown in Figure 5. In the buffer-injected group, as shown in Figures 5(a) and 5(b), left heat maps, there was high theta-gamma PAC from the contralateral CA1L electrode to the ipsilateral CA1R electrode and vice versa. It is also of note that mean CA1L > CA1R PAC and mean CA1R > CA1L PAC were almost equal. However, in the K18-injected group, as shown in Figures 5(a) and 5(b), right heat maps, PAC between CA1L and CA1R was reduced in both directions as compared to that in the buffer group, although this reduction seems slightly greater in the CA1R > CA1L direction (Figures 5(a) and 5(b), bar plots). The mean phase of theta frequency oscillations in the frontal and CA3 regions and the amplitude of CA1 gamma frequency were also significantly reduced ($p < 0.05$, two-sample t-test, Figure 5(b), bar plots).

4.7. Tau Seeding Alters the Functional Cortical Network. Coherence characterizes synchronous oscillations in different networks and deduces functional coupling among these networks. As shown in Figure 6(a), there was an early relatively weak ($p < 0.05$, two-sample t-test) mean global coherence efficiency in K18-injected animals estimated for a whole network of our recordings, as compared to buffer-injected animals. This reduction in a whole network coherence was primarily driven by the coherence between the CA1L and CA1R recording sites. CA1L-CA1R coherence function, which peaks in the theta and high gamma frequency bands, shows generalized decrease ($p < 0.05$, two-sample t-test) in the 4-70 Hz frequency range at recording week 10 in the K18-injected group, as shown by the accompanying bar charts (Figure 6(b), upper graph and bar chart).

Partial coherence analysis is similar to the previously mentioned coherence analysis but removes the influence of indirect connections, in order to focus on robust connections and remove the possible effects of volume conduction. Due to

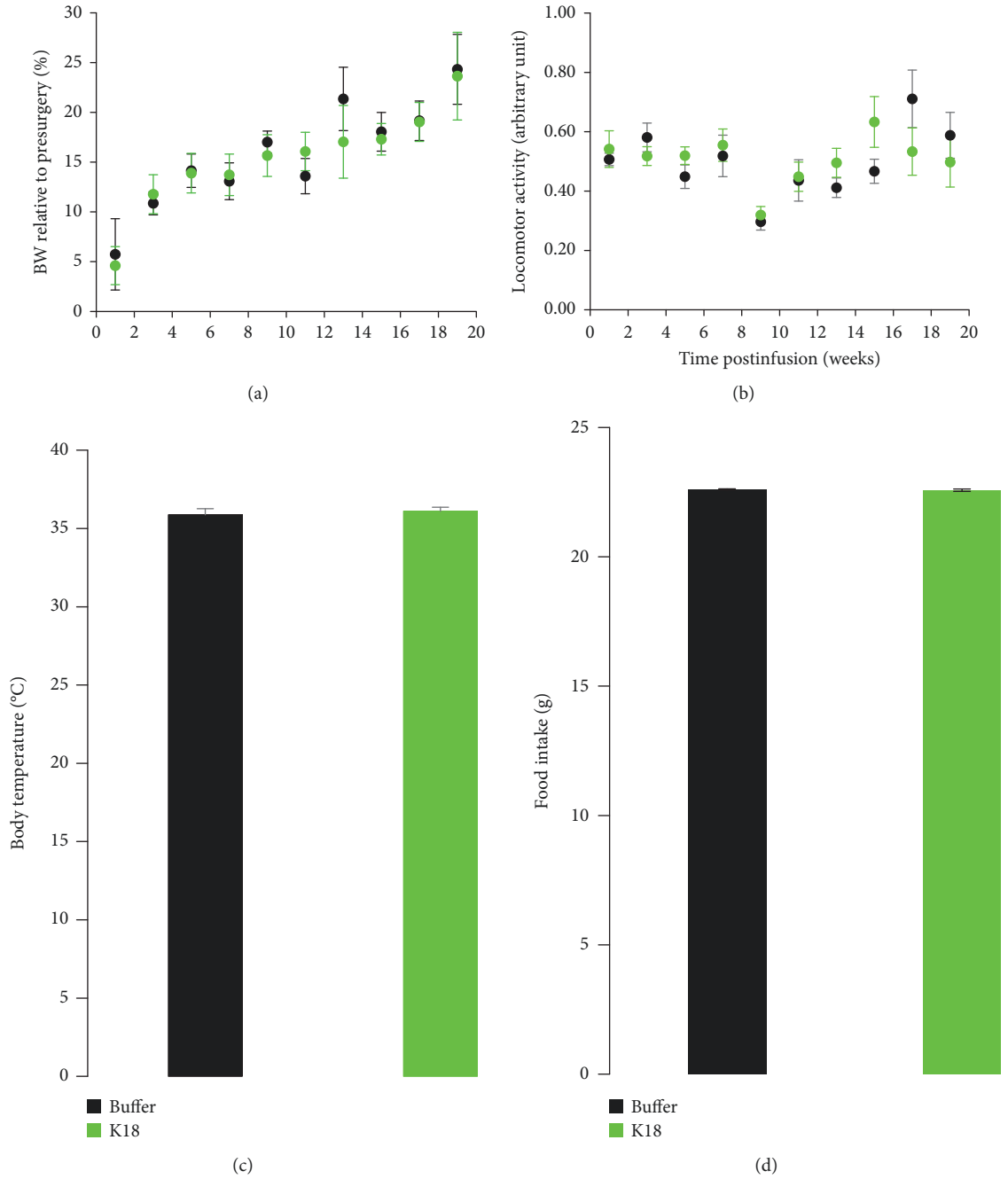

Figure 4: Mean locomotor activity, body weight, body temperature, and food intake in buffer- (black, $n = 7$) and K18- (green, $n = 8$) injected mice. (a) Body weight relative to presurgery and (b) locomotor activity were monitored daily prior and during EEG recording sessions, respectively. (c) Body temperature was measured in the middle of the study, and (d) food intake was measured daily during the first week postinfusion of K18 and buffer in the LC area. No changes in the mean activity levels, body weight, body temperature, and food intake were observed between the study groups. Data are expressed as mean ± sem.

this removal, partial coherence is lower in comparison to coherence, as it can also be seen for CA1L-CA1R results for week 10 (Figure 6(b), lower graph and bar chart). Mean partial coherence levels were significantly ($p < 0.05$, two-sample t-test) decreased between CA1L and CA1R electrode pairs in the 4-70 Hz frequency range in the K18-injected group, as compared to the buffer-injected group.

Partial directed coherence, which is an extension of partial coherence, probes time lags in signals to investigate the directionality of these coherent interactions and focuses on causal functional relationships. As shown in Figure 6(c), at recording week 10, there were changes in mean extended partial directed coherence between CA1L-CA3R electrode pairs. A consistent decrease in the extended PDC levels was observed for low and high gamma oscillations from CA1R > CA1L ($p < 0.05$, two-sample t-test, Figure 6(c)). However, there seems to be no significant difference (two-sample t-test) in the level of directional interactions

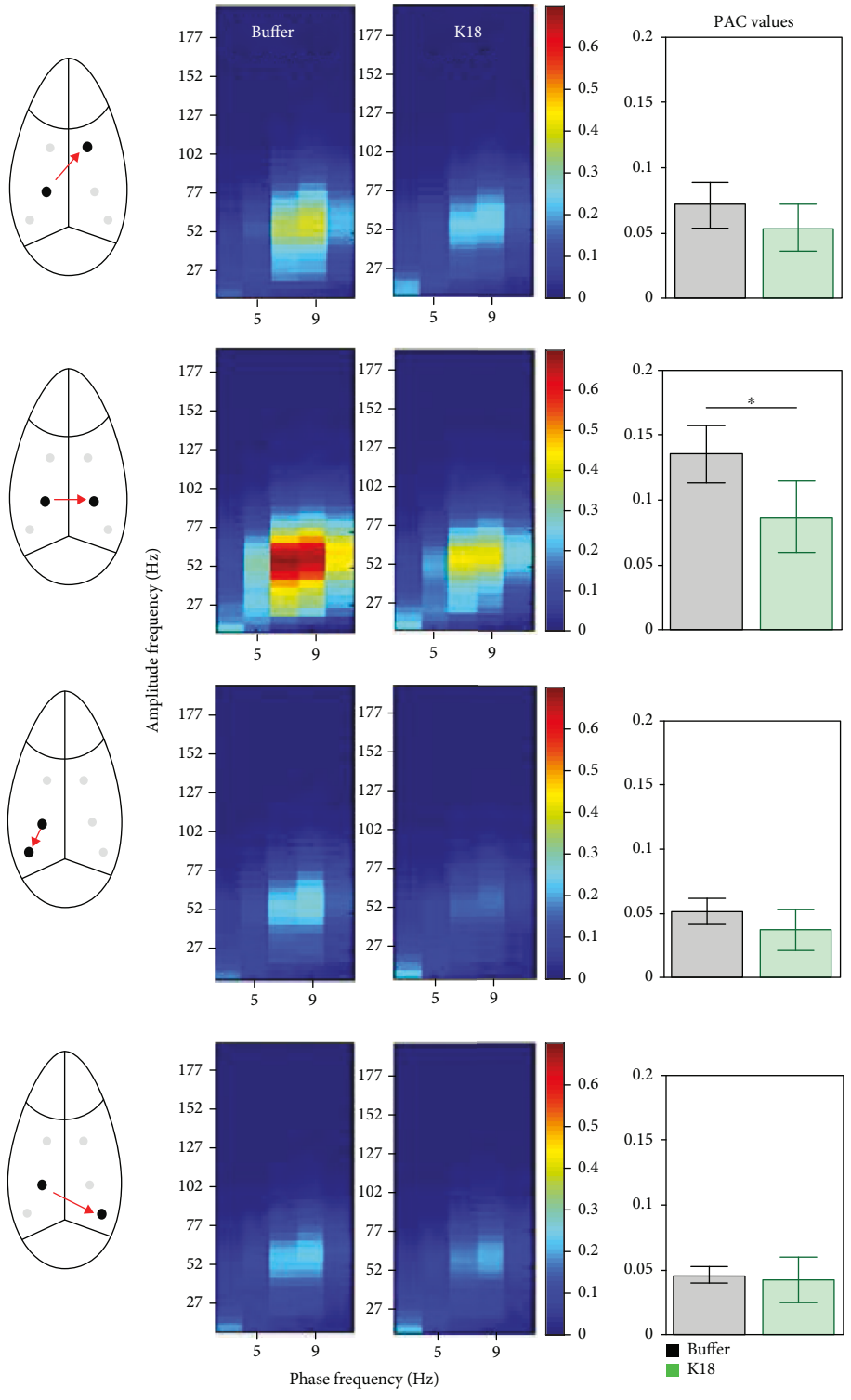

(a)

Figure 5: Continued.

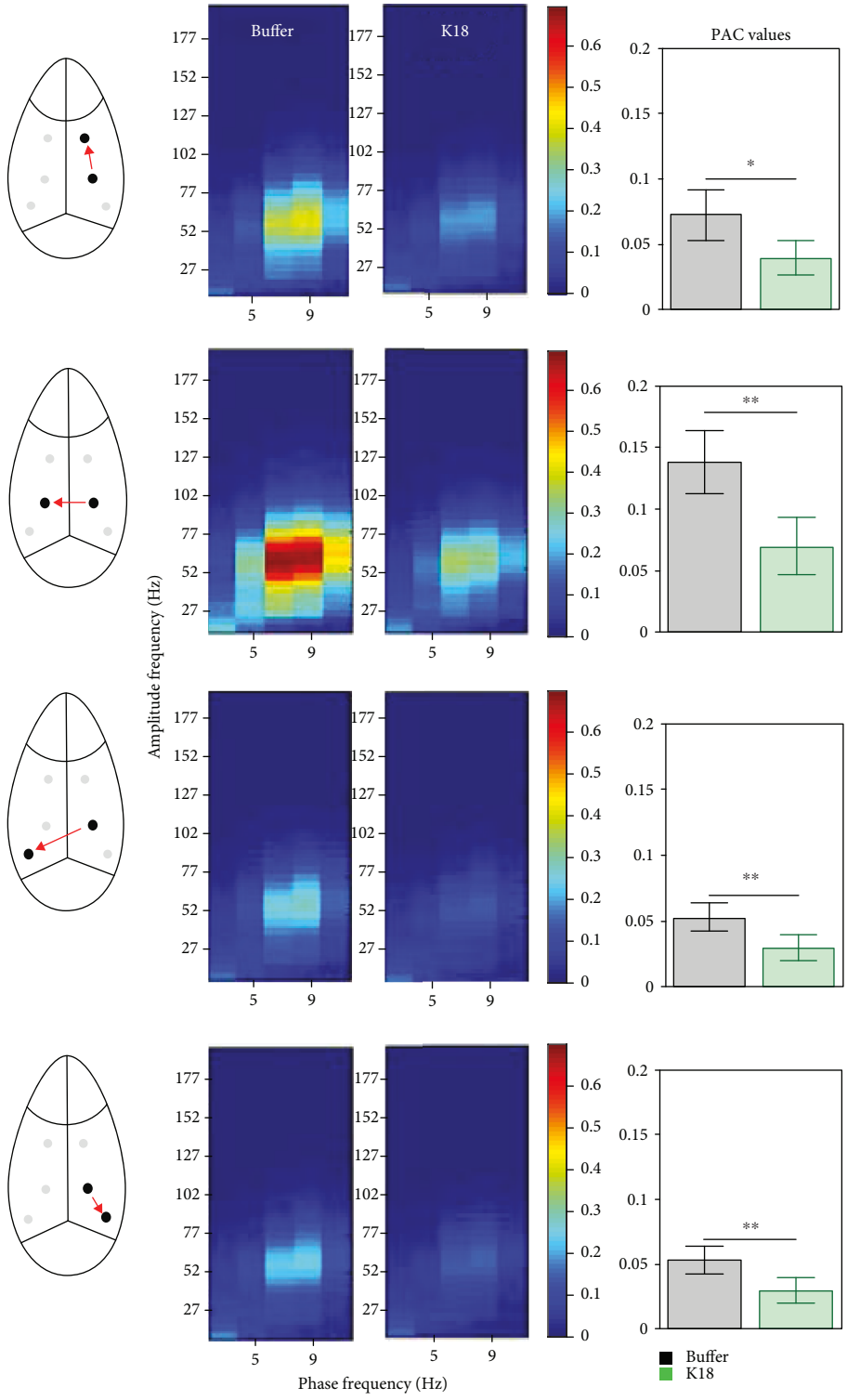

Figure 5: Heat maps showing the mean phase-amplitude coupling (PAC) between contralateral CA1L and ipsilateral CA1R electrodes for buffer- (left heat maps in each frame) and K18- (right heat maps in each frame) injected animals at recording week 1 (buffer $n = 7$, K18 $n = 8$). (a) CA1L > CA1R represents the strength of PAC between theta oscillations (phase) from CA1L and gamma oscillations (amplitude) at CA1R, while (b) CA1R > CA1L represents the strength of PAC between theta oscillations from CA1R and gamma oscillations at CA1L. Bar charts quantifying the mean PAC between the stated electrodes (shown with 95% CI) for buffer- (black) and K18- (green) injected animals. These mean PAC values are calculated as the average PAC for the window of phase frequency: 3.5–11 Hz, and amplitude frequency: 32–100 Hz, to focus on theta-gamma PAC. Horizontal lines above the bar plots with asterisks indicate the presence of significant difference between buffer- and K18-injected animals (two-sample t-test; $^{*}p$ value < 0.05 and $^{**}p$ value < 0.01).

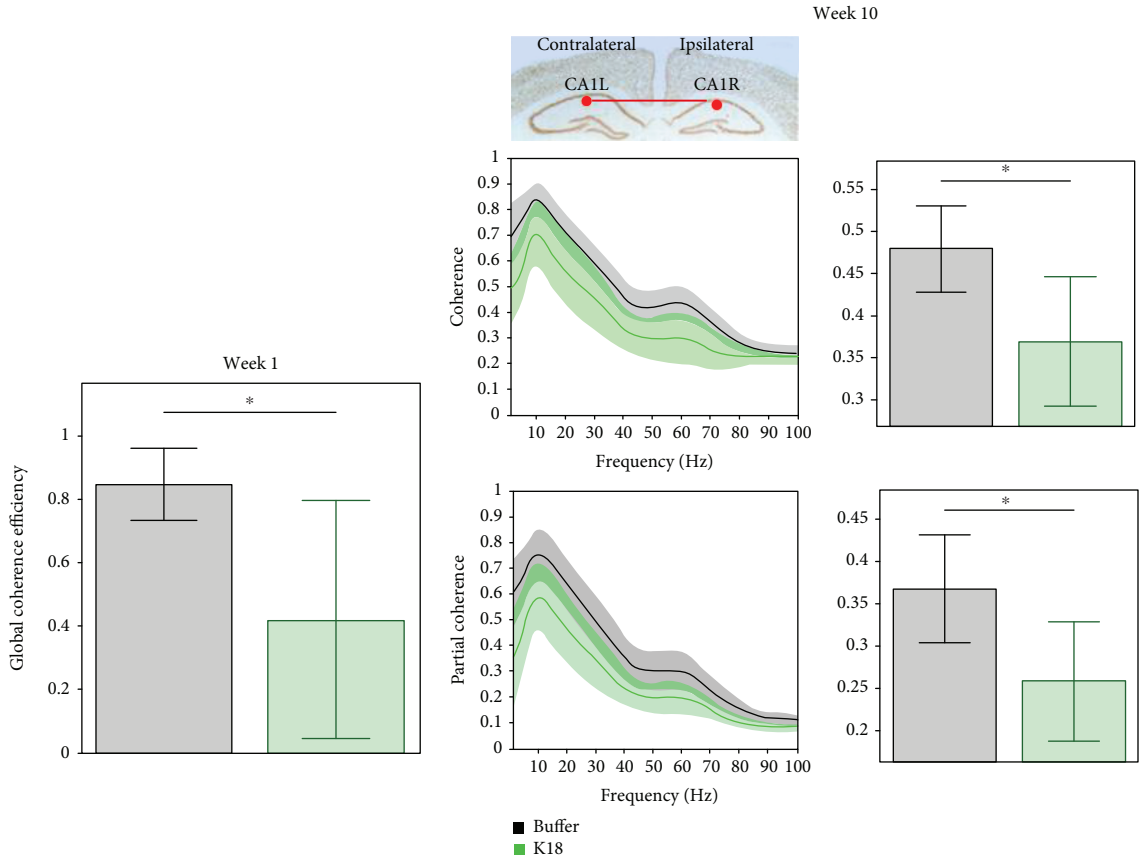

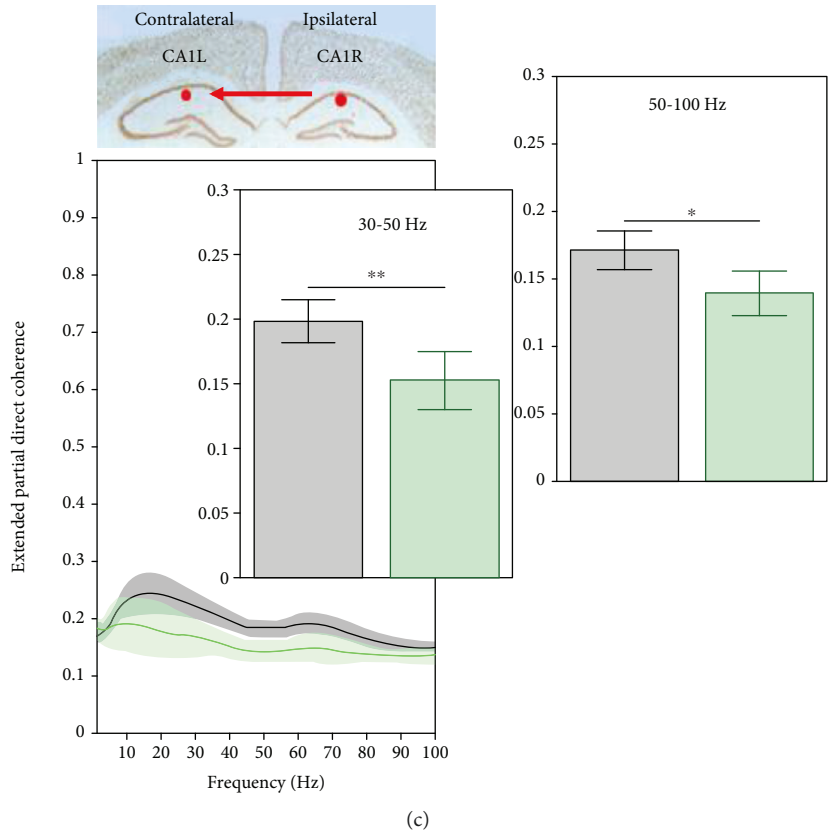

Figure 6: Continued.

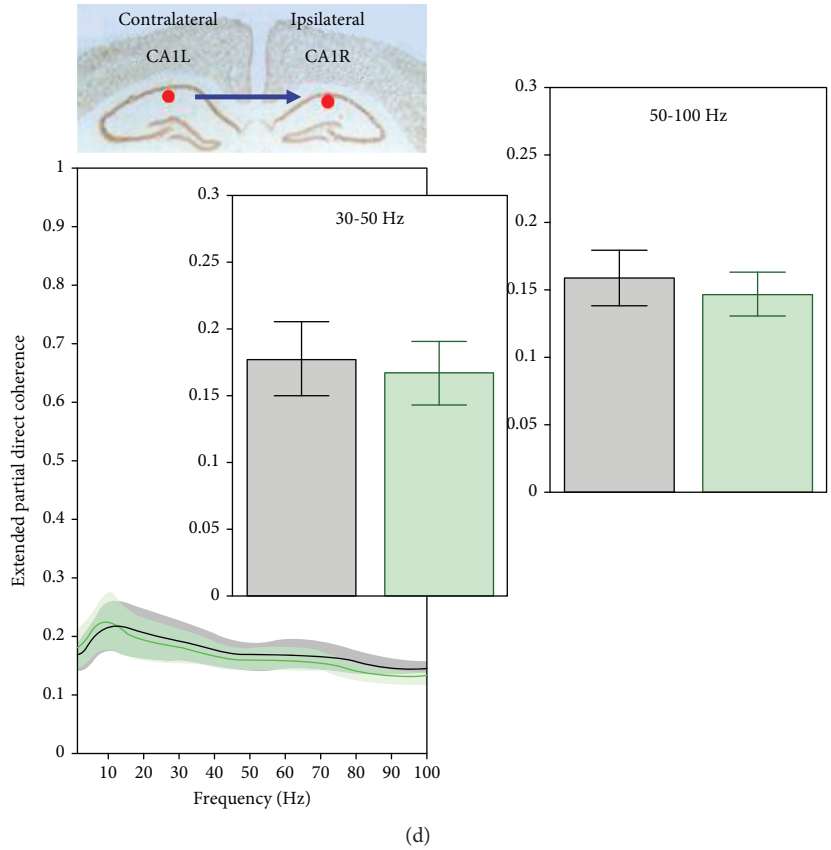

FIGURE 6: (a) Graphs showing the mean (across animals) global coherence efficiency (with 95% CI) for buffer-injected (black) and K18-injected (green) mice, at week 1 (buffer $n = 7$, K18 $n = 8$). Horizontal lines above bar plots with asterisks indicate the presence of significant difference between buffer- and K18-injected animals (two-sample t-test: $^{*}p$ value < 0.05). (b) The top line graph shows the mean (across animals) coherence values (with 95% CI) between CA1L and CA1R electrodes for buffer-injected (black) and K18-injected (green) mice, at week 10 for the frequency range 0-100 Hz. On the right-hand side, bar charts show the mean (across animals) coherence (with 95% CI) for both groups for the frequency range of interest. Bottom line graphs show the mean (across animals) partial coherence values (with 95% CI) between the same electrodes. On the right-hand side, bar charts show the mean partial coherence (with 95% CI) for both groups for the same frequency range, 0-100 Hz. Horizontal lines above bar plots with asterisks indicate the presence of significant difference between buffer- and K18-injected animals (two-sample t-test; $^{*}p$ value < 0.05). (c) Graphs showing the mean (across animals) extended partial directed coherence (with 95% CI) from CA1R to CA1L and (d) CA1L to CA1R for buffer-injected (black) and K18-injected (green) mice, at recording week 10. On the left-hand side, these data are presented in the form of a line graph, showing mean (across animal) extended partial directed coherence as a function of frequency (with 95% CI) for both groups for the frequency range 0-100 Hz. On the right-hand side, bar charts show the mean (across animals) extended partial directed coherence (with 95% CI) for both groups for frequency ranges 30-50 and 50-100 Hz. Horizontal lines above the bar plots with asterisks indicate the presence of significant difference between buffer- and K18-injected animals (two-sample t-test; $^{*}p$ value < 0.05 and $^{**}p$ value < 0.01).

from CA1L > CA1R (Figure 6(d)) or within the FL-FR and CA3L-CA3R (data not shown) electrode pairs.

5. Discussion

K18 seeding in the brainstem LC elicited early robust alterations in distant hippocampal functional networks, and as seen before, the pathology spread from the deeper LC seeding area to the hippocampus and frontal cortex was not observed [30].

While no current tau transgenic mouse models of AD fully recreate the spatiotemporal progression of tau in humans, they have taught us a great deal about the nature of tau pathology and its direct involvement in AD. Human tauopathies and numerous tau transgenic mouse models have demonstrated that tau pathology can cause neurodegeneration and cognitive impairment in the absence of Aβ [15, 16, 52]. However, various studies have also shown that tau pathology causes functional alterations in affected neurons aside from neuronal injury. One such study by [16] found that suppressing the human mutant tau transgene in the aforementioned rTg4510 tau transgenic mouse line restored cognitive function and prevented further neuronal loss, while aggregation of tau into NFTs continued. This recovery of cognitive function implied that these early impairments were due to "reversible neuronal dysfunction" and not necessarily due to neurodegeneration. These results also suggest that the pathological form of tau may in fact be the soluble tau oligomers, rather than the insoluble NFTs, a theory echoed by others in the field [53]. A seminal study by

[33] demonstrated that neurons with intracellular tau show reduced activity and a relatively small number of pathological neurons can affect the activity of whole networks. From the various electrophysiological alterations seen in our mouse model, we expected that the cause of these alterations would be due to the rapid spread of tau pathology from the seeded locus coeruleus to the ipsilateral hippocampus and its direct effects on this region. However, surprisingly, no tau pathology was seen in the hippocampus of a previous LC tau-seeding model [30]. A possible explanation suggests that this previous result may be due to strain-specific effects; however, a pilot study revealed no tau deposits at the level of the CA1 (data not shown). One possible explanation for this lack of tau pathology in the hippocampus could be due to the relatively short time frame of the study and that the spread of tau pathology to the hippocampus may occur in a given time. Another possibility is that tau pathology could have spread to the hippocampus but, by 20 weeks postinjection, was effectively removed by different clearance systems in the brain. However, there is also another possibility that has been brought up in a recent paper [54], in which the authors suggest that the spread of tau beyond the earliest Braak stages could be accelerated by increasing concentrations of Aβ, through "cross-seeding" of tau by Aβ [25]. Therefore, it could be that the lack of high levels of Aβ in the hippocampus and frontal cortex prevents rapid spread of tau pathology to these areas. One way of investigating this could be to seed tau pathology in the LC of an amyloid transgenic mouse model and investigate the subsequent pathology. One caveat to this however is the possibility that the lack of mutant tau transgenes in these animals could prevent effective tau seeding in these animals. Further work down this line of investigation could be rewarding, as any AD model is limited in its usefulness without the presence of both tau and amyloid pathologies. Regardless, the robust functional alterations seen in the hippocampus in our model in the absence of tau pathology challenge the classic prion hypothesis that the spread of tau pathology to areas of the brain may not be the sole causal factor that results in functional impairments in these areas [21].

To understand the causes of the various functional alterations demonstrated in the LC seeding model, it is salient to first look at them individually, as there is nothing to imply that they are resulting from a single common factor.

5.1. Hippocampal Spectral Changes Seem to Demonstrate Altered Neural Network Activity. Firstly, the most notable change in hippocampal power spectra is the early entrainment shift in relative power oscillations of a range of frequencies at the CA1 contralateral and ipsilateral to the injection site of K18. At the first week post-K18 injection, there was a shift in the peak theta frequency oscillation towards slow rhythm and reduction in the peak gamma frequency oscillations. Furthermore, at 20 weeks post-K18 injection, the sustained entrainment shifts in relative power seem to slightly reflect the "slowing" of the EEG, which refers to a shift in the power spectrum due to decreased high-frequency oscillations and subsequently increased low-frequency oscillations as seen in AD [9]. Therefore, our observation in the CA1R of tau-seeded animals may be indicative of the beginnings of this EEG slowing. The cause of this slowing in AD is currently not certain, but earlier works have shown that combined cholinergic and monoaminergic blockade in rats can effectively recreate this slowing and also results in severe cognitive impairments [7, 55, 56]. It is highly possible that tau pathology in the noradrenergic LC and nearby cholinergic nuclei could result in reduced noradrenergic and cholinergic signalling to the hippocampus, resulting in this slowing. Clinical evidence has demonstrated that there is an upregulation of beta-2 adrenoceptors at the hippocampus and frontal cortex of AD patients, suggesting a compensation for reduced noradrenergic input, while muscarinic M1 receptor densities have been shown to be largely unchanged, suggesting reduced cholinergic innervation as the cause of loss of cholinergic signalling in AD [57]. The maintenance of theta power in this region seems to be extremely fortuitous, as the importance of hippocampal theta rhythms in cognition and short-term memory has been well documented [58]. It has also been suggested that impairments of hippocampal theta through functional means may be as detrimental to mental health as impairment of hippocampal theta through structural damage [59]. Due to the generally unidirectional nature of information flow in the hippocampal trisynaptic circuit, one of the main inputs to the CA1 is the CA3 region. No differences were found in the ipsilateral CA3 power spectra between K18- and buffer-injected animals. However, there seems to be a slight, nonsignificant decrease in slow and fast theta power at this electrode for the 10-20-week period. The power spectra of the contralateral CA1L show no significant differences in K18-injected animals in any frequency band, at any week, and show no notable changes either. However, interestingly, the power spectra of the contralateral CA3L region show nonsignificant changes in theta power. Although the hippocampi of both hemispheres are separate, they are strongly interconnected through the hippocampal commissure, and while there is a weak commissural connection between CA1 regions, one of the main origins of hippocampal commissural fibers is CA3 pyramidal cells [60]. These commissural fibers innervate the CA1, CA2, and CA3 regions of the contralateral hippocampus. Therefore, it is entirely possible that any change in the theta power at the CA3L region is maintaining theta power at the CA1R through commissural fibers.

5.2. Reduced Theta-Gamma PAC at the Ipsilateral CA1 Region Could Result in Impaired Synaptic Plasticity in This Region. Theta-gamma PAC has been widely researched due to its possible roles in learning and memory. PAC strength has been shown to correlate with cognitive performance [48], and as demonstrated in numerous in vitro electrophysiology protocols, gamma frequency stimulation bursts repeated at theta frequency effectively induce long-term potentiation, a type of synaptic plasticity in the hippocampal CA1 area [61, 62]. Impaired theta-gamma PAC has been demonstrated prior to Aβ accumulation in an amyloid mouse model AD [36] and in the tau-seeding model [24] and has been suggested to be a possible early functional biomarker of AD [63]. Here, K18 seeding in the LC resulted in

reduced theta-gamma PAC at the ipsilateral CA1R region, from 1 week postinjection, and persisted throughout the 20-week recording period. This significant early impairment occurs in the CA1R of these animals prior to a significant reduction in gamma power and in the absence of changes in the phase angle or theta power. Additionally, theta-gamma PAC at the contralateral CA1 was shown to steadily deteriorate throughout this 20-week recording period. Similarly, this reduction in theta-gamma PAC in the contralateral CA1L occurs in the absence of significant changes in theta or gamma power. One possible explanation for this is due to a reduction in cholinergic signalling from affected cholinergic nuclei in the brainstem. It has been shown that reduced cholinergic signalling, through systemic administration of the muscarinic antagonist scopolamine, causes impaired theta-gamma PAC in the entorhinal cortex of freely moving rats [64]. Intracellular tau has been shown to reduce the firing rates of neurons prior to neurodegeneration [32], so developing tau pathology in brainstem cholinergic nuclei could reduce cholinergic signalling as a robust reduction in the number of choline acetyltransferase- (ChAT-) immunopositive cholinergic neurons that has been previously seen in the medial septum of a tau transgenic mouse model [65].

In Alzheimer's disease, reduced cholinergic signalling has been established as a cause of cognitive impairment and has been attributed to reduced cholinergic innervation [54]. The deterioration of theta-gamma PAC in the contralateral CA1L could also be explained by this, as tau pathology in the brainstem spreading to the contralateral side would result in increasing numbers of affected cholinergic neurons on that side and therefore decreasing signalling. While the cause of impaired theta-gamma PAC in the aforementioned amyloid model was likely resulting from the local electrophysiological alterations caused by increasing levels of Aβ in the hippocampus, in the context of AD, the combination of these two different pathologies could conceivably result in an even greater theta-gamma PAC impairment.

5.3. Bidirectional Theta-Gamma PAC Impairments between CA1L and CA1R in Seeded Animals. Theta-gamma PAC has also been suggested to facilitate communication between distant brain regions [66]. Intersite PAC analysis was used to investigate changes in the coupling of oscillations between contralateral and ipsilateral CA1 regions. This allows understanding of functional changes in the dynamics of this network and allows possible further insight into the nature of localized PAC changes at these regions. At recording week 1, there was significantly reduced coupling of contralateral CA1L theta with ipsilateral CA1R gamma oscillations in seeded animals. This could result from the reduced slow gamma power at the ipsilateral CA1R around this time. There is also reduced coupling of ipsilateral CA1R theta with contralateral CA1L gamma oscillations. The impaired high-theta activity in the ipsilateral CA1R may contribute to this impairment, and the possible compensatory CA1L-enhanced theta power may not be completely effective in maintaining the normal CA1 circuit's function. This impaired intersite PAC suggests a bidirectional impairment in effective communication between both hippocampal CA1 regions.

5.4. Various Changes in Different Coherence Measures between Electrodes Suggest Altered Neural Network Dynamics. The main goal of coherence function is to reveal synchronous oscillations in different networks to deduce functional coupling among these networks. Highly coherent oscillations between two structures can occur because they are functionally connected or because they share a common input; e.g., coherence analysis considers all possible interactions, including those from mutual sources. However, due to a high sensitivity to noise and the possibility of volume conduction-related effects, variability can be high. K18-seeded animals showed an early deteriorating global coherence efficiency network and coherence between contralateral CA1L and ipsilateral CA1R regions for the frequency range 4-70 Hz. The shift towards slow theta observed in the power spectra may be indicatory of the beginnings of adaptive increases in intercortical connectivity and may further support the possibility of enhanced theta power to overcome impaired interhippocampal connectivity.

Partial coherence and extended PDC allowed further investigation into changes in functional network connectivity observed in the results from the standard coherence analysis. Partial coherence analysis, unlike coherence analysis, only investigates direct interactions between the two electrodes of interest and removes any possible mutual connections. Interestingly, a significant decrease in partial coherence between CA1L and CA1R was observed in tau-seeded animals at recording week 10. There are numerous physical hippocampal commissural fibers between these two regions, so this functional disconnection may not be robust enough to overcome this anatomical connectivity. Unlike with the aforementioned coherence analysis, there are no significant differences in partial coherence between FL and FR or CA3L and CA3R. This is interesting as it suggests that the changes in coherence seen between these electrode pairs may be due to changes in their coherence with mutual connections.

Extended PDC analysis is a slightly more advanced function than partial coherence and involves time lags between coherent signals, to investigate causal relationships and directionality between these network locations. Interestingly, in support of differences in partial coherence between K18- and buffer-injected animals at recording week 10 for CA1 electrode pairs, this analysis highlighted some possible directional network changes occurring. There seems to be a consistent decrease in the extended PDC index in the direction of CA1R to CA1L and other electrodes, whereas there seems to be no changes in the PDC levels in the direction of CA1L to CA1R and other electrodes. This is surprising but could be indicative of this possible compensatory activity from the contralateral CA1L region, which attempts to maintain a level of functional network connectivity with the ipsilateral hippocampus.

5.5. Possible Functional Biomarkers and Considerations of the Novel Brainstem Tau Pathology Mouse Model. As we have demonstrated, tau seeding in the brainstem LC was sufficient to cause early functional alterations in distant hippocampi ipsilateral to the injection site as well as the contralateral hippocampus. These functional alterations have been shown to

take the form of localized changes, as well as changes in the dynamics of functional hippocampal networks. We have also seen some changes in the contralateral hippocampus to suggest a possible attempt to maintain normal function. If the contralateral hippocampus was found to be compensating for these changes, it is possible that without this compensation, the functional alterations seen in the hippocampus ipsilateral to the injection site could be far greater. As this study is focused on investigating possible functional biomarkers in this model, we have attempted to critically analyze each measure to determine its value. In this study, the earliest and most robust changes were the leftward shift to slow power spectra, impaired global coherence, and intrasite theta-gamma PAC at the CA1R. There were significant reductions seen in tau-seeded animals at 1 week postinjection, which persist throughout the recording period. Similarly, deteriorating theta-gamma PAC was found at the contralateral CA1L as well. Hippocampal theta-gamma PAC has been implicated as an important process in learning and memory in humans and rodents, giving this measure translational value [43]. This functional index may be extremely valuable, as a functional correlate of the early pathology load in live animals and how it progresses, without the need for labor-intensive immunohistochemistry. It is worth mentioning that variability in functional measures may arise from the high variability in the underlying tau pathology load between tau-seeded animals. The subsequent development of tau pathology following seeding is not completely uniform between different animals. Differences in the brain's ability to clear this pathology, as well as differences in the vulnerability of the brain to these changes, are two of many possible factors that may affect the development of tau pathology. During the stereotaxic injection of compounds into the brain, it is possible for the compound to flow back up along the needle track and out of the brain. This "backflow" could be avoided using smaller volumes of compounds, as this could result in reduced pressure at the injection site. However, one problem with reducing the amount of seed material injected into the brain could be a subsequent reduction in tau pathology.

From the translational perspective, the present model could be improved as tau pathology was unilaterally seeded in the right-side locus coeruleus, whereas tau pathology in AD initiates bilaterally, in the LC of both hemispheres [25]. To better recreate the early pathological process of AD in this model, tau pathology could be seeded bilaterally, in the LC of both hemispheres. Bilateral tau seeding in this model could also conceivably result in more severe functional changes, by removing any possible compensatory changes seen in this unilateral seeding model, and could also result in more extensive tau pathology spread within the brain. Another possible benefit of bilateral seeding could be that smaller volumes of seed material could be used, as tau spreading from both LCs may overcome the possible reduction in seeding mentioned earlier.

One final possible methodological improvement relates to the form of seed material that we have used in our model. In the previous tau-seeding models, the tau-seeding material has taken various forms. Clavaguera et al. have demonstrated the in vivo seeding potential of brain homogenates from both tau transgenic P301S mice [23] and brain extracts from humans who had died from various tauopathies [67], while we have used synthetic preformed fibrils of K18 [24]. A study by [68] found that the seeding potential of different tau aggregates is affected by the conformation of the aggregates, and as it is currently unknown which form of tau is implicated in the spread of tau between neurons, it could be beneficial to experiment with different seed materials, to determine whether this has an effect on the spatiotemporal progression of tau pathology as compared to our model. While seeding with K18 aggregates has the disadvantage of being artificial, brain homogenates may contain a few other pathogenic molecules, which could cause pathology unrelated to tau pathology. The paired helical filaments (PHFs), which are the main components of neurofibrillary tangles that are naturally found in AD, could act as a more natural seed [69].

In addition, a few other measures of health of these animals were also taken throughout the study, including body weight, 6-day food intake, and core body temperature. Regular weighing also allowed us to investigate the animal's health, as well as monitor the tau-seeded animals for the motor impairments seen in other tau transgenic mouse models with heavy hindbrain pathology. It is of note that none of the animals suffered from any hind limb clasping behavior as seen in the JNPL3 mouse model [15]. It is our view that this novel mouse model along with the robust functional alterations seen in the brains of these animals could be used as a platform for testing experimental therapeutic compounds that target tau pathology early in AD. As mentioned before, it is extremely valuable to have an indication that a therapeutic compound is resulting in a functional improvement in animals, aside from its effects on the pathology itself [11]. Moreover, with some of the possible methodological improvements mentioned earlier, this mouse model could be used to further attempt to understand the nature of the marked functional impairments that have been observed in early stages of AD using EEG rhythms. In particular, reduced EEG coherence has previously been found in individuals homozygous for the APOE $\varepsilon 4$ allele [70]. EEG/EMG connectivity data have been shown to correlate with structural and functional hallmarks of neurodegeneration such as hippocampal atrophy [71]. In recent years, many studies have combined EEG/MEG techniques to graph theories to investigate brain connectivity in AD [9, 41, 72–78]. AD patients are characterized by loss of EEG synchrony among distributed functional networks [79] and significantly reduced interhemispheric theta coherence [79]. Other studies reported the increased delta coherence, decreased theta and alpha coherence, higher alpha and lower delta, and beta small world characteristics of connectivity [80, 81]. A global reduction of functional long-distance brain connectivity and transhemispheric coherence were found in EEG resting states of AD patients [82]. A decreased coherence of high-frequency gamma rhythms has been identified as a specifically predictive sign of conversion from MCI to initial AD [83]. In addition, reduced complex EEG activity and decrease in coherence of fast EEG rhythms were described in EEG of AD patients [9, 84, 85]. Further evidence for a close relation

between dysfunction of cortical connectivity and AD comes from studies investigating effective connectivity of neuronal systems based on Granger causality estimates. Reduced effective connectivity in high-frequency rhythms from parietal to frontal electrodes was observed in AD and MCI patients [86, 87].

Additional newly emerging stimulation techniques such as noninvasive transcranial magnetic stimulation (TMS) have proven reliability in probing selective impairment of specific intracortical circuits in neurodegenerative disorders with primary or secondary tauopathy and in assessing the underlying neurotransmitter deficits [88]. Cerebrospinal fluid tau levels mediate abnormal cortical excitatory activity [89], associated with prominent long-term depression (LTD) mechanisms of cortical plasticity and faster cognitive decline [90]. In animal models of AD, hippocampal long-term potentiation (LTP), which is an electrophysiological correlate of learning and memory, is impaired by Aβ peptides and tau proteins [91–93]. New models of AD pathophysiology have suggested a primary dysfunction of midbrain catecholaminergic systems [94–96]. Aβ-induced dopamine depletion has been suggested as a core mechanism underlying the early synaptopathy and memory alterations observed in AD models and acts by modifying the threshold for the induction of cortical LTP and/or LTD [97]. Dopamine agonists could restore the altered mechanisms of LTP-like cortical plasticity in AD patients, thus providing novel implications for therapies based on dopaminergic stimulation [98]. Early loss of noradrenergic drive contributes to the impairment of cerebellar synaptic plasticity and motor learning [99, 100], and restoration of the noradrenergic tone has been shown to reverse these effects and slow neurodegeneration in animal models of AD [101, 102]. Cortical plasticity measures such as LTP/LTD can be obtained by applying noninvasive repetitive TMS over the primary motor cortex, using theta burst stimulation protocols that mimic those described in animal models. TMS combined with simultaneous EEG provides unique possibilities to study and map the excitability and plasticity of the brain as well as its functional connectivity in a much deeper and time-resolved manner [103–107]. The primary disintegration of hippocampal networks observed in the present mouse model of tauopathy could be used in translational studies in samples of populations with primary tauopathies or of AD patients with high tau accumulation in the brain. Simultaneous recording of TMS-EEG thus offers an important means of directly testing the model.

6. Conclusion

To conclude, we have seen numerous robust functional changes in the hippocampus of mice seeded with K18 aggregates in the deeper brainstem LC area. These changes are indicative of decreasing neuronal activity at the ipsilateral hippocampus, along with some possible compensatory increases in neuronal activity in the contralateral hippocampus, alterations in the functional connectivity of specific functional neural network connections, and decreased theta-gamma PAC, suggesting impaired synaptic plasticity. It is our hope that these results will highlight to the field the relevance of the development of tau pathology in the brainstem early in AD and challenge the belief that it is the spread of tau pathology to a region of the brain in tauopathy which is the necessary sole causal factor for severe functional deterioration of this region.

Data Availability

All relevant data within the article are fully available.

Conflicts of Interest

No conflicts of interest, financial or otherwise, are declared by the authors.

Acknowledgments

We are grateful to L. Raeymaekers and E. Broeckx for their technical assistance. We wish to thank K. Van Kolen PhD for providing the K18 material and D. Moechars PhD for his comments during the initial stage of this research.

References

[1] M. Prince, A. Wimo, M. Guerchet, A. Gemma-Claire, Y. T. Wu, and M. Prina, "The global impact of dementia - an analysis of prevalence, incidence, cost and trends," *Alzheimer's Disease International, 2015 World Alzheimer Report*, vol. 84, 2015.

[2] Alzheimer's Association, "2015 Alzheimer's disease facts and figures," *Alzheimer's & Dementia*, vol. 11, no. 3, pp. 332–384, 2015.

[3] H. Bickel, "Dementia in advanced age: estimating incidence and health care costs," *Zeitschrift für Gerontologie und Geriatrie*, vol. 34, no. 2, pp. 108–115, 2001.

[4] G. G. Glenner and C. W. Wong, "Alzheimer's disease: initial report of the purification and characterization of a novel cerebrovascular amyloid protein," *Biochemical and Biophysical Research Communications*, vol. 120, no. 3, pp. 885–890, 1984.

[5] K. S. Kosik, C. L. Joachim, and D. J. Selkoe, "Microtubule-associated protein tau (tau) is a major antigenic component of paired helical filaments in Alzheimer disease," *Proceedings of the National Academy of Sciences of the United States of America*, vol. 83, no. 11, pp. 4044–4048, 1986.

[6] J. L. Cummings, T. Morstorf, and K. Zhong, "Alzheimer's disease drug-development pipeline: few candidates, frequent failures," *Alzheimer's Research & Therapy*, vol. 6, no. 4, p. 37, 2014.

[7] A. Ahnaou, H. Huysmans, T. Jacobs, and W. H. I. M. Drinkenburg, "Cortical EEG oscillations and network connectivity as efficacy indices for assessing drugs with cognition enhancing potential," *Neuropharmacology*, vol. 86, pp. 362–377, 2014.

[8] A. Horvath, A. Szucs, G. Csukly, A. Sakovics, G. Stefanics, and A. Kamondi, "EEG and ERP biomarkers of Alzheimer's disease: a critical review," *Frontiers in Bioscience*, vol. 23, no. 1, pp. 183–220, 2018.

[9] J. Jeong, "EEG dynamics in patients with Alzheimer's disease," *Clinical Neurophysiology*, vol. 115, no. 7, pp. 1490–1505, 2004.

[10] R. A. Sperling, P. S. Aisen, L. A. Beckett et al., "Toward defining the preclinical stages of Alzheimer's disease: recommendations from the National Institute on Aging-Alzheimer's Association workgroups on diagnostic guidelines for Alzheimer's disease," *Alzheimer's & Dementia*, vol. 7, no. 3, pp. 280–292, 2011.

[11] C. Walsh, W. H. I. M. Drinkenburg, and A. Ahnaou, "Neurophysiological assessment of neural network plasticity and connectivity: progress towards early functional biomarkers for disease interception therapies in Alzheimer's disease," *Neuroscience and Biobehavioral Reviews*, vol. 73, pp. 340–358, 2017.

[12] M. Goedert and M. G. Spillantini, "Tau mutations in frontotemporal dementia FTDP-17 and their relevance for Alzheimer's disease," *Biochimica et Biophysica Acta - Molecular Basis of Disease*, vol. 1502, no. 1, pp. 110–121, 2000.

[13] M. Hutton, C. L. Lendon, P. Rizzu et al., "Association of missense and $5'$-splice-site mutations in tau with the inherited dementia FTDP-17," *Nature*, vol. 393, no. 6686, pp. 702–705, 1998.

[14] O. Bugiani, J. R. Murrell, G. Giaccone et al., "Frontotemporal dementia and corticobasal degeneration in a family with a P301S mutation in *tau*," *Journal of Neuropathology and Experimental Neurology*, vol. 58, no. 6, pp. 667–677, 1999.

[15] J. Lewis, E. McGowan, J. Rockwood et al., "Neurofibrillary tangles, amyotrophy and progressive motor disturbance in mice expressing mutant (P301L) tau protein," *Nature Genetics*, vol. 25, no. 4, pp. 402–405, 2000.

[16] K. Santacruz, J. Lewis, T. Spires et al., "Tau suppression in a neurodegenerative mouse model improves memory function," *Science*, vol. 309, no. 5733, pp. 476–481, 2005.

[17] M. Ramsden, L. Kotilinek, C. Forster et al., "Age-dependent neurofibrillary tangle formation, neuron loss, and memory impairment in a mouse model of human tauopathy (P301L)," *The Journal of Neuroscience*, vol. 25, no. 46, pp. 10637–10647, 2005.

[18] H. Braak and E. Braak, "Neuropathological stageing of Alzheimer-related changes," *Acta Neuropathologica*, vol. 82, no. 4, pp. 239–259, 1991.

[19] D. R. Thal, U. Rüb, M. Orantes, and H. Braak, "Phases of Aβ-deposition in the human brain and its relevance for the development of AD," *Neurology*, vol. 58, no. 12, pp. 1791–1800, 2002.

[20] H. Braak and K. del Tredici, "Alzheimer's pathogenesis: is there neuron-to-neuron propagation?," *Acta Neuropathologica*, vol. 121, no. 5, pp. 589–595, 2011.

[21] P. Brundin, R. Melki, and R. Kopito, "Prion-like transmission of protein aggregates in neurodegenerative diseases," *Nature Reviews Molecular Cell Biology*, vol. 11, no. 4, pp. 301–307, 2010.

[22] H. F. Baker, R. M. Ridley, L. W. Duchen, T. J. Crow, and C. J. Bruton, "Induction of β(A4)-amyloid in primates by injection of Alzheimer's disease brain homogenate. Comparison with transmission of spongiform encephalopathy," *Molecular Neurobiology*, vol. 8, no. 1, pp. 25–39, 1994.

[23] F. Clavaguera, T. Bolmont, R. A. Crowther et al., "Transmission and spreading of tauopathy in transgenic mouse brain," *Nature Cell Biology*, vol. 11, no. 7, pp. 909–913, 2009.

[24] A. Ahnaou, D. Moechars, L. Raeymaekers et al., "Emergence of early alterations in network oscillations and functional connectivity in a tau seeding mouse model of Alzheimer's disease pathology," *Scientific Reports*, vol. 7, no. 1, article 14189, 2017.

[25] H. Braak and K. Del Tredici, "The pathological process underlying Alzheimer's disease in individuals under thirty," *Acta Neuropathologica*, vol. 121, no. 2, pp. 171–181, 2011.

[26] J. Brettschneider, K. D. Tredici, V. M.-Y. Lee, and J. Q. Trojanowski, "Spreading of pathology in neurodegenerative diseases: a focus on human studies," *Nature Reviews Neuroscience*, vol. 16, no. 2, pp. 109–120, 2015.

[27] H. Braak and K. Del Tredici, "Alzheimer's disease: pathogenesis and prevention," *Alzheimer's & Dementia*, vol. 8, no. 3, pp. 227–233, 2012.

[28] S. J. Sara, "The locus coeruleus and noradrenergic modulation of cognition," *Nature Reviews Neuroscience*, vol. 10, no. 3, pp. 211–223, 2009.

[29] E. Shibata, M. Sasaki, K. Tohyama et al., "Age-related changes in locus ceruleus on neuromelanin magnetic resonance imaging at 3 Tesla," *Magnetic Resonance in Medical Sciences*, vol. 5, no. 4, pp. 197–200, 2006.

[30] M. Iba, J. D. McBride, J. L. Guo, B. Zhang, J. Q. Trojanowski, and V. M.-Y. Lee, "Tau pathology spread in PS19 tau transgenic mice following locus coeruleus (LC) injections of synthetic tau fibrils is determined by the LC's afferent and efferent connections," *Acta Neuropathologica*, vol. 130, no. 3, pp. 349–362, 2015.

[31] Y. Yoshiyama, M. Higuchi, B. Zhang et al., "Synapse loss and microglial activation precede tangles in a P301S tauopathy mouse model," *Neuron*, vol. 53, no. 3, pp. 337–351, 2007.

[32] J. J. Palop and L. Mucke, "Amyloid-β-induced neuronal dysfunction in Alzheimer's disease: from synapses toward neural networks," *Nature Neuroscience*, vol. 13, no. 7, pp. 812–818, 2010.

[33] N. Menkes-Caspi, H. G. Yamin, V. Kellner, T. L. Spires-Jones, D. Cohen, and E. A. Stern, "Pathological tau disrupts ongoing network activity," *Neuron*, vol. 85, no. 5, pp. 959–966, 2015.

[34] W. H. I. M. Drinkenburg, G. S. F. Ruigt, and A. Ahnaou, "Pharmaco-EEG studies in animals: an overview of contemporary translational applications," *Neuropsychobiology*, vol. 72, no. 3-4, pp. 151–164, 2016.

[35] P. Bazzigaluppi, T. L. Beckett, M. M. Koletar et al., "Early-stage attenuation of phase-amplitude coupling in the hippocampus and medial prefrontal cortex in a transgenic rat model of Alzheimer's disease," *Journal of Neurochemistry*, vol. 144, no. 5, pp. 669–679, 2018.

[36] C. A. Booth, T. Ridler, T. K. Murray et al., "Electrical and network neuronal properties are preferentially disrupted in dorsal, but not ventral, medial entorhinal cortex in a mouse model of tauopathy," *The Journal of Neuroscience*, vol. 36, no. 2, pp. 312–324, 2016.

[37] R. Goutagny, N. Gu, C. Cavanagh et al., "Alterations in hippocampal network oscillations and theta-gamma coupling arise before Aβ overproduction in a mouse model of Alzheimer's disease," *The European Journal of Neuroscience*, vol. 37, no. 12, pp. 1896–1902, 2013.

[38] T. Nakazono, T. N. Lam, A. Y. Patel et al., "Impaired *in vivo* gamma oscillations in the medial entorhinal cortex of knock-in Alzheimer model," *Frontiers in Systems Neuroscience*, vol. 11, p. 48, 2017.

[39] X. Zhang, W. Zhong, J. Brankačk et al., "Impaired theta-gamma coupling in APP-deficient mice," *Scientific Reports*, vol. 6, no. 1, article 21948, 2016.

[40] J. W. Kowalski, M. Gawel, A. Pfeffer, and M. Barcikowska, "The diagnostic value of EEG in Alzheimer disease: correlation with the severity of mental impairment," *Journal of Clinical Neurophysiology*, vol. 18, no. 6, pp. 570–575, 2001.

[41] G. G. Yener and E. Başar, "Biomarkers in Alzheimer's disease with a special emphasis on event-related oscillatory responses," *Supplements to Clinical Neurophysiology*, vol. 62, pp. 237–273, 2013.

[42] E. Peeraer, A. Bottelbergs, K. van Kolen et al., "Intracerebral injection of preformed synthetic tau fibrils initiates widespread tauopathy and neuronal loss in the brains of tau transgenic mice," *Neurobiology of Disease*, vol. 73, pp. 83–95, 2015.

[43] G. Paxinos and K. Franklin, *Paxinos and Franklin's the mouse brain in stereotaxic coordinates*, Academic Press, 2012.

[44] R. T. Canolty, E. Edwards, S. S. Dalal et al., "High gamma power is phase-locked to theta oscillations in human neocortex," *Science*, vol. 313, no. 5793, pp. 1626–1628, 2006.

[45] A. Ahnaou, H. Huysmans, R. Biermans, N. V. Manyakov, and W. H. I. M. Drinkenburg, "Ketamine: differential neurophysiological dynamics in functional networks in the rat brain," *Translational Psychiatry*, vol. 7, no. 9, p. e1237, 2017.

[46] V. Latora and M. Marchiori, "Efficient behavior of small-world networks," *Physical Review Letters*, vol. 87, no. 19, p. 198701, 2001.

[47] K. J. Blinowska, "Review of the methods of determination of directed connectivity from multichannel data," *Medical & Biological Engineering & Computing*, vol. 49, no. 5, pp. 521–529, 2011.

[48] L. Faes and G. Nollo, "Multivariate frequency domain analysis of causal interactions in physiological time series," in *Biomedical Engineering, Trends in Electronics, Communications and Software*, InTech, 2011.

[49] A. B. L. Tort, R. W. Komorowski, J. R. Manns, N. J. Kopell, and H. Eichenbaum, "Theta–gamma coupling increases during the learning of item–context associations," *Proceedings of the National Academy of Sciences of the United States of America*, vol. 106, no. 49, pp. 20942–20947, 2009.

[50] N. Axmacher, M. M. Henseler, O. Jensen, I. Weinreich, C. E. Elger, and J. Fell, "Cross-frequency coupling supports multi-item working memory in the human hippocampus," *Proceedings of the National Academy of Sciences of the United States of America*, vol. 107, no. 7, pp. 3228–3233, 2010.

[51] R. T. Canolty and R. T. Knight, "The functional role of cross-frequency coupling," *Trends in Cognitive Sciences*, vol. 14, no. 11, pp. 506–515, 2010.

[52] V. M. Y. Lee, T. K. Kenyon, and J. Q. Trojanowski, "Transgenic animal models of tauopathies," *Biochimica et Biophysica Acta - Molecular Basis of Disease*, vol. 1739, no. 2-3, pp. 251–259, 2005.

[53] K. J. Kopeikina, B. T. Hyman, and T. L. Spires-Jones, "Soluble forms of tau are toxic in Alzheimer's disease," *Translational Neuroscience*, vol. 3, no. 3, pp. 223–233, 2012.

[54] B. Vasconcelos, I. C. Stancu, A. Buist et al., "Heterotypic seeding of tau fibrillization by pre-aggregated Abeta provides potent seeds for prion-like seeding and propagation of Tau-pathology in vivo," *Acta Neuropathologica*, vol. 131, no. 4, pp. 549–569, 2016.

[55] H. C. Dringenberg, "Alzheimer's disease: more than a 'cholinergic disorder' - evidence that cholinergic-monoaminergic interactions contribute to EEG slowing and dementia," *Behavioural Brain Research*, vol. 115, no. 2, pp. 235–249, 2000.

[56] A. Ahnaou, R. Biermans, and W. H. I. M. Drinkenburg, "Cholinergic mechanisms of target oddball stimuli detection: the late "P300-like" event-related potential in rats," *Neural Plasticity*, vol. 2018, Article ID 4270263, 15 pages, 2018.

[57] R. N. Kalaria, A. C. Andorn, M. Tabaton, P. J. Whitehouse, S. I. Harik, and J. R. Unnerstall, "Adrenergic receptors in aging and Alzheimer's disease: increased beta 2-receptors in prefrontal cortex and hippocampus," *Journal of Neurochemistry*, vol. 53, no. 6, pp. 1772–1781, 1989.

[58] R. P. Vertes, "Hippocampal theta rhythm: a tag for short-term memory," *Hippocampus*, vol. 15, no. 7, pp. 923–935, 2005.

[59] G. Buzsáki, "Theta oscillations in the hippocampus," *Neuron*, vol. 33, no. 3, pp. 325–340, 2002.

[60] D. Amaral and P. Lavenex, "Hippocampal neuroanatomy," in *The hippocampus book*, P. Andersen, R. Morris, D. Amaral, T. Bliss, and J. O'Keefe, Eds., p. 37, Oxford University Press, New York, NY, USA, 1st edition, 2007.

[61] T. V. P. Bliss and G. L. Collingridge, "A synaptic model of memory: long-term potentiation in the hippocampus," *Nature*, vol. 361, no. 6407, pp. 31–39, 1993.

[62] L. M. Grover, E. Kim, J. D. Cooke, and W. R. Holmes, "LTP in hippocampal area CA1 is induced by burst stimulation over a broad frequency range centered around delta," *Learning & Memory*, vol. 16, no. 1, pp. 69–81, 2009.

[63] V. Drago, C. Babiloni, D. Bartrés-Faz et al., "Disease tracking markers for Alzheimer's disease at the prodromal (MCI) stage," *Journal of Alzheimer's Disease*, vol. 26, no. s3, pp. 159–199, 2011.

[64] E. L. Newman, S. N. Gillet, J. R. Climer, and M. E. Hasselmo, "Cholinergic blockade reduces theta-gamma phase amplitude coupling and speed modulation of theta frequency consistent with behavioral effects on encoding," *The Journal of Neuroscience*, vol. 33, no. 50, pp. 19635–19646, 2013.

[65] K. Belarbi, S. Burnouf, F. J. Fernandez-Gomez et al., "Loss of medial septum cholinergic neurons in THY-Tau22 mouse model: what links with tau pathology?," *Current Alzheimer Research*, vol. 8, no. 6, pp. 633–638, 2011.

[66] A. Sirota, S. Montgomery, S. Fujisawa, Y. Isomura, M. Zugaro, and G. Buzsaki, "Entrainment of neocortical neurons and gamma oscillations by the hippocampal theta rhythm," *Neuron*, vol. 60, no. 4, pp. 683–697, 2008.

[67] F. Clavaguera, H. Akatsu, G. Fraser et al., "Brain homogenates from human tauopathies induce tau inclusions in mouse brain," *Proceedings of the National Academy of Sciences of the United States of America*, vol. 110, no. 23, pp. 9535–9540, 2013.

[68] B. Falcon, A. Cavallini, R. Angers et al., "Conformation determines the seeding potencies of native and recombinant Tau aggregates," *The Journal of Biological Chemistry*, vol. 290, no. 2, pp. 1049–1065, 2015.

[69] I. Grundke-Iqbal, K. Iqbal, M. Quinlan, Y. C. Tung, M. S. Zaidi, and H. M. Wisniewski, "Microtubule-associated protein tau. A component of Alzheimer paired helical filaments," *Journal of Biology*, vol. 261, pp. 6084–6089, 1986.

[70] V. Jelic, P. Julin, M. Shigeta et al., "Apolipoprotein E ε4 allele decreases functional connectivity in Alzheimer's disease as measured by EEG coherence," *Journal of Neurology, Neurosurgery, and Psychiatry*, vol. 63, no. 1, pp. 59–65, 1997.

[71] C. Babiloni, G. B. Frisoni, M. Pievani et al., "Hippocampal volume and cortical sources of EEG alpha rhythms in mild cognitive impairment and Alzheimer disease," *NeuroImage*, vol. 44, no. 1, pp. 123–135, 2009.

[72] M. D'Amelio and P. M. Rossini, "Brain excitability and connectivity of neuronal assemblies in Alzheimer's disease: from animal models to human findings," *Progress in Neurobiology*, vol. 99, no. 1, pp. 42–60, 2012.

[73] C. Babiloni, R. Lizio, N. Marzano et al., "Brain neural synchronization and functional coupling in Alzheimer's disease as revealed by resting state EEG rhythms," *International Journal of Psychophysiology*, vol. 103, pp. 88–102, 2016.

[74] C. J. Stam, "Use of magnetoencephalography (MEG) to study functional brain networks in neurodegenerative disorders," *Journal of the Neurological Sciences*, vol. 289, no. 1-2, pp. 128–134, 2010.

[75] S. Teipel, M. J. Grothe, J. Zhou et al., "Measuring cortical connectivity in Alzheimer's disease as a brain neural network pathology: toward clinical applications," *Journal of the International Neuropsychological Society*, vol. 22, no. 2, pp. 138–163, 2016.

[76] C. J. Stam, T. Montez, B. F. Jones et al., "Disturbed fluctuations of resting state EEG synchronization in Alzheimer's disease," *Clinical Neurophysiology*, vol. 116, no. 3, pp. 708–715, 2005.

[77] C. J. Stam, W. de Haan, A. Daffertshofer et al., "Graph theoretical analysis of magnetoencephalographic functional connectivity in Alzheimer's disease," *Brain*, vol. 132, no. 1, pp. 213–224, 2009.

[78] J. Dauwels, F. Vialatte, and A. Cichocki, "Diagnosis of Alzheimer's disease from EEG signals: where are we standing?," *Current Alzheimer Research*, vol. 7, no. 6, pp. 487–505, 2010.

[79] G. Adler, S. Brassen, and A. Jajcevic, "EEG coherence in Alzheimer's dementia," *Journal of Neural Transmission*, vol. 110, no. 9, pp. 1051–1058, 2003.

[80] S. Marceglia, S. Mrakic-Sposta, M. Rosa et al., "Transcranial direct current stimulation modulates cortical neuronal activity in Alzheimer's disease," *Frontiers in Neuroscience*, vol. 10, p. 134, 2016.

[81] F. Vecchio, F. Miraglia, F. Piludu et al., ""Small world" architecture in brain connectivity and hippocampal volume in Alzheimer's disease: a study via graph theory from EEG data," *Brain Imaging and Behavior*, vol. 11, no. 2, pp. 473–485, 2017.

[82] S. J. Teipel, O. Pogarell, T. Meindl et al., "Regional networks underlying interhemispheric connectivity: an EEG and DTI study in healthy ageing and amnestic mild cognitive impairment," *Human Brain Mapping*, vol. 30, no. 7, pp. 2098–2119, 2009.

[83] P. M. Rossini, C. del Percio, P. Pasqualetti et al., "Conversion from mild cognitive impairment to Alzheimer's disease is predicted by sources and coherence of brain electroencephalography rhythms," *Neuroscience*, vol. 143, no. 3, pp. 793–803, 2006.

[84] J. Dauwels, F. Vialatte, C. Latchoumane, J. Jeong, and A. Cichocki, "EEG synchrony analysis for early diagnosis of Alzheimer's disease: a study with several synchrony measures and EEG data sets," in *2009 Annual International Conference of the IEEE Engineering in Medicine and Biology Society*, pp. 2224–2227, Minneapolis, MN, USA, 2009.

[85] F. J. Fraga, T. H. Falk, P. A. M. Kanda, and R. Anghinah, "Characterizing Alzheimer's disease severity via resting-awake EEG amplitude modulation analysis," *PLoS One*, vol. 8, no. 8, article e72240, 2013.

[86] K. J. Blinowska, F. Rakowski, M. Kaminski et al., "Functional and effective brain connectivity for discrimination between Alzheimer's patients and healthy individuals: a study on resting state EEG rhythms," *Clinical Neurophysiology*, vol. 128, no. 4, pp. 667–680, 2017.

[87] C. Babiloni, R. Ferri, G. Binetti et al., "Directionality of EEG synchronization in Alzheimer's disease subjects," *Neurobiology of Aging*, vol. 30, no. 1, pp. 93–102, 2009.

[88] A. Benussi, V. Dell'Era, V. Cantoni et al., "Discrimination of atypical parkinsonisms with transcranial magnetic stimulation," *Brain Stimulation*, vol. 11, no. 2, pp. 366–373, 2018.

[89] G. Koch, Z. Esposito, H. Kusayanagi et al., "CSF tau levels influence cortical plasticity in Alzheimer's disease patients," *Journal of Alzheimer's Disease*, vol. 26, no. 1, pp. 181–186, 2011.

[90] G. Koch, F. di Lorenzo, M. F. del Olmo et al., "Reversal of LTP-like cortical plasticity in Alzheimer's disease patients with tau-related faster clinical progression," *Journal of Alzheimer's Disease*, vol. 50, no. 2, pp. 605–616, 2016.

[91] S. Gelman, J. Palma, G. Tombaugh, and A. Ghavami, "Differences in synaptic dysfunction between rTg4510 and APP/PS1 mouse models of Alzheimer's disease," *Journal of Alzheimer's Disease*, vol. 61, no. 1, pp. 195–208, 2017.

[92] I. Klyubin, V. Betts, A. T. Welzel et al., "Amyloid β protein dimer-containing human CSF disrupts synaptic plasticity: prevention by systemic passive immunization," *The Journal of Neuroscience*, vol. 28, no. 16, pp. 4231–4237, 2008.

[93] D. Puzzo, R. Piacentini, M. Fá et al., "LTP and memory impairment caused by extracellular Aβ and tau oligomers is APP-dependent," *eLife*, vol. 6, article e26991, 2017.

[94] G. D. Femminella, D. Leosco, N. Ferrara, and G. Rengo, "Adrenergic drugs blockers or enhancers for cognitive decline? What to choose for Alzheimer's disease patients?," *CNS & Neurological Disorders Drug Targets*, vol. 15, no. 6, pp. 665–671, 2016.

[95] S. C. Kelly, B. He, S. E. Perez, S. D. Ginsberg, E. J. Mufson, and S. E. Counts, "Locus coeruleus cellular and molecular pathology during the progression of Alzheimer's disease," *Acta Neuropathologica Communications*, vol. 5, no. 1, p. 8, 2017.

[96] A. Martorana and G. Koch, "Is dopamine involved in Alzheimer's disease?," *Frontiers in Aging Neuroscience*, vol. 6, p. 252, 2014.

[97] P. Moreno-Castilla, L. F. Rodriguez-Duran, K. Guzman-Ramos, A. Barcenas-Femat, M. L. Escobar, and F. Bermudez-Rattoni, "Dopaminergic neurotransmission dysfunction induced by amyloid-β transforms cortical long-term potentiation into long-term depression and produces memory impairment," *Neurobiology of Aging*, vol. 41, pp. 187–199, 2016.

[98] G. Koch, F. Di Lorenzo, S. Bonnì et al., "Dopaminergic modulation of cortical plasticity in Alzheimer's disease patients," *Neuropsychopharmacology*, vol. 39, no. 11, pp. 2654–2661, 2014.

[99] M. Gannon, P. Che, Y. Chen, K. Jiao, E. D. Roberson, and Q. Wang, "Noradrenergic dysfunction in Alzheimer's disease," *Frontiers in Neuroscience*, vol. 9, p. 220, 2015.

[100] T. Hammerschmidt, M. P. Kummer, D. Terwel et al., "Selective loss of noradrenaline exacerbates early cognitive dysfunction and synaptic deficits in APP/PS1 mice," *Biological Psychiatry*, vol. 73, no. 5, pp. 454–463, 2013.

[101] T. Chalermpalanupap, B. Kinkead, W. T. Hu et al., "Targeting norepinephrine in mild cognitive impairment and Alzheimer's disease," *Alzheimer's Research & Therapy*, vol. 5, no. 2, p. 21, 2013.

[102] J. A. Ross, P. McGonigle, and E. J. Van Bockstaele, "Locus coeruleus, norepinephrine and Aβ peptides in Alzheimer's disease," *Neurobiology of Stress*, vol. 2, pp. 73–84, 2015.

[103] F. Ferreri and P. M. Rossini, "TMS and TMS-EEG techniques in the study of the excitability, connectivity, and plasticity of the human motor cortex," *Reviews in the Neurosciences*, vol. 24, no. 4, pp. 431–442, 2013.

[104] F. Ferreri, F. Vecchio, L. Vollero et al., "Sensorimotor cortex excitability and connectivity in Alzheimer's disease: a TMS-EEG co-registration study," *Human Brain Mapping*, vol. 37, no. 6, pp. 2083–2096, 2016.

[105] A. Guerra, F. Assenza, F. Bressi et al., "Transcranial magnetic stimulation studies in Alzheimer's disease," *International Journal of Alzheimer's Disease*, vol. 2011, article 263817, pp. 1–9, 2011.

[106] R. J. Ilmoniemi and D. Kičić, "Methodology for combined TMS and EEG," *Brain Topography*, vol. 22, no. 4, pp. 233–248, 2010.

[107] G. Thut and A. Pascual-Leone, "A review of combined TMS-EEG studies to characterize lasting effects of repetitive TMS and assess their usefulness in cognitive and clinical neuroscience," *Brain Topography*, vol. 22, no. 4, pp. 219–232, 2010.

Hindawi
Neural Plasticity
Volume 2019, Article ID 1619290, 11 pages
https://doi.org/10.1155/2019/1619290

Research Article

Aging Does Not Affect Beta Modulation during Reaching Movements

Serena Ricci,[1,2] **Ramtin Mehraram**,[1,3] **Elisa Tatti**,[1] **Aaron B. Nelson**,[1] **Martina Bossini-Baroggi**,[2] **Priya Panday**,[1] **Nancy Lin**,[1] **and M. Felice Ghilardi**[1]

[1]*CUNY Medical School, New York, NY 10031, USA*
[2]*DIBRIS University of Genoa, 16145, Italy*
[3]*Institute of Neuroscience, Newcastle University, NE17RU, UK*

Correspondence should be addressed to Serena Ricci; ricci_serena@ymail.com and M. Felice Ghilardi; lice.mg79@gmail.com

Received 1 February 2019; Revised 9 April 2019; Accepted 17 April 2019; Published 15 May 2019

Guest Editor: Giovanni Pellegrino

During movement, modulation of beta power occurs over the sensorimotor areas, with a decrease just before its start (event-related desynchronization, ERD) and a rebound after its end (event-related synchronization, ERS). We have recently found that the depth of ERD-to-ERS modulation increases during practice in a reaching task and the following day decreases to baseline levels. Importantly, the magnitude of the beta modulation increase during practice is highly correlated with the retention of motor skill tested the following day. Together with other evidence, this suggests that the increase of practice-related modulation depth may be the expression of sensorimotor cortex's plasticity. Here, we determine whether the practice-related increase of beta modulation depth is equally present in a group of younger and a group of older subjects during the performance of a 30-minute block of reaching movements. We focused our analyses on two regions of interest (ROIs): the left sensorimotor and the frontal region. Performance indices were significantly different in the two groups, with the movements of older subjects being slower and less accurate. Importantly, both groups presented a similar increase of the practice-related beta modulation depth in both ROIs in the course of the task. Peak latency analysis revealed a progressive delay of the ERS peak that correlated with the total movement time. Altogether, these findings support the notion that the depth of beta modulation in a reaching movement task does not depend on age and confirm previous findings that only ERS peak latency but not ERS magnitude is related to performance indices.

1. Introduction

Movement is associated with changes of the electroencephalographic (EEG) activity in the beta frequency range from 15 to 30 Hz recorded mainly over the sensorimotor cortex. During movement planning, beta power decreases reaching a minimum at the end of the movement, event-related desynchronization (ERD) [1]. After the movement, beta power shows a rebound, defined as event-related synchronization (ERS) [2]. Likely, ERD reflects the increased excitability of the motor cortex and the deactivation of somatosensory areas. ERS, instead, may represent the reactivation of the somatosensory area following the motor activity [3, 4]. There is no clear evidence as to whether ERD and ERS characteristics are related to specific movement attributes [5–7] or whether they change with aging or neurodegenerative processes [8–10]. Interestingly, we have recently found that during practice in a reaching task, ERS magnitude increases [11, 12], independently of possible changes in mean power. Such practice-related increases are also evident in the beta modulation depth, computed as the ERS-ERD peak-to-peak difference. Importantly, we have also found that beta modulation decreased to baseline levels twenty-four hours later and that the magnitude of its increase during practice was correlated with retention of motor skill tested the following day [10]. Thus, we interpreted the beta modulation changes occurring during practice as reflecting plasticity-related phenomena: indeed, human and animal studies have shown that beta power increases in parallel with a reduction of cortical excitability and with an increase of GABA levels [13, 14]. In

this context, the recurring activation and inactivation of the sensory and motor areas during our task with repetitive reaching movements may be an appropriate scenario to trigger long-term potentiation- (LTP-) related phenomena and may result in an increase of beta modulation depth. In turn, such an increase may reflect a progressive saturation of the mechanisms related to LTP-like plasticity. This idea is supported by work in animal and humans. In particular, high beta power likely reflects high GABA levels [14–20], thus linking increases in beta power to increases of inhibitory processes as well as to decreases of cortical excitability and LTP-related processes. Furthermore, theta burst TMS protocols that modulate local plasticity also induce local changes not only in cortical excitability but also in beta power [13, 21, 22]. Finally, in Parkinson's disease (PD), which is characterized by alterations in the beta frequency range [23–25] and impaired plasticity [26–31], we did not find either the practice-related increases of beta power or the retention of motor improvement that was present in normal subjects. As neural plasticity declines with increasing age [32], it is possible that practice-related beta modulation would also be affected by aging. However, studies on either beta oscillatory activity or plasticity of the sensorimotor cortex report controversial results. For instance, a recent work with a motor sequence task reported increased ERD amplitude over the contralateral sensorimotor area in older (aged from 54 to 75 years) compared to younger adults (aged from 20 to 42 years) [8]. In contrast, another study with a grip task [19] showed a lack of correlation between age and movement-related beta ERD in the contralateral motor area. Similarly, the studies testing LTP-like plasticity of the sensorimotor cortex with paired-associative stimulation (PAS) protocols yielded contrasting results [33–35].

In the present study, we ascertain in a group of younger and older adults whether healthy aging affects practice-related changes both in terms of magnitude and peak latency of ERD and ERS during a reaching task with the right hand. We focused on the left sensorimotor cortex and on a frontal region that, in previous studies, showed robust beta modulation [11, 12].

2. Materials and Methods

2.1. Subjects. We tested two groups of subjects: a younger group, with thirteen subjects (mean age ± SD: 24.2 ± 4.5 years, ten women) and an older group with thirteen subjects (mean age ± SD: 57.5 ± 8.2 years, six women). All subjects were right-handed, as determined by the Edinburgh inventory [36], and had no history of neurological or psychiatric disorders. Experiments were conducted with the approval of our Institutional Review Board, and written informed consent was obtained from all participants.

2.2. Experimental Design and Motor Task. All experiments were run in the morning. Subjects were fitted with high-density 256-electrode EEG cap. The two groups of subjects performed a reaching task (MOT) for 30 minutes. Specifically, as described in previous papers [37, 38], subjects were seated in front of a computer screen and moved a hand-held cursor on a digitizing tablet with their right upper limb that was hidden by an opaque surface (Figure 1(a)). On the screen, an array of eight targets (1 cm diameter circles) that was equidistant (4 cm) from a central starting point was present at all times together with the position of the cursor. One of the eight targets blackened with a 1.5 s interval for 400 ms in a random order; subjects were instructed to move as soon as possible, minimizing reaction time but avoiding anticipation or guessing, to make overlapping out-and-back movements without corrections or stops with sharp reversal within the target (Figure 1(b)). Before the first testing session, all subjects were trained in this task to reach a hit rate of at least 95%.

The session encompassed a total of 840 target presentations divided into 15 sets of 56 each. Between two consecutive sets, subjects paused for an average of 30 seconds.

For each movement, we computed the following: reaction time, defined as the time from the target appearance to the movement onset; total movement time, defined as the time from movement onset to the end of the out and back stroke; peak velocity; and hand-path area, a measure that reflects interjoint coordination, computed as the area included in the trajectory normalized by path length squared (Figure 1(b)). For each subject, we discarded outlier movements that met one of the following criteria: reaction time exceeding 2 SD from the subject's mean, directional error greater than 22°, and movement end less than 100 ms before the presentation of the next target.

2.3. EEG

2.3.1. EEG Recording. A high-density EEG was recorded from 256 electrodes (HydroCel net, Electrical Geodesics Inc.) for the entire duration of the experiment with a sampling rate of 250 Hz, using the high impedance amplifier Net Amp 300 and Net Station 4.3. Impedances were kept below 30 kΩ, and the signal was referenced to the vertex Cz.

2.3.2. EEG Data Preprocessing. Data were preprocessed using the public Matlab toolbox EEGLAB [39]. The continuous EEG signal was filtered with a passband two-way least-square FIR filter between 1 and 80 Hz and a notch filter centered at 60 Hz. Then, signal was divided into 4-second epochs, centered at the stimulus onset (-1 to 3 seconds). Also, recordings were visually inspected to define artefactual epochs and channels. Channels affected by bad scalp-electrode contact were replaced with spherical spline interpolation, and artefactual epochs were removed from the recording. Stereotypical artifacts, such as blinks, eye movements, and motion-related signals, were removed with Independent Component Analysis (ICA) with Principal Component Analysis- (PCA-) based dimension reduction [40]. Briefly, we visually inspected the power spectral density, topographical maps, and time activations of each estimated component. The components identified as "artefactual" were removed from the raw EEG signal. Finally, the signal was averaged referenced to proceed with the analyses and reduced to 180 channels, removing 76 channels located on the cheeks and the neck.

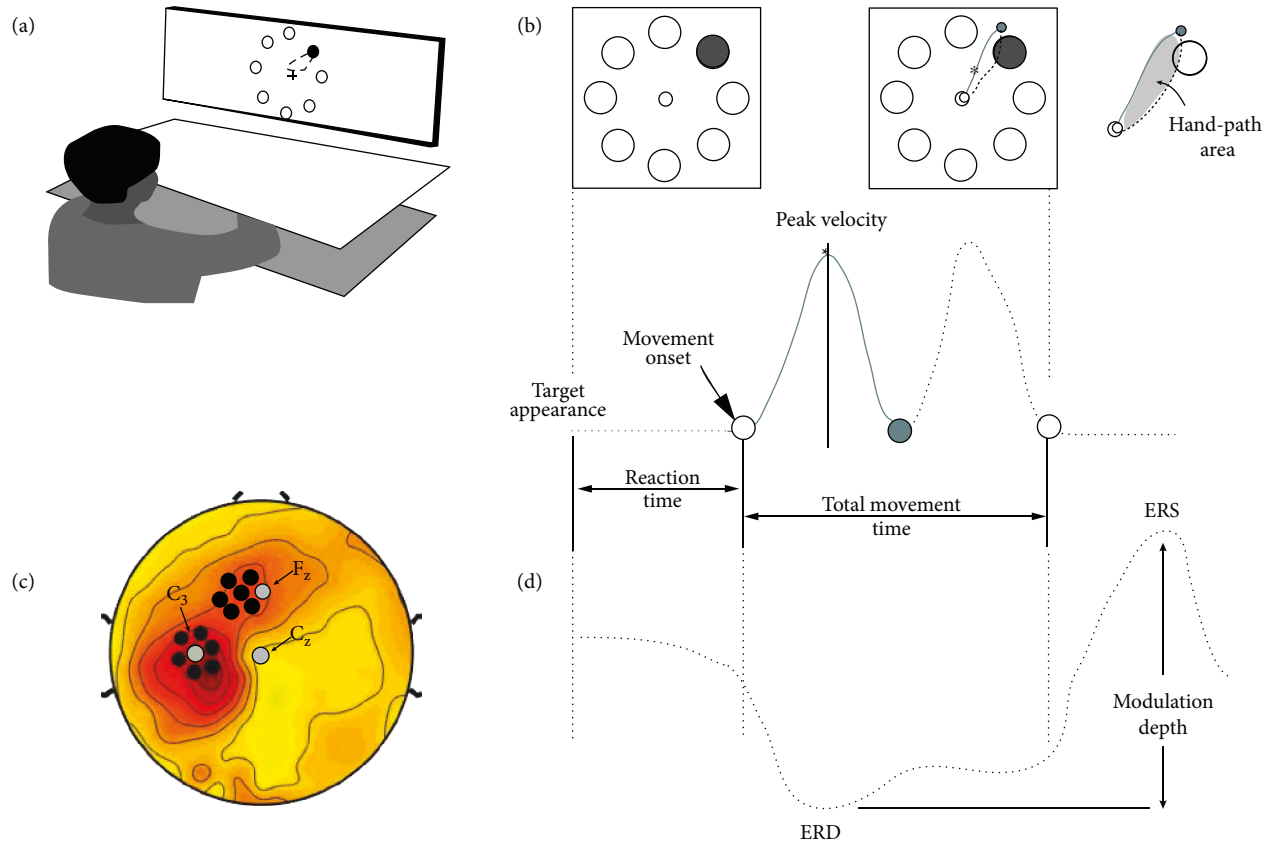

Figure 1: Experimental design and kinematic measures. (a) Testing set up. (b) Upper line: target display on the screen with the appearance of the target (left); the hand-path display during the movement (center); in grey, the hand-path area (left). Bottom line: temporal profile of trajectory velocity with the kinematic parameters used in the analyses. (c) Definition of the regions of interest (ROIs): the left and the frontal ROIs (black dots) with Cz, Fz, and C3 (grey dots). (d) Representation of beta power changes related to target appearance, movement onset, and end. The peak of event-related desynchronization (ERD) is followed by a rebound (or event-related synchronization, ERS) after the movement end. Beta modulation is defined as the difference between ERD and ERS power.

2.3.3. EEG Data Analyses. As a first step, we aligned each valid trial (i.e., trials that were not discarded from either EEG or kinematic preprocessing) to the time of movement onset; then, we computed time-frequency representations in the 15 to 30 Hz range (0.25 Hz steps), using a short-time Fourier transform approach (Hanning taper, time step-size of 20 ms, 5 cycles adaptive window width). Beta power of each trial and region of interest (ROI) was normalized using the average beta power value computed over the entire motor session as such: $\sum_i^{i=1:\text{trials}}((\text{BetaEEG}i - \text{TotPower})/\text{TotPower})$, with TotPower defined as the total beta power across all the trials. First, we ascertained whether the two groups of subjects had a comparable beta power in both ROIs with nonparametric permutation testing with false discovery rate correction. Then, we determined the amplitudes of ERD and ERS: ERD amplitude was defined as the minimum value of beta power within an interval between 200 ms before movement onset to 700 ms after it; ERS amplitude was the maximum value in the interval from 500 to 1500 ms. Beta modulation depth was computed as the difference between ERS and ERD. We then averaged the data of all the subjects to define two ROIs centered where beta modulation was maximal. Specifically, we defined a left sensorimotor ROI, which was centered on C3 with six neighbor electrodes, and a frontal ROI, which was centered on the electrode between Fz and F3 and its six neighbors (Figure 1(c)).

Afterwards, trials were averaged across sets to determine time and group differences, as well as across all trials to assess time differences in the two groups. All the analyses have been implemented using the FieldTrip toolbox for Matlab [41].

2.4. Statistical Analysis. To quantify the changes of EEG (ERD and ERS magnitude and peak latency) and kinematic measures (reaction time, peak velocity, hand-path area, and total movement time) across sets, we performed repeated measure multivariate ANOVAs (MANOVA) with Group (younger, older) as between-subject effect and practice (15 sets) and parameters and ROI (left and front, only for the EEG analysis) as within-subject effects. We also used univariate mixed model ANOVA for EEG parameters for each ROI (including beta modulation depth) and for kinematic measurements with practice (15 sets) as within-subject effect. All the results had been Greenhouse-Geisser corrected since the assumption of sphericity was violated (Mauchly's test). Pearson coefficients were used to explore significant correlations between kinematic and EEG peak latency parameters.

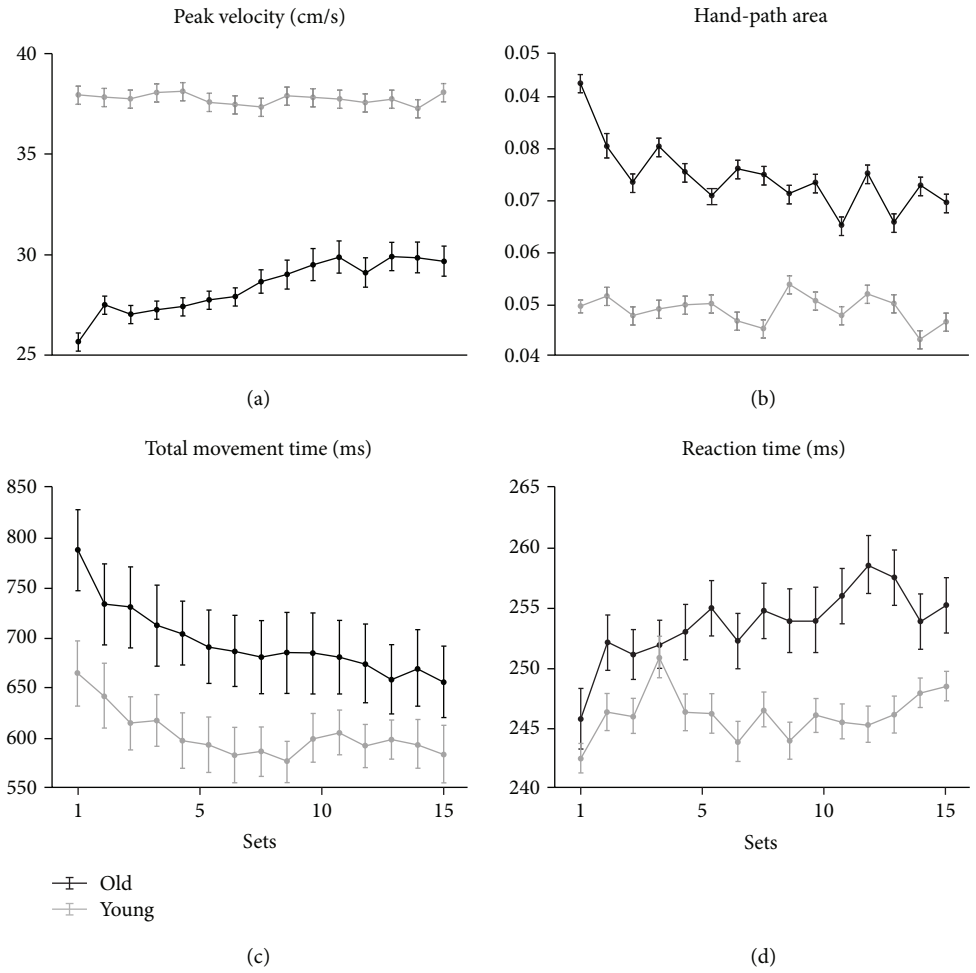

Figure 2: Average of kinematic measures of each set (56 movements each) for the younger (grey lines and dots) and older (black lines and dots) groups. The vertical bars represent standard errors of the mean.

Normality was tested with the Lilliefors test. We used two-tailed paired t-tests to determine a significant group difference for both ERD and ERS peak latency. Results were considered significant with a p value < 0.05. All statistical analyses were conducted using SPSS v25 and Matlab 2017b.

3. Results and Discussion

3.1. Motor Performance Differs in Younger and Older Subjects. All participants completed the session without any difficulty. In general, movements were mostly straight with bell-shaped velocity profiles in all subjects. The performance measures of the two groups across sets are illustrated in Figure 2. The results of the repeated measure MANOVA revealed an overall effect of practice ($F_{(56,1297.47)} = 2.86$, $p < 0.001$) and group ($F_{(4,21)} = 8.80$, $p < 0.001$) and a trend toward significance in the Practice∗ Group interaction ($F_{(56,1297.47)} = 1.26$, $p = 0.096$). Results of the univariate tests are reported in Table 1. Specifically, peak velocity values were significantly greater in the younger group without significant changes across sets (Table 1, Figure 2(a)). However, inspection of the data showed some increase across sets, although not significant, only in the older group (Figure 2(a)). In parallel, total movement time was significantly longer in older subjects, with significant decreases across sets in both groups (Table 1, Figure 2(c)). Hand-path area, an inverse measure of spatial accuracy that depends on velocity, was greater in the older participants but decreased in both groups across sets, as shown by a borderline p value (Table 1, Figure 2(b)). Finally, reaction times were rather stable across sets and were slightly longer in the older group, despite mixed model ANOVA did not reveal any main effect or interaction (Table 1, Figure 2(d)). In summary, these results suggest that movements in the older group were slower and spatially less accurate than in the younger group, as confirmed by correlations between the mean values of kinematic parameters and age (peak velocity: $R^2 = 0.43$, $p < 0.001$; hand-path area: $R^2 = 0.28$, $p = 0.006$; total movement time: $R^2 = 0.30$, $p = 0.004$). Additionally, we found a strong correlation between age and the decrease of hand-path area from the first to the last set ($R^2 = 0.29$, $p = 0.005$, Supplementary Table 1). Deterioration of motor performance in the elderly has been reported in several publications, involving spatial and temporal characteristics of motor performance.

Table 1: Results of the repeated measure ANOVA, univariate tests of peak velocity, hand-path area, and reaction time comparing groups across practice.

	Group		Practice		GroupXPractice	
	$F_{(1,24)}$	p	$F_{(14,336)}$	p	$F_{(14,336)}$	p
Peak velocity	**9.51**	**0.005**	1.32	0.277	1.63	0.209
Hand-path area	**8.63**	**0.007**	2.02	0.059	1.80	0.095
Reaction time	0.47	0.501	1.52	0.189	0.92	0.468
Total movement time	**4.82**	**0.038**	**14.94**	**<0.001**	0.78	0.515

Table 2: Results of mixed model univariate ANOVAs for the magnitude of ERD and ERS and beta modulation depth.

	Group (G)		Practice (P)		ROI (R)		P∗G		R∗G		P∗R		P∗R∗G	
	F	p	F	p	F	p	F	p	F	p	F	p	F	p
ERD	0.07	0.788	**2.48**	**0.035**	**6.88**	**0.015**	0.51	0.770	3.05	0.094	1.01	0.424	1.39	0.225
ERS	0.68	0.417	**8.97**	**<0.001**	1.09	0.307	0.67	0.654	1.59	0.219	0.69	0.626	0.83	0.526
β Modulation	0.56	0.460	**9.13**	**<0.001**	1.44	0.241	0.67	0.657	1.78	0.195	0.71	0.614	0.78	0.563

The causes of this decline are multiple and may involve, singly or in combination, muscular, skeletal, and the central and peripheral nervous systems. During aging, progressive muscle deterioration [42], increased muscle fatigability, and sarcopenia [43–46] may occur with loss of motor units, remodeling of neuromuscular junctions, and eventually with alteration of peripheral and neuromuscular transmissions [47–49]. Besides decreasing muscle strength [50], aging may also impair proprioceptive processing [51], as well as the function of cortical motor regions [48] and the basal ganglia [52]. This can result in mobility problems and an increased risk of falling [53]. Our results showed that, besides being slower, the movements of the older group had greater hand-path area values, suggesting a worse interjoint coordination [54–56]. This occurred despite the older groups' movements were slower, and thus, the interaction torques developing during movement should have been easier to counteract, and movements should have had overlapping trajectories. Intact proprioception is necessary for overcoming these forces not only by providing feedback during the movement but also by updating the sensorimotor memories used to program movements through feedforward mechanisms [54–56]. Therefore, even small problems in proprioception information processing, as the ones reported in aging, may produce deficits of intersegmental dynamics, despite low movement velocities, thus resulting in increases of both interjoint timing and hand-path area. Importantly, the older group also showed a decrease of hand-path area across sets with values approaching the range of the younger group in the last sets. This decrease occurred together with an increase of peak velocity, suggesting that some skill learning occurred in the older group. These practice-related improvements also indicate a shift toward the use of feedforward mechanisms and possibly suggest memory formation in this particular aspect of performance [11]. To be noticed, performance of the younger group reached a plateau already in the first set, thus minimizing the significance of the improvements during the last set. This conclusion is supported also by the fact that the values of hand-path area in the older group hardly reached those of the younger subjects (see Figure 2(b)). Therefore, our results suggest that, despite average differences, both groups displayed some learning.

3.2. Beta Modulatory Activity Is Similar in Younger and Older Subjects. We next analyzed the power changes across sets of beta ERD and ERS in the two groups for the left and frontal ROIs. Results are reported in Table 2 and Supplementary Table 2 and illustrated in Figure 3. Multivariate tests with ERD and ERS magnitude did not reveal significant group differences or interactions (Group: $F_{(2,23)} = 1.121$, $p = 0.343$; Practice∗Group: $F_{(28,672)} = 0.548$, $p = 0.973$; ROI∗Group: $F_{(2,23)} = 1.47$, $p = 0.251$; Practice∗ROI: $F_{(28,670)} = 0.899$, $p = 0.618$; Practice∗ROI∗Group: $F_{(28,670)} = 1.00$, $p = 0.465$). Nevertheless, we found the main effects of practice and ROI ($F_{(28,672)} = 4.69$, $p < 0.001$; $F_{(2,23)} = 3.71$, $p = 0.040$, respectively). The results of univariate mixed model ANOVAs for ERD and ERS (Table 2) confirmed a significant effect of practice for both measures. They also revealed a difference between ROIs for ERD magnitude (see also: Supplementary Table 2 and Figure 3). Over the frontal ROI, the significant across-set increase extended also to beta ERD (Supplementary Table 2): inspection of the data in Figure 3 suggests that such an effect was more evident, although not significantly so, in the older group. Indeed, some works have shown that older participants need to recruit additional resources in sensorimotor and premotor areas to achieve normal movement execution [57–61]. Thus, the progressive increase of ERD magnitude in older subjects over the frontal ROI may reflect an increased recruitment to improve performance across sets. Univariate mixed model ANOVA for beta modulation depth (Table 2) revealed only a main effect of practice, without any interaction between variables. Finally, as in previous studies [11, 12], we found no significant

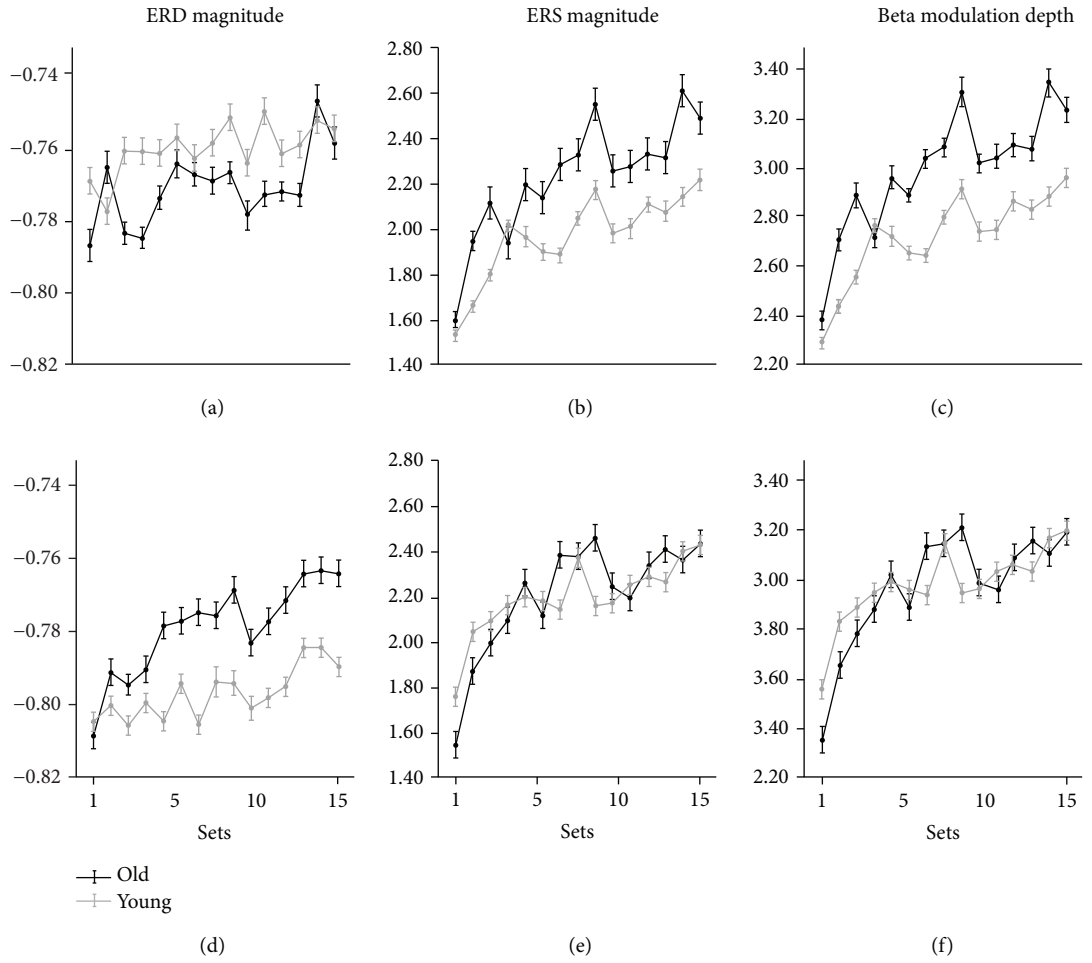

Figure 3: Average of ERD (a, d), ERS (b, e), and beta modulation (c, f) magnitudes for the left (upper row) and frontal (lower row) ROIs for each set in the younger (grey lines and dots) and older (black lines and dots) groups. The vertical bars represent the standard errors of the mean.

correlation between the practice-related changes of ERD, ERS, or beta modulation and the performance changes across sets. Altogether, these results suggest that practice-related changes of beta modulation in both ROIs are very similar in the two groups. Further analyses on all subjects showed no correlation between the mean values of ERD, ERS, and modulation depth and the subjects' age for both left and frontal ROIs (all: $R^2 < 0.01$, $p > 0.50$). Also, correlations between magnitude difference across sets and age did not reveal any direct link between beta modulation and anagraphical age (Supplementary Table 1). These results are in agreement with a study showing no age effect on the mean value of ERD recorded over the left sensorimotor area with a grip task [19], but at odds with a work demonstrating that mean ERD amplitude was greater in older subjects during a motor sequence task [8]. It is conceivable that such discrepant results may originate from differences in task characteristics and sample size. Also, anagraphical age may not be the only and best predictor of changes in cortical function and performance, as it is increasingly more evident that exercise and other factors play important roles in decreasing or accelerating aging processes.

As mentioned earlier, the most novel result is that the increases of beta modulation across sets are similar in the younger and older groups, and notably, this occurs despite important group differences in performance indices (see Figure 2). This result prompts two sets of considerations. First, the magnitude of movement-related beta oscillations does not directly reflect movement characteristics, in line with other studies reporting a lack of correlation between ERD ERS and speed [5, 62], force [63–65], movement type [6], or muscle pattern [7]. Specifically, previous studies found beta oscillatory differences in slow versus fast movements [5]; however, a correlation between EMG burst and ERS latency was detected only for slow movements. Similarly, no direct relationship between movement parameters and ERS, despite an ERS difference between extension-flexion and flexion-extension movements, had been found [66]. Also, a recent work from our research group indicated that no link between movement extent and beta modulation magnitude is detected in upper limb reaching movements [67]. Indeed, movement-related beta oscillations may be related to sensorimotor integration processes associated with movement planning and execution rather than explicitly reflecting the coding of

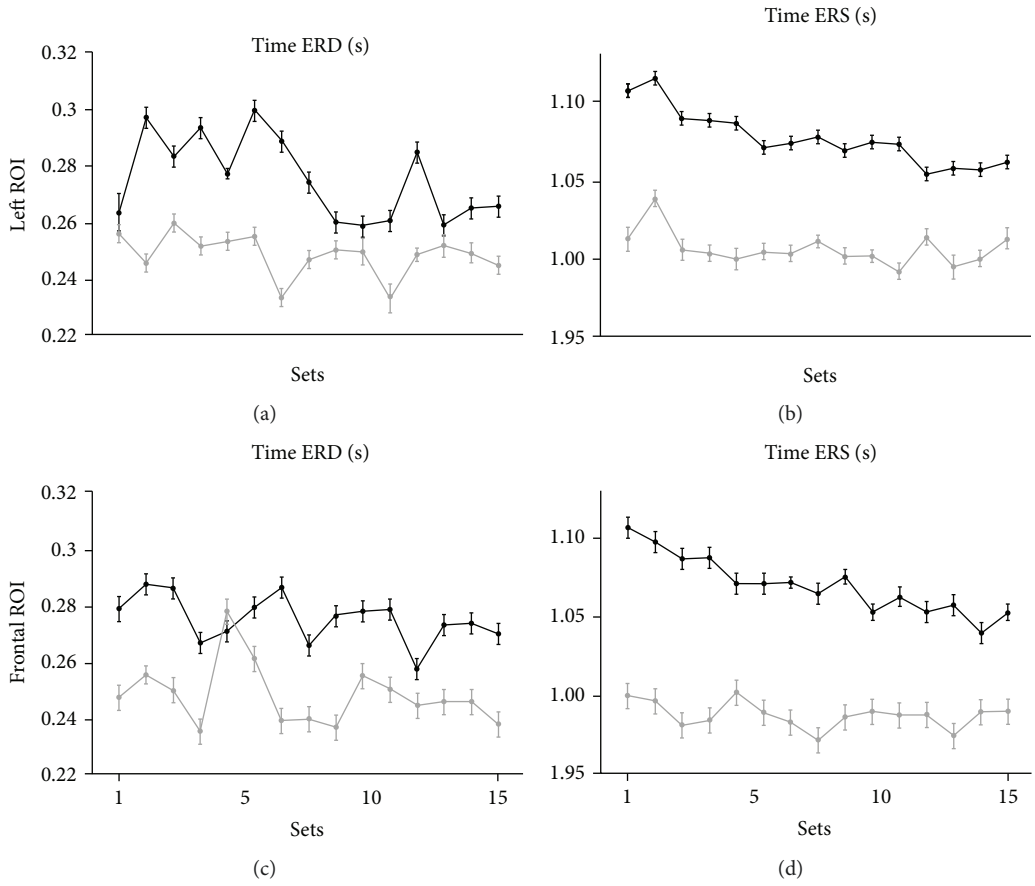

Figure 4: Average peak latencies of ERD (a, c) and ERS (b, d) for each set in the younger (grey circles and lines) and older (black circles and lines) groups for the left (upper graphs, a and b) and frontal (lower graphs, c and d) ROIs. The vertical bars represent the standard error of the mean.

Table 3: Result of repeated measure ANOVAs for ERD and ERS peak latency.

	Group (G)		Practice (P)		ROI (R)		P∗G		R∗G		P∗R		P∗R∗G	
	F	*p*	*F*	*p*	*F*	*p*	*F*	*p*	*F*	*p*	*F*	*p*	*F*	*p*
ERD	**4.35**	**0.048**	1.07	0.386	0.00	0.959	0.78	0.649	0.00	0.975	1.03	0.419	0.93	0.501
ERS	**12.42**	**0.002**	**2.74**	**0.015**	3.96	0.058	1.13	0.350	1.14	0.296	0.65	0.747	0.66	0.730

distinct movement features [68, 69]. The second set of considerations is based on the fact that the continuous performance in our motor tasks should induce constant and regular interplay of sensory and motor regions' activities [68, 69], thus providing the bases for use-dependent LTP induction. Improvements of velocity and interjoint coordination indices during the task in the older group indicate a major shift of the performance toward a reinforcement of the feedforward mechanisms, and thus of memory formation. Practice-related beta modulation increase may reflect this phenomenon [11]. If indeed, as also suggested by other evidence [13, 14], beta modulation depth increases reflect LTP-like phenomena in the sensorimotor cortex; then, one may speculate that plasticity-related mechanisms in the sensorimotor cortex should not be particularly affected by age. Studies testing the effect of age on the plasticity of the sensorimotor cortex with transcranial magnetic stimulation (TMS) have not shown clear differences between younger and older subjects, and the picture may be further complicated by the influence of hormonal levels on PAS results [33, 70] and neural plasticity in general [71, 72]. Indeed, our results need to be replicated in a larger population, also taking into account the factors other than age that could affect cortical plasticity mechanisms, such as motor and cognitive reserves.

3.3. ERS Peak Latency Occurs Later in Older Adults and Correlates with Total Movement Time. We finally focused on the peak latency of ERD and ERS peaks and determined whether they changed across sets and groups. Indeed, inspection of the data suggests that ERS peak latency was higher in the older but decreased with practice in both groups (Figure 4). Statistical analyses (Table 3, Supplementary Table 3) showed a significant group difference ($F_{(2,23)} = 7.93$, $p = 0.002$) and a significant effect of practice

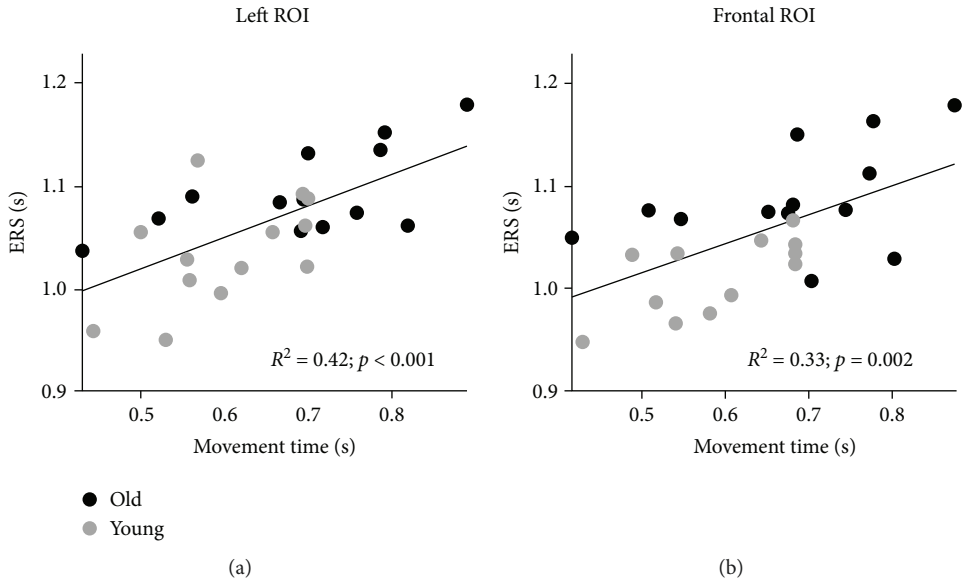

Figure 5: Correlations of total movement time with ERS peak latency in the left (a) and frontal (b) ROIs for younger (gray points) and older (black points) subjects combined.

($F_{(28,670)} = 1.75$, $p = 0.010$). However, we found no significant effect of ROI ($F_{(2,23)} = 2.30$, $p = 0.123$) and interactions (ROI∗Group: $F_{(2,23)} = 0.634$, $p = 0.540$; Practice∗Group: $F_{(28,670)} = 0.95$, $p = 0.535$; Practice∗ROI: $F_{(28,670)} = 0.84$, $p = 0.705$; and Practice∗ROI∗Group: $F_{(28,670)} = 0.80$, $p = 0.766$). Importantly, the temporal occurrence of ERS peak was linked to total movement time in both the left and the frontal ROIs ($R^2 = 0.42$, $p < 0.0001$; $R^2 = 0.33$, $p = 0.002$, respectively; Figure 5). However, ERS peak latency did not correlate with other kinematic parameters and with either ERS amplitude or beta modulation depth in both the left and the frontal ROI ($R^2 < 0.08$, $p > 0.16$). Altogether, these results show no effect of aging on ERS and ERD peak latency but only a strong dependence of ERS peak latency on movement duration. This is further supported by the lack of significant correlation between changes in peak latency across sets and age (Supplementary Table 1).

Only a few studies have focused on the ERS peak latency or its duration. It is generally accepted that ERS occurs 300-1000 ms after movement ends and lasts several seconds [2, 5, 63, 73–75]. Indeed, the present study with fast reaching movements at a pace of 1.5 s in a choice reaction time task showed that, on average, the peak latency of peak ERS is highly correlated with the total movement time and that it occurs from 300 to 400 ms from the end of the out-and-back movement. This observation is in agreement with the idea that ERS peak coincides with a deactivated state of the motor cortex and thus to a reduced excitability of the neuronal populations [76]. The peak latency characteristics of ERS are linked to the type of task and the movement duration. In tasks with isometric wrist contractions, ERS occurrence is related to the rate of force development but not the force output [63, 64]. During a task with repetitive movements, ERS occurs earlier than in a task with discrete finger movements [65]. Another work demonstrated that ERS lasts longer after withholding of real foot movements compared to imagined foot movements [77], with the faster movements showing earlier ERS peak occurrence.

4. Conclusions

The main result of this study is that, despite being slower and less accurate, the reaching movements of older subjects are associated with beta oscillatory activity that is no different from that accompanying the faster and more precise performance of younger subjects. Importantly, in both groups, the magnitude of beta modulation depth increases to the same degree during practice in both the left and the frontal ROIs. To address the discrepancy between performance and EEG, the results of this study need to be replicated in a larger population and also to take into account the factors other than anagraphical age.

Data Availability

Data that support the findings of this study are available from the corresponding authors upon reasonable request.

Conflicts of Interest

The authors declare no competing interests.

Acknowledgments

All the kinematic data were collected with MotorTaskManager software (designed by E.T.T. Srl, Genova Italy). We would like to thank Maura Casadio, Gabriele Arnulfo, and Andrea Canessa for their insights during data analyses and

also Giorgia Marchesi, Jing Lin, Shaina George, Francesco Della Gatta, Adhvik Kanagala, and Giulia Aurora Albanese for their help during data acquisition and preprocessing. This work was supported by NIH P01 NS083514 (MFG).

Supplementary Materials

Supplementary Table 1: correlations between Behavioral parameters and age. Supplementary Table 2: results of the Mixed Model ANOVA for ERD, ERS, and beta modulation comparing groups across practice in the two ROIs. Supplementary Table 3: results of the Mixed Model ANOVA for ERD, ERS, and beta modulation peak latency. *(Supplementary Materials)*

References

[1] G. Pfurtscheller and A. Aranibar, "Event-related cortical desynchronization detected by power measurements of scalp EEG," *Electroencephalography and Clinical Neurophysiology*, vol. 42, no. 6, pp. 817–826, 1977.

[2] G. Pfurtscheller, A. Stancak Jr, and C. Neuper, "Event-related synchronization (ERS) in the alpha band—an electrophysiological correlate of cortical idling: a review," *International Journal of Psychophysiology*, vol. 24, no. 1–2, pp. 39–46, 1996.

[3] S. Rossi, F. Tecchio, P. Pasqualetti et al., "Somatosensory processing during movement observation in humans," *Clinical Neurophysiology*, vol. 113, no. 1, pp. 16–24, 2002.

[4] A. M. Cebolla and G. Cheron, "Sensorimotor and cognitive involvement of the beta–gamma oscillation in the frontal N30 component of somatosensory evoked potentials," *Neuropsychologia*, vol. 79, Part B, pp. 215–222, 2015.

[5] A. Stancák Jr and G. Pfurtscheller, "Desynchronization and recovery of β rhythms during brisk and slow self-paced finger movements in man," *Neuroscience Letters*, vol. 196, no. 1–2, pp. 21–24, 1995.

[6] B. E. Kilavik, M. Zaepffel, A. Brovelli, W. A. MacKay, and A. Riehle, "The ups and downs of beta oscillations in sensorimotor cortex," *Experimental Neurology*, vol. 245, pp. 15–26, 2013.

[7] R. Salmelin, N. Forss, J. Knuutila, and R. Hari, "Bilateral activation of the human somatomotor cortex by distal hand movements," *Electroencephalography and Clinical Neurophysiology*, vol. 95, no. 6, pp. 444–452, 1995.

[8] E. Heinrichs-Graham, T. J. McDermott, M. S. Mills et al., "The lifespan trajectory of neural oscillatory activity in the motor system," *Developmental Cognitive Neuroscience*, vol. 30, pp. 159–168, 2018.

[9] W. Gaetz, M. Macdonald, D. Cheyne, and O. C. Snead, "Neuromagnetic imaging of movement-related cortical oscillations in children and adults: age predicts post-movement beta rebound," *NeuroImage*, vol. 51, no. 2, pp. 792–807, 2010.

[10] J. Dushanova, D. Philipova, and G. Nikolova, "Beta and gamma frequency-range abnormalities in parkinsonian patients under cognitive sensorimotor task," *Journal of the Neurological Sciences*, vol. 293, no. 1–2, pp. 51–58, 2010.

[11] A. B. Nelson, C. Moisello, J. Lin et al., "Beta oscillatory changes and retention of motor skills during practice in healthy subjects and in patients with Parkinson's disease," *Frontiers in Human Neuroscience*, vol. 11, 2017.

[12] C. Moisello, D. Blanco, J. Lin et al., "Practice changes beta power at rest and its modulation during movement in healthy subjects but not in patients with Parkinson's disease," *Brain and Behavior*, vol. 5, no. 10, article e00374, 2015.

[13] C. J. McAllister, K. C. Rönnqvist, I. M. Stanford, G. L. Woodhall, P. L. Furlong, and S. D. Hall, "Oscillatory beta activity mediates neuroplastic effects of motor cortex stimulation in humans," *Journal of Neuroscience*, vol. 33, no. 18, pp. 7919–7927, 2013.

[14] S. D. Hall, G. R. Barnes, P. L. Furlong, S. Seri, and A. Hillebrand, "Neuronal network pharmacodynamics of GABAergic modulation in the human cortex determined using pharmaco-magnetoencephalography," *Human Brain Mapping*, vol. 31, no. 4, pp. 581–594, 2010.

[15] S. D. Hall, I. M. Stanford, N. Yamawaki et al., "The role of GABAergic modulation in motor function related neuronal network activity," *NeuroImage*, vol. 56, no. 3, pp. 1506–1510, 2011.

[16] O. Jensen, P. Goel, N. Kopell, M. Pohja, R. Hari, and B. Ermentrout, "On the human sensorimotor-cortex beta rhythm: sources and modeling," *NeuroImage*, vol. 26, no. 2, pp. 347–355, 2005.

[17] S. D. Muthukumaraswamy, J. F. M. Myers, S. J. Wilson et al., "The effects of elevated endogenous GABA levels on movement-related network oscillations," *NeuroImage*, vol. 66, pp. 36–41, 2013.

[18] A. K. Roopun, S. J. Middleton, M. O. Cunningham et al., "A beta2-frequency (20–30 Hz) oscillation in nonsynaptic networks of somatosensory cortex," *Proceedings of the National Academy of Sciences of the United States of America*, vol. 103, no. 42, pp. 15646–15650, 2006.

[19] H. E. Rossiter, E. M. Davis, E. V. Clark, M.-H. Boudrias, and N. S. Ward, "Beta oscillations reflect changes in motor cortex inhibition in healthy ageing," *NeuroImage*, vol. 91, no. 100, pp. 360–365, 2014.

[20] N. Yamawaki, I. M. Stanford, S. D. Hall, and G. L. Woodhall, "Pharmacologically induced and stimulus evoked rhythmic neuronal oscillatory activity in the primary motor cortex *in vitro*," *Neuroscience*, vol. 151, no. 2, pp. 386–395, 2008.

[21] Y.-F. Hsu, K. K. Liao, P. L. Lee et al., "Intermittent theta burst stimulation over primary motor cortex enhances movement-related beta synchronisation," *Clinical Neurophysiology*, vol. 122, no. 11, pp. 2260–2267, 2011.

[22] N. A. Noh, G. Fuggetta, P. Manganotti, and A. Fiaschi, "Long lasting modulation of cortical oscillations after continuous theta burst transcranial magnetic stimulation," *PLoS One*, vol. 7, no. 4, article e35080, 2012.

[23] M. Cassidy, P. Mazzone, A. Oliviero et al., "Movement-related changes in synchronization in the human basal ganglia," *Brain*, vol. 125, no. 6, pp. 1235–1246, 2002.

[24] R. Levy, P. Ashby, W. D. Hutchison, A. E. Lang, A. M. Lozano, and J. O. Dostrovsky, "Dependence of subthalamic nucleus oscillations on movement and dopamine in Parkinson's disease," *Brain*, vol. 125, no. 6, pp. 1196–1209, 2002.

[25] A. A. Kühn, T. Trottenberg, A. Kivi, A. Kupsch, G.-H. Schneider, and P. Brown, "The relationship between local field potential and neuronal discharge in the subthalamic nucleus of patients with Parkinson's disease," *Experimental Neurology*, vol. 194, no. 1, pp. 212–220, 2005.

[26] P. Bedard and J. N. Sanes, "Basal ganglia-dependent processes in recalling learned visual-motor adaptations," *Experimental Brain Research*, vol. 209, no. 3, pp. 385–393, 2011.

[27] A. Kishore, T. Joseph, B. Velayudhan, T. Popa, and S. Meunier, "Early, severe and bilateral loss of LTP and LTD-like plasticity in motor cortex (M1) in *de novo* Parkinson's disease," *Clinical Neurophysiology*, vol. 123, no. 4, pp. 822–828, 2012.

[28] F. Morgante, A. J. Espay, C. Gunraj, A. E. Lang, and R. Chen, "Motor cortex plasticity in Parkinson's disease and levodopa-induced dyskinesias," *Brain*, vol. 129, no. 4, pp. 1059–1069, 2006.

[29] C. Moisello, D. Blanco, C. Fontanesi et al., "TMS enhances retention of a motor skill in Parkinson's disease," *Brain Stimulation*, vol. 8, no. 2, pp. 224–230, 2015.

[30] L. Marinelli, D. Crupi, A. di Rocco et al., "Learning and consolidation of visuo-motor adaptation in Parkinson's disease," *Parkinsonism & Related Disorders*, vol. 15, no. 1, pp. 6–11, 2009.

[31] Y. Ueki, T. Mima, M. Ali Kotb et al., "Altered plasticity of the human motor cortex in Parkinson's disease," *Annals of Neurology*, vol. 59, no. 1, pp. 60–71, 2006.

[32] S. N. Burke and C. A. Barnes, "Neural plasticity in the ageing brain," *Nature Reviews Neuroscience*, vol. 7, no. 1, pp. 30–40, 2006.

[33] F. Tecchio, F. Zappasodi, P. Pasqualetti et al., "Age dependence of primary motor cortex plasticity induced by paired associative stimulation," *Clinical Neurophysiology*, vol. 119, no. 3, pp. 675–682, 2008.

[34] R. Polimanti, I. Simonelli, F. Zappasodi et al., "Biological factors and age-dependence of primary motor cortex experimental plasticity," *Neurological Sciences*, vol. 37, no. 2, pp. 211–218, 2016.

[35] J. F. M. Müller-Dahlhaus, Y. Orekhov, Y. Liu, and U. Ziemann, "Interindividual variability and age-dependency of motor cortical plasticity induced by paired associative stimulation," *Experimental Brain Research*, vol. 187, no. 3, pp. 467–475, 2008.

[36] R. C. Oldfield, "The assessment and analysis of handedness: the Edinburgh inventory," *Neuropsychologia*, vol. 9, no. 1, pp. 97–113, 1971.

[37] M.-F. Ghilardi, C. Ghez, V. Dhawan et al., "Patterns of regional brain activation associated with different forms of motor learning," *Brain Research*, vol. 871, no. 1, pp. 127–145, 2000.

[38] C. Moisello, D. Crupi, E. Tunik et al., "The serial reaction time task revisited: a study on motor sequence learning with an arm-reaching task," *Experimental Brain Research*, vol. 194, no. 1, pp. 143–155, 2009.

[39] A. Delorme and S. Makeig, "EEGLAB: an open source toolbox for analysis of single-trial EEG dynamics including independent component analysis," *Journal of Neuroscience Methods*, vol. 134, no. 1, pp. 9–21, 2004.

[40] T.-P. Jung, S. Makeig, C. Humphries et al., "Removing electroencephalographic artifacts by blind source separation," *Psychophysiology*, vol. 37, no. 2, pp. 163–178, 2000.

[41] R. Oostenveld, P. Fries, E. Maris, and J.-M. Schoffelen, "FieldTrip: open source software for advanced analysis of MEG, EEG, and invasive electrophysiological data," *Computational Intelligence and Neuroscience*, vol. 2011, Article ID 156869, 9 pages, 2011.

[42] S. K. Hunter, H. M. Pereira, and K. G. Keenan, "The aging neuromuscular system and motor performance," *Journal of Applied Physiology*, vol. 121, no. 4, pp. 982–995, 2016.

[43] J. A. Kent-Braun, D. M. Callahan, J. L. Fay, S. A. Foulis, and J. P. Buonaccorsi, "Muscle weakness, fatigue, and torque variability: effects of age and mobility status," *Muscle & Nerve*, vol. 49, no. 2, pp. 209–217, 2014.

[44] C. J. McNeil and C. L. Rice, "Fatigability is increased with age during velocity-dependent contractions of the dorsiflexors," *The Journals of Gerontology Series A: Biological Sciences and Medical Sciences*, vol. 62, no. 6, pp. 624–629, 2007.

[45] E. J. Metter, N. Lynch, R. Conwit, R. Lindle, J. Tobin, and B. Hurley, "Muscle quality and age: cross-sectional and longitudinal comparisons," *The Journals of Gerontology Series A: Biological Sciences and Medical Sciences*, vol. 54, no. 5, pp. B207–B218, 1999.

[46] I. S. Raj, S. R. Bird, and A. J. Shield, "Aging and the force–velocity relationship of muscles," *Experimental Gerontology*, vol. 45, no. 2, pp. 81–90, 2010.

[47] M. J. Campbell, A. J. McComas, and F. Petito, "Physiological changes in ageing muscles," *Journal of Neurology, Neurosurgery & Psychiatry*, vol. 36, no. 2, pp. 174–182, 1973.

[48] R. D. Seidler, J. A. Bernard, T. B. Burutolu et al., "Motor control and aging: links to age-related brain structural, functional, and biochemical effects," *Neuroscience & Biobehavioral Reviews*, vol. 34, no. 5, pp. 721–733, 2010.

[49] R. T. Hepple and C. L. Rice, "Innervation and neuromuscular control in ageing skeletal muscle," *The Journal of Physiology*, vol. 594, no. 8, pp. 1965–1978, 2016.

[50] M. C. Perry, S. F. Carville, I. C. H. Smith, O. M. Rutherford, and D. J. Newham, "Strength, power output and symmetry of leg muscles: effect of age and history of falling," *European Journal of Applied Physiology*, vol. 100, no. 5, pp. 553–561, 2007.

[51] H. B. Skinner, R. L. Barrack, and S. D. Cook, "Age-related decline in proprioception," *Clinical Orthopaedics and Related Research*, vol. 184, pp. 208–211, 1984.

[52] N. Raz, K. M. Rodrigue, K. M. Kennedy, D. Head, F. Gunning-Dixon, and J. D. Acker, "Differential aging of the human striatum: longitudinal evidence," *American Journal of Neuroradiology*, vol. 24, no. 9, pp. 1849–1856, 2003.

[53] J. Verghese, A. LeValley, C. B. Hall, M. J. Katz, A. F. Ambrose, and R. B. Lipton, "Epidemiology of gait disorders in community-residing older adults," *Journal of the American Geriatrics Society*, vol. 54, no. 2, pp. 255–261, 2006.

[54] R. L. Sainburg, M. F. Ghilardi, H. Poizner, and C. Ghez, "Control of limb dynamics in normal subjects and patients without proprioception," *Journal of Neurophysiology*, vol. 73, no. 2, pp. 820–835, 1995.

[55] R. Huber, M. F. Ghilardi, M. Massimini et al., "Arm immobilization causes cortical plastic changes and locally decreases sleep slow wave activity," *Nature Neuroscience*, vol. 9, no. 9, pp. 1169–1176, 2006.

[56] C. Moisello, M. Bove, R. Huber et al., "Short-term limb immobilization affects motor performance," *Journal of Motor Behavior*, vol. 40, no. 2, pp. 165–176, 2008.

[57] A. Sailer, J. Dichgans, and C. Gerloff, "The influence of normal aging on the cortical processing of a simple motor task," *Neurology*, vol. 55, no. 7, pp. 979–985, 2000.

[58] S. Heuninckx, N. Wenderoth, F. Debaere, R. Peeters, and S. P. Swinnen, "Neural basis of aging: the penetration of cognition into action control," *Journal of Neuroscience*, vol. 25, no. 29, pp. 6787–6796, 2005.

[59] S. Heuninckx, N. Wenderoth, and S. P. Swinnen, "Systems neuroplasticity in the aging brain: recruiting additional neural resources for successful motor performance in elderly persons," *Journal of Neuroscience*, vol. 28, no. 1, pp. 91–99, 2008.

[60] S. P. Swinnen, S. Heuninckx, A. Van Impe, D. J. Goble, J. P. Coxon, and N. Wenderoth, "Aging and movement control: the neural basis of age-related compensatory recruitment," *Motor Control*, vol. 17, pp. 383–413, 2010.

[61] A. Vallesi, A. R. McIntosh, and D. T. Stuss, "Overrecruitment in the aging brain as a function of task demands: evidence for a compensatory view," *Journal of Cognitive Neuroscience*, vol. 23, no. 4, pp. 801–815, 2011.

[62] A. Stancák Jr and G. Pfurtscheller, "Event-related desynchronisation of central beta-rhythms during brisk and slow self-paced finger movements of dominant and nondominant hand," *Cognitive Brain Research*, vol. 4, no. 3, pp. 171–183, 1996.

[63] A. Fry, K. J. Mullinger, G. C. O'Neill et al., "Modulation of post-movement beta rebound by contraction force and rate of force development," *Human Brain Mapping*, vol. 37, no. 7, pp. 2493–2511, 2016.

[64] S. Cremoux, J. Tallet, E. Berton, F. Dal Maso, and D. Amarantini, "Motor-related cortical activity after cervical spinal cord injury: multifaceted EEG analysis of isometric elbow flexion contractions," *Brain Research*, vol. 1533, pp. 44–51, 2013.

[65] Y.-Z. Wu, D. M. Niddam, C. C. Chen et al., "Effects of cognitive demands on postmovement motor cortical deactivation," *NeuroReport*, vol. 17, no. 4, pp. 371–375, 2006.

[66] A. Stančák Jr, "The electroencephalographic β synchronization following extension and flexion finger movements in humans," *Neuroscience Letters*, vol. 284, no. 1–2, pp. 41–44, 2000.

[67] E. Tatti, S. Ricci, R. Mehraram et al., "Beta modulation depth is not linked to movement features," *Frontiers in Behavioral Neuroscience*, vol. 13, p. 49, 2019.

[68] H. Shimazu, R. Kaji, N. Murase et al., "Pre-movement gating of short-latency somatosensory evoked potentials," *NeuroReport*, vol. 10, no. 12, pp. 2457–2460, 1999.

[69] F. Cassim, W. Szurhaj, H. Sediri et al., "Brief and sustained movements: differences in event-related (de) synchronization (ERD/ERS) patterns," *Clinical Neurophysiology*, vol. 111, no. 11, pp. 2032–2039, 2000.

[70] G. Fernández, S. Weis, B. Stoffel-Wagner et al., "Menstrual cycle-dependent neural plasticity in the adult human brain is hormone, task, and region specific," *The Journal of Neuroscience*, vol. 23, no. 9, pp. 3790–3795, 2003.

[71] M. M. Adams and J. H. Morrison, "Estrogen and the aging hippocampal synapse," *Cerebral Cortex*, vol. 13, no. 12, pp. 1271–1275, 2003.

[72] H. A. Hofmann, "Gonadotropin-releasing hormone signaling in behavioral plasticity," *Current Opinion in Neurobiology*, vol. 16, no. 3, pp. 343–350, 2006.

[73] G. Pfurtscheller, "Event-related synchronization (ERS): an electrophysiological correlate of cortical areas at rest," *Electroencephalography and Clinical Neurophysiology*, vol. 83, no. 1, pp. 62–69, 1992.

[74] R. Salmelin and R. Hari, "Spatiotemporal characteristics of sensorimotor neuromagnetic rhythms related to thumb movement," *Neuroscience*, vol. 60, no. 2, pp. 537–550, 1994.

[75] M. T. Jurkiewicz, W. C. Gaetz, A. C. Bostan, and D. Cheyne, "Post-movement beta rebound is generated in motor cortex: evidence from neuromagnetic recordings," *NeuroImage*, vol. 32, no. 3, pp. 1281–1289, 2006.

[76] R. Chen, Z. Yaseen, L. G. Cohen, and M. Hallett, "Time course of corticospinal excitability in reaction time and self-paced movements," *Annals of Neurology*, vol. 44, no. 3, pp. 317–325, 1998.

[77] T. Solis-Escalante, G. R. Müller-Putz, G. Pfurtscheller, and C. Neuper, "Cue-induced beta rebound during withholding of overt and covert foot movement," *Clinical Neurophysiology*, vol. 123, no. 6, pp. 1182–1190, 2012.

Hindawi
Neural Plasticity
Volume 2019, Article ID 2057308, 12 pages
https://doi.org/10.1155/2019/2057308

Research Article

Effects of Electroacupuncture on Pain Memory-Related Behaviors and Synchronous Neural Oscillations in the Rostral Anterior Cingulate Cortex in Freely Moving Rats

Zui Shen, Yilin Zhu, Boyi Liu, Yi Liang, Qiaoying He, Jing Sun, Zemin Wu, Haiyan Zhang, Shujing Yao, Xiaofen He, Jianqiao Fang, and Xiaomei Shao

Department of Neurobiology and Acupuncture Research, The Third Clinical College, Zhejiang Chinese Medical University, Key Laboratory of Acupuncture and Neurology of Zhejiang Province, Hangzhou 310053, China

Correspondence should be addressed to Jianqiao Fang; fangjianqiao7532@163.com and Xiaomei Shao; 13185097375@163.com

Received 28 December 2018; Revised 20 March 2019; Accepted 11 April 2019; Published 15 May 2019

Guest Editor: John-Stuart Brittain

Our previous studies have confirmed that electroacupuncture (EA) can effectively intervene in pain memory, but the neural mechanism involved remains unclear. In this study, we observed the effects of EA in regulating pain memory-related behaviors and synchronous neural oscillations in the rostral anterior cingulate cortex (rACC). During nociceptive behavioral testing, pain memory induced a nonpain stimulus that spurred a neural oscillatory reaction similar to that caused by pain stimuli in the rACC. After EA, nonpain stimuli did not induce decreased neural oscillatory activity in the rACC until the presentation of pain stimuli. During aversive behavioral testing, EA, through the downregulation of theta power, inhibited the retrieval of aversive memory and relieved pain memory-induced aversive behaviors. These changes of oscillatory activity may be the hallmarks of EA therapy for pain memory.

1. Introduction

Many studies have proven that initial injury-induced indelible pain memory is often a key factor of long-term unhealed chronic pain [1–4]. Pain memory has been a new focus on chronic pain research [5–7]. Therefore, the eradication of pain memory may be the key to relieving chronic pain. Our previous studies and other studies have shown that the "pain memory" phenomenon can be reproduced in a rat pain memory model, and the present study is also based on this model [2, 3, 8].

The rostral anterior cingulate cortex (rACC) is an important brain area for the modulation of pain memory [2, 3, 9]. Our previous study showed that the cAMP/PKA/CREB signaling pathway in the rACC relating to memory storage and retrieval is involved in regulating pain memory-induced nociceptive behavior in a rat pain memory model [2]. In addition, a previous study indicated that rACC is also involved in the processing of aversive behavior [10]. Thus, whether pain memory induces changes in aversive behavior and rACC is certainly worthy of further study.

Neural oscillation is a rhythmic fluctuation of neuronal excitability. It is a combination of neural ensemble firing with distinct levels of frequency. Delta band oscillation is usually closely related to decision making, attentional process, and expectation [11, 12]. Oscillation in the theta band is related to memory encoding and retrieval [13, 14]. Alpha and beta oscillations are associated with top-down cognitive processes, including attention and preparation of movements [15–17]. Gamma oscillation is commonly observed in many brain regions during both waking and sleep states [18].

Recent studies indicate that the neural oscillation mechanism is central to studying the brain neural network of chronic pain [19–22]. Evidence suggests that neural oscillations in multiple frequency bands modulate different levels of information integration, playing an important role in perceptions, emotions, and behaviors [23–26]. Additionally, pain can induce a change in neural oscillations in brain

regions, as recent researches show that acute pain can spur changes in local field potentials (LFPs) in multiple frequency bands in ACC [27–29]. However, whether pain memory induces a change in neural oscillations requires further observation.

Electroacupuncture (EA), a form of acupuncture involving electronic stimulation, is widely applied as an analgesic for chronic pain in clinics [30–32]. EA can regulate the prefrontal neural network which basically overlaps with the neural network of cognition [33]. Additionally, EA can modulate a change in brain oscillatory activity in a rat model of acute pain, regulating the neural network of central processes and spontaneous injury information integration [34]. Our previous research has also indicated that EA can alleviate the retrieval of nociceptive behavior induced by pain memory [2, 3]. However, how EA modulates the neural network in the rat model of pain memory remains unknown and deserves further observation. In this study, to explore the effect of electroacupuncture on pain memory-related synchronous neural oscillations in the rACC in freely moving rats, we observe pain memory-induced nociceptive and aversive behaviors and synchronous LFPs via extracellular multichannel recording in vivo.

2. Materials and Methods

2.1. Animals and Groups. Male adult Sprague-Dawley (SD) rats of 250-300 g in body weight were obtained from the Experimental Animal Center of Zhejiang Chinese Medical University. The animals were housed in groups of five in plastic cages with soft bedding at the University Animal Care Facility with an artificial 12/12 h light-dark cycle (lights on at 8 a.m.). Animals received food and water ad libitum at a constant room temperature of 23 to 25°C and at a relative humidity of 40% to 70%. Prior to experimental manipulations, rats were given a period of 1 week to adjust to their new surroundings. The whole experiment was performed in accordance with the guidelines of the International Association for the Study of Pain and the Institutional Animal Ethical Committee (IAEC).

Adult male SD rats were randomly divided into a blank control (Control) group, pain memory model (Model) group, and model+electroacupuncture (EA) group.

2.2. Surgeries. Animals were anesthetized with urethane anesthesia (1.2 g/kg i.p., Sigma-Aldrich) and fixed to a stereotaxic apparatus (68025, RWD Life Science, China). Rats were placed in a stereotaxic frame on a heated surgical platform maintained at a constant temperature of 37°C. A midline scalp incision was made to expose the skull to allow for the implantation of a microwire array, which was fixed to the skull with surface screws and dental cement. Rats received surgery for neural recordings.

To record the LFPs of rACC neural activity, one recording microwire array was surgically implanted. Surgical procedures used were the same as those used in our previous studies [12]. The array was driven into the right rACC at a twenty-degree angle using a hydraulic microdrive (model 51421, Stoelting Co., Wood Dale, USA). Each microwire array consisted of eight filaments of nickel-chromium wire (35 μm diameter, Stablohm 675; California Fine Wire Company, Grover Beach, CA, USA). The array was constructed in 4×2 architecture with 200 μm between the recording wires. The following coordinates (relative to the bregma) were used to center the array: rACC (+2.7 mm rostrocaudal, +0.8 mm mediolateral, and 2.0 mm dorsoventral).

2.3. Pain Memory Model. In our previous study, the pain memory model was induced by two injections of carrageenan [2, 3]. The first carrageenan injection was placed into the left hind paw plantar surface via the subcutaneous injection of 0.1 mL of 2% carrageenan (Sigma-Aldrich, St. Louis, MO, USA) to induce acute inflammatory pain. After a 14-day recovery period, when the right hind paw was also injected with the same carrageenan, the pain threshold of the recovered left hind paw dropped again. This shows that the pain memory model was successfully prepared. The basic experimental procedure is shown in Figure 1.

2.4. Electroacupuncture. Electroacupuncture treatment was applied in rats of the EA group. In a previous study [2, 3], we found that EA treatment at bilateral acupoints "Zusanli" (ST36) and the reference electrode (1 cm inferior of "Zusanli") were effective for impairing the retrieval of pain memory. Therefore, we used the same methods including the acupoints and EA parameters in this study. The acupoints were needled with stainless acupuncture needles (0.25 mm in diameter × 13 mm in length) and electrically stimulated with a Hans Acupoint Nerve Stimulator (HANS 200E; Huawei Co. Ltd., Beijing, China). The EA parameters were set as follows: 2/100 Hz of the frequency with automatic shifting between 2 Hz and 100 Hz stimulation for 3 s each; a square wave current output (pulse width: 0.2 ms); and an intensity range of about 1-2 mA adjusted to the animals' local muscle contractions. The treatment was administered at 5 h, 1-5 d after the first carrageenan injection. In the whole procedure, all rats maintained relatively comfortable states without any struggling and screaming.

2.5. Nociceptive Behavioral Testing. As described above, paw withdrawal thresholds (PWTs) were measured automatically using a dynamic plantar aesthesiometer (model 37450; Ugo Basile, Comerio, Italy) [12, 35]. A paw-flick response was elicited by applying an increasing vertical force (increased steadily from 0 to 50 grams over 20 s) using a stainless steel probe (a straight 0.5 mm diameter shaft) placed underneath the mesh floor and focused at the middle of the plantar surface of the ipsilateral hind paw. According to our previous study, PWT was determined as the mean of four subsequent measurements except for the first at intervals of 1 min [12]. Moreover, all manipulations were made under the guidance of an operator.

2.6. Aversive Behavioral Testing. Two carrageenan injections that induced aversive behavior were performed using a modified conditioned place aversion (CPA) paradigm [36]. The plexiglas paradigm consists of two equally sized cabinets ($35 \times 28 \times 45$ cm) that can be controlled by opening or closing with a baffle. The two cabinets are composed of wallpaper

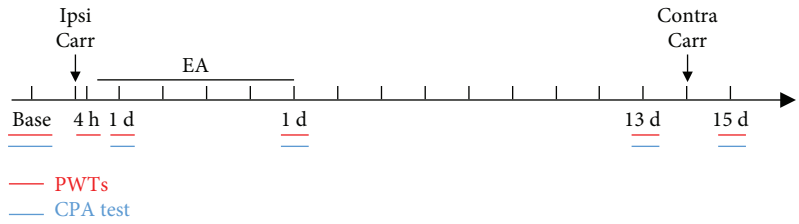

Figure 1: The basic experimental procedure.

strips of different widths (3 cm and 9 cm wide) and colors (black and white). One side of the cabinets is 3 cm of alternating black and white colors, and the other side is 9 cm of alternating black and white colors. The base is hollowed out and can be fully placed on the perforated platform which is fitted with a dynamic plantar aesthesiometer.

At baseline, the rats were left free in an open (middle without baffle) paradigm for 30 min, and the activity time of the rats in the two compartments was recorded separately. Pain- and non-pain-paired compartments for each rat were randomly assigned according to the activity time of the rats in the two compartments at baseline. On day 0, the two compartments were separated with the baffle and the rats were placed in a non-pain-paired compartment for free activity for 30 min (unconditioned phase). After the rats were placed back into a cage to rest for 30 min, control rats were given a left hind paw injection of 0.1 mL of 0.9% NaCl and model and EA rats were injected with 0.1 mL of 2% carrageenan in the left hind paw. Four hours later, the rats were placed into pain-paired compartments (conditioning phase), and after a 5 min period of habituation, each left hind paw was stimulated every minute for 25 min using a dynamic plantar aesthesiometer. The rats were placed in the two compartments (middle without a baffle) for free movement for 30 min on day 1, day 5, and day 13, and their activity time in the two compartments was recorded. On day 14, the control rats were given 0.1 mL of 0.9% NaCl in the right hind paw. The model and EA rats were injected with 0.1 mL of 2% carrageenan in the right hind paw. On day 15, the rats moved freely between the two compartments for 30 min, and their activity time was recorded.

Aversive behavior was measured with the CPA score, which is the difference in time between the test day (day 1, day 5, day 13, and day 15) and baseline for the pain-paired compartment. The formula is shown as follows:

$$T_{\text{score}} = T_{\text{test day}} - T_{\text{baseline}}. \quad (1)$$

During the experiment, the rats were lightly placed in the central area of the two compartments. After the rats acclimated for 1 min, the video acquisition software automatically started timing and tracking the activity of the rats for 30 min. Real-time recording and data analysis were performed using the SMART video tracking software (v3.0, Panlab, Spain). After the test of the previous rats, the two compartments were thoroughly scrubbed with 10% alcohol to eliminate residual traces and odors that could have affected the activity of the next rats tested.

2.7. Neural Recordings. LFPs were recorded from the implanted microwire array with a Cerebus neural signal processing system (Blackrock Microsystems, Salt Lake City, UT, USA). LFP signals were preamplified (300x), bandpass filtered (0.3–250 Hz), and sampled at 1 kHz. Neural recordings were obtained in nociceptive behavioral testing environments in quiet states. A plantar video camera and video tracking system (ANY-maze, Stoelting, CO, USA) was used to generate real-time imaging of the rats' plantar and the stimulus probe in the dynamic plantar aesthesiometer, permitting the synchronization of the probe's stimulus process with the acquired neuronal data. No animals were removed from the study due to the poor placement of recording wires.

2.8. Spectral Analysis. Data were processed and validated by offline analysis using NeuroExplorer 5.021 (NEX, Plexon Inc.) and were exported to MATLAB 2014a (MathWorks, Natick, MA) for complementary analysis.

A spectrogram analysis was used to visualize LFP power levels at different frequency bands as a function of time for each condition. The raw rACC LFPs were bandpass filtered at 2-45 Hz using a noncausal zero-phase-shift filter (fourth-order Butterworth). Next, the power spectral densities (PSD) were calculated with Hanning window 2^{10} frequency bins over the 2-45 Hz range and with 50% overlapping windows. The power was normalized by the logarithm of the PSD (in decibels), and smoothing was applied (Gaussian filter, width = 3). The following five frequency band intervals were considered: delta (2–4 Hz), theta (4–9 Hz), alpha (9–15 Hz), beta (15–30 Hz), and gamma (30–45 Hz).

2.9. Statistical Analysis. All averaged values are given as the mean ± SEM. One- or two-way repeated measures analyses of variance (rm ANOVA) with Bonferroni post hoc analysis were used when the variances were equal. In all cases, the results were considered to be statistically significant at $p < 0.05$.

3. Results

3.1. Pain Memory-Related Behaviors Observed during Nociceptive Behavioral Testing. As shown in Figure 2, we tested paw withdrawal thresholds (PWTs) of the ipsilateral (left) hind paws in the control, model, and EA groups (two-way rm ANOVA; groups: $F_{(2,60)} = 99.973$, $p < 0.001$; time: $F_{(5,60)} = 62.303$, $p < 0.001$; and groups × time:

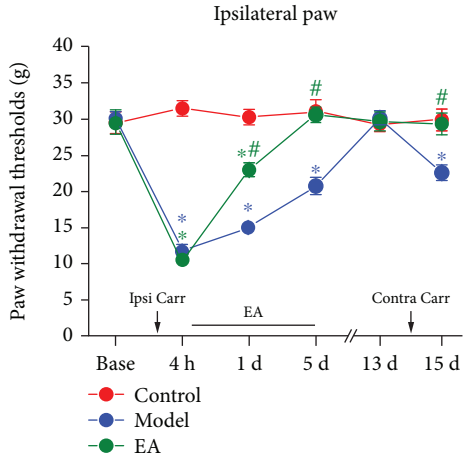

Figure 2: Mechanical withdrawal thresholds of the ipsilateral (left) hind paws in each group. $^{*}p < 0.05$ compared to the control group and $^{\#}p < 0.05$ compared to the model group. $N = 7$. Abbreviation: Ipsi Carr = ipsilateral carrageenan injection, Contra Carr = contralateral carrageenan injection.

$F_{(10,60)} = 18.026$, $p < 0.001$; $n = 7$). Post hoc analysis shows that there were no significant differences in each group before the first carrageenan injection was made into the ipsilateral hind paws ($p > 0.05$, Bonferroni test). Furthermore, PWTs in the model and EA groups were significantly decreased compared to those of the control group at 4 h ($p < 0.05$, Bonferroni test). The PWTs of the model group at 1 d and 5 d and the PWTs of the EA group at 1 d were significantly lower than those of the control group at the same time ($p < 0.05$, Bonferroni test), and the PWTs of the EA group at 1 d and 5 d were significantly higher than those of the model group ($p < 0.05$, Bonferroni test). At 13 d, there were no statistically significant differences between each group ($p > 0.05$, Bonferroni test), and at 14 d, the same doses of carrageenan were injected into the contralateral hind paw of the model and EA groups. At 15 d, the PWTs of the ipsilateral hind paw of the model group were significantly decreased relative to those of rats of the control group ($p < 0.05$, Bonferroni test), and compared to those of the model group, the PWTs of ipsilateral hind paws of the EA group were significantly increased ($p < 0.05$, Bonferroni test).

3.2. Synchronous Neural Oscillations of Pain Memory-Related Behaviors Observed during Nociceptive Behavioral Testing. Compared to those of the prestimulus phase (-5 s to 0 s), the amplitude and PSD values observed during the stimulus phase (0 s to paw withdrawal (upward arrow)) showed early downtrends in the rACC at 1 d, 13 d, and 15 d (Figure 3(a)). As the maintenance times of rats in response to the paw withdrawal stimulus varied, we selected mean PSD as the observation target. At -1 d, there was no significant difference in the mean PSD within 2-45 Hz between the prestimulus and stimulus phases (one-way rm ANOVA; $F_{(1,7)} = 2{,}337$, $p > 0.05$). At 1 d, 13 d, and 15 d, the mean PSD of the stimulus phase was lower than those of the prestimulus phase (one-way rm ANOVA; $F_{(1,7)} = 662.202$, $p < 0.05$; $F_{(1,6)} = 1114.916$, $p < 0.05$; and $F_{(1,6)} = 454.370$, $p < 0.05$) (Figure 3(b)).

The analysis results of each frequency band are as follows (Figure 3(c)): At -1 d, the mean PSD of the theta frequency band increased during the stimulus phase (one-way rm ANOVA; $F_{(1,7)} = 288.803$, $p < 0.05$) and showed a decrease in the alpha frequency band (one-way rm ANOVA; $F_{(1,7)} = 1909.767$, $p < 0.05$) compared to those of the prestimulus phase. At 1 d, the mean PSD of the stimulus phase decreased in the delta, theta, alpha, and beta bands (one-way rm ANOVA; $F_{(1,7)} = 111.719$, $p < 0.05$; $F_{(1,7)} = 360.460$, $p < 0.05$; $F_{(1,7)} = 850.932$, $p < 0.05$; and $F_{(1,7)} = 830.523$, $p < 0.05$) compared to those of the prestimulus phase. At 13 d, the mean PSD of the stimulus phase showed a significant decrease in the delta and theta bands (one-way rm ANOVA; $F_{(1,6)} = 1243.328$, $p < 0.05$ and $F_{(1,6)} = 296.415$, $p < 0.05$) compared to those of the prestimulus phase. At 15 d, the mean PSD of the delta, theta, alpha, beta, and gamma bands significantly decreased during the stimulus phase (one-way rm ANOVA; $F_{(1,6)} = 68.989$, $p < 0.05$; $F_{(1,6)} = 1015.063$, $p < 0.05$; $F_{(1,6)} = 191.674$, $p < 0.05$; $F_{(1,6)} = 2297.207$, $p < 0.05$; and $F_{(1,6)} = 42.677$, $p < 0.05$) compared to those of the prestimulus phase (Figure 3(c)).

3.3. After EA, Synchronous Neural Oscillations of Pain Memory-Related Behaviors Were Observed during Nociceptive Behavioral Testing. After EA, compared to the prestimulus phase, the early declining amplitude and PSD of the stimulus phase were not observed at 1 d, 13 d, and 15 d (Figure 4(a)).

At -1 d, 1 d, 13 d, and 15 d, there were no significant differences in the mean PSD of the prestimulus and stimulus phases (one-way rm ANOVA; all $p > 0.05$) (Figure 4(b)). Furthermore, Figure 4(c) shows that at -1 d, 13 d, and 15 d, there was no significant difference in the mean PSD of each frequency band between the stimulus and prestimulus phases (one-way rm ANOVA; all $p > 0.05$). At 1 d, the mean PSD in the delta band during the stimulus phase was higher than that during the prestimulus phase (one-way rm ANOVA; $F_{(1,6)} = 17.453$, $p < 0.05$).

3.4. Pain Memory-Related Behaviors Observed during Aversive Behavioral Testing. Figure 5 shows that there were changes between the control, model, and EA groups at 1 d, 5 d, 13 d, and 15 d (two-way rm ANOVA; groups: $F_{(2,36)} = 2.892$, $p > 0.05$; time: $F_{(3,60)} = 1.066$, $p > 0.05$; and groups × time: $F_{(6,60)} = 3.079$, $p < 0.05$; $n = 7$). The results observed at 15 d show that score values of the model group were lower than those of the control group ($p < 0.05$, Bonferroni test); compared to those of the model group, the score values of the EA group were significantly increased ($p < 0.05$, Bonferroni test). Together, these data suggest that the second injury stimulated the aversive memory in the pain-paired compartments (conditioning phase) of the model rats, spurring significantly aversive avoidance behaviors. EA can inhibit

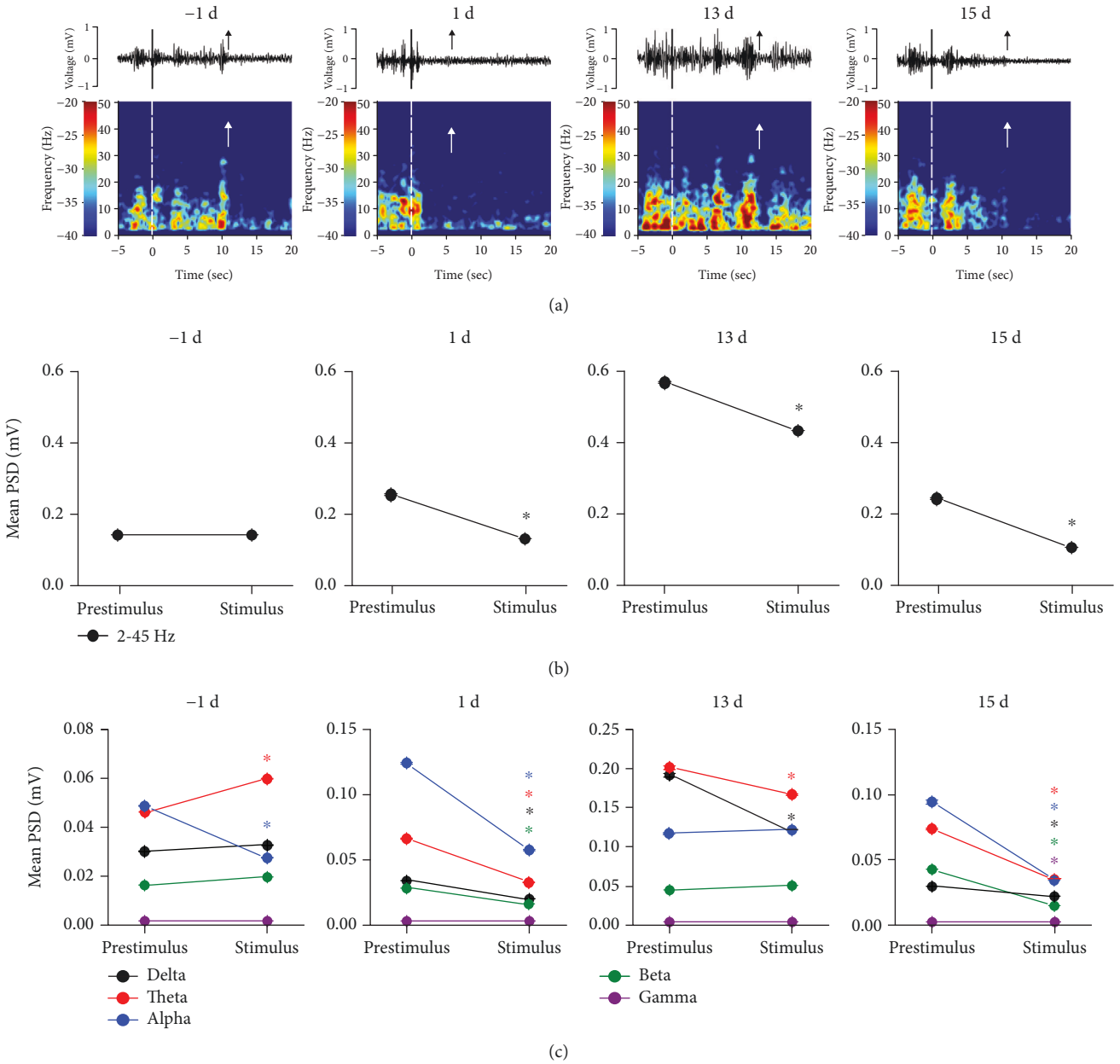

Figure 3: Synchronous LFPs observed during nociceptive behavioral testing. (a) A spontaneous recording and real-time spectrogram for LFP signals of the prestimulus, stimulus, and poststimulus phases (black and white dashed lines indicate the start of the stimulus and the upward arrow represents paw withdrawal). (b) The change in the mean PSD observed within 2-45 Hz between the prestimulus and stimulus phases in the rACC. $^{*}p < 0.05$ compared to the prestimulus phase. (c) The change in the mean PSD in different frequency bands between the prestimulus and stimulus phases in the rACC. $^{*}p < 0.05$ compared to the prestimulus phase of the same band. Five frequency band intervals were considered: delta (2–4 Hz), theta (4–9 Hz), alpha (9–15 Hz), beta (15–30 Hz), and gamma (30–45 Hz).

aversive memory induced by a second injury, and the rats exhibited no aversive avoidance behaviors.

3.5. Synchronous Neural Oscillations of Pain Memory-Related Behaviors Observed during Aversive Behavioral Testing. Our data indicate that when rats were moving freely in the non-pain-paired compartments, the mean PSD gradually increased, and specifically at 15 d, the mean PSD in the theta band reached a pronounced peak value (Figure 6(a)). When the rats were moving in the pain-paired compartment, the mean PSD also gradually increased, and at 15 d, the mean PSD in the theta band also increased (Figure 6(b)).

Next, we analyzed the mean PSD in five frequency bands. Compared to that observed at -1 d, the mean PSD observed at 1 d in the theta and alpha bands decreased in the pain-paired compartment (one-way rm ANOVA; $F_{(1,7)} = 52.347$, $p < 0.05$ and $F_{(1,7)} = 60.954$, $p < 0.05$; Figure 6(d)). The mean PSD at 5 d in the delta band increased

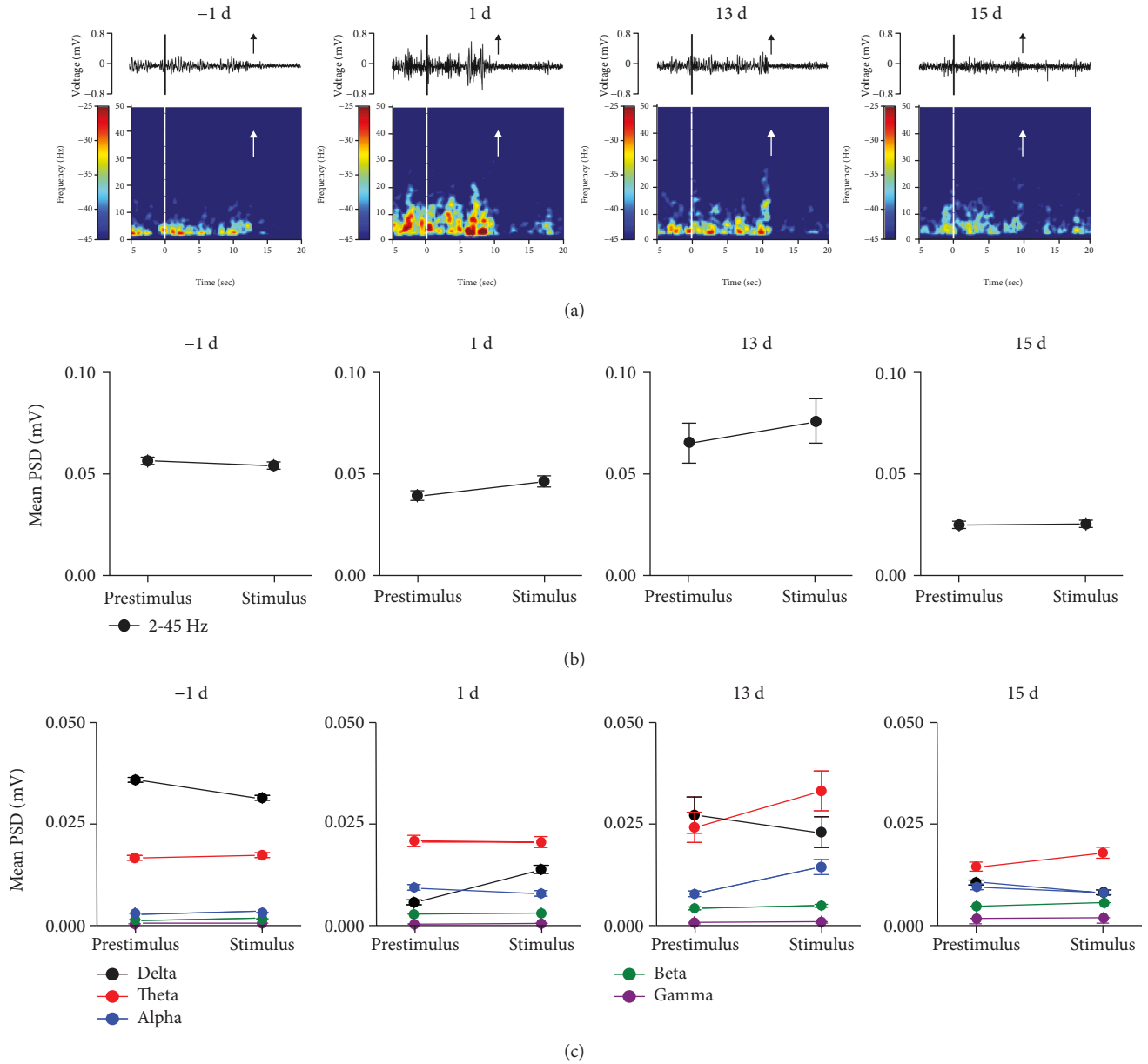

Figure 4: After EA, synchronous LFPs were observed during nociceptive behavioral testing. (a) After EA, a spontaneous recording and real-time spectrogram of LFP signals of the prestimulus, stimulus, and poststimulus phases. (b) After EA, the change in the mean PSD (2-45 Hz) was observed between the prestimulus and stimulus phases in the rACC. (c) After EA, the change in the mean PSD was observed at different frequency bands between the prestimulus and stimulus phases in the rACC. $^{*}p < 0.05$ compared to the prestimulus phase of the same band. Five frequency band intervals were considered: delta (2–4 Hz), theta (4–9 Hz), alpha (9–15 Hz), beta (15–30 Hz), and gamma (30–45 Hz).

but that of the alpha band decreased in the non-pain-paired compartment (one-way rm ANOVA; $F_{(1,7)} = 90.105$, $p < 0.05$ and $F_{(1,7)} = 54.211$, $p < 0.05$; Figure 6(c)). The mean PSD at 13 d in the delta, theta, alpha, and beta bands were increased in the non-pain-paired compartment (one-way rm ANOVA; $F_{(1,7)} = 754.585$, $p < 0.05$; $F_{(1,7)} = 656.647$, $p < 0.05$; $F_{(1,7)} = 178.395$, $p < 0.05$; and $F_{(1,7)} = 62.780$, $p < 0.05$; Figure 6(c)), while it increased in the theta and alpha bands in the pain-paired compartment at the same time (one-way rm ANOVA; $F_{(1,7)} = 161.090$, $p < 0.05$ and $F_{(1,7)} = 56.208$, $p < 0.05$; Figure 6(d)). The mean PSD at 15 d in the delta, theta, alpha, and beta bands increased in the non-pain-paired compartment (one-way rm ANOVA; $F_{(1,6)} = 40.680$, $p < 0.05$; $F_{(1,6)} = 371.190$, $p < 0.05$; $F_{(1,6)} = 444.247$, $p < 0.05$; and $F_{(1,6)} = 139.694$, $p < 0.05$; Figure 6(c)), while in the theta, alpha, and beta bands, it increased in the pain-paired compartment (one-way rm ANOVA; $F_{(1,6)} = 83.732$, $p < 0.05$; $F_{(1,6)} = 124.425$, $p < 0.05$; and $F_{(1,6)} = 63.617$, $p < 0.05$; Figure 6(d)). Note that compared to the mean PSD at 13 d, the PSD of the theta, alpha, and beta bands significantly increased in the two compartments at 15 d (one-way rm ANOVA; non-pain-paired compartment: $F_{(1,6)} = 194.174$,

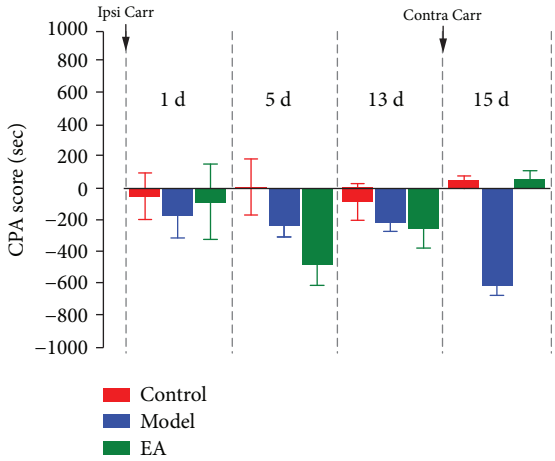

Figure 5: Values of aversive behavioral testing. $^{*}p < 0.05$ compared to the control group at the same time; $^{\#}p < 0.05$ compared to the model group at the same time. $N = 7$. Abbreviation: Ipsi Carr = ipsilateral carrageenan injection, Contra Carr = contralateral carrageenan injection.

$p < 0.05$, $F_{(1,6)} = 163.629$, $p < 0.05$, and $F_{(1,6)} = 58.376$, $p < 0.05$; pain-paired compartment: $F_{(1,6)} = 50.593$, $p < 0.05$, $F_{(1,6)} = 84.377$, $p < 0.05$, and $F_{(1,6)} = 41.596$, $p < 0.05$; Figures 6(c) and 6(d)).

3.6. After EA, Synchronous Neural Oscillations of Pain Memory-Related Behaviors Were Observed during Aversive Behavioral Testing. After EA, when the rats were moving freely in the pain-paired compartments at 15 d, the mean PSD in the alpha band reached an obvious peak value rather than in the theta band (Figure 7(b)).

We further analyzed the mean PSD in five frequency bands. Compared to the mean PSD observed at -1 d, the PSD observed at 1 d in the delta and theta bands increased in the pain-paired compartment at 1 d (one-way rm ANOVA; $F_{(1,7)} = 156.429$, $p < 0.05$ and $F_{(1,7)} = 88.682$, $p < 0.05$; Figure 7(d)). The PSD at 5 d in the delta and alpha bands decreased in the non-pain-paired compartment (one-way rm ANOVA; $F_{(1,7)} = 121.593$, $p < 0.05$ and $F_{(1,7)} = 30.721$, $p < 0.05$; Figure 7(c)). The PSD at 13 d in the delta and alpha bands decreased in the non-pain-paired compartment (one-way rm ANOVA; $F_{(1,7)} = 95.330$, $p < 0.05$ and $F_{(1,7)} = 31.672$, $p < 0.05$; Figure 7(c)), while in the beta and gamma bands, it increased in the pain-paired compartment (one-way rm ANOVA; $F_{(1,7)} = 39.571$, $p < 0.05$ and $F_{(1,7)} = 67.012$, $p < 0.05$; Figure 7(d)). The PSD at 15 d in the delta, beta, and gamma bands increased in the non-pain-paired compartment (one-way rm ANOVA; $F_{(1,7)} = 57.185$, $p < 0.05$; $F_{(1,7)} = 222.434$, $p < 0.05$; and $F_{(1,7)} = 36.979$, $p < 0.05$; Figure 7(c)), while in the theta, alpha, beta, and gamma bands, it increased in the pain-paired compartment (one-way rm ANOVA; $F_{(1,7)} = 95.254$, $p < 0.05$; $F_{(1,7)} = 444.281$, $p < 0.05$; $F_{(1,7)} = 408.482$, $p < 0.05$; and $F_{(1,7)} = 95.737$, $p < 0.05$; Figure 7(d)). Note that compared to the mean PSD observed at 13 d, the PSD of the alpha and beta bands significantly increased in the two compartments at 15 d (one-way rm ANOVA; $F_{(1,7)} = 127.105$, $p < 0.05$ and $F_{(1,7)} = 54.631$, $p < 0.05$; Figures 7(c) and 7(d)) rather than in the theta band.

4. Discussion

The results showed that EA plays an important role in regulating pain memory-related behavior and synchronous neural oscillations in the rACC. During pain memory retrieval, a nonpain stimulus generates a neural oscillatory reaction similar to the pain stimulus in the rACC. This may be a mechanism of the decrease in PWTs induced by pain memory. After EA, the nonpain stimulus did not induce decreased neural oscillatory activity in advance in the rACC. It may be that EA suppresses pain memory in nociceptive behavior. In addition, we observed an extensive change in neural oscillations in rats with aversive behavior, including power enhancement in the theta, alpha, and beta bands. EA only inhibited theta power in the rACC, and alpha and beta power levels still increased. These results indicate that EA, through the downregulation of theta power, inhibited the retrieval of aversive memory and regulated pain memory-induced aversive behavior.

4.1. The Paw Stimulus-Induced Changes in Neural Oscillations in the rACC. Our data show that the PWTs of the model group were significantly decreased compared to the control group at 15 d. This means that the pain memory in the model group was retrieved after the injury of the contralateral hind paws. It has previously been reported that a pain stimulus can rapidly inhibit spontaneous neural oscillations that can open the gates of sensory and motor systems, and a predictive warning of pain can be used to prepare for subsequent individual processing and for responses to external stimuli [37]. However, according to our results, a nonpain stimulus can also inhibit spontaneous neural oscillations. At 15 d, neural oscillations in the rACC were inhibited during tactile and pressure sensation. Then, the gate of the motor system opened in advance, and a paw withdraw response occurred.

Remarkably, neural oscillations declined early, but not for PWTs at 13 d. However, neural oscillations were inhibited early on, and PWTs also declined at 15 d. This suggests that at 13 d, the rats were hypersensitive to the nonpain stimulus, but they only paid attention to the nonpain stimulus rather than exhibiting paw withdrawal behaviors to escape. At 15 d, the rats were more sensitive after the second injury. Although the primary tissue injury to the left hind paw has recovered at 15 d, an early warning and attention can still be dedicated to the nonpain stimulus to withdraw paws early to avoid potential damage. This suggests that the paw withdrawal reaction induced by acute injury may be an escape reaction occurring through the transmission of peripheral sensory information to the central system (bottom-up), while the paw withdrawal reaction induced by pain memory may serve as a predictive warning and a protective reaction through the transmission of the central cognitive information to the periphery (top-down).

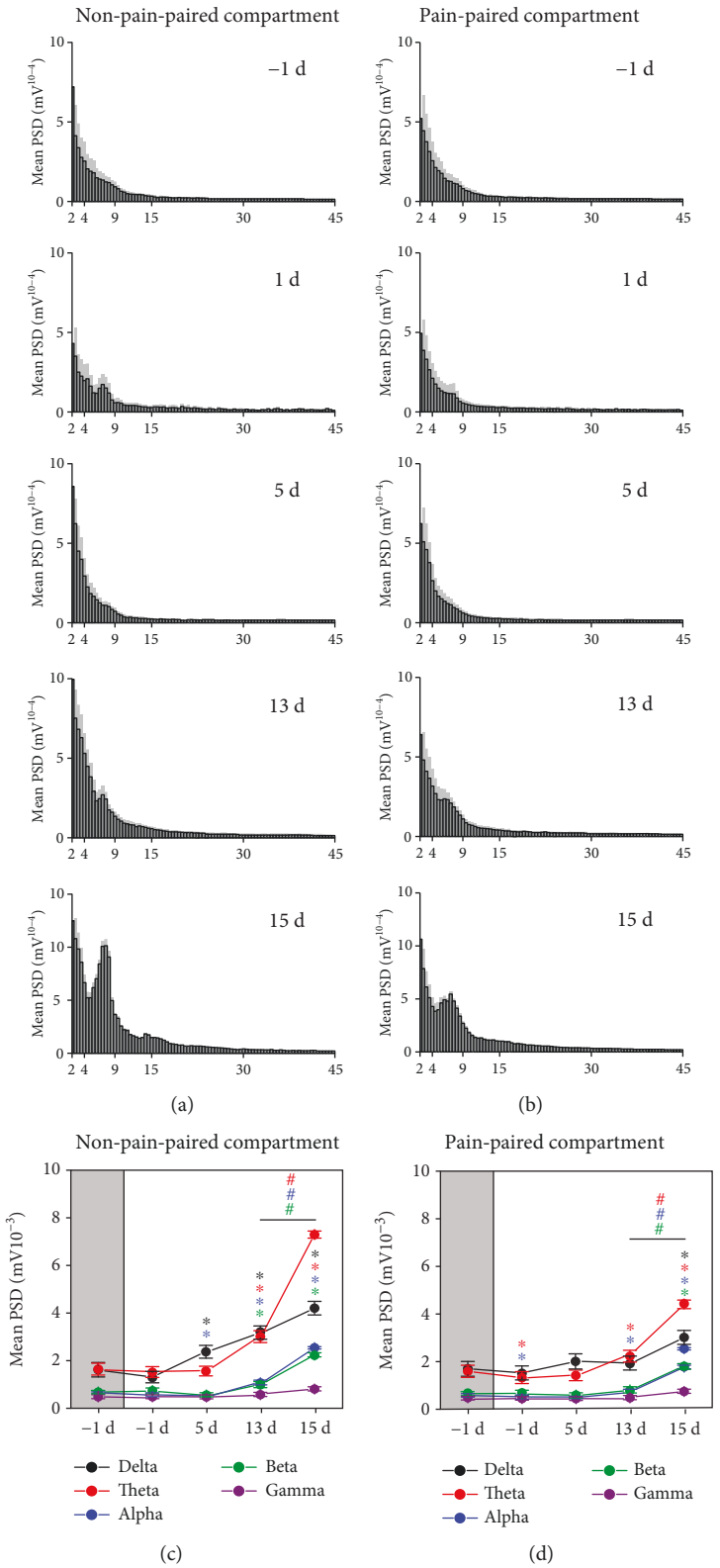

Figure 6: Synchronous LFPs during aversive behavioral testing. (a) Mean PSD histogram of the non-pain-paired compartment (the gray area indicates the standard deviation). (b) Mean PSD histogram of the pain-paired compartment (the gray area indicates the standard deviation). (c) Mean PSD of rACC LFPs for five frequency bands in the non-pain-paired compartment. $^{*}p < 0.05$ compared to -1 d; $^{\#}p < 0.05$ compared to 13 d. (d) Mean PSD of rACC LFPs for five frequency bands in the pain-paired compartment. $^{*}p < 0.05$ compared to -1 d; $^{\#}p < 0.05$ compared to 13 d. Five frequency band intervals were considered: delta (2–4 Hz), theta (4–9 Hz), alpha (9–15 Hz), beta (15–30 Hz), and gamma (30–45 Hz).

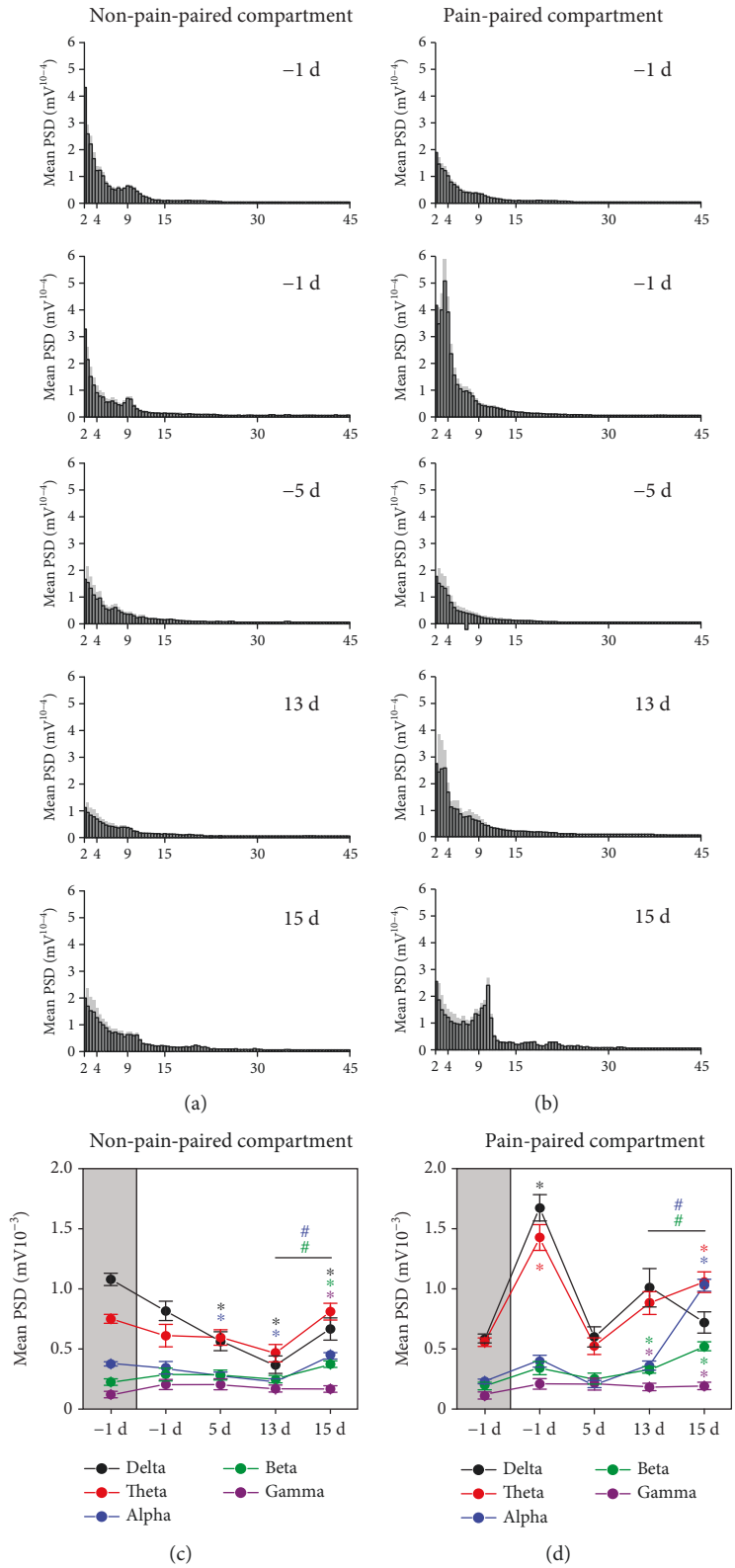

Figure 7: After EA, synchronous LFPs were observed during aversive behavioral testing. (a) After EA, the mean PSD histogram of the non-pain-paired compartment (the gray area indicates the standard deviation). (b) After EA, the mean PSD histogram of the pain-paired compartment (the gray area indicates the standard deviation). (c) After EA, the mean PSD of rACC LFPs for five frequency bands in the non-pain-paired compartment. $^{*}p < 0.05$ compared to -1 d; $^{\#}p < 0.05$ compared to 13 d. (d) After EA, the mean PSD of rACC LFPs for five frequency bands in the pain-paired compartment. $^{*}p < 0.05$ compared to -1 d; $^{\#}p < 0.05$ compared to 13 d. Five frequency band intervals were considered: delta (2–4 Hz), theta (4–9 Hz), alpha (9–15 Hz), beta (15–30 Hz), and gamma (30–45 Hz).

4.2. After EA, the Paw Stimulus Induced Changes in Neural Oscillations in the rACC. The PWTs of the EA group were significantly increased compared to those of the model group at 15 d. This indicates that EA suppresses the pain memory retrieval of left paws.

In addition, at 1 d, the PWTs of the EA group were enhanced relative to those of the model group, which means that EA likely recovers the acute pain threshold by modulating the rACC. However, the early declining PSD of rACC was not observed during the stimulus period. This indicates that EA may suppress the rACC prereaction to the nonpain stimulus during the acute period. At 13 d and 15 d, the paw nonnoxious stimulus did not induce the early decline of neural oscillations in the rACC. This could partly explain why we did not observe hyperpathia induced by pain memory. This also shows that EA may inhibit the oversensitive protective response induced by pain memory by regulating early warning information processing in the rACC.

In addition, the application of EA started 4 h after carrageenan injection and it ended at 5 d. Although the application of EA was not continued, the pain memory did not occur in the EA group after the second injury. Therefore, EA not only plays an acute analgesic role but also eliminates the subsequent long-term overprotection effect induced by pain memory.

4.3. Aversive Stimuli Induced Changes in Neural Oscillations in the rACC. CPA scores represent the time spent in the pain-paired compartment in the test session minus the time spent in the same compartment in the preconditioning (baseline) session. The CPA score obtained in this way is the difference between each rat before and after, and it can better show the changes before and after itself. Therefore, the CPA score shows the changes in the degree of aversion to the pain-paired compartment over time. Score values of the pain-paired compartment show that pain-related aversive behaviors did not appear after primary paw injury but appeared after the second paw injury, showing that pain-related aversive memory caused the rats to escape from the pain-paired compartments.

Many studies show that the increased theta band is related to memory loss and that the decreased theta band denotes memory arousal [38–40]. In our study, the PSD of the theta band gradually increased over time in pain and non-pain-paired compartments after primary paw injury. These results suggest that the memory for two compartments fades after a conditioning phase at 4 h. Note that the memory of the non-pain-paired compartment fades more quickly than that of the pain-paired compartment, especially at 15 d. Therefore, the PSD of the theta band may be a key mechanism of pain-related aversive memory processing.

4.4. After EA, an Aversive Stimulus Induced Changes in Neural Oscillations in the rACC. Rats of the EA group did not exhibit aversive escape reactions after a second paw injury. This shows that EA may suppress aversive memory retrieval by intervening with rACC. However, how EA intervenes with the neural oscillation activity in the rACC is in need of further observation.

Studies have shown that the alpha and beta bands participate in the control of top-down cognitive processes [41], especially alpha bands which are involved in internally directed cognitive processes [42–44]. Our results show that after EA, the PSD at day 15 show no changes in the theta band but show a significant increase in the alpha and beta bands after the second paw injury. Taken together, EA could not only inhibit aversive memory retrieval by intervening in the theta power but could also strengthen the inhibition of top-down control by enhancing the alpha and beta power levels. These two processes work together to suppress aversive memory induced by pain memory.

5. Conclusions

Our research, in relation to pain memory, reveals the possible intervening mechanisms of EA in long-term pain. In this study, we observe the effects of EA on pain memory-induced nociceptive and aversive behaviors and on synchronous neural oscillations in the rACC. During nociceptive behavioral testing, a pain memory-induced nonpain stimulus spurred a neural oscillatory reaction in the rACC similar that of a pain stimulus. After EA, the nonpain stimulus did not induce decreased neural oscillatory activity in the rACC until a pain stimulus was applied. During aversive behavioral testing, EA, through the downregulation of theta power, inhibited the retrieval of aversive memory and relieved pain memory-induced aversive behaviors. These results extend previous studies on pain memory and EA. These changes of oscillatory activity may be the hallmarks of EA therapy for pain memory.

Data Availability

The data used to support the findings of this study are available from the corresponding authors upon request.

Conflicts of Interest

The authors have no conflicts of interest to declare.

Authors' Contributions

Zui Shen and Yilin Zhu contributed equally to this work as co-first authors. Xiaomei Shao and Jianqiao Fang designed the experimental protocols. Zui Shen, Qiaoying He, and Jing Sun performed microwire implantation surgeries. Zemin Wu and Haiyan Zhang performed nociceptive behavioral experiments. Shujing Yao and Xiaofen He performed aversive behavioral experiments. Boyi Liu and Yi Liang performed the recording of LFPs. Zui Shen and Yilin Zhu performed data analysis and manuscript writing.

Acknowledgments

This study was supported by the National Natural Science Foundation of China (81574056, 81804183, and 81873365), the Special Financial Grant from the China Postdoctoral Science Foundation (2016T90552), the Project Supported by Zhejiang Province Top Key Discipline of Chinese Medicine-

Acupuncture and Tuina, the Class General Financial Grant from the China Postdoctoral Science Foundation (2015 M580527 and 2018M642492), and the Medicine and Health Science and Technology Plan projects of Zhejiang Province (2017KY123).

References

[1] A. V. Apkarian, M. N. Baliki, and P. Y. Geha, "Towards a theory of chronic pain," *Progress in Neurobiology*, vol. 87, no. 2, pp. 81–97, 2009.

[2] X. M. Shao, J. Sun, Y. L. Jiang et al., "Inhibition of the cAMP/P-KA/CREB pathway contributes to the analgesic effects of electroacupuncture in the anterior cingulate cortex in a rat pain memory model," *Neural Plasticity*, vol. 2016, Article ID 5320641, 16 pages, 2016.

[3] J. Sun, X. M. Shao, F. Fang, Z. Shen, Y. Y. Wu, and J. Q. Fang, "Electroacupuncture alleviates retrieval of pain memory and its effect on phosphorylation of cAMP response element-binding protein in anterior cingulate cortex in rats," *Behavioral and Brain Functions*, vol. 11, no. 1, p. 9, 2015.

[4] M. Yi and H. Zhang, "Nociceptive memory in the brain: cortical mechanisms of chronic pain," *Journal of Neuroscience*, vol. 31, no. 38, pp. 13343–13345, 2011.

[5] H. Flor, "Painful memories. Can we train chronic pain patients to 'forget' their pain?," *EMBO Reports*, vol. 3, no. 4, pp. 288–291, 2002.

[6] J. Adler, "Erasing painful memories," *Scientific American*, vol. 306, no. 5, pp. 56–61, 2012.

[7] D. S. Choi, D. Y. Choi, R. A. Whittington, and S. S. Nedeljkovic, "Sudden amnesia resulting in pain relief: the relationship between memory and pain," *Pain*, vol. 132, no. 1, pp. 206–210, 2007.

[8] I. Kissin, C. F. Freitas, and E. L. Bradley Jr., "Memory of pain: the effect of perineural resiniferatoxin," *Anesthesia and Analgesia*, vol. 103, no. 3, pp. 721–728, 2006.

[9] S. Kelly, D. Lloyd, T. Nurmikko, and N. Roberts, "Retrieving autobiographical memories of painful events activates the anterior cingulate cortex and inferior frontal gyrus," *The Journal of Pain*, vol. 8, no. 4, pp. 307–314, 2007.

[10] N. Yan, B. Cao, J. Xu, C. Hao, X. Zhang, and Y. Li, "Glutamatergic activation of anterior cingulate cortex mediates the affective component of visceral pain memory in rats," *Neurobiology of Learning and Memory*, vol. 97, no. 1, pp. 156–164, 2012.

[11] B. Guntekin and E. Basar, "Review of evoked and event-related delta responses in the human brain," *International Journal of Psychophysiology*, vol. 103, pp. 43–52, 2016.

[12] Z. Shen, J. Sun, B. Liu et al., "Mechanical stimulus-induced withdrawal behavior increases subsequent pre-stimulus local field potential power in the rostral anterior cingulate cortex in unanesthetized rats," *Medical Science Monitor*, vol. 23, pp. 1099–1105, 2017.

[13] T. Staudigl, S. Hanslmayr, and K.-H. T. Bauml, "Theta oscillations reflect the dynamics of interference in episodic memory retrieval," *Journal of Neuroscience*, vol. 30, no. 34, pp. 11356–11362, 2010.

[14] L. T. Hsieh and C. Ranganath, "Frontal midline theta oscillations during working memory maintenance and episodic encoding and retrieval," *NeuroImage*, vol. 85, Part 2, pp. 721–729, 2014.

[15] P. J. Uhlhaas and W. Singer, "Neural synchrony in brain disorders: relevance for cognitive dysfunctions and pathophysiology," *Neuron*, vol. 52, no. 1, pp. 155–168, 2006.

[16] J. J. Foxe and A. C. Snyder, "The role of alpha-band brain oscillations as a sensory suppression mechanism during selective attention," *Frontiers in Psychology*, vol. 2, p. 154, 2011.

[17] M. Alegre, I. G. de Gurtubay, A. Labarga, J. Iriarte, A. Malanda, and J. Artieda, "Alpha and beta oscillatory activity during a sequence of two movements," *Clinical Neurophysiology*, vol. 115, no. 1, pp. 124–130, 2004.

[18] G. Buzsaki and X. J. Wang, "Mechanisms of gamma oscillations," *Annual Review of Neuroscience*, vol. 35, no. 1, pp. 203–225, 2012.

[19] S. Ahn, J. H. Prim, M. L. Alexander, K. L. McCulloch, and F. Frohlich, "Identifying and engaging neuronal oscillations by transcranial alternating current stimulation in patients with chronic low back pain: a randomized, crossover, double-blind, sham-controlled pilot study," *The Journal of Pain*, vol. 20, no. 3, pp. 277.e1–277.e11, 2019.

[20] B. Fu, S. N. Wen, B. Wang, K. Wang, J. Y. Zhang, and S. J. Liu, "Acute and chronic pain affects local field potential of the medial prefrontal cortex in different band neural oscillations," *Molecular Pain*, vol. 14, 2018.

[21] H. Y. Zhao, L. Y. Liu, J. Cai, Y. J. Cui, and G. G. Xing, "Electroacupuncture treatment alleviates the remifentanil-induced hyperalgesia by regulating the activities of the ventral posterior lateral nucleus of the thalamus neurons in rats," *Neural Plasticity*, vol. 2018, Article ID 6109723, 15 pages, 2018.

[22] B. Cao, J. Wang, L. Mu, D. C.-H. Poon, and Y. Li, "Impairment of decision making associated with disruption of phase-locking in the anterior cingulate cortex in viscerally hypersensitive rats," *Experimental Neurology*, vol. 286, pp. 21–31, 2016.

[23] S. Northon, N. Rustamov, and M. Piche, "Cortical integration of bilateral nociceptive signals: when more is less," *Pain*, vol. 160, no. 3, pp. 724–733, 2019.

[24] J. Horvath, B. Barkoczi, G. Muller, and V. Szegedi, "Anxious and nonanxious mice show similar hippocampal sensory evoked oscillations under urethane anesthesia: difference in the effect of buspirone," *Neural Plasticity*, vol. 2015, Article ID 186323, 9 pages, 2015.

[25] H. Shin, R. Law, S. Tsutsui, C. I. Moore, and S. R. Jones, "The rate of transient beta frequency events predicts behavior across tasks and species," *eLife*, vol. 6, 2017.

[26] B. Lee, D. Shin, S. P. Gross, and K. H. Cho, "Combined positive and negative feedback allows modulation of neuronal oscillation frequency during sensory processing," *Cell Reports*, vol. 25, no. 6, pp. 1548–1560.e3, 2018.

[27] Q. Zhang, Z. Xiao, C. Huang et al., "Local field potential decoding of the onset and intensity of acute pain in rats," *Scientific Reports*, vol. 8, no. 1, p. 8299, 2018.

[28] X. Li, Z. Zhao, J. Ma et al., "Extracting neural oscillation signatures of laser-induced nociception in pain-related regions in rats," *Frontiers in Neural Circuits*, vol. 11, p. 71, 2017.

[29] J. Wang, B. Cao, T. R. Yu et al., "Theta-frequency phase-locking of single anterior cingulate cortex neurons and synchronization with the medial thalamus are modulated by visceral noxious stimulation in rats," *Neuroscience*, vol. 298, pp. 200–210, 2015.

[30] S. Y. Seo, K. B. Lee, J. S. Shin et al., "Effectiveness of acupuncture and electroacupuncture for chronic neck pain: a systematic review and meta-analysis," *The American Journal of Chinese Medicine*, vol. 45, no. 8, pp. 1573–1595, 2017.

[31] R. Zhang, L. Lao, K. Ren, and B. M. Berman, "Mechanisms of acupuncture-electroacupuncture on persistent pain," *Anesthesiology*, vol. 120, no. 2, pp. 482–503, 2014.

[32] Z. Y. Ju, K. Wang, H. S. Cui et al., "Acupuncture for neuropathic pain in adults," *Cochrane Database of Systematic Reviews*, vol. 12, article CD012057, 2017.

[33] J. Fang, X. Wang, H. Liu et al., "The limbic-prefrontal network modulated by electroacupuncture at CV4 and CV12," *Evidence-Based Complementary and Alternative Medicine*, vol. 2012, Article ID 515893, 11 pages, 2012.

[34] J. Wang, J. Wang, X. Li et al., "Modulation of brain electroencephalography oscillations by electroacupuncture in a rat model of postincisional pain," *Evidence-Based Complementary and Alternative Medicine*, vol. 2013, Article ID 160357, 11 pages, 2013.

[35] X. M. Shao, Z. Shen, J. Sun et al., "Strong manual acupuncture stimulation of "Huantiao" (GB 30) reduces pain-induced anxiety and p-ERK in the anterior cingulate cortex in a rat model of neuropathic pain," *Evidence-Based Complementary and Alternative Medicine*, vol. 2015, Article ID 235491, 11 pages, 2015.

[36] M. Hummel, P. Lu, T. A. Cummons, and G. T. Whiteside, "The persistence of a long-term negative affective state following the induction of either acute or chronic pain," *Pain*, vol. 140, no. 3, pp. 436–445, 2008.

[37] M. Ploner, J. Gross, L. Timmermann, B. Pollok, and A. Schnitzler, "Pain suppresses spontaneous brain rhythms," *Cerebral Cortex*, vol. 16, no. 4, pp. 537–540, 2006.

[38] L. Meyer, M. Grigutsch, N. Schmuck, P. Gaston, and A. D. Friederici, "Frontal-posterior theta oscillations reflect memory retrieval during sentence comprehension," *Cortex*, vol. 71, pp. 205–218, 2015.

[39] L. Fuentemilla, "Memory: theta rhythm couples periodic reactivation during memory retrieval," *Current Biology*, vol. 28, no. 21, pp. R1243–R1245, 2018.

[40] H. Cardoso-Cruz, M. Sousa, J. B. Vieira, D. Lima, and V. Galhardo, "Prefrontal cortex and mediodorsal thalamus reduced connectivity is associated with spatial working memory impairment in rats with inflammatory pain," *Pain*, vol. 154, no. 11, pp. 2397–2406, 2013.

[41] E. K. Miller, M. Lundqvist, and A. M. Bastos, "Working memory 2.0," *Neuron*, vol. 100, no. 2, pp. 463–475, 2018.

[42] M. E. López, P. Garcés, P. Cuesta et al., "Synchronization during an internally directed cognitive state in healthy aging and mild cognitive impairment: a MEG study," *AGE*, vol. 36, no. 3, p. 9643, 2014.

[43] S. Palva and J. M. Palva, "New vistas for alpha-frequency band oscillations," *Trends in Neurosciences*, vol. 30, no. 4, pp. 150–158, 2007.

[44] W. Peng, C. Babiloni, Y. Mao, and Y. Hu, "Subjective pain perception mediated by alpha rhythms," *Biological Psychology*, vol. 109, pp. 141–150, 2015.

Hindawi
Neural Plasticity
Volume 2019, Article ID 7084618, 11 pages
https://doi.org/10.1155/2019/7084618

Research Article

Longitudinal Analysis of Stroke Patients' Brain Rhythms during an Intervention with a Brain-Computer Interface

Ruben I. Carino-Escobar,[1,2] **Paul Carrillo-Mora**,[3] **Raquel Valdés-Cristerna**,[1] **Marlene A. Rodriguez-Barragan**,[4] **Claudia Hernandez-Arenas**,[4] **Jimena Quinzaños-Fresnedo**,[4] **Marlene A. Galicia-Alvarado**,[5] **and Jessica Cantillo-Negrete**[2]

[1]*Electrical Engineering Department, Universidad Autónoma Metropolitana Unidad Iztapalapa, Mexico City 09340, Mexico*
[2]*Division of Research in Medical Engineering, Instituto Nacional de Rehabilitación "Luis Guillermo Ibarra Ibarra", Mexico City 14389, Mexico*
[3]*Neuroscience Division, Instituto Nacional de Rehabilitación "Luis Guillermo Ibarra Ibarra", Mexico City 14389, Mexico*
[4]*Division of Neurological Rehabilitation, "Instituto Nacional de Rehabilitación Luis Guillermo Ibarra Ibarra", Mexico City 14389, Mexico*
[5]*Department of Electrodiagnostic.National Institute of Rehabilitation, "Luis Guillermo Ibarra Ibarra", Mexico City 14389, Mexico*

Correspondence should be addressed to Jessica Cantillo-Negrete; jessica.cantillo.negrete@gmail.com

Received 28 December 2018; Revised 13 March 2019; Accepted 25 March 2019; Published 14 April 2019

Guest Editor: Andrea Guerra

Stroke is a leading cause of motor disability worldwide. Upper limb rehabilitation is particularly challenging since approximately 35% of patients recover significant hand function after 6 months of the stroke's onset. Therefore, new therapies, especially those based on brain-computer interfaces (BCI) and robotic assistive devices, are currently under research. Electroencephalography (EEG) acquired brain rhythms in alpha and beta bands, during motor tasks, such as motor imagery/intention (MI), could provide insight of motor-related neural plasticity occurring during a BCI intervention. Hence, a longitudinal analysis of subacute stroke patients' brain rhythms during a BCI coupled to robotic device intervention was performed in this study. Data of 9 stroke patients were acquired across 12 sessions of the BCI intervention. Alpha and beta event-related desynchronization/synchronization (ERD/ERS) trends across sessions and their association with time since stroke onset and clinical upper extremity recovery were analyzed, using correlation and linear stepwise regression, respectively. More EEG channels presented significant ERD/ERS trends across sessions related with time since stroke onset, in beta, compared to alpha. Linear models implied a moderate relationship between alpha rhythms in frontal, temporal, and parietal areas with upper limb motor recovery and suggested a strong association between beta activity in frontal, central, and parietal regions with upper limb motor recovery. Higher association of beta with both time since stroke onset and upper limb motor recovery could be explained by beta relation with closed-loop communication between the sensorimotor cortex and the paralyzed upper limb, and alpha being probably more associated with motor learning mechanisms. The association between upper limb motor recovery and beta activations reinforces the hypothesis that broader regions of the cortex activate during movement tasks as a compensatory mechanism in stroke patients with severe motor impairment. Therefore, EEG across BCI interventions could provide valuable information for prognosis and BCI cortical activity targets.

1. Introduction

Stroke is one of the leading causes of disability worldwide [1]. Ischemic stroke is the most common type and has a global incidence of approximately 11.6 million new cases per year [1]. One of the most disabling motor impairments produced by stroke is hemiparesis which is comprised by the complete or partial paralysis of one of the body sides, including the arm, leg, foot, and hand. Furthermore, after six months of the stroke's onset, only 35% of patients recover enough hand

motor function to be able to use it in daily activities [2]. Therefore, research involving new therapies focused on stroke patients' upper limb rehabilitation is needed to increase the number of patients that achieve hand function recovery. Particularly, therapies based on robot assistive devices have shown potential for increasing stroke patients' neuroplasticity, the main recovery mechanism of stroke [2]. Some of these devices are specifically designed for upper limb motor rehabilitation by applying passive movement to stroke patients' paralyzed hand [3–6]. Another promising technology for upper limb rehabilitation of stroke patients is brain-computer interfaces (BCI). BCI allow control of external devices by decoding users' intentions from central nervous system sources such as the electroencephalogram (EEG) [7]. BCI systems are comprised by EEG signal acquisition, signal preprocessing, feature extraction, feature selection, classification, and external device communication stages [7]. Several paradigms allow BCI users to achieve control of the system, one of them is motor imagery/intention (MI), which is the mental rehearsal (motor imagery) or intention (motor intention) of movement execution and elicits similar cortical activations as actual movement [8]. MI elicits a power decrease and/or increase in alpha (8 to 13 Hz) and/or beta EEG frequencies (14 to 30 Hz) with respect to a baseline, known as event-related desynchronization or synchronization (ERD/ERS) [9]. Studies have described that stroke patients can still elicit ERD/ERS during MI of their paralyzed hand [10, 11] and during passive movement provided by robotic assistive devices [12]. Since ERD/ERS is associated with increased or decreased brain activity, it has been hypothesized that BCI systems controlled by hand MI and coupled to robotic assistive devices could be used to promote stroke patients' neuroplasticity processes, increasing the probability of upper limb function recovery [13, 14].

Although some studies have evaluated the effectiveness of a BCI coupled to robotic assistive devices for upper limb rehabilitation of stroke patients [15–18], to the authors' knowledge, none has evaluated the longitudinal changes and the relationship between upper limb motor recovery with brain rhythms recorded during a complete BCI intervention, in subacute stroke patients. Stroke patients' EEG, recorded during a BCI intervention, offers the possibly of evaluating this relationship, since changes in EEG brain rhythms have been related to neuroplasticity induced by different types of noninvasive stimulation. For example, Pellegrino et al. reported changes in EEG connectivity in stroke patients before and after a robotic hand therapy. The intervention lasted for 12 weeks, and changes in functional connectivity were reported to correlate with improvement in upper limb motor control [19]. In addition, Shindo et al. reported alpha and beta power differences in EEG electrodes placed above the somatosensory cortex of 8 stroke patients before and after 4 to 7 months intervention with a BCI coupled to a robotic hand orthosis. Half of the patients that showed more pronounced ERD over the affected hemisphere also had increased cortical excitability, measured by means of transcranial magnetic stimulation (TMS), implying a relationship between EEG power and brain plasticity [20]. Both studies reported preintervention and postintervention EEG changes; however, a trend analysis performed from several intraintervention EEG measurements could provide additional insights of neuroplasticity mechanisms involved in upper limb motor recovery. This trend analysis could comprise a longitudinal study of ERD/ERS features which could offer additional information of the neuroplasticity meaning of brain rhythms during a noninvasive intervention for stroke patients' hand rehabilitation.

The purposes of the present study are to describe changes in cortical activations across a BCI intervention and to analyze possible relationships between ERD/ERS trends and upper limb motor recovery in stroke patients. The BCI intervention was comprised by passive hand movement provided by means of a robotic hand orthosis driven by MI of the paralyzed hand of patients, undergoing an intervention as part of a larger study. EEG alpha and beta brain rhythms were recorded across 12 intervention sessions, and its association with upper limb motor recovery was analyzed.

2. Materials and Methods

2.1. Stroke Patients. Data of 9 stroke patients were included for the present study. Patients were recruited as part of a BCI validation study being conducted in the National Institute of Rehabilitation "Luis Guillermo Ibarra Ibarra" with the approval of its research committee. All patients read and signed an informed consent approved by the institute's ethical committee. Patients had an ischemic stroke diagnosis confirmed through neuroimaging by a neurologist. During the BCI intervention, patients were in the subacute phase of their stroke; therefore, no more than 10 months and no less than 2 months had passed since the stroke onset [21]. Patients were right handed before the stroke and had no previous history of neurological lesions and showed a cognitive performance with slight alterations in attention and memory processes, as well as adequate understanding of instructions, according to the neuropsychological test NEUROPSI [22]. Table 1 shows patients' information.

2.2. BCI System. The BCI system acquisition stage was comprised by a g.USBamp biosignal amplifier from g.tec and an electrode cap with 11 g.LADYbird electrodes placed in the $F3$, $F4$, Fz, $P3$, $P4$, Pz, $C3$, $C4$, Cz, $T3$, and $T4$ positions of the international 10-20 system; ground electrode was placed in the AFz position and reference electrode in the right earlobe. All EEG recordings used for the BCI system were performed with electrode impedances below 5 KΩ. A computer monitor was also part of the system and allowed showing and playing visual and auditory cues to patients. Preprocessing and processing stages of the BCI system were programmed in a PC. The preprocessing stage of the BCI was comprised by a notch 60 Hz filter and bandpass filters in the following frequency bands: 8-12 Hz, 12-16 Hz, 16-20 Hz, 20-24 Hz, 24-28 Hz, and 28-32 Hz, all are of FIR type and order 30. The processing stage's feature extraction algorithm was a common spatial pattern (CSP) filter, applied to each one of the 6 frequency subbands [24], following a methodology similar to the Filter Bank Common Spatial Patterns (FBCSP) [25]. Features extracted with the spatial

Table 1: Clinical and demographic information of stroke patients' data included in the present study. Each patient's time since the beginning of the BCI of intervention, relative to stroke onset, and time at the end of the BCI intervention is shown. Percentage of infarct in regions related to the middle cerebral artery was assessed using the ASPECTS scale [23].

Patients' identifier	Age (years)	Gender	BCI intervention period relative to stroke onset (days)	Paralyzed hand	Lesion, type, and location of the affected area	Percentage of infarct in the middle cerebral artery
*P*1	54	Female	280 - 302	Right	Subcortical. L. lentiform nucleus, L. internal capsule, and L. thalamus	50%
*P*2	85	Female	111 - 137	Left	Subcortical. R. pontine tegmentum	NM
*P*3	58	Female	190 - 222	Right	Subcortical. L. lentiform nucleus and L. internal capsule	30%
*P*4	54	Female	176 - 204	Left	Cortical-subcortical. R. insula, R. lentiform nucleus, and R. internal capsule	40%
*P*5	43	Male	61 - 90	Left	Subcortical. R. pontine tegmentum	NM
*P*6	48	Male	99 - 125	Right	Subcortical. L. internal capsule	20%
*P*7	53	Male	127 - 156	Right	Cortical. L. insula	20%
*P*8	63	Male	260 - 285	Right	Subcortical. L. lentiform nucleus and L. internal capsule	20%
*P*9	65	Male	119 - 142	Left	Subcortical. R. internal capsule and R. thalamus	10%
Mean (±STD)	59.9 (±2.8)		158 (±74) – 185 (±73)			

NM: not measured if location did not comprise the middle cerebral artery; L.: left; R.: right.

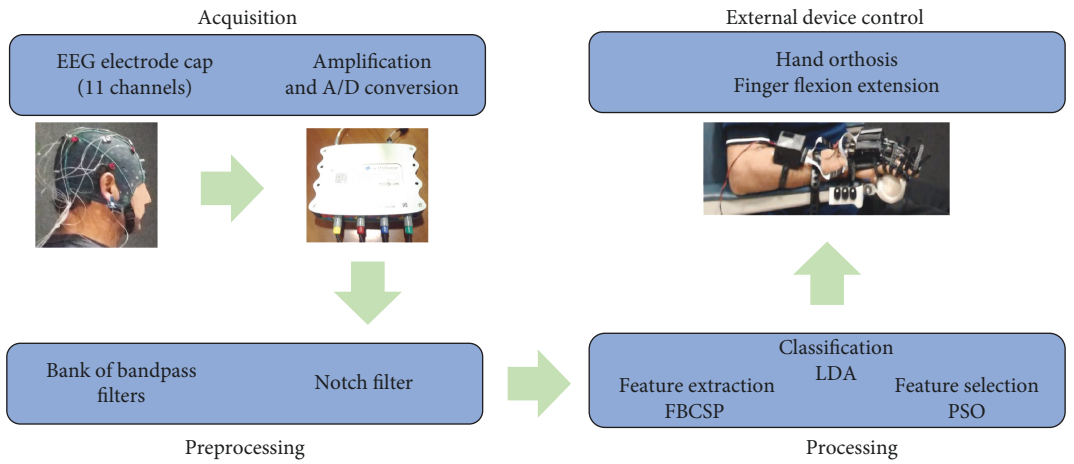

Figure 1: Stages of the BCI system employed for stroke patients' intervention.

filters were selected using particle swarm optimization (PSO) and classified with linear discriminant analysis (LDA) [26]. The system's classification output was sent to a robotic hand orthosis through wireless communication. When activated by the BCI system, the robotic orthosis provided passive flexion followed by extension of the fingers of the hand. A more detailed description of the BCI system can be found in the work by Cantillo-Negrete et al. [27]. A depiction of the BCI system is shown in Figure 1.

2.3. BCI Intervention. Patients underwent therapy with the BCI system during a 4-week intervention, with 3 sessions per week. Therefore, each patient had 12 BCI intervention sessions. Each session was comprised by 3 runs of 20 trials and lasted between 45 and 60 minutes. Patients rested for at least 3 minutes between runs. BCI sessions were conducted in a sound-attenuated room with the same illumination conditions and at the same time of the day. Patients were instructed to sit in a comfortable armed chair, with a computer monitor placed at approximately 1.5 m in front of them. The trials' time structure was based on the Graz paradigm [28] and was comprised by a first rest period of 3 s in which patients observed a white cross on the computer screen. At 2 s from initiating this rest period, a beep sound was played by the monitor's loudspeakers, notifying the patient that the task is about to begin. Three seconds after trials' onset, an arrow pointing to the direction of the patient's paralyzed hand appeared in the computer screen,

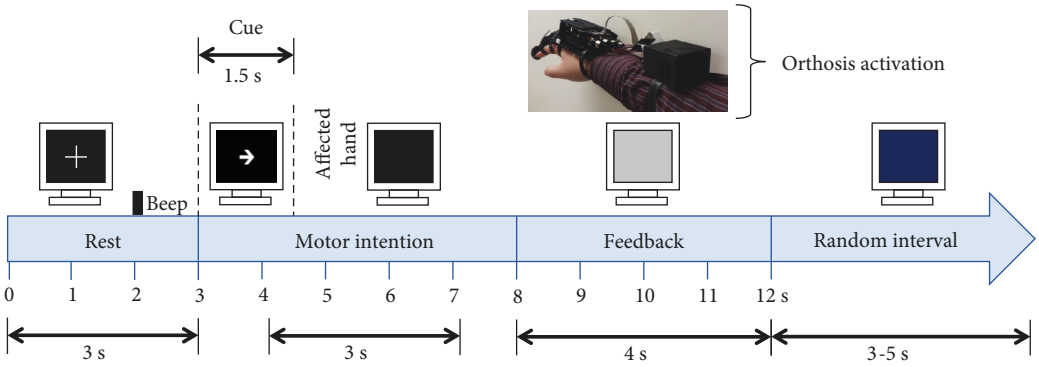

Figure 2: Structure of trials during the BCI intervention.

signaling the patient to perform MI of the affected hand. This arrow lasted 1.5 s and afterwards disappeared with the monitor's screen turning black for another 3.5 s. During this time (arrow or black screen shown in the monitor), patients were instructed to perform MI of their paralyzed hand. After this time, the BCI system processed 3 s of EEG data segmented in 1-second length windows, from 4 to 7 seconds of the trial's structure. If 2 of these time windows were classified as MI, then the robotic orthosis was activated; if 1 or no time windows were classified as MI, then the robotic orthosis was not activated. Regardless of the orthosis activation, after 8 s from the trial onset, the screen turned grey for 4 s. Finally, each trial ended with a blue screen that lasted between 3 and 5 s, to prevent habituation, in which patients could blink their eyes, move, and rest. Figure 2 shows a trial's structure.

2.4. Patients' Clinical Assessment. Clinical assessment of patients' upper extremity motor recovery after the BCI intervention was performed using the upper extremity Fugl-Meyer assessment (FMA-UE) [29], by applying the scale to each patient before and after the BCI intervention. FMA-UE ranks upper extremity motor recovery in a 0-66 scale, with a lower score representing a lower motor impairment. Differences in the scale's scores between preintervention and postintervention were used as clinical upper limb motor recovery markers.

2.5. EEG Signal Processing. Patients' raw EEG data recorded from each session were analyzed. Data were preprocessed with a 30th-order FIR filter from 8 to 32 Hz and a common average reference (CAR) spatial filter for reducing ground placement effects in EEG data [30]. For each trial and EEG channel, alpha and beta time-frequency features were computed by means of the Morlet wavelet transform as explained by Tallon-Baudry et al. [31]. In order to eliminate trials with excessive noise artifacts, the interquartile ranges from the 60 trials of each patients' session were computed. Trials that exceeded power values 3 times higher than the 3rd quartile or 3 times lower than the 1st quartile were regarded as outliers and eliminated from the session's trial sample. Less than 5% of the total recorded trials were eliminated with this procedure. Afterwards, percentage of ERD/ERS was computed for each trial by subtracting averaged power from the 3 s time interval that comprised the rest condition (0-3 s of the trials' time structure) from the trial's power during MI (4-7 s of the trials' time structure) and dividing it by the rest condition's averaged power and afterwards multiplying it by 100 [32]; this procedure is described in

$$\frac{\%\text{ERD}}{\text{ERS}} = \left(\frac{P_{\text{MI}} - P_{\text{rest}}}{P_{\text{rest}}}\right) * 100, \quad (1)$$

with P_{MI} being MI task's power and P_{rest} averaged power during the rest condition. Alpha features were extracted by averaging ERD/ERS values from the 8-13 Hz band and beta features by averaging values from 14-32 Hz. Afterwards, averaged MI-related ERD/ERS (4-7 s of the trials' time structure) were computed from alpha and beta bands. Therefore, for all patients' EEG channels to represent information from the same affected and unaffected hemisphere, regardless of the lesioned hemisphere, ERD/ERS for the left hemisphere's channels ($F3$, $C3$, $T3$, and $P3$) of patients with right hemisphere lesions were interchanged with those for the right hemisphere's channels ($F4$, $C4$, $T4$, and $P4$). This allowed the affected hemisphere's (AH) cortical activity to be shown over the left hemisphere's channels (F_{AH}, C_{AH}, T_{AH}, and P_{AH}) and unaffected hemisphere's (UH) activity to be shown over the right channels (F_{UH}, C_{UH}, T_{UH}, and P_{UH}). Grand average brain topographic maps of ERD/ERS were computed for each of the 12 intervention sessions, separately for alpha and beta frequency bands. To quantitatively analyze ERD/ERS across sessions, a trend analysis, proposed by López-Larraz et al., was performed by computing the slope of a least squares fitted linear regression model from the averaged ERD/ERS values of each session and sessions' time since stroke onset (stated in days), separately, for each channel and for alpha and beta bands [33].

2.6. ERD/ERS Association with Clinical Recovery. A stepwise linear regression model [34] was used to explore the relationship between clinical hand motor recovery and ERD/ERS trends across BCI intervention sessions. The predicted variable (dependent variable) was set as each patients' differences between preintervention and postintervention of the FMA-UE scores. Predictor variables (independent variables) were set as computed ERD/ERS slopes for each channel and patient. All possible combinations of initial predictor variables included in the model were assessed. Models

were calculated separately for alpha and beta ERD/ERS slopes.

2.7. Statistical Analysis. ERD/ERS data were tested for Gaussian distribution by means of a Lilliefors-corrected Kolmogorov-Smirnov test ($\alpha = 0.05$) [35]. After this test implied non-Gaussian distribution, statistically significant ($\alpha = 0.05$) differences between ERD/ERS across sessions were assessed for each channel, separately for alpha and beta bands, with Friedman nonparametric tests for repeated measures design [36]. ERD/ERS linear trends across sessions were evaluated for significance by computing the Spearman correlation between mean ERD/ERS with time since stroke's onset, as performed by López-Larraz et al. [33]. Slope significance values were FDR corrected for multiple comparisons. For the stepwise linear regression analysis, only models that presented a statistically significant ($\alpha = 0.05$) prediction of the dependent variable, measured by means of p values obtained from an F distribution and whose coefficients' confidence intervals ($\alpha = 0.05$) did not included the 0 value, were included. If more than one model was statistically significant per frequency band, then the model with the lowest p value was presented for each band as advised by Draper and Smith [37]. All computations were performed using MATLAB® software from MathWorks.

3. Results

3.1. Patients' Clinical Assessment. Table 2 shows the FMA-UE scores obtained for each of the 9 patients that underwent the BCI intervention. Three patients (*P*3, *P*5, and *P*9) had score gains equal or higher than 3. Three patients (*P*4, *P*7, and *P*8) had score gains between 2 and 1, while 3 other patients (*P*1, *P*2, and *P*6) did not have score gains.

3.2. ERD/ERS Longitudinal Brain Maps. Figure 3 shows grand average ERD/ERS topographic maps separately for alpha and beta bands. In the alpha band, significant ($p < 0.05$) differences across sessions were observed in AH frontal, central, and temporal electrodes (F_{AH}, C_{AH}, and T_{AH}). In the UH, significant ($p < 0.05$) differences were observed in central, temporal, and parietal electrodes (C_{UH}, T_{UH}, and P_{UH}). In the sagittal region, only the central channel (C_Z) showed significant ($p < 0.05$) differences across sessions. In beta, all channels in the AH (F_{AH}, C_{AH}, T_{AH}, and P_{AH}) and UH (F_{UH}, C_{UH}, T_{UH}, and P_{UH}) presented significant ($p < 0.05$) differences across sessions, while only the central channel (C_Z) of the sagittal region did not present significant ($p < 0.05$) differences. Therefore, for four channels in alpha and one in beta, significant ERD/ERS ($p < 0.05$) differences were not observed across sessions. Since maps showed ERD (cortical activations) mainly in frontal and central areas, Wilcoxon signed-rank tests were used to assess if significant ($\alpha = 0.05$) differences were found between central and frontal ERD/ERS for each session. In both alpha and beta, the comparisons that showed consistent differences across sessions were the ones observed between F_{AH} and C_{UH}. In alpha, F_{AH} and C_{UH} were not significantly different in sessions 1 to 6 and 12, while more pronounced ($p < 0.05$) ERD in F_{AH} compared to C_{UH} were observed in sessions 7 to 11, while in beta, F_{AH} and C_{UH} were not significantly different in sessions 1 to 6 and 9, while more pronounced ($p < 0.05$) ERD in F_{AH} compared to C_{UH} were observed in sessions 7, 8, 10, 11, and 12.

Table 2: FMA-UE scores for 9 patients. Score ranges from 0 to 66; higher score's values imply lesser upper limb motor impairment.

Patient	Pre-BCI intervention	Post-BCI intervention	Intervention difference
*P*1	12	12	0
*P*2	13	13	0
*P*3	9	12	3
*P*4	11	12	1
*P*5	32	36	4
*P*6	15	14	-1
*P*7	16	17	1
*P*8	59	61	2
*P*9	16	20	4

3.3. ERD/ERS Longitudinal Trends. Central channel's (C_{AH} and C_{UH}) linear trends computed from patient *P*5 mean %ERD/ERS across sessions can be observed in Figure 4. In alpha, a negative slope implied a trend towards ERD in the central AH, while a positive slope suggested a trend towards ERS in the central UH. In beta, trends towards ERS were observed in both AH and UH central channels.

Table 3 shows ERD/ERS slopes computed from each patient and channel calculated for alpha. A total of 45 slopes implied more pronounced ERD trends (negative slope), while the other 54 suggested less pronounced ERS (positive slope) across intervention sessions. Negative and positive ERD/ERS slopes that presented significant correlation with stroke's onset were observed in 24 and 36 channels, respectively. The trend with more pronounced ERD (lowest ERD/ERS slope) was observed in the UH parietal channel (P_{UH}) of *P*5 (-2.81). The trend with less pronounced ERD (highest ERD/ERS slope) was observed in the UH central channel (C_{UH}) of *P*5 (2.12).

Table 4 shows ERD/ERS slopes computed from each patient and channel calculated for beta. Approximately half of the slopes (49) implied more pronounced ERD trends (negative slope), while the others suggested (50) less pronounced ERS (positive slope) across intervention sessions. Negative and positive ERD/ERS slopes that presented significant correlation with stroke's onset were observed in 34 and 39 channels, respectively. The trend with more pronounced ERD (lowest ERD/ERS slope) was observed in the UH parietal channel (F_{UH}) of *P*4 (-1.23). The trend with more pronounced ERD (highest ERD/ERS slope) was observed in the UH temporal channel (T_{UH}) of *P*4 (2.09).

3.4. ERD/ERS Association with Clinical Recovery. Equations (2) and (3) show linear models computed with alpha and beta

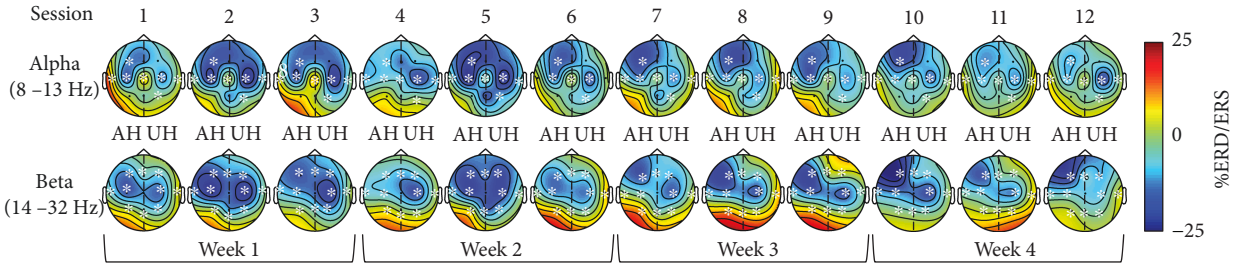

Figure 3: Grand average topographic maps of ERD/ERS during MI are observed across each session. Blue tones show ERD and red tones show ERS. All maps are plotted using the same scale. Affected (AH) and unaffected hemispheres (UH) are shown. Channels with significant differences across sessions are marked (*).

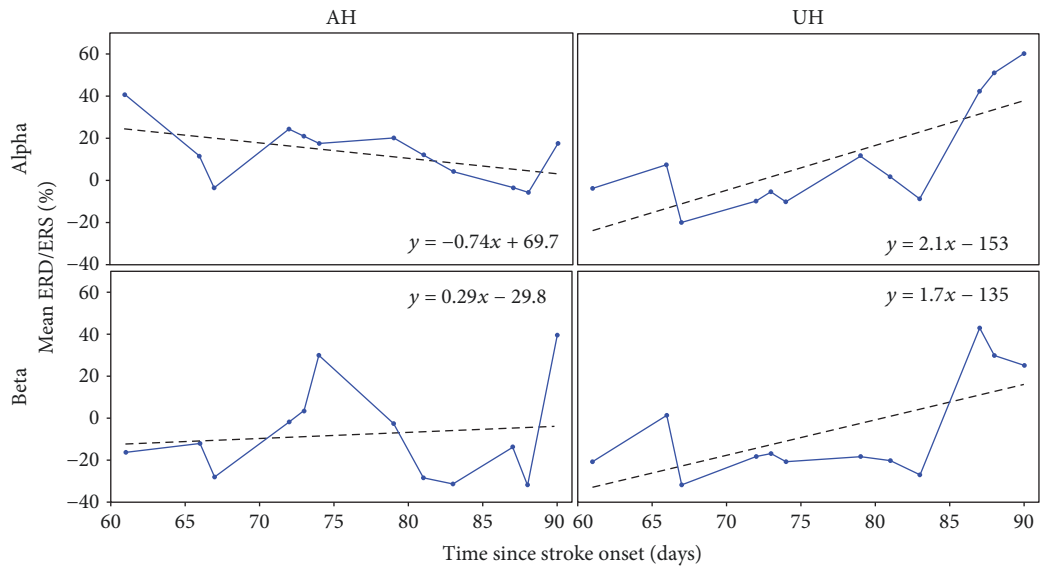

Figure 4: Example of linear trends, computed from average ERD/ERS across sessions and taking into account days since stroke onset. Slopes were calculated from central channels of the AH and UH of patient *P*5. Trends were computed separately for alpha and beta bands.

Table 3: Slopes of ERD/ERS computed for each patient in the alpha band and for each AH (F_{AH}, C_{AH}, T_{AH}, and P_{AH}), sagittal (*Fz*, *Cz*, and *Pz*), and UH (F_{UH}, C_{UH}, T_{UH}, and P_{UH}) channels. Slopes computed from ERD/ERS with a significant correlation with time since stroke onset (*) are shown.

Patient	F_{AH}	C_{AH}	T_{AH}	P_{AH}	*Fz*	*Cz*	*Pz*	F_{UH}	C_{UH}	T_{UH}	P_{UH}
*P*1	0.73*	-0.05	0.17	0.52*	0.41*	0.10	0.13	0.65*	0.43*	0.43*	-0.28
*P*2	0.09	0.34*	0.00	0.13	0.18	0.03	0.07	-0.19	0.32*	-0.20*	0.22*
*P*3	1.01*	-0.14	0.34*	0.60*	0.98*	0.20*	0.51*	0.69*	0.22*	0.25*	0.22*
*P*4	-0.29*	-0.27*	-0.13	-0.41*	-0.19	-0.44*	-0.30*	-1.10*	-0.40*	-0.13*	-0.02
*P*5	-0.38*	-0.74*	0.35*	-1.05*	-1.03*	-2.03*	-0.46	-0.92*	2.12*	-1.63*	-2.81*
*P*6	0.23*	0.47*	0.35*	-1.12*	-0.02	-0.80	-0.11	-0.22*	1.14*	-0.19	0.45*
*P*7	0.09	0.66*	-0.52*	0.43*	0.44*	0.10	-0.31*	0.17*	0.50*	0.68	0.62*
*P*8	-0.16	-0.15	-0.07	-0.32*	-0.11	-0.07	0.18	-0.11	-0.55*	-0.03	-0.25*
*P*9	0.49*	0.06	0.71	0.65	0.54*	0.74*	-0.16	-0.09	0.06	0.93*	0.32

ERD/ERS trends' slopes, respectively. Negative coefficients in the models implied that a negative channel trend slope, observed when more pronounced ERD was presented across sessions, was associated with lower upper limb motor impairment after the BCI intervention. On the other hand, positive coefficients in the model suggested that a positive channel trend slope, which was observed when less pronounced ERD was presented across sessions, was associated

Table 4: Slopes of ERD/ERS computed for each patient in the beta band and for each AH (F_{AH}, C_{AH}, T_{AH}, and P_{AH}), sagittal (Fz, Cz, and Pz), and UH (F_{UH}, C_{UH}, T_{UH}, and P_{UH}) channels. Slopes computed from ERD/ERS with a significant correlation with time since stroke onset (*) are shown.

Patient	F_{AH}	C_{AH}	T_{AH}	P_{AH}	Fz	Cz	Pz	F_{UH}	C_{UH}	T_{UH}	P_{UH}
$P1$	-0.02	0.10*	0.05	0.10*	0.24*	0.08	0.13*	-0.02	0.04	0.25*	0.10
$P2$	0.69*	1.05*	0.24*	0.99*	0.69*	1.36*	0.77*	0.32*	0.58*	0.69*	0.62*
$P3$	-0.42*	-0.58*	-0.50*	-0.05*	-0.02	-0.08	-0.24*	-0.28*	-0.06	-0.36*	-0.46*
$P4$	1.37*	-0.17	-0.03	1.03*	2.02*	0.42*	1.24*	-1.23*	-0.35	-0.26	0.17
$P5$	0.24	0.29	0.50*	-0.07	0.04	0.05	0.10*	-0.54*	1.68*	0.05	-0.47*
$P6$	-1.11*	-0.90*	-0.81*	-1.09*	-0.52*	-0.97*	-0.46*	-0.12*	-0.34*	-0.31*	-0.44*
$P7$	0.41*	0.93*	-0.17*	0.97*	0.90*	0.54*	0.44*	0.88*	1.87*	2.09*	0.85*
$P8$	-0.03	0.46*	0.50*	-0.23*	-0.23*	-0.34*	-0.30*	-0.21*	-0.46*	-1.13*	-0.16*
$P9$	-0.12	-0.22*	0.75*	0.28*	-0.27	-0.58*	-0.24*	-0.23	-0.03	1.12*	0.08

with lower upper limb motor impairment after the BCI intervention. The intercept term shows how much changes in motor impairment could be observed if a patient did not present ERD/ERS trends in channels included in the model (zero-magnitude slopes).

Equation (2) shows the linear model, obtained through stepwise regression that best fitted stroke patient's hand motor recovery for the alpha band ($p = 0.02$). Channels from the frontal and temporal AH (F_{AH} and T_{AH}), frontal sagittal (Fz), and parietal UH (P_{UH}) regions were included in the model. Coefficients' confidence intervals ($\alpha = 0.05$) were not zero inclusive. The model's adjusted R^2 was of 0.83, implying that the model successfully predicts 83% of FMA-UE scores' variability. The alpha model implies that trends across the intervention of more pronounced ERD in the F_{AH} and P_{UH}, coupled to less pronounced ERD in the T_{AH} and Fz, are associated with less upper limb motor impairment at the end of the BCI intervention. The intercept term of the model implies an average gain of 0.89 points in patients' post-BCI intervention FMA-UE, if no changes of included channels' ERD/ERS were presented across the intervention sessions (channels' slopes included in the model equal to zero).

$$\begin{aligned}\mathrm{FMUE}_{\mathrm{post}} - \mathrm{FMUE}_{\mathrm{pre}} = {} & -(8.64[-13.8,-3.4])(F_{\mathrm{AH}}) \\ & + (3.9[1.1, 6.8])(T_{\mathrm{AH}}) \ldots \\ & + (10.19[4.8, 15.1])(F_{\mathrm{z}}) \\ & - (3.16[-4.7,-1.6])(P_{\mathrm{UH}}) + 0.89.\end{aligned} \tag{2}$$

Equation 3 shows the linear model, obtained with stepwise regression, that best fitted stroke patients' hand motor recovery for the beta band ($p = 0.001$). The ERD/ERS slopes of the parietal (P_{AH}) channel of the AH(PAH), coupled to the parietal sagittal (Pz) and frontal (F_{UH}) and central (C_{UH}) UH channels were included in the model. All coefficient confidence intervals ($\alpha = 0.05$) were not zero inclusive. The model's adjusted R^2 was of 0.96, implying that the model successfully predicts approximately 96% of patients' FMA-UE scores' variability. The beta model implies that more pronounced ERD in F_{UH} and Pz regions, coupled to less pronounced ERD in P_{AH} and C_{UH}, are associated with less motor impairment at the end of the BCI intervention. The intercept term of the model was of 0.7; therefore, if no changes of included channels' mean ERD/ERS were presented across the intervention session (channels' slopes included in the model equal to zero), patients would have a 0.7 increase in their FMA-UE scores after the BCI intervention.

$$\begin{aligned}\mathrm{FMUE}_{\mathrm{post}} - \mathrm{FMUE}_{\mathrm{pre}} = {} & (4.11[2.9, 5.3])(P_{\mathrm{AH}}) \\ & - (6.25[-7.8,-4.8])(Pz) \ldots \\ & - (3.55[-4.4,-2.7])(F_{\mathrm{UH}}) \\ & + (1.28[0.8, 1.8])(C_{\mathrm{UH}}) + 0.7.\end{aligned} \tag{3}$$

4. Discussion

Cortical activation differences were observed in several regions across sessions of the BCI intervention. In both alpha and beta, activation changes were observed over the somatosensory cortex, which could be expected since MI-BCI systems coupled to robotic assistive devices have shown to elicit activity above this area in stroke patients [15, 27]. However, these central area significant changes across sessions were not associated in all patients with time since stroke onset. Other areas such as frontal, temporal, and parietal regions also showed significant changes across sessions in alpha and/or beta and in some patients these changes presented a significant association with time since stroke. This implied that regions usually not associated with motor tasks could be recruited in stroke patients during MI of their impaired upper limb. This is also reinforced by the observed evolution of compared activity in frontal AH and central UH across sessions, since similar activations were more likely to be observed over these regions in alpha and beta in earlier sessions and afterwards changed towards more pronounced activations in frontal AH compared to central UH, in later

sessions of the intervention. This could suggest that the frontal region of the AH could have been recruited, during the contralateral MI task, as a compensatory mechanism enhanced across the intervention. Recruitment of parietal and frontal regions has also been reported during stroke patients' evolution using fMRI by Ward et al. and hypothesized a possible enlargement of the motor region for compensating damage of the corticospinal tract [38]. Fewer patients' cortical areas in the alpha band showed activation trends across sessions, which had a significant association with stroke's onset, compared to beta. This could imply that a BCI intervention in stroke patients is more likely to elicit beta band modulation across time. It has been theorized that beta oscillations are associated with neural networks that propagate activity between primary motor cortex and muscles [39], while alpha has been related to motor information processes, such as learning of motor tasks [40]. Therefore, less ERD/ERS significant trends associated with time since stroke onset in alpha could be related to these processes, since patients' changes in alpha activity across sessions could be more associated with learning of the MI task. On the other hand, beta could reflect changes in motor cortex information processing within the corticospinal tract, as a consequence of neuroplasticity mechanisms, and thus could have a closer relationship with stroke time evolution compared to alpha oscillations. A similar hypothesis was also suggested by Gandolfi et al. since alpha and beta changes were also presented across a BCI intervention in a single stroke patient. The authors proposed that the alpha band was related with MI training processes, which could have aided to modulate beta, associated with corticospinal excitability [41].

An association between alpha ERD/ERS trends in frontal, temporal, and parietal regions with upper limb motor recovery was observed. However, the model's significance is less than the one recommended for linear regression analysis [37] and its prediction of upper limb recovery is moderate; therefore, it needs to be further confirmed with a higher sample of patients. A possible reason for this moderate association could be that alpha rhythm evolution across sessions is more related to the learning of the MI task, rather than to upper limb motor recovery, as previously suggested [39, 40, 42]. Interestingly, the alpha model did not include activity over electrodes directly located above the somatosensory cortex; this could also highlight the need for a larger sample of patients, to further assess somatosensory cortex alpha oscillation's association with upper limb motor recovery. On the other hand, an association with a recommended significance [36], between beta cortical activity trends across sessions in frontal, central, and parietal areas, with upper limb motor recovery, was observed. The model included the central UH implying that less pronounced cortical activity across sessions in this region was related to upper limb motor recovery during the intervention. However, it did not include an association between motor impairment with central AH cortical activity across sessions. Kaiser et al. reported in the alpha band of 27 stroke patients (which performed MI of their affected hand) that less pronounced cortical activation (less pronounced ERD) in the central UH, during patients' affected hand MI, was related to less motor impairment, while no association was found between cortical activations in the central AH with motor impairment [11]. Although, Kaiser et al. only reported similar central region observations in alpha, both alpha and beta have been associated with motor-related processes. Therefore, both Kaiser et al. observations and those of the present study's suggest that less pronounced central UH cortical activity could be related to less motor impairment, while AH activity could not be as associated with motor impairment. A possible explanation for these similar observations could be that it is more likely that patients' UH somatosensory cortex becomes less involved in ipsilateral motor processes as the corticospinal tract becomes more functional, compared to the possibility of the AH somatosensory cortex becoming more involved in contralateral motor processes, due to lesion heterogeneity presented in stroke. This hypothesis is reinforced by the observations reported by Lotze et al. in well-recovered subcortical stroke patients using MRI-derived measurements and TMS, since higher AH corticospinal tract integrity was associated with less pronounced activity in areas within the UH motor cortex [42]. The present study's beta model also implies that activation trends in areas usually not related with motor processes such as frontal and parietal regions could be associated with upper limb motor recovery after stroke. The model suggests that higher cortical activity trends (more pronounced ERD) in the UH frontal and parietal sagittal regions, combined with lower activity trends (more pronounced ERS) in parietal AH and central UH, were associated with higher motor recovery during the intervention. This could imply that an enlargement of the motor area, by including frontal and parietal regions, during motor-related processes, could be a neuroplasticity mechanism for improving upper limb function. Therefore, different degrees of activation in areas less related with motor processing, implied by the beta model, further reinforce previously observed enlargement of motor-processing areas during stroke recovery [38]. In addition, involvement of larger AH and UH areas during motor tasks has been described as a possible compensatory mechanism in patients with severe stroke motor impairment as reviewed by Cassidy and Cramer [43]. This could possibly explain the association of these regions in the present study, with upper limb motor impairment, as implied by alpha and beta linear models, since most patients included in the present study had moderate to severe upper limb stroke impairment. This is reinforced by the observations reported by Rondina et al. when predicting motor recovery in patients with severe stroke upper limb impairment, using features extracted from structural MRI and machine learning, to classify good or poor motor recovery, and suggested that prediction accuracy increased when larger areas of the somatosensory cortex were included in the model [44]. Furthermore, the longitudinal observations of Park et al. in stroke patients' resting state functional connectivity, computed from fMRI, reported connectivity changes comprising frontal and parietal cortex AH regions [45], reinforcing the hypothesis that normally non-motor-related regions could play a significant role during stroke recovery.

It has also been reported that interhemispheric differences in beta, between homologous somatosensory cortex

areas, could play an important role in stroke motor recovery processes. For example, Shiner et al. reported an association between higher central AH and lower UH cortical activity in stroke patients' beta band, with lower motor impairment using magnetoencephalography, a high spatial and temporal resolution acquisition modality [46]. Furthermore, Pichiorri et al. reported that interhemispheric connectivity measurements, computed from EEG over somatosensory cortex regions in lower beta, can be associated with corticospinal integrity, evaluated by means of TMS [47]. Although the present work did not explore connectivity measurements among interhemispheric homologous areas, the beta model in the present work included the somatosensory cortex in the UH and implied that less beta cortical activity in this region was associated with higher motor recovery. Therefore, a trend towards less activity in the UH somatosensory cortex could be related with the recovery of interhemispheric balance across the BCI intervention. This could further reinforce the hypothesis of an association between interhemispheric differences with upper limb motor recovery; however, a larger sample and functional connectivity measurements should be computed in order to further assess this relationship.

According to the FMA-UE, patients' motor recovery was heterogenous along the sample. After the BCI intervention, 6 of 9 patients showed gains in upper limb motor recovery, while 2 patients showed no gains and one patient showed a decrease. All FMA-UE gains were in the range (4.55 ± 6.07) reported by Ang et al. with a 1-month intervention with a BCI coupled to a robotic assistive device [16]. Two-thirds of the patients with higher FMA-UE gains were in the range of other BCI stroke intervention studies, such as the one reported by Frolov et al. (5.25 ± 4.5) with a 1.5-month intervention [17] and Ramos-Murguialday et al. (3.4 ± 2.2) with a 1-month intervention [18]. Therefore, patients' clinical assessments show that the BCI intervention allowed most patients to achieve some degree of upper extremity motor recovery and that these recoveries are similar to the ones reported with other BCI interventions.

The present study has limitations that need to be acknowledged. One of them is the limited spatial resolution of EEG. This limited resolution, although acceptable for BCI applications, makes the association of more specific brain regions with upper limb recovery unfeasible, requiring the use of modalities like fMRI for further description of the evolution of brain rhythms across BCI interventions. Another limitation is the small sample of 9 patients' data, with heterogenous motor impairment (9 to 59 in the FMA), analyzed in the current study. This limited sample makes necessary the confirmation in a higher sample of patients of the presented regression models' association with upper limb motor impairment, especially the model computed from alpha ERD/ERS trends which showed lower than recommended significance. Also, most patients in the present study presented moderate to severe upper limb motor impairment and computed linear models could be mostly applicable to patients with these degrees of impairment. Therefore, studies that include a more balanced sample of patients with different degrees of stroke upper limb impairment are still needed for a more complete description of associations between upper limb impairment and brain rhythms. Taking into account these limitations, the present study's beta rhythm-described associations with upper limb motor recovery, which is thought to be more involved in closed-loop motor training processes [39], could bring more insight to the neuroplasticity mechanisms associated to good or poor upper limb recovery prognosis. This is important for establishing EEG brain rhythm longitudinal analysis as a complementary tool to other clinical assessments, for stroke patients' upper limb function prognosis. Also, specifically targeting trends and regions of AH and UH cortical activations during hand rehabilitation interventions, such as the ones implemented with BCI systems coupled to robotic devices, could potentially increase the number of patients that can achieve good rehabilitation outcomes.

5. Conclusion

This study presents a trend analysis of stroke patients' cortical activity during a BCI intervention aimed for hand rehabilitation. EEG trends in alpha seemed to be moderately related with time since stroke onset and recovery of upper limb motor function, probably reflecting neuroplasticity effects related to learning of the hand motor tasks. On the other hand, EEG trends in beta showed a higher association with time since stroke onset, compared to alpha, and a strong association with upper limb motor recovery. These beta band changes in hemispheres' nonhomologous activity along the BCI intervention suggested that longitudinal measurements could be associated with motor recovery of the upper limb. Although these findings need to be further confirmed with studies with higher spatial resolution and larger patient samples, it can be inferred that longitudinal analysis of EEG brain rhythms during stroke patients' hand rehabilitation interventions could provide valuable clinical information for both stroke prognosis and BCI intervention goals.

Data Availability

The EEG data used to support the findings of this study are restricted by the National Institute of Rehabilitation Luis Guillermo Ibarra Ibarra ethics committee, in order to protect patient privacy. Data are available from Dr. Jessica Cantillo-Negrete for researchers who meet the criteria for access to confidential data.

Conflicts of Interest

The authors declare that they have no conflicts of interest.

Acknowledgments

The authors would like to thank all the patients that participated in this study. This work was supported by Consejo Nacional de Ciencia y Tecnología (CONACYT) (SALUD-2015-2-262061).

References

[1] E. J. Benjamin, M. J. Blaha, S. E. Chiuve et al., "Executive summary: heart disease and stroke statistics-2017 update: a report from the American Heart Association," *Circulation*, vol. 135, no. 10, pp. 399–410, 2017.

[2] B. H. Dobkin, "Rehabilitation after stroke," *New England Journal of Medicine*, vol. 352, no. 16, pp. 1677–1684, 2005.

[3] R. Bertani, C. Melegari, M. C. de Cola, A. Bramanti, P. Bramanti, and R. S. Calabrò, "Effects of robot-assisted upper limb rehabilitation in stroke patients: a systematic review with meta-analysis," *Neurological Sciences*, vol. 38, no. 9, pp. 1561–1569, 2017.

[4] F. Orihuela-Espina, G. F. Roldán, I. Sánchez-Villavicencio et al., "Robot training for hand motor recovery in subacute stroke patients: a randomized controlled trial," *Journal of Hand Therapy*, vol. 29, no. 1, pp. 51–57, 2016.

[5] J. Iqbal, H. Khan, N. G. Tsagarakis, and D. G. Caldwell, "A novel exoskeleton robotic system for hand rehabilitation – conceptualization to prototyping," *Biocybernetics and Biomedical Engineering*, vol. 34, no. 2, pp. 79–89, 2014.

[6] X. L. Hu, K. Y. Tong, X. J. Wei, W. Rong, E. A. Susanto, and S. K. Ho, "The effects of post-stroke upper-limb training with an electromyography (EMG)-driven hand robot," *Journal of Electromyography and Kinesiology*, vol. 23, no. 5, pp. 1065–1074, 2013.

[7] J. R. Wolpaw, N. Birbaumer, D. J. McFarland, G. Pfurtscheller, and T. M. Vaughan, "Brain–computer interfaces for communication and control," *Clinical Neurophysiology*, vol. 113, no. 6, pp. 767–791, 2002.

[8] S. Kraeutner, A. Gionfriddo, T. Bardouille, and S. Boe, "Motor imagery-based brain activity parallels that of motor execution: evidence from magnetic source imaging of cortical oscillations," *Brain Research*, vol. 1588, pp. 81–91, 2014.

[9] G. Pfurtscheller, C. Brunner, A. Schlögl, and F. H. Lopes da Silva, "Mu rhythm (de)synchronization and EEG single-trial classification of different motor imagery tasks," *NeuroImage*, vol. 31, no. 1, pp. 153–159, 2006.

[10] K. K. Ang, C. Guan, K. S. G. Chua et al., "A large clinical study on the ability of stroke patients to use an EEG-based motor imagery brain-computer interface," *Clinical EEG and Neuroscience*, vol. 42, no. 4, pp. 253–258, 2011.

[11] V. Kaiser, I. Daly, F. Pichiorri, D. Mattia, G. R. Müller-Putz, and C. Neuper, "Relationship between electrical brain responses to motor imagery and motor impairment in stroke," *Stroke*, vol. 43, no. 10, pp. 2735–2740, 2012.

[12] M. Caimmi, E. Visani, F. Digiacomo et al., "Predicting functional recovery in chronic stroke rehabilitation using event-related desynchronization-synchronization during robot-assisted movement," *BioMed Research International*, vol. 2016, Article ID 7051340, 11 pages, 2016.

[13] S. R. Soekadar, N. Birbaumer, M. W. Slutzky, and L. G. Cohen, "Brain-machine interfaces in neurorehabilitation of stroke," *Neurobiology of Disease*, vol. 83, pp. 172–179, 2015.

[14] A. Remsik, B. Young, R. Vermilyea et al., "A review of the progression and future implications of brain-computer interface therapies for restoration of distal upper extremity motor function after stroke," *Expert Review of Medical Devices*, vol. 13, no. 5, pp. 445–454, 2016.

[15] K. K. Ang, C. Guan, K. S. Phua et al., "Brain-computer interface-based robotic end effector system for wrist and hand rehabilitation: results of a three-armed randomized controlled trial for chronic stroke," *Frontiers in Neuroengineering*, vol. 7, p. 30, 2014.

[16] K. K. Ang, K. S. G. Chua, K. S. Phua et al., "A randomized controlled trial of EEG-based motor imagery brain-computer interface robotic rehabilitation for stroke," *Clinical EEG and Neuroscience*, vol. 46, no. 4, pp. 310–320, 2015.

[17] A. A. Frolov, O. Mokienko, R. Lyukmanov et al., "Post-stroke rehabilitation training with a motor-imagery-based brain-computer interface (BCI)-controlled hand exoskeleton: a randomized controlled multicenter trial," *Frontiers in Neuroscience*, vol. 11, p. 400, 2017.

[18] A. Ramos-Murguialday, D. Broetz, M. Rea et al., "Brain-machine interface in chronic stroke rehabilitation: a controlled study," *Annals of Neurology*, vol. 74, no. 1, pp. 100–108, 2013.

[19] G. Pellegrino, L. Tomasevic, M. Tombini et al., "Inter-hemispheric coupling changes associate with motor improvements after robotic stroke rehabilitation," *Restorative Neurology and Neuroscience*, vol. 30, no. 6, pp. 497–510, 2012.

[20] K. Shindo, K. Kawashima, J. Ushiba et al., "Effects of neurofeedback training with an electroencephalogram-based brain–computer Interface for hand paralysis in patients with chronic stroke: a preliminary case series study," *Journal of Rehabilitation Medicine*, vol. 43, no. 10, pp. 951–957, 2011.

[21] H.-Y. Jung, "Rehabilitation in subacute and chronic stage after stroke," in *Stroke revisited: diagnosis and treatment of ischemic stroke*, S. H. Lee, Ed., pp. 351–360, Springer, Singapore, 2017.

[22] E. Ostrosky-Solis, A. Gómez-Pérez, M. Ardilla, E. Rosselli, E. Matute, and D. Pineda, *Batería Neuropsicológica Neuro PSI Atención y Memoria, 6 a 85 años de edad*, Bookstore, 2003.

[23] P. A. Barber, A. M. Demchuk, J. Zhang, and A. M. Buchan, "Validity and reliability of a quantitative computed tomography score in predicting outcome of hyperacute stroke before thrombolytic therapy," *The Lancet*, vol. 355, no. 9216, pp. 1670–1674, 2000.

[24] B. Blankertz, R. Tomioka, S. Lemm, M. Kawanabe, and K. R. Muller, "Optimizing spatial filters for robust EEG single-trial analysis," *IEEE Signal Processing Magazine*, vol. 25, no. 1, pp. 41–56, 2008.

[25] K. K. Ang, Z. Y. Chin, H. Zhang, and C. Guan, "Filter bank common spatial pattern (FBCSP) in brain-computer interface," in *2008 IEEE International Joint Conference on Neural Networks (IEEE World Congress on Computational Intelligence)*, Hong Kong, China, June 2008.

[26] Y. Shi and R. C. Eberhart, "A modified particle swarm optimizer," in *IEEE International Conference on Evolutionary Computation Proceedings. IEEE World Congress on Computational Intelligence (Cat. No.98TH8360)*, Anchorage, Alaska, USA, 1998.

[27] J. Cantillo-Negrete, R. I. Carino-Escobar, P. Carrillo-Mora, D. Elias-Vinas, and J. Gutierrez-Martinez, "Motor imagery-based brain-computer Interface coupled to a robotic hand orthosis aimed for neurorehabilitation of stroke patients," *Journal of Healthcare Engineering*, vol. 2018, Article ID 1624637, 10 pages, 2018.

[28] G. Pfurtscheller and C. Neuper, "Motor imagery and direct brain-computer communication," *Proceedings of the IEEE*, vol. 89, no. 7, pp. 1123–1134, 2001.

[29] A. R. Fugl-Meyer, L. Jääskö, I. Leyman, S. Olsson, and S. Steglind, "The post-stroke hemiplegic patient. 1. A method

for evaluation of physical performance," *Scandinavian Journal of Rehabilitation Medicine*, vol. 7, no. 1, pp. 13–31, 1975.

[30] R. Oostenveld, P. Fries, E. Maris, and J. M. Schoffelen, "Fieldtrip: open source software for advanced analysis of MEG, EEG, and invasive electrophysiological data," *Computational Intelligence and Neuroscience*, vol. 2011, Article ID 156869, 9 pages, 2011.

[31] C. Tallon-Baudry, O. Bertrand, C. Delpuech, and J. Pernier, "Oscillatory γ-band (30–70 Hz) activity induced by a visual search task in humans," *The Journal of Neuroscience*, vol. 17, no. 2, pp. 722–734, 1997.

[32] G. Pfurtscheller and F. H. Lopes da Silva, "Event-related EEG/MEG synchronization and desynchronization: basic principles," *Clinical Neurophysiology*, vol. 110, no. 11, pp. 1842–1857, 1999.

[33] E. López-Larraz, L. Montesano, Á. Gil-Agudo, J. Minguez, and A. Oliviero, "Evolution of EEG motor rhythms after spinal cord injury: a longitudinal study," *PLoS One*, vol. 10, no. 7, article e0131759, 2015.

[34] N. R. Draper and H. Smith, "Selecting the "best" regression equation," *Applied Regression Analysis*, N. R. Draper and S. H. Wiley, Eds., 327–368, 2014.

[35] H. W. Lilliefors, "On the Kolmogorov-Smirnov test for normality with mean and variance unknown," *Journal of the American Statistical Association*, vol. 62, no. 318, pp. 399–402, 1967.

[36] D. W. Zimmerman and B. D. Zumbo, "Relative power of the Wilcoxon test, the Friedman test, and repeated-measures ANOVA on ranks," *The Journal of Experimental Education*, vol. 62, no. 1, pp. 75–86, 1993.

[37] N. R. Draper and H. Smith, "On worthwhile regressions, big F's, and R^2," *Applied Regression Analysis*, N. R. Draper and S. H. Wiley, Eds., pp. 243–250, JOHN WILEY SONS, 2014.

[38] N. S. Ward, M. M. Brown, A. J. Thompson, and R. S. Frackowiak, "Neural correlates of motor recovery after stroke: a longitudinal fMRI study," *Brain*, vol. 126, no. 11, pp. 2476–2496, 2003.

[39] T. D. Aumann and Y. Prut, "Do sensorimotor β-oscillations maintain muscle synergy representations in primary motor cortex?," *Trends in Neurosciences*, vol. 38, no. 2, pp. 77–85, 2015.

[40] R. Kawai, T. Markman, R. Poddar et al., "Motor cortex is required for learning but not for executing a motor skill," *Neuron*, vol. 86, no. 3, pp. 800–812, 2015.

[41] M. Gandolfi, E. Formaggio, C. Geroin et al., "Electroencephalographic changes of brain oscillatory activity after upper limb somatic sensation training in a patient with somatosensory deficit after stroke," *Clinical EEG and Neuroscience*, vol. 46, no. 4, pp. 347–352, 2014.

[42] M. Lotze, W. Beutling, M. Loibl et al., "Contralesional motor cortex activation depends on ipsilesional corticospinal tract integrity in well-recovered subcortical stroke patients," *Neurorehabilitation and Neural Repair*, vol. 26, no. 6, pp. 594–603, 2012.

[43] J. M. Cassidy and S. C. Cramer, "Spontaneous and therapeutic-induced mechanisms of functional recovery after stroke," *Translational Stroke Research*, vol. 8, no. 1, pp. 33–46, 2017.

[44] J. M. Rondina, C. H. Park, and N. S. Ward, "Brain regions important for recovery after severe post-stroke upper limb paresis," *Journal of Neurology, Neurosurgery & Psychiatry*, vol. 88, no. 9, pp. 737–743, 2017.

[45] C. Park, W. H. Chang, S. H. Ohn et al., "Longitudinal changes of resting-state functional connectivity during motor recovery after stroke," *Stroke*, vol. 42, no. 5, pp. 1357–1362, 2011.

[46] C. T. Shiner, H. Tang, B. W. Johnson, and P. A. McNulty, "Cortical beta oscillations and motor thresholds differ across the spectrum of post-stroke motor impairment, a preliminary MEG and TMS study," *Brain Research*, vol. 1629, pp. 26–37, 2015.

[47] F. Pichiorri, M. Petti, S. Caschera, L. Astolfi, F. Cincotti, and D. Mattia, "An EEG index of sensorimotor interhemispheric coupling after unilateral stroke: clinical and neurophysiological study," *European Journal of Neuroscience*, vol. 47, no. 2, pp. 158–163, 2018.

Hindawi
Neural Plasticity
Volume 2019, Article ID 6263907, 13 pages
https://doi.org/10.1155/2019/6263907

Research Article

Phase-Amplitude Coupling of Neural Oscillations Can Be Effectively Probed with Concurrent TMS-EEG

Sarah Glim,[1,2,3] Yuka O. Okazaki,[1] Yumi Nakagawa,[1] Yuji Mizuno,[1,4] Takashi Hanakawa,[1,4] and Keiichi Kitajo[1,4,5,6]

[1]*RIKEN CBS-TOYOTA Collaboration Center, RIKEN Center for Brain Science, 2-1 Hirosawa, Wako, Saitama 351-0198, Japan*
[2]*Department of Neuroradiology, Technical University of Munich, Ismaninger Straße 22, 81675 Munich, Germany*
[3]*Graduate School of Systemic Neurosciences, LMU Munich, Großhaderner Straße 2, 82152 Planegg-Martinsried, Germany*
[4]*Integrative Brain Imaging Center, National Center of Neurology and Psychiatry, 4-1-1 Ogawa-Higashi, Kodaira, Tokyo 187-8551, Japan*
[5]*Division of Neural Dynamics, Department of System Neuroscience, National Institute for Physiological Sciences, National Institutes of Natural Sciences, Okazaki, Aichi 444-8585, Japan*
[6]*Department of Physiological Sciences, School of Life Science, The Graduate University for Advanced Studies (SOKENDAI), Okazaki, Aichi 444-8585, Japan*

Correspondence should be addressed to Keiichi Kitajo; kkitajo@nips.ac.jp

Received 3 November 2018; Revised 12 January 2019; Accepted 23 January 2019; Published 31 March 2019

Guest Editor: Andrea Guerra

Despite the widespread use of transcranial magnetic stimulation (TMS), knowledge of its neurophysiological mode of action is still incomplete. Recently, TMS has been proposed to synchronise neural oscillators and to thereby increase the detectability of corresponding oscillations at the population level. As oscillations in the human brain are known to interact within nested hierarchies via phase-amplitude coupling, TMS might also be able to increase the macroscopic detectability of such coupling. In a concurrent TMS-electroencephalography study, we therefore examined the technique's influence on theta-gamma, alpha-gamma, and beta-gamma phase-amplitude coupling by delivering single-pulse TMS (sTMS) and repetitive TMS (rTMS) over the left motor cortex and right visual cortex of healthy participants. The rTMS pulse trains were of 5 Hz, 11 Hz, and 23 Hz for the three coupling variations, respectively. Relative to sham stimulation, all conditions showed transient but significant increases in phase-amplitude coupling at the stimulation site. In addition, we observed enhanced coupling over various other cortical sites, with a more extensive propagation during rTMS than during sTMS. By indicating that scalp-recorded phase-amplitude coupling can be effectively probed with TMS, these findings open the door to the technique's application in manipulative dissections of such coupling during human cognition and behaviour in healthy and pathological conditions.

1. Introduction

Due to its extensive effects on human perception, cognition, and action, transcranial magnetic stimulation (TMS) is nowadays widely used in both basic neuroscientific research (e.g., during investigations of visual awareness [1], attention [2], speech [3], and motor processing [4]) and in clinical practice (with potential treatment domains (see guidelines on therapeutic use [5]) including medication-resistant major depressive disorder [6], poststroke motor impairment [7], aphasia [8], and schizophrenia [9]). Despite this broad scope of application, knowledge of the precise neurophysiological effects of TMS is still incomplete.

Over the past decade, interest has arisen in the effects of TMS on macroscopic neural oscillations, as measured with noninvasive recording techniques such as electroencephalography (EEG) [10–14]. In this context, Kawasaki et al. [13] demonstrated a direct modulation of the temporal dynamics of these oscillations by showing that the consistency of oscillatory phases across stimulation trials, so-called phase locking, is transiently enhanced after single-pulse TMS (sTMS). Even though this effect can occur within a wide oscillatory

spectrum, sTMS is assumed to act on intrinsic neural systems, and thus to be most effective for those frequencies that arise naturally within particular corticothalamic modules [15]. Accordingly, a highly probable candidate mechanism behind the observed increase in macroscopic across-trial phase locking is the phase resetting of underlying intrinsic oscillators (but see Sauseng et al. [16] for a critical discussion of phase locking). Considering that such resets would simultaneously pertain to a multitude of coexistent oscillators, transiently enhanced synchronisation would also unfold within stimulation trials. As Thut et al. [12, 17] argued, rhythmic stimulation via repetitive TMS (rTMS) can foster such a synchronisation through neural entrainment, during which individual oscillators start to cycle with the same period as pulses delivered at their eigenfrequency, and thus become more and more aligned to such pulses, and consequently also to each other. Interestingly, this synchronisation or alignment of coexistent neural oscillators has been argued to prevent population-level signal nullifications, and to thereby enhance the detectability of macroscopic oscillations with scalp-based measurement techniques [17]. Associated EEG-recorded oscillatory power increases have de facto been reported for both sTMS [15, 18] and rTMS [12].

To fully appreciate the neurophysiological effects of TMS, it is necessary to consider that the human brain is unlikely to be a composition of neatly separated neural modules whose oscillatory signatures can be manipulated independently from each other. Rather, its essence lies in a myriad of dynamic neural interactions that serve the integration of information across various temporal and spatial processing scales [19]. One promising mechanism for how such integration may be implemented in the brain is through a nested hierarchy of neural oscillations [20]. In particular, studies have shown that the phase of oscillations arising from slower global computations can flexibly modulate the amplitude of faster local oscillations [21–25], a mechanism that might enable the coordination of multiple specialised processing nodes across large-scale brain networks. The functional relevance of such phase-amplitude coupling is supported by findings associating its strength with behavioural outcomes, e.g., success in a visual motion discrimination task [26]. Given that phase-amplitude coupling is an inherent property of neural systems, the alignment of oscillators by TMS should enhance not only the detectability of individual macroscopic oscillations, but also the detectability of their coupling to other oscillations. As this feature would greatly facilitate the investigation of phase-amplitude coupling with noninvasive measurement techniques such as scalp EEG, which often require extensive recordings to cope with only moderate signal-to-noise ratios, its clear demonstration would be of high relevance for both TMS methodologists and cognitive neuroscientists.

Attempts have already been made to demonstrate an enhancement of EEG-recorded phase-amplitude coupling by TMS [27] and other noninvasive brain stimulation techniques, specifically transcranial alternating current stimulation (tACS) [28]. Even though Noda et al. [27] demonstrated the enhancement of preexisting intrinsic theta-gamma coupling within an offline paradigm following several sessions of rTMS in patients with depression, conclusive evidence from a sham-controlled examination of online EEG recordings during TMS in the healthy population is still missing. With the present study, we set out to provide such evidence, thereby using TMS to shed light on the transient modulation of the human brain's nested oscillations. To this end, we delivered both sTMS and rTMS over the left motor cortex and right visual cortex of healthy participants while simultaneously collecting EEG. To ensure coverage of a wide range of the oscillatory nesting observable in neural systems [20, 29, 30], the enhancement of phase-amplitude coupling relative to sham stimulation was assessed separately for theta-gamma, alpha-gamma, and beta-gamma coupling, with the alpha and beta bands, in particular, having been related to the stimulated visual and motor cortex, respectively [15]. The rTMS frequency always equalled the frequency of the slower modulating oscillation to allow for this oscillation's direct entrainment. We designed the experiments to evaluate the following theoretical reasoning. As enhanced oscillatory power has been reported for both sTMS [15, 18] and rTMS [12], scalp-recorded phase-amplitude coupling should likewise be transiently enhanced for both stimulation paradigms. As both paradigms were further shown to modulate phase dynamics not only locally at the stimulation site, but also with network-wide signal propagation [13, 14], the enhancement of phase-amplitude coupling might likewise propagate across the cortex. Finally, we directly compared the neurophysiological effects of sTMS and rTMS by examining whether an rTMS-induced entrainment of neural oscillators can induce a locally stronger and/or globally more widespread enhancement of phase-amplitude coupling relative to sTMS.

2. Materials and Methods

2.1. Participants. Fourteen right-handed healthy participants (two females, twelve males; mean age ± SD, 30.8 ± 5.5 years) were recruited in this study. Written informed consent was obtained from all participants prior to the experimental sessions. The study was approved by the RIKEN Ethics Committee and was conducted in accordance with the code of ethics of the World Medical Association for research involving humans (Declaration of Helsinki).

2.2. TMS Design. TMS pulses were delivered through a figure-of-eight coil with a 70 mm wing diameter, connected to a biphasic magnetic stimulator unit (Magstim Rapid, The Magstim Company Ltd., UK). Stimulation intensity was fixed at 90% of a participant's active motor threshold, which was determined for the right first dorsal interosseous (FDI) muscle. During the entire experimental procedure, participants fixated on a central grey cross on a black computer monitor background and wore earplugs to reduce stimulation-evoked auditory potentials in neural activity.

An overview of the experimental design is presented in Figure 1. Each participant received stimulation at three different sites in randomly ordered sessions. In one session, TMS was applied over the left motor cortex (approximately between electrodes C1 and C3, with the exact position being

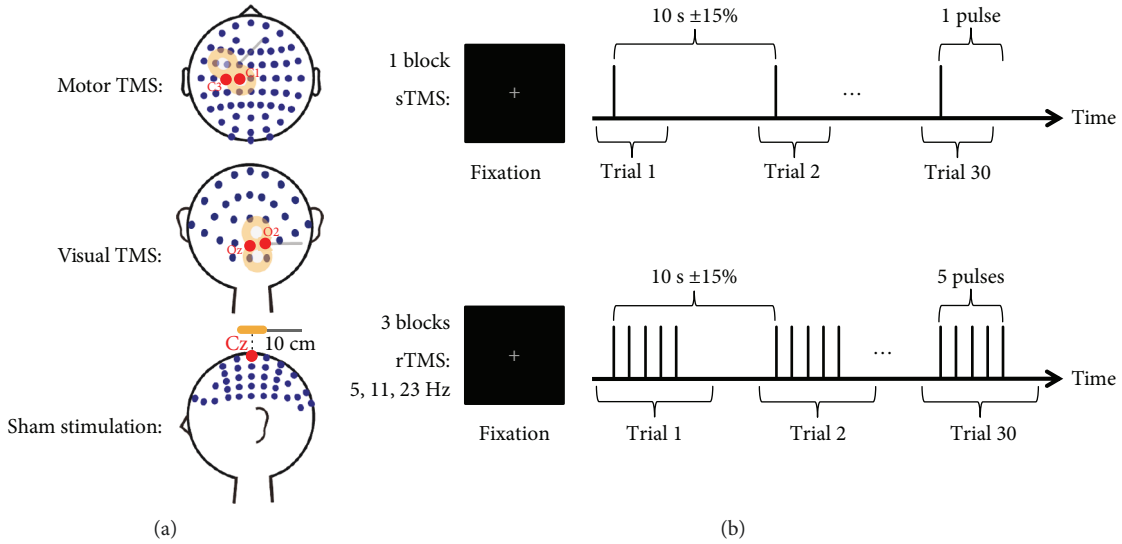

Figure 1: Experimental design. (a) The EEG electrode layout used in the present study is displayed along with the different stimulation sites. In separate sessions, TMS was applied over the left motor cortex (first row), over the right visual cortex (second row), and as sham stimulation 10 cm above the vertex of the head (third row). (b) Each session contained four blocks of 30 trials each, in which we performed sTMS (first row) as well as 5 Hz, 11 Hz, and 23 Hz rTMS (second row). During rTMS trials, stimulation was delivered in trains of five consecutive pulses.

determined by the individual hotspot of the right FDI muscle stimulation; coil handle perpendicular to the central sulcus; anteroposterior current direction of the waveform's first phase) and in a second session, it was applied over the right visual cortex (between electrodes Oz and O2; coil handle perpendicular to the midsagittal plane). In a third session, sham stimulation was delivered at a location 10 cm above the vertex of the head (electrode Cz; coil handle directed posteriorly). Each of these sessions comprised four different blocks, with each block consisting of 30 trials with intertrial intervals of 10 s ± 15%. Depending on the block, trials contained either single TMS pulses or trains of five consecutive pulses delivered at 5 Hz, 11 Hz, or 23 Hz. The different rTMS frequencies were selected so that they are not multiples of each other.

2.3. EEG Recording and Preprocessing. During the entire stimulation procedure, EEG (left earlobe reference; AFz as ground) was recorded from 63 TMS-compatible Ag/AgCl scalp electrodes (Easy Cap, EASYCAP GmbH, Germany; see Figure 1(a) for the electrode layout), which were positioned according to the international 10/10 system with lead wires rearranged orthogonally to the TMS coil handle to reduce TMS-induced artefacts [31]. In addition, horizontal and vertical electrooculography (EOG; ground electrode on the left mastoid) was recorded to monitor eye movements and blinks. All signals were sampled at a rate of 5,000 Hz, filtered online from DC to 1,000 Hz, and amplified using the TMS-compatible BrainAmp MR plus system (Brain Products GmbH, Germany). Impedances were kept below 10 kΩ.

We preprocessed the EEG data by first segmenting it into epochs starting 2 s before the first (or single) TMS pulse and ending 3 s after the last (or single) pulse of a train, and then rereferencing these epochs to the averaged recordings from electrodes positioned on the left and right earlobe. To remove the TMS-induced ringing artefact in the EEG signals, we substituted all values within an interval of 0-8 ms after each pulse with replacement values estimated using linear interpolation. In those cases where the interval was deemed to be too short via visual inspection, it was manually extended to 12 ms after the pulse. The longer-lasting exponential decay artefact was attenuated by identifying components capturing this artefact with an independent component analysis (ICA), and then removing them from the data [18, 32]. Next, we rejected trials with signal values exceeding ±200 μV within an interval of −1 s to +1 s around the stimulation to exclude any remaining artefacts. Out of 30 collected trials per block, 24.8 ± 2.6 trials (mean ± SD) were retained. After performing a current source density (CSD) transformation of the surface voltage distribution using spherical splines to reduce the effects of volume conduction [33, 34], the data were downsampled to a rate of 1,000 Hz.

2.4. EEG Analysis. To compute phase-amplitude coupling, we first convolved the preprocessed time series with complex Morlet wavelets $w(t, f)$ [35, 36]:

$$w(t,f) = \sqrt{f}\,\exp\left(-\frac{t^2}{2\sigma_t^2}\right)\exp\left(i2\pi f t\right), \tag{1}$$

with t denoting time, f denoting the central frequency of interest, σ_t denoting the SD of the Gaussian window, and the number of wavelet cycles within a $6\sigma_t$ interval $n_{co} = 3$ determining the approximate width of the frequency bands [37]:

$$\left[f - \frac{4f}{n_{co}}, f + \frac{4f}{n_{co}}\right]. \tag{2}$$

The central frequencies f were chosen to be 5 Hz, 11 Hz, and 23 Hz for phase extraction and 30 Hz to 45 Hz in 1 Hz steps for amplitude extraction. The upper limit was fixed at 45 Hz to diminish potential artefacts from muscular activity and power line noise. The instantaneous phase ϕ at each time point was then defined as the angle of the resulting complex-plane vector with respect to the positive real axis, while the magnitude of this vector was utilised as a measure of instantaneous amplitude a. For each combination of phase and amplitude frequency and for each trial time point, we separately computed the event-related phase-amplitude coupling (ERPAC) $\rho_{\phi a}$, which was defined as the circular-linear correlation of phase and amplitude values across stimulation trials [38, 39]:

$$\rho_{\phi a} = \sqrt{\frac{r_{ca}^2 + r_{sa}^2 - 2r_{ca}r_{sa}r_{cs}}{1 - r_{cs}^2}}, \quad (3)$$

where $r_{ca} = c(\cos\phi[n], a[n])$, $r_{sa} = c(\sin\phi[n], a[n])$, and $r_{cs} = c(\sin\phi[n], \cos\phi[n])$ with $c(x, y)$ being the Pearson correlation between x and y.

As the sixteen amplitude frequencies were pooled together in each ERPAC analysis, three different phase-amplitude combinations existed (5 Hz, 11 Hz, or 23 Hz phase coupled to amplitudes at 30-45 Hz, i.e., theta-gamma coupling, alpha-gamma coupling, and beta-gamma coupling), which were examined separately for motor and visual TMS. Analyses of the resulting six conditions focused on contrasting motor or visual TMS with sham stimulation to account for any indirect effects of stimulation; they were either performed individually for sTMS and rTMS (first and third analysis), or they directly compared the two stimulation paradigms (second and fourth analysis), as detailed in the following discussion. Whenever statistical tests were performed, the (multiple-comparison-corrected) significance level was set at $p \leq .05$. With regard to rTMS, it is important to note that the frequency of a condition's respective phase angle time series always corresponded to the applied stimulation frequency. This approach allowed us to directly assess how targeting a particular oscillation via repetitive stimulation affected this oscillation's scalp-recorded coupling to faster oscillations.

We first examined whether sTMS and rTMS led to an increase in phase-amplitude coupling at the stimulation site by analysing ERPAC as a function of amplitude frequency and time, spanning −0.5 cycles to +4.5 cycles of a condition's phase-providing oscillation around the onset of the first (or single) pulse. Statistically significant enhancements of ER PAC were determined via nonparametric permutation testing in the following way. To evaluate the observed set of time-frequency representations encompassing the ERPAC data from the two local electrodes of interest (C1 and C3 for motor TMS; Oz and O2 for visual TMS), the two modes of stimulation (TMS and sham), and each of the fourteen participants, we created 500 sets of corresponding surrogate representations by computing ERPAC between the unchanged phase values and the trial-shuffled amplitude values. As we randomised the relative trial structure between phase and amplitude while maintaining the temporal structure, and thus left any pulse-evoked changes intact, significant differences to the observed data could not arise from spurious stimulus-evoked relationships between phase and amplitude values [39]. We next averaged each set's ERPAC data over the electrodes of interest, then took the difference between motor or visual TMS and sham stimulation, and averaged resulting values over participants. One observed time-frequency representation and a distribution of 500 surrogate representations emerged, all of which were subsequently binarised by thresholding them with the 95th percentile of the surrogate distribution at each time-frequency point. Contiguous suprathreshold points were clustered, and the sum of ERPAC values within each cluster was determined. To account for multiple comparisons, we removed from the observed time-frequency representation those clusters whose cluster sum of ERPAC values was below the 95th percentile of the distribution of maximum cluster sums, obtained by taking the highest sum within each surrogate representation.

Second, to investigate whether the local enhancement of phase-amplitude coupling differed between sTMS and rTMS, we took the mean ERPAC over the local electrodes of interest (C1 and C3 for motor TMS; Oz and O2 for visual TMS), subtracted corresponding mean data obtained from sham stimulation, and averaged values over a time window of interest, covering ±1/10th of the respective phase-providing oscillation's cycle around either the sTMS pulse or the last pulse of the rTMS trains, as well as over the sixteen amplitude frequencies. By selecting a narrow time window around the last rTMS pulse, we aimed to minimise the potential contamination of the rTMS data from surrounding pulses. Resulting values were then compared between sTMS and rTMS using a two-tailed paired-sample Student's t-test over participants.

Third, we assessed whether an enhancement of phase-amplitude coupling by sTMS and rTMS was observable not only at the stimulation site, but also over other cortical regions. ERPAC was therefore computed at all scalp electrodes for each time point within nine different time windows of interest, centred at −2 cycles to +6 cycles of a condition's phase-providing oscillation in 1-cycle steps around the onset of the first (or single) pulse and spanning ±1/10th of this cycle. Topographic maps were created by taking the difference between motor or visual TMS and sham stimulation, and then averaging the resulting values over time points within the respective window of interest, over the sixteen amplitude frequencies as well as over participants.

Fourth, to analyse whether the global propagation of phase-amplitude coupling differed between sTMS and rTMS, we counted the number of electrodes that showed significantly higher ERPAC during motor or visual TMS than during sham stimulation using one-tailed paired-sample Student's t-tests over participants. Tests were performed for windows of ±1/10th of a condition's phase-providing oscillation's cycle around the sTMS pulse and each of the five rTMS pulses, with ERPAC values averaged over the respective time

points as well as over amplitude frequencies. The extent of propagation induced by each of the five rTMS pulses was then compared to the sTMS-induced extent of propagation using exact binomial tests with parameters n_{el_1} = number of electrodes with a significant TMS-sham difference during a particular rTMS pulse but not the sTMS pulse, n_{el_2} = number of electrodes with a significant TMS-sham difference during the sTMS pulse but not a particular rTMS pulse, and the total number of discordant electrodes $n_{el} = n_{el\_1} + n_{el\_2}$. As the assignment of these electrodes to either n_{el_1} or n_{el_2} would have happened with equal probability under the null hypothesis of no sTMS-rTMS difference, the p-value was defined as the probability of n_{el_1} reaching the observed or a higher value. Since we performed five tests per condition, multiple comparisons were subsequently accounted for by adjusting p-values with the false discovery rate (FDR) procedure [40].

All analyses were performed in MATLAB (The MathWorks Inc., USA), using the CSD toolbox [34], the CircStat toolbox [38], the FieldTrip toolbox [41], and custom-written scripts.

3. Results

3.1. Local Modulation of Phase-Amplitude Coupling. Time-frequency representations of the local change in ERPAC relative to the sham stimulation revealed that both motor TMS, analysed at electrodes C1 and C3, and visual TMS, analysed at electrodes Oz and O2, led to an enhancement of phase-amplitude coupling in all assessed phase-amplitude combinations (Figure 2). For sTMS (Figure 2(a)), significant time-frequency clusters ($p \leq .05$, one-tailed cluster-based permutation tests) were found around the onset of the single pulse at 0 ms in all conditions but one: the ERPAC increase around the time of the pulse did not reach significance for the effect of visual sTMS on alpha-gamma coupling. However, later clusters of significant increases suggested an effect of sTMS on local ERPAC in this condition as well. For rTMS (Figure 2(b)), significant time-frequency clusters of increased ERPAC could likewise be observed around the onset times of almost all pulses. Interestingly, whereas the ERPAC increases induced by the individual pulses were clearly separated in time in the 5 Hz and 11 Hz stimulation, which related to theta-gamma and alpha-gamma coupling, respectively, the effects were more strongly merged for the beta-gamma coupling occurring during the faster 23 Hz stimulation. Although clusters in all conditions could spread out symmetrically in time because of the temporal smoothing introduced by the wavelet convolution, it should be noted that their spreading was generally biased towards poststimulation rather than prestimulation time points. While the ERPAC enhancement induced by the present TMS design thus seemed to linger for some tens of milliseconds, it was still transient in nature, with individual effects typically lasting for less than 50 ms. The abovementioned temporal smoothing also explains the observation of enhanced ERPAC during the interpolation intervals, which did not carry meaningful information per se. Since enhanced ERPAC could be found further away from the pulses and interpolation intervals as well (e.g., enhanced theta-gamma coupling more than 3 theta cycles after motor sTMS), these intervals were unlikely to be causally related to the observed effects.

A comparison of the local change in phase-amplitude coupling induced by sTMS and rTMS revealed that in all but one condition, the mean ERPAC increase relative to the sham stimulation was higher for the last rTMS pulse than for the sTMS pulse, with the opposite pattern being observable for beta-gamma coupling during visual TMS (Figure 3). However, because of high variability over participants, the p-values from two-tailed paired-sample Student's t-tests did not reach statistical significance (all $p > .05$), there being merely a statistical trend ($t(13) = -1.93$, $p = .076$) observable for alpha-gamma coupling during visual TMS, suggesting stronger ERPAC enhancement by rTMS than by sTMS.

3.2. Global Modulation of Phase-Amplitude Coupling. To illustrate the change in ERPAC relative to the sham stimulation at all 63 scalp electrodes, nine topographic maps were computed for each condition and stimulation paradigm (Figure 4). The first two maps represented prestimulation time windows, the next one (sTMS) or next five (rTMS) represented windows centred on the individual pulses, and all remaining maps represented poststimulation time windows. In accordance with the transient character of the assessed effects, an enhancement of ERPAC was most noticeable within the topographic maps centred on the pulses. Visual inspection further revealed that sTMS-induced increases in ERPAC were prominent primarily over the site of stimulation, with sporadic enhancements also occurring at other sites (Figure 4(a)). By contrast, the effects of rTMS within the five topographic maps centred on the five pulses appeared to be more strongly distributed over the entire cortex (Figure 4(b)).

We quantified this observation by determining the number of electrodes with significantly higher ERPAC during motor or visual TMS than during sham stimulation ($p \leq .05$, one-tailed paired-sample Student's t-tests), and then comparing the electrode numbers between sTMS and the five rTMS pulses (Figure 5). As expected, in most cases, the number of significant electrodes was larger for a particular rTMS pulse than for the sTMS pulse of the same condition. With regard to motor stimulation, this difference was statistically significant ($p_{FDR} \leq .05$, exact binomial tests) for three out of five rTMS pulses when investigating alpha-gamma coupling (pulses 1, 2, and 3: each $p_{FDR} = .041$) and for one rTMS pulse when investigating beta-gamma coupling (pulse 3: $p_{FDR} = .019$). With regard to visual stimulation, three out of five rTMS pulses showed a significantly larger propagation when investigating theta-gamma coupling (pulse 1: $p_{FDR} = .019$; pulse 4: $p_{FDR} = .009$; and pulse 5: $p_{FDR} = .006$), whereas two rTMS pulses were significant for beta-gamma coupling (pulses 2 and 3: each $p_{FDR} = .021$). Thus, while significant sTMS-sham differences were still found at five or more electrodes in all conditions, indicating a certain extent of propagation in this stimulation paradigm as well, rTMS induced a considerably more widespread propagation of ERPAC enhancement overall.

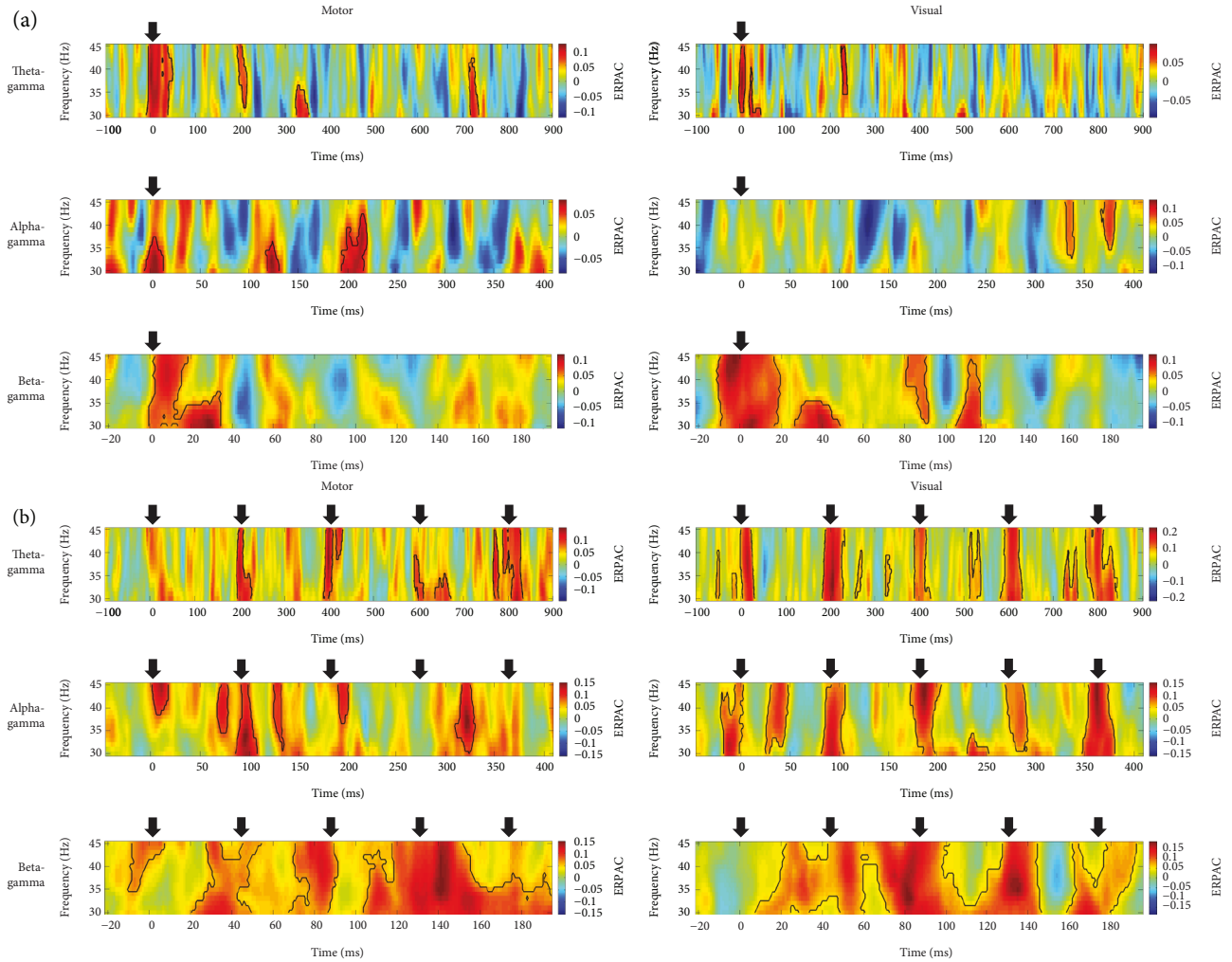

FIGURE 2: Grand average time-frequency representations of phase-amplitude coupling. Plots show the strength of motor-TMS-induced (left column) and visual-TMS-induced (right column) theta-gamma (first row), alpha-gamma (second row), and beta-gamma (third row) event-related phase-amplitude coupling (ERPAC) as a function of trial time and amplitude frequency. Stimulation paradigms are (a) sTMS and (b) rTMS, with the rTMS frequency always corresponding to the frequency of the phase series. We extracted TMS effects by averaging ERPAC over electrodes C1 and C3 for motor TMS and electrodes Oz and O2 for visual TMS, subtracting corresponding mean data obtained during sham stimulation, and averaging the resulting values over the fourteen assessed participants. Time points of pulses are indicated by black arrows and significant time-frequency clusters ($p \leq .05$, one-tailed cluster-based permutation tests) by black contours.

4. Discussion

With the present study, we provide compelling evidence that both sTMS and rTMS can transiently enhance phase-amplitude coupling of neural oscillations, as measured with concurrent EEG. This enhancement was found not only locally at the stimulation site, but also over various other cortical sites, with the propagation induced by rTMS outperforming that induced by sTMS. By demonstrating enhanced theta-gamma, alpha-gamma, and beta-gamma phase-amplitude coupling during motor and visual TMS, our results have relevance for a wide range of the nested oscillatory signatures inherent to neural processing [20, 21, 42, 43] and are highly consistent with the hypothesised population-level increase in intrinsic coupling brought about by oscillatory phase alignment. We hence propose that concurrent TMS-EEG can be utilised to effectively probe such coupling in humans, a feature making it a highly promising technique for future noninvasive investigations of this important mechanism.

At the site of stimulation, all of the assessed conditions showed significant increases in phase-amplitude coupling strength during or slightly after TMS. As the phase-amplitude coupling in the present study was operationalised as the circular-linear correlation of phase and amplitude values at each time point across stimulation trials [38, 39], changes in coupling strength could be assessed without the loss of temporal resolution inherent to most other coupling measures [21, 22, 29]. Given that the enhancement of local phase-amplitude coupling typically lasted for less than 50 ms around the pulse, a finding consistent with the previously reported short-lived character of TMS-induced phase dynamics [13], this approach was vital to quantify transient effects that would otherwise be barely detectable in scalp

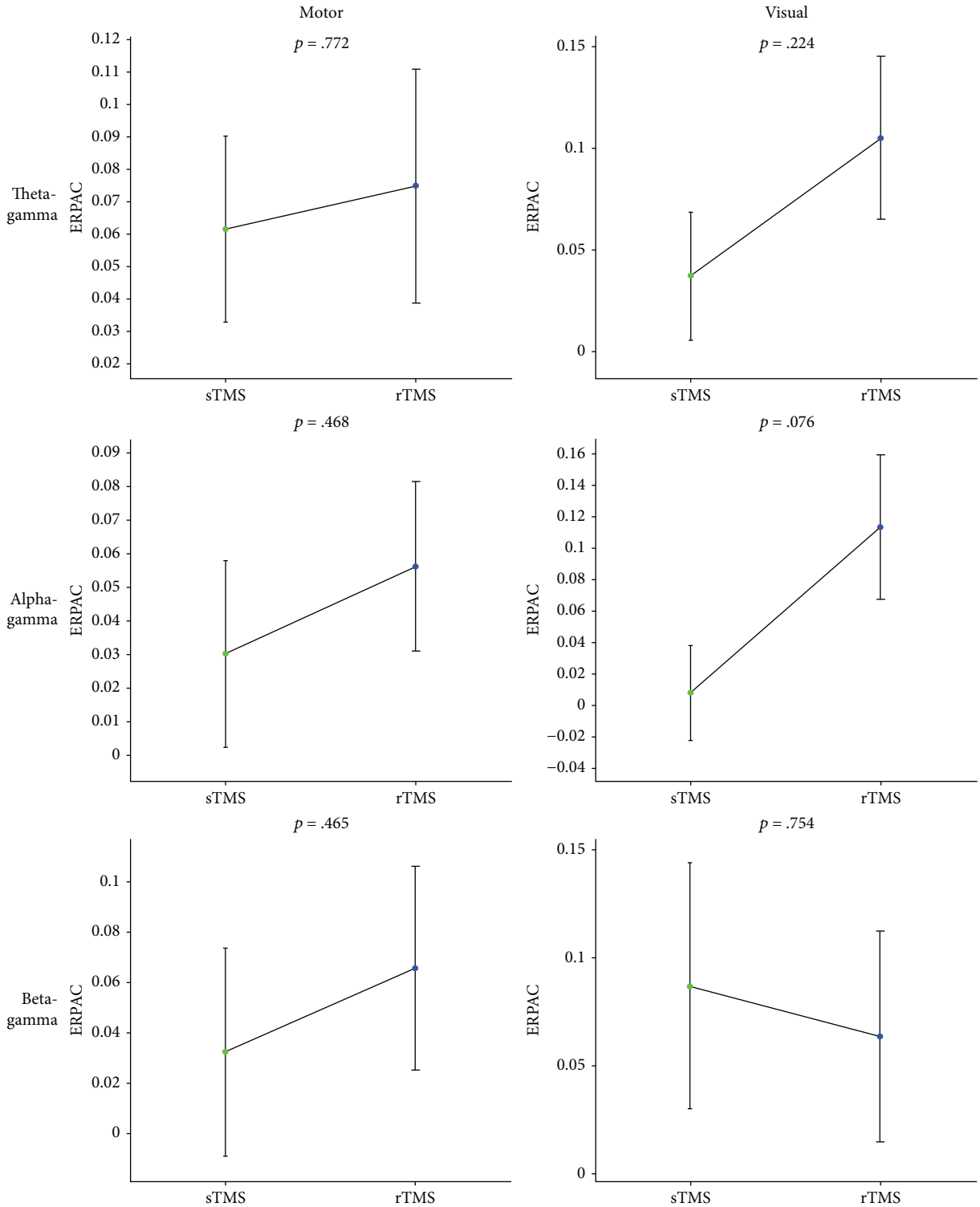

Figure 3: Local comparisons of phase-amplitude coupling between sTMS and rTMS. Plots show the strength of motor-TMS-induced (left column) and visual-TMS-induced (right column) theta-gamma (first row), alpha-gamma (second row), and beta-gamma (third row) event-related phase-amplitude coupling (ERPAC) during the sTMS pulse in green and the last rTMS pulse in blue, with the rTMS frequency always corresponding to the frequency of the phase series. We extracted TMS effects by averaging ERPAC over electrodes C1 and C3 for motor TMS and electrodes Oz and O2 for visual TMS, subtracting corresponding mean data obtained during sham stimulation, and averaging the resulting values over predefined time windows of interest around the respective pulses and over the sixteen amplitude frequencies. Bars of sTMS and rTMS represent mean values ± 1 SEM over the fourteen assessed participants; each displayed p-value is based on a two-tailed paired-sample Student's t-test between the stimulation paradigms.

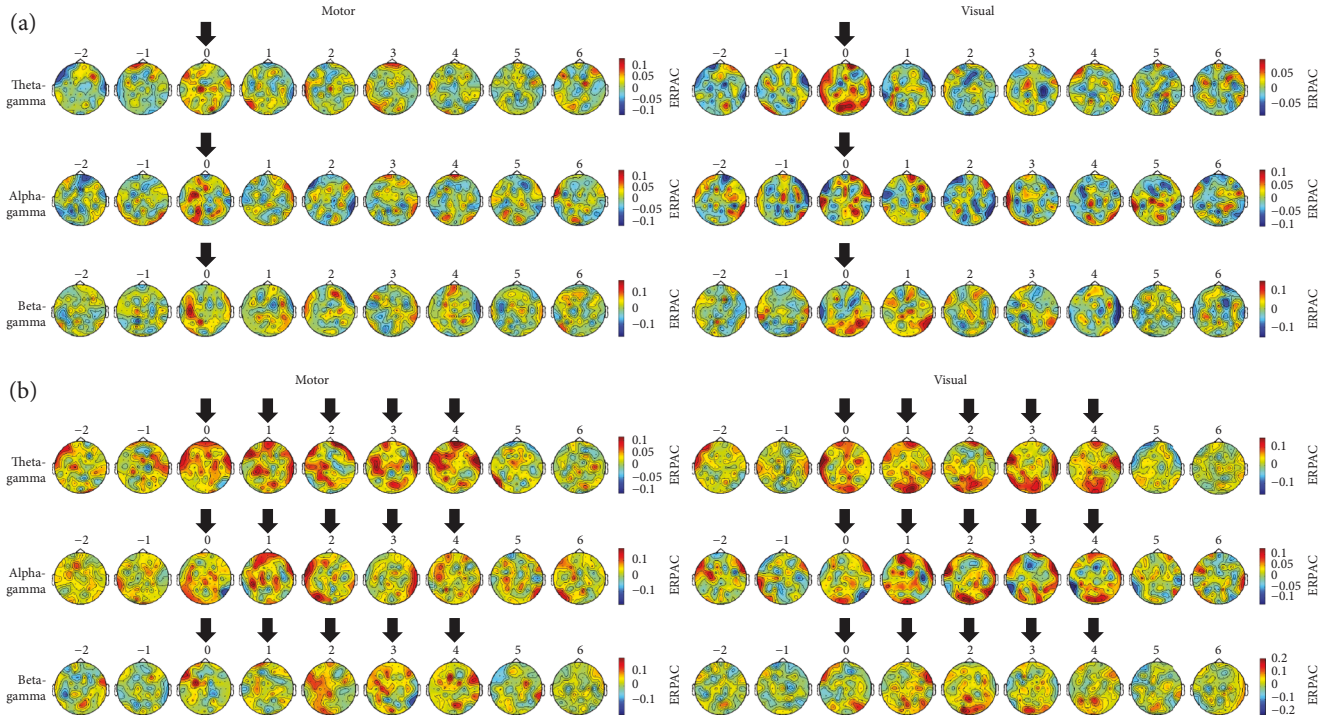

Figure 4: Grand average topographic maps of phase-amplitude coupling. Plots show the strength of motor-TMS-induced (left column) and visual-TMS-induced (right column) theta-gamma (first row), alpha-gamma (second row), and beta-gamma (third row) event-related phase-amplitude coupling (ERPAC) at all scalp electrodes within nine time windows of interest. Stimulation paradigms are (a) sTMS and (b) rTMS, with the rTMS frequency always corresponding to the frequency of the phase series. We extracted TMS effects by subtracting ERPAC obtained during sham stimulation from that obtained during motor or visual TMS and averaging the resulting values over predefined time windows of interest, positioned at −2 cycles to +6 cycles of a condition's phase-providing oscillation around the onset of the first (or single) pulse, over the sixteen amplitude frequencies and fourteen assessed participants. Topographic maps centred on pulses are indicated by black arrows.

EEG recordings. We took the following steps to ensure that the observed effects did indeed reflect a direct enhancement of macroscopic phase-amplitude coupling by TMS. First, to account for any indirect effects of stimulation, particularly for auditory-evoked changes in brain activity including cross-modally triggered phase locking after salient sounds [44], phase-amplitude coupling was always assessed relative to the sham stimulation, which was applied over the vertex of the head. Second, by statistically comparing the observed TMS-sham differences to surrogate distributions of trial-shuffled data with unmodified temporal structure [39], we confirmed that the observed enhancement of phase-amplitude coupling was based on a specific statistical relationship between phase and amplitude values across trials, rather than on spurious relationships induced by unrelated neural effects of the pulse or any sharp edge artefacts [45]. Thanks to these methodological approaches, a clear demonstration of TMS-induced changes in phase-amplitude coupling was made possible. Even though such changes seemed to be stronger for the last pulse of the delivered rTMS trains (targeted at the phase-providing lower-frequency oscillations) than for the sTMS pulse in almost all conditions, the statistical power was not high enough to enable a conclusion regarding local phase-amplitude coupling differences between stimulation paradigms. It has to be acknowledged in this context that 30 collected trials per block might have been insufficient to yield significant difference effects. Due to the already long overall testing duration of 4-5 h per participant though, a higher number of trials was practically not feasible in our study. Notably, a slight modification of the rTMS paradigm could potentially facilitate the detection of significant local differences. Successful neural entrainment, which might underlie a potential rTMS benefit by enabling stronger oscillatory phase alignment relative to sTMS, requires the existence of a neural population that can oscillate at the stimulation frequency under natural conditions [17]. As such eigenfrequencies differ between cortical regions [15] and individuals [46], the entrainment capability of rTMS should be enhanced by tuning its frequency to the local power spectrum peak frequencies of participants. Recent evidence has indeed demonstrated the benefits of such an individualised targeting of intrinsic oscillations by rTMS [14], making a comparison of local phase-amplitude coupling strength between this rTMS paradigm and sTMS promising. Importantly, even though the perturbation of intrinsic oscillations is potentially stronger in the case of individualised rTMS frequencies, previously reported effects of nonindividualised stimulation on human cognition [47] suggest successful entrainment in this case as well. As Thut et al. [12] noted, such effects might be enabled by intraindividual frequency fluctuations as well as a loosening relationship between eigenfrequency and effective stimulation frequency

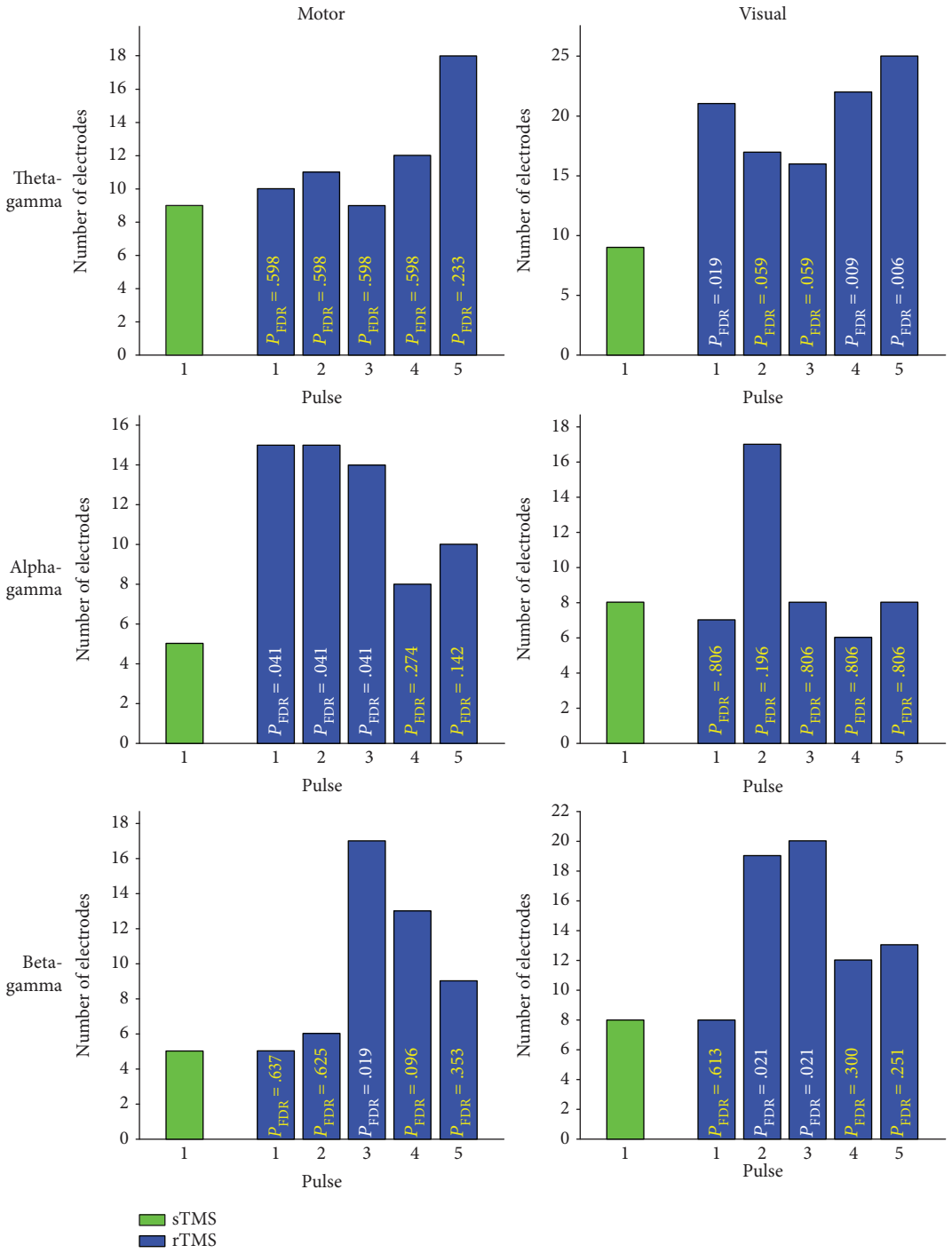

Figure 5: Global comparisons of phase-amplitude coupling between sTMS and rTMS. Plots show the spatial extent of motor-TMS-induced (left column) and visual-TMS-induced (right column) theta-gamma (first row), alpha-gamma (second row), and beta-gamma (third row) event-related phase-amplitude coupling (ERPAC) during the sTMS pulse in green and the five rTMS pulses in blue, with the rTMS frequency always corresponding to the frequency of the phase series. We extracted TMS effects by averaging ERPAC at all electrodes over predefined time windows of interest around the respective pulses and over the sixteen amplitude frequencies, comparing the resulting values between motor or visual TMS and sham stimulation with one-tailed paired-sample Student's t-tests, and counting the number of electrodes with a statistically significant difference ($p \leq .05$; drawn on y-axis). The spatial extent of TMS effects was subsequently compared between the sTMS pulse and each of the five rTMS pulses with exact binomial tests. Corresponding p-values, adjusted for multiple comparisons with the false discovery rate (FDR) procedure, are superimposed onto the rTMS bars in all plots; significant p-values ($p_{FDR} \leq .05$) are displayed in white, while all other p-values are displayed in yellow.

at higher stimulation intensities (see also Gouwens et al. [48]). A decision in favour of nonindividualised stimulation paradigms may eventually also be driven by the increased expenditure of time and resources associated with the preexperimental determination of individual peak frequencies, especially when testing clinical populations.

Alongside the described local effects of sTMS and rTMS, we found that TMS can enhance population-level measures of phase-amplitude coupling over various other cortical sites. In line with this finding, the propagation of neural activation related to either sTMS or rTMS has been shown in a number of previous studies [13, 14, 49–54]. In particular, Kawasaki et al. [13] demonstrated an sTMS-induced large-scale propagation of oscillatory phase locking, which was accompanied by increased directional information flow of phase dynamics from the occipital stimulation site to an examined distant site over the motor cortex, as assessed by transfer entropy. Since the therein-suggested alignment of phases of individual oscillators should increase the detectability of intrinsic phase-amplitude coupling at the population level, the propagation of enhanced coupling observed here is highly consistent with this report. The pathways of such propagation are not arbitrary, but should follow the brain's intrinsic organizational structure, which is characterised by frequency-specific functional networks [55]. We thus propose that the applied stimulation drove particular cortical systems via successive interactions with functionally coupled neural oscillators in a frequency-dependent manner, resulting in different propagation patterns for the different conditions. However, knowledge of any propagation differences between sTMS and rTMS is sparse. In the present study, rTMS enhanced scalp-recorded phase-amplitude coupling at considerably more sites than sTMS. This difference was particularly pronounced for alpha-gamma coupling during 11 Hz motor stimulation and theta-gamma coupling during 5 Hz visual stimulation, with three out of five rTMS pulses outperforming the respective sTMS pulse in each case. As (nested) intrinsic oscillations are believed to play an important role in neural signal transmission [42, 56], their entrainment by rTMS may again be at the bottom of the observed benefit. In accordance with this idea, Romei et al. [14] demonstrated that rTMS pulses propagate from the sensorimotor cortex to spinal levels only when sensorimotor oscillations are specifically targeted via their eigenfrequency, with stimulation at other frequencies having little impact on corticospinal signal interactions. Likewise, the impact of sTMS on relevant oscillations might have been too weak to reach the extent of propagation achieved by rTMS in the present study. Before alternatively ascribing the observed propagation benefit of rTMS to a methodological contamination of rTMS pulses by surrounding pulses, it should be noted that during rTMS, both local alpha-gamma coupling and local theta-gamma coupling typically returned to baseline long before the next pulse arrived. Still, one could argue that we had already observed a more widespread distribution of enhanced phase-amplitude coupling during the first rTMS pulse in several conditions. As an rTMS-induced synchronisation of neural oscillators might have progressively strengthened within entire rTMS blocks, including multiple stimulation trials, in these cases, the assessed correlation of phase and amplitude values could have been driven by the intensified entrainment present only in later trials. Nonetheless, conclusive evidence on this matter is so far missing and future studies are needed to shed light on the exact cause of the observed sTMS-rTMS differences in phase-amplitude coupling propagation.

As phase-amplitude coupling is believed to play a fundamental role in the transfer of neural information across diverse spatial and temporal processing scales, thereby serving the dynamic integration of global computations with fast local processing, it may be extremely relevant for cognitive functioning [42]. Recent evidence has started to support this claim by hinting at its functional significance for visual perception [26], feedback processing [57], memory recall [58], visuomotor mapping [59], and movement planning and execution [60]. Accordingly, a dysfunction in phase-amplitude coupling has been identified in several clinical conditions such as Parkinson's disease [61], autism spectrum disorders [62], and epilepsy [63]. Still, our current understanding of this intriguing mechanism is far from exhaustive. Investigations of phase-amplitude coupling in the human population are hampered by the inherent shortcomings of established noninvasive measurement techniques. As methods such as EEG capture the summed potentials of tens of thousands of synchronously activated neurons, scalp-recorded oscillations inevitably reflect the summation of multiple underlying neural oscillators. Consequently, even strong phase-amplitude coupling can only be detected with EEG if a considerable quantity of those oscillators are in phase, and thus are not cancelling out at the population level. We suggest that by aligning the phases of individual oscillators, TMS fosters this setting, and thereby facilitates the noninvasive detection of intrinsic phase-amplitude coupling with an improved signal-to-noise ratio. The proposed perturbational approach therefore holds great promise for future investigations aimed at further unravelling the association between such oscillatory nesting on the one hand, and healthy or pathological human functioning on the other hand. By probing the intrinsic capacity of individuals for phase-amplitude coupling, concurrent TMS-EEG might, in this regard, prove particularly useful for the reliable development of coupling-based biomarkers, as have already been presented for amnestic mild cognitive impairment [64]. Besides opening the door to a deeper understanding of the functional role of phase-amplitude coupling, the present results add to the constantly growing body of knowledge regarding the neurophysiological mode of action underlying TMS (see Klomjai et al. [65] for a review). By actively modulating nested intrinsic oscillations, TMS impacts on the gating of information along interconnected neural ensembles, and consequently affects a fundamental property of neural processing in the human brain.

On a final note, we would like to point out that direct evidence for this assumed mode of action is still missing. Even though our results are highly consistent with the hypothesised population-level increase in intrinsic phase-amplitude coupling, it cannot be fully excluded that TMS instead gave rise to novel coupling overlaid on top of ongoing brain

activity (see Sauseng et al. [16] for a similar discussion on the generation of event-related potentials). One might argue in favour of the latter mechanism in particular by pointing at the lack of observable differences between motor and visual TMS in our study. However, the abovementioned loosened relationship (at higher stimulation intensities) between a region's eigenfrequency, which most likely differs between the motor and visual cortex [15], and the region's effective stimulation frequency may have contributed to this observation as well. The former, hypothesised mechanism on the contrary might be supported by evidence for the pre-TMS existence of relevant phase-amplitude coupling that is then enhanced after TMS. While the current ERPAC method is not suited for the assessment of non-event-related data, phase-amplitude coupling has indeed been demonstrated in the human resting state [23, 27]. The presence or absence of coupled macroscopic oscillations alone, however, is an insufficient marker of the existence of underlying intrinsic oscillators [16], which in turn does not automatically entail that these oscillators are directly modulated by TMS. Thus, although TMS has generally been shown to interact with intrinsic brain activity [66], the unequivocal disentanglement of both mechanisms in the context of the present study requires access to the level of individual oscillators with measurements of a considerably higher temporal and spatial resolution compared to that achieved by time-frequency-resolved scalp EEG.

In conclusion, we used a concurrent TMS-EEG study design to demonstrate that TMS can transiently enhance scalp-recorded phase-amplitude coupling. This enhancement was found for both sTMS and rTMS, with a more widespread propagation of effects being observed during the latter stimulation paradigm. We thus recommend the perturbational approach of concurrent TMS-EEG as a novel experimental technique to effectively probe intrinsic phase-amplitude coupling in humans. The utility of this design for future studies investigating the functional roles of phase-amplitude coupling in the healthy population, as well as plastic changes of phase-amplitude coupling in pathological conditions, awaits confirmation.

Data Availability

The TMS-EEG data used to support the findings of this study are available from the corresponding author upon request.

Conflicts of Interest

The authors declare that there is no conflict of interest regarding the publication of this article.

Acknowledgments

KK was supported by JST PRESTO, MEXT Grants-in-Aid for Scientific Research 26282169 and 15H05877 and a research grant from Toyota Motor Corporation.

References

[1] T. A. de Graaf, M. Koivisto, C. Jacobs, and A. T. Sack, "The chronometry of visual perception: review of occipital TMS masking studies," *Neuroscience and Biobehavioral Reviews*, vol. 45, pp. 295–304, 2014.

[2] B. Olk, C. Peschke, and C. C. Hilgetag, "Attention and control of manual responses in cognitive conflict: findings from TMS perturbation studies," *Neuropsychologia*, vol. 74, pp. 7–20, 2015.

[3] T. Murakami, Y. Ugawa, and U. Ziemann, "Utility of TMS to understand the neurobiology of speech," *Frontiers in Psychology*, vol. 4, p. 446, 2013.

[4] L. J. Volz, M. Hamada, J. C. Rothwell, and C. Grefkes, "What makes the muscle twitch: motor system connectivity and TMS-induced activity," *Cerebral Cortex*, vol. 25, no. 9, pp. 2346–2353, 2015.

[5] J.-P. Lefaucheur, N. André-Obadia, A. Antal et al., "Evidence-based guidelines on the therapeutic use of repetitive transcranial magnetic stimulation (rTMS)," *Clinical Neurophysiology*, vol. 125, no. 11, pp. 2150–2206, 2014.

[6] T. Perera, M. S. George, G. Grammer, P. G. Janicak, A. Pascual-Leone, and T. S. Wirecki, "The Clinical TMS Society consensus review and treatment recommendations for TMS therapy for major depressive disorder," *Brain Stimulation*, vol. 9, no. 3, pp. 336–346, 2016.

[7] G. Di Pino, G. Pellegrino, G. Assenza et al., "Modulation of brain plasticity in stroke: a novel model for neurorehabilitation," *Nature Reviews Neurology*, vol. 10, no. 10, pp. 597–608, 2014.

[8] E. G. Chrysikou and R. H. Hamilton, "Noninvasive brain stimulation in the treatment of aphasia: exploring interhemispheric relationships and their implications for neurorehabilitation," *Restorative Neurology and Neuroscience*, vol. 29, no. 6, pp. 375–394, 2011.

[9] J. C. Cole, C. Green Bernacki, A. Helmer, N. Pinninti, and J. P. O'Reardon, "Efficacy of transcranial magnetic stimulation (TMS) in the treatment of schizophrenia: a review of the literature to date," *Innovations in Clinical Neuroscience*, vol. 12, no. 7-8, pp. 12–19, 2015.

[10] G. Fuggetta, A. Fiaschi, and P. Manganotti, "Modulation of cortical oscillatory activities induced by varying single-pulse transcranial magnetic stimulation intensity over the left primary motor area: a combined EEG and TMS study," *NeuroImage*, vol. 27, no. 4, pp. 896–908, 2005.

[11] P. C. J. Taylor, V. Walsh, and M. Eimer, "Combining TMS and EEG to study cognitive function and cortico-cortico interactions," *Behavioural Brain Research*, vol. 191, no. 2, pp. 141–147, 2008.

[12] G. Thut, D. Veniero, V. Romei, C. Miniussi, P. Schyns, and J. Gross, "Rhythmic TMS causes local entrainment of natural oscillatory signatures," *Current Biology*, vol. 21, no. 14, pp. 1176–1185, 2011.

[13] M. Kawasaki, Y. Uno, J. Mori, K. Kobata, and K. Kitajo, "Transcranial magnetic stimulation-induced global propagation of transient phase resetting associated with directional information flow," *Frontiers in Human Neuroscience*, vol. 8, p. 173, 2014.

[14] V. Romei, M. Bauer, J. L. Brooks et al., "Causal evidence that intrinsic beta-frequency is relevant for enhanced signal propagation in the motor system as shown through rhythmic TMS," *NeuroImage*, vol. 126, pp. 120–130, 2016.

[15] M. Rosanova, A. Casali, V. Bellina, F. Resta, M. Mariotti, and M. Massimini, "Natural frequencies of human corticothalamic circuits," *The Journal of Neuroscience*, vol. 29, no. 24, pp. 7679–7685, 2009.

[16] P. Sauseng, W. Klimesch, W. R. Gruber, S. Hanslmayr, R. Freunberger, and M. Doppelmayr, "Are event-related potential components generated by phase resetting of brain oscillations? A critical discussion," *Neuroscience*, vol. 146, no. 4, pp. 1435–1444, 2007.

[17] G. Thut, P. G. Schyns, and J. Gross, "Entrainment of perceptually relevant brain oscillations by non-invasive rhythmic stimulation of the human brain," *Frontiers in Psychology*, vol. 2, p. 170, 2011.

[18] J. D. Herring, G. Thut, O. Jensen, and T. O. Bergmann, "Attention modulates TMS-locked alpha oscillations in the visual cortex," *The Journal of Neuroscience*, vol. 35, no. 43, pp. 14435–14447, 2015.

[19] G. Tononi, "Information integration: its relevance to brain function and consciousness," *Archives Italiennes de Biologie*, vol. 148, no. 3, pp. 299–322, 2010.

[20] P. Lakatos, A. S. Shah, K. H. Knuth, I. Ulbert, G. Karmos, and C. E. Schroeder, "An oscillatory hierarchy controlling neuronal excitability and stimulus processing in the auditory cortex," *Journal of Neurophysiology*, vol. 94, no. 3, pp. 1904–1911, 2005.

[21] R. T. Canolty, E. Edwards, S. S. Dalal et al., "High gamma power is phase-locked to theta oscillations in human neocortex," *Science*, vol. 313, no. 5793, pp. 1626–1628, 2006.

[22] A. B. L. Tort, R. Komorowski, H. Eichenbaum, and N. Kopell, "Measuring phase-amplitude coupling between neuronal oscillations of different frequencies," *Journal of Neurophysiology*, vol. 104, no. 2, pp. 1195–1210, 2010.

[23] F. Roux, M. Wibral, W. Singer, J. Aru, and P. J. Uhlhaas, "The phase of thalamic alpha activity modulates cortical gamma-band activity: evidence from resting-state MEG recordings," *The Journal of Neuroscience*, vol. 33, no. 45, pp. 17827–17835, 2013.

[24] M. Bonnefond and O. Jensen, "Gamma activity coupled to alpha phase as a mechanism for top-down controlled gating," *PLoS One*, vol. 10, no. 6, article e0128667, 2015.

[25] T. Kajihara, M. N. Anwar, M. Kawasaki, Y. Mizuno, K. Nakazawa, and K. Kitajo, "Neural dynamics in motor preparation: from phase-mediated global computation to amplitude-mediated local computation," *NeuroImage*, vol. 118, pp. 445–455, 2015.

[26] B. Händel and T. Haarmeier, "Cross-frequency coupling of brain oscillations indicates the success in visual motion discrimination," *NeuroImage*, vol. 45, no. 3, pp. 1040–1046, 2009.

[27] Y. Noda, R. Zomorrodi, T. Saeki et al., "Resting-state EEG gamma power and theta-gamma coupling enhancement following high-frequency left dorsolateral prefrontal rTMS in patients with depression," *Clinical Neurophysiology*, vol. 128, no. 3, pp. 424–432, 2017.

[28] R. F. Helfrich, C. S. Herrmann, A. K. Engel, and T. R. Schneider, "Different coupling modes mediate cortical cross-frequency interactions," *NeuroImage*, vol. 140, pp. 76–82, 2016.

[29] B. Voytek, R. T. Canolty, A. Shestyuk, N. E. Crone, J. Parvizi, and R. T. Knight, "Shifts in gamma phase–amplitude coupling frequency from theta to alpha over posterior cortex during visual tasks," *Frontiers in Human Neuroscience*, vol. 4, p. 191, 2010.

[30] L. Wang, Y. B. Saalmann, M. A. Pinsk, M. J. Arcaro, and S. Kastner, "Electrophysiological low-frequency coherence and cross-frequency coupling contribute to BOLD connectivity," *Neuron*, vol. 76, no. 5, pp. 1010–1020, 2012.

[31] H. Sekiguchi, S. Takeuchi, H. Kadota, Y. Kohno, and Y. Nakajima, "TMS-induced artifacts on EEG can be reduced by rearrangement of the electrode's lead wire before recording," *Clinical Neurophysiology*, vol. 122, no. 5, pp. 984–990, 2011.

[32] R. J. Korhonen, J. C. Hernandez-Pavon, J. Metsomaa, H. Mäki, R. J. Ilmoniemi, and J. Sarvas, "Removal of large muscle artifacts from transcranial magnetic stimulation-evoked EEG by independent component analysis," *Medical & Biological Engineering & Computing*, vol. 49, no. 4, pp. 397–407, 2011.

[33] F. Perrin, J. Pernier, O. Bertrand, and J. F. Echallier, "Spherical splines for scalp potential and current density mapping," *Electroencephalography and Clinical Neurophysiology*, vol. 72, no. 2, pp. 184–187, 1989.

[34] J. Kayser and C. E. Tenke, "Principal components analysis of Laplacian waveforms as a generic method for identifying ERP generator patterns: I. Evaluation with auditory oddball tasks," *Clinical Neurophysiology*, vol. 117, no. 2, pp. 348–368, 2006.

[35] R. Kronland-Martinet, J. Morlet, and A. Grossmann, "Analysis of sound patterns through wavelet transforms," *International Journal of Pattern Recognition and Artificial Intelligence*, vol. 1, no. 02, pp. 273–302, 1987.

[36] C. Tallon-Baudry, O. Bertrand, C. Delpuech, and J. Pernier, "Stimulus specificity of phase-locked and non-phase-locked 40 Hz visual responses in human," *The Journal of Neuroscience*, vol. 16, no. 13, pp. 4240–4249, 1996.

[37] J.-P. Lachaux, E. Rodriguez, M. L. V. Quyen, A. Lutz, J. Martinerie, and F. J. Varela, "Studying single-trials of phase synchronous activity in the brain," *International Journal of Bifurcation and Chaos*, vol. 10, no. 10, pp. 2429–2439, 2000.

[38] P. Berens, "CircStat: a MATLAB toolbox for circular statistics," *Journal of Statistical Software*, vol. 31, no. 10, 2009.

[39] B. Voytek, M. D'Esposito, N. Crone, and R. T. Knight, "A method for event-related phase/amplitude coupling," *NeuroImage*, vol. 64, pp. 416–424, 2013.

[40] Y. Benjamini and Y. Hochberg, "Controlling the false discovery rate: a practical and powerful approach to multiple testing," *Journal of the Royal Statistical Society: Series B (Methodological)*, vol. 57, no. 1, pp. 289–300, 1995.

[41] R. Oostenveld, P. Fries, E. Maris, and J.-M. Schoffelen, "FieldTrip: open source software for advanced analysis of MEG, EEG, and invasive electrophysiological data," *Computational Intelligence and Neuroscience*, vol. 2011, Article ID 156869, 9 pages, 2011.

[42] R. T. Canolty and R. T. Knight, "The functional role of cross-frequency coupling," *Trends in Cognitive Sciences*, vol. 14, no. 11, pp. 506–515, 2010.

[43] R. C. Sotero, "Modeling the generation of phase-amplitude coupling in cortical circuits: from detailed networks to neural mass models," *BioMed Research International*, vol. 2015, Article ID 915606, 12 pages, 2015.

[44] V. Romei, J. Gross, and G. Thut, "Sounds reset rhythms of visual cortex and corresponding human visual perception," *Current Biology*, vol. 22, no. 9, pp. 807–813, 2012.

[45] M. A. Kramer, A. B. L. Tort, and N. J. Kopell, "Sharp edge artifacts and spurious coupling in EEG frequency comodulation measures," *Journal of Neuroscience Methods*, vol. 170, no. 2, pp. 352–357, 2008.

[46] S. Haegens, H. Cousijn, G. Wallis, P. J. Harrison, and A. C. Nobre, "Inter- and intra-individual variability in alpha peak frequency," *NeuroImage*, vol. 92, pp. 46–55, 2014.

[47] P. Sauseng, W. Klimesch, K. F. Heise et al., "Brain oscillatory substrates of visual short-term memory capacity," *Current Biology*, vol. 19, no. 21, pp. 1846–1852, 2009.

[48] N. W. Gouwens, H. Zeberg, K. Tsumoto, T. Tateno, K. Aihara, and H. P. C. Robinson, "Synchronization of firing in cortical fast-spiking interneurons at gamma frequencies: a phase-resetting analysis," *PLoS Computational Biology*, vol. 6, no. 9, article e1000951, 2010.

[49] R. J. Ilmoniemi, J. Virtanen, J. Ruohonen et al., "Neuronal responses to magnetic stimulation reveal cortical reactivity and connectivity," *Neuroreport*, vol. 8, no. 16, pp. 3537–3540, 1997.

[50] M. Massimini, F. Ferrarelli, R. Huber, S. K. Esser, H. Singh, and G. Tononi, "Breakdown of cortical effective connectivity during sleep," *Science*, vol. 309, no. 5744, pp. 2228–2232, 2005.

[51] Y. Morishima, R. Akaishi, Y. Yamada, J. Okuda, K. Toma, and K. Sakai, "Task-specific signal transmission from prefrontal cortex in visual selective attention," *Nature Neuroscience*, vol. 12, no. 1, pp. 85–91, 2009.

[52] A. G. Casali, S. Casarotto, M. Rosanova, M. Mariotti, and M. Massimini, "General indices to characterize the electrical response of the cerebral cortex to TMS," *NeuroImage*, vol. 49, no. 2, pp. 1459–1468, 2010.

[53] N. A. Parks, E. L. Maclin, K. A. Low, D. M. Beck, M. Fabiani, and G. Gratton, "Examining cortical dynamics and connectivity with simultaneous single-pulse transcranial magnetic stimulation and fast optical imaging," *NeuroImage*, vol. 59, no. 3, pp. 2504–2510, 2012.

[54] M. Zanon, P. P. Battaglini, J. Jarmolowska, G. Pizzolato, and P. Busan, "Long-range neural activity evoked by premotor cortex stimulation: a TMS/EEG co-registration study," *Frontiers in Human Neuroscience*, vol. 7, p. 803, 2013.

[55] A. Hillebrand, G. R. Barnes, J. L. Bosboom, H. W. Berendse, and C. J. Stam, "Frequency-dependent functional connectivity within resting-state networks: an atlas-based MEG beamformer solution," *NeuroImage*, vol. 59, no. 4, pp. 3909–3921, 2012.

[56] T. Akam and D. M. Kullmann, "Oscillations and filtering networks support flexible routing of information," *Neuron*, vol. 67, no. 2, pp. 308–320, 2010.

[57] M. X. Cohen, C. E. Elger, and J. Fell, "Oscillatory activity and phase-amplitude coupling in the human medial frontal cortex during decision making," *Journal of Cognitive Neuroscience*, vol. 21, no. 2, pp. 390–402, 2009.

[58] A. B. L. Tort, R. W. Komorowski, J. R. Manns, N. J. Kopell, and H. Eichenbaum, "Theta–gamma coupling increases during the learning of item–context associations," *Proceedings of the National Academy of Sciences of the United States of America*, vol. 106, no. 49, pp. 20942–20947, 2009.

[59] E. Tzvi, R. Verleger, T. F. Münte, and U. M. Krämer, "Reduced alpha-gamma phase amplitude coupling over right parietal cortex is associated with implicit visuomotor sequence learning," *NeuroImage*, vol. 141, pp. 60–70, 2016.

[60] E. Combrisson, M. Perrone-Bertolotti, J. L. P. Soto et al., "From intentions to actions: neural oscillations encode motor processes through phase, amplitude and phase-amplitude coupling," *NeuroImage*, vol. 147, pp. 473–487, 2017.

[61] C. de Hemptinne, E. S. Ryapolova-Webb, E. L. Air et al., "Exaggerated phase-amplitude coupling in the primary motor cortex in Parkinson disease," *Proceedings of the National Academy of Sciences of the United States of America*, vol. 110, no. 12, pp. 4780–4785, 2013.

[62] S. Khan, A. Gramfort, N. R. Shetty et al., "Local and long-range functional connectivity is reduced in concert in autism spectrum disorders," *Proceedings of the National Academy of Sciences of the United States of America*, vol. 110, no. 8, pp. 3107–3112, 2013.

[63] K. Edakawa, T. Yanagisawa, H. Kishima et al., "Detection of epileptic seizures using phase-amplitude coupling in intracranial electroencephalography," *Scientific Reports*, vol. 6, no. 1, p. 25422, 2016.

[64] S. I. Dimitriadis, N. A. Laskaris, M. P. Bitzidou, I. Tarnanas, and M. N. Tsolaki, "A novel biomarker of amnestic MCI based on dynamic cross-frequency coupling patterns during cognitive brain responses," *Frontiers in Neuroscience*, vol. 9, p. 350, 2015.

[65] W. Klomjai, R. Katz, and A. Lackmy-Vallée, "Basic principles of transcranial magnetic stimulation (TMS) and repetitive TMS (rTMS)," *Annals of Physical and Rehabilitation Medicine*, vol. 58, no. 4, pp. 208–213, 2015.

[66] B. Kundu, J. S. Johnson, and B. R. Postle, "Prestimulation phase predicts the TMS-evoked response," *Journal of Neurophysiology*, vol. 112, no. 8, pp. 1885–1893, 2014.

Hindawi
Neural Plasticity
Volume 2019, Article ID 3540898, 15 pages
https://doi.org/10.1155/2019/3540898

Clinical Study

Investigating the Efficacy of an Individualized Alpha/Delta Neurofeedback Protocol in the Treatment of Chronic Tinnitus

Dominik Güntensperger[1,2], **Christian Thüring**[3], **Tobias Kleinjung**[3], **Patrick Neff**[2,4] and **Martin Meyer**[1,2,5]

[1]*Division of Neuropsychology, Department of Psychology, University of Zurich, Zurich, Switzerland*
[2]*University Research Priority Program "Dynamics of Healthy Aging", University of Zurich, Zurich, Switzerland*
[3]*Department of Otorhinolaryngology, University Hospital Zurich, Zurich, Switzerland*
[4]*Center for Neuromodulation, University of Regensburg, Regensburg, Germany*
[5]*Tinnitus-Zentrum, Charité-Universitätsmedizin, Berlin, Germany*

Correspondence should be addressed to Dominik Güntensperger; dominik.guentensperger@uzh.ch

Received 13 November 2018; Revised 24 January 2019; Accepted 10 February 2019; Published 26 March 2019

Guest Editor: Giovanni Pellegrino

First attempts have demonstrated that the application of alpha/delta neurofeedback in the treatment of chronic tinnitus leads to a reduction of symptoms at the group level. However, recent research also suggests that chronic tinnitus is a decidedly heterogeneous phenomenon, one that requires treatment of distinct subgroups or even on an individual level. Thus, the purpose of this study was to evaluate an individually adjusted alpha/delta neurofeedback protocol. Following previous studies, the delta band fixed between 3 and 4 Hz was chosen as the frequency for inhibition. However, unlike the previous studies, the frequency range for the rewarded alpha band was not fixed between 8 and 12 Hz but rather individually determined according to each patient's specific alpha peak frequency (IAF). Twenty-six chronic tinnitus patients participated in 15 weekly neurofeedback training sessions and extensive pre- and post-tests, as well as follow-up testing 3 and 6 months after training. The main outcome measures were tinnitus-related distress measured with the Tinnitus Handicap Inventory (THI) and Tinnitus Questionnaire (TQ), tinnitus loudness, and pre- and post-training resting-state EEG activity in trained frequency bands. In Results, the neurofeedback protocol led to a significant reduction of tinnitus-related distress and tinnitus loudness. While distress remained on a low level even 6 months after the completion of training, loudness returned to baseline levels in the follow-up period. In addition, resting-state EEG activity showed an increase in the trained alpha/delta ratio over the course of the training. This ratio increase was related to training-induced changes of tinnitus-related distress as measured with TQ, mainly due to increases in the alpha frequency range. In sum, this study confirms the alpha/delta neurofeedback as a suitable option for the treatment of chronic tinnitus and represents a first step towards the development of individual neurofeedback protocols. This clinical trial was registered online at ClinicalTrials.gov (NCT02383147) and kofam.ch (SNCTP000001313).

1. Introduction

Approximately 5-15% of the Western population suffers from a permanent sensation of ringing or hissing in their ears, a phenomenon also known as chronic subjective tinnitus [1]. According to Henry et al. [1], around 20% of affected people suffer considerably from this constant perception of sound which, in some cases, can result in a substantial reduction of quality of life. Often, chronic tinnitus can induce related issues, some of which include problems sleeping or concentrating, experiencing difficulty in social interactions, and perhaps even resulting in severe depression or anxiety [2–4]. An effective treatment to completely alleviate the symptoms of tinnitus has not yet been discovered, and thus, many sufferers do not receive the help that they need. As a consequence, this lack of sustained and effective intervention

can lead to increased levels of stress and frustration which, in turn, compound the negative impact of tinnitus on the quality of life for many patients [5].

While in early research subjective tinnitus was assumed to be a problem associated with the peripheral hearing system only [6, 7], the currently widely accepted view is that this auditory phantom percept emerges as a result of unsuccessful compensatory mechanisms in the brain in consequence of inner ear receptor damage [8–11]. Further to this, electrophysiological recordings with electroencephalography (EEG) and/or magnetoencephalography (MEG) have led to the recognition of tinnitus-related abnormalities in spontaneous resting-state brain activity. According to recent studies in which the resting-state activity of tinnitus patients and healthy controls was compared, the resting brain of tinnitus patients typically shows enhanced activity in the delta (0.5-4 Hz) and gamma (35.5-45 Hz) frequency bands and a comparative reduction of alpha (8.5-12 Hz) oscillations over temporal areas [11–18]. The theoretical frameworks on which these findings are based are the thalamocortical dysrhythmia (TCD) model [19] and the synchronization-by-loss-of-inhibition model (SLIM) [11]. The TCD model describes the emergence of spontaneous firing of thalamic fibers due to auditory input deprivation as an essential factor for tinnitus genesis [19]. Specifically, when thalamic relay cells are deprived of excitatory sensory input from the inner ear, the hyperpolarized cell membrane causes these neurons to fire low-threshold calcium spike bursts in a slow-wave mode. Thalamocortical feedback loops then lead to the establishment of this slow-wave rhythm in cortical neurons, which is measurable as ongoing delta activity on the scalp. Llinás et al. [19] further propose that an *edge effect* resulting from these increased gamma oscillations is responsible for perceptive disturbances, such as tinnitus. Furthermore, it is suggested in the SLIM that this increase in the gamma frequency range may also be driven by decreased lateral inhibition processes in auditory cortex areas due to an underactivation of inhibitory neurons [11]. This imbalance between cortical inhibition and excitation thus provides a theoretical explanation for the alpha-down, delta-up pattern typically found in the resting-state M/EEG data of tinnitus patients [20].

Recently, neurofeedback has received increasing attention regarding its potential in the treatment of a variety of psychological and neurological disorders. In the process of neurofeedback, electrophysiological brain activity is recorded noninvasively, immediately analyzed in real-time, and certain aspects of it (e.g., frequency band power) extracted, which are then directly used for feedback to the subject. The rewarding of desired changes and inhibiting of undesired changes in the signal pattern by providing directly perceivable visual, auditory, and/or tactile feedback is proposed to trigger a learning process during which the patients learn to voluntarily control their brain activity and to adjust it in the desired direction. Neurofeedback has been in development since the late 1960s [21, 22] and is currently an established treatment method for attention deficit hyperactivity disorder (ADHD) [23–27]. Furthermore, first attempts have already been made to implement it as an effective treatment for chronic tinnitus (for a review, see [28]). In this context, the training of frequency bands linked to the aforementioned abnormalities in resting-state brain activity has been shown to be a highly promising approach. Two research groups reported that neurofeedback training aimed at increasing alpha and decreasing delta activity over auditory areas led to significant reductions in tinnitus-related symptoms (i.e., tinnitus distress and loudness) and that these behavioral changes were also linked to the trained resting-state activity [29, 30]. The gamma frequency band, however, has been largely neglected in neurofeedback treatments for chronic tinnitus. The reason for this is based on current debate, namely, that activity in the gamma band may reflect an attempt of the brain to suppress tinnitus rather than cause it [31, 32] or may be involved in the communication of prediction errors [33]. Given these inconsistencies, the inclusion of gamma oscillations in neurofeedback protocols for the treatment of tinnitus is unsuitable until their specific role is better understood. Furthermore, the usability of gamma for neurofeedback protocols is limited by its rather broad and unspecific bandwidth and a decreasing signal-to-noise ratio for higher frequencies.

The aim of this clinical study was thus to contribute to the development of effective neurofeedback protocols for tinnitus patients and to build on as well as extend the previously applied auditory alpha/delta training. For the recording of brain activity used for the feedback, the same EEG electrodes (FC1, FC2, F3, and F4) were chosen as in the previously mentioned studies [29, 30] to guarantee comparability. Regarding the frequency bands used for the training, however, we chose a novel approach. This was based on the recognition that chronic tinnitus is a very multifaceted and complex phenomenon, as noted in recent studies (e.g., [10, 34]). For this reason, we considered it extremely important to conceive the applied neurofeedback treatment on an individualized basis, thereby attempting to meet the specific needs of each tinnitus patient. This project takes the first step in this direction. In particular, we took into account observations that the individual alpha peak frequency (IAF) can vary considerably among individuals [35]. Using the fixed alpha band (generally defined between 8 and 12 Hz) for power analysis, therefore, does not reflect alpha band power for each subject appropriately. We believe that these interindividual differences should be considered when alpha is targeted in a neurofeedback training protocol. Further to this argument, a recent study with tinnitus patients has underlined the importance of taking the interindividual alpha variability into account for this group [36]. Based on this reasoning, we did not choose the standard alpha band (8-12 Hz) as a fixed reward frequency for each patient, which has customarily been the case in previous studies. Instead, an individual alpha peak frequency was determined for each tinnitus patient before the first neurofeedback session and an individually adjusted alpha band was then used for the generation of the neurofeedback reward.

In addition, we placed great emphasis on efforts to make our results replicable and comparable to other studies. Accordingly, we designed our study closely following the

guidelines of the Tinnitus Research Initiative (TRI) on outcome measures for tinnitus intervention studies [37, 38]. We combined our training with a wide variety of questionnaires and tests at different time points while also using different measurements for tinnitus-related distress and other health-related variables. In addition, the classical pre-post design, generally used in treatment studies, was supplemented by two follow-up measurements in order to investigate longevity and persistence of the potential effects. The main behavioral outcome measures of this study were tinnitus-related distress, measured with two well-established tinnitus questionnaires, and tinnitus loudness. Both variables were hypothesized to decrease over the course of the neurofeedback training and to remain on a stable lower level at the follow-up time points. Furthermore, in order to examine whether the neurofeedback training indeed evoked the desired effects in EEG activity, the ratio between the rewarded alpha- and the inhibited delta band was compared across time points. It was expected that the alpha/delta ratio would change significantly between pre- and post-tests and would remain on a stable level in the follow-up period.

2. Methods

2.1. Participants. Participants were recruited at the Department of Otorhinolaryngology (University Hospital Zurich). In order to be eligible for study inclusion, patients had to be diagnosed with chronic subjective tinnitus (>0.5 years), be between 18 and 75 years old, have adequate knowledge of the German language, suffer from no other psychiatric or neurological disorder, and have no acute suicidal tendency. Furthermore, patients with drug or alcohol addiction, cochlear implants, and current prescriptions for tranquilizers, neuroleptics, or antiepileptics were not considered. It should be mentioned that this study is part of a comprehensive clinical project, and participants were randomly assigned to one of two study groups (single-blind randomized controlled trial). Both groups underwent the exact same procedure (see Section 2.2) with the sole difference being a technical aspect of feedback generation. The group reported here followed the neurofeedback application closely related to prior studies (see Section 2.5) in which the activity included for calculating reward and inhibit rates was limited to four electrodes. The other group used a marginally different approach in that more EEG electrodes in addition to source estimation algorithms were involved in feedback generation. The results of this group as well as between-group comparisons will be discussed elsewhere. According to the aforementioned criteria, 26 suitable patients with chronic subjective tinnitus were identified and included. Participants were between 24 and 71 years old with a mean age of 46.15 (SD: 12.33). The sample consisted of 20 males and 6 females. The study was approved by the appropriate Ethics Committee (Kantonale Ethikkommission Project KEK-ZH-Nr. 2014-0594) and was registered online at ClinicalTrials.gov (NCT02383147) and kofam.ch (SNCTP000001313).

2.2. Procedure. This prospective clinical trial consisted of 20 visits in total. In the first appointment, 1-2 weeks before the start of the neurofeedback training phase, patients were extensively informed about the purpose and exact procedure of the study and signed their informed consent in the presence of a qualified medical professional at the Department of Otorhinolaryngology. In the same visit, participants further underwent the audiometric screening in which their pure tone hearing thresholds at 0.25, 0.5, 1, 2, 4, 6, and 8 kHz as well as other audiometric measurements (speech audiogram and speech-in-noise test) were determined. In the second screening visit, a baseline resting-state EEG measurement was performed and patients were asked to complete questionnaires covering demographics and tinnitus-related symptoms, as well as several other psychological and health-related questions (details in Section 2.3).

After the two baseline appointments (t1), patients participated in a total of 15 neurofeedback training sessions on a weekly basis. Occasional rescheduling of individual sessions as well as absences due to holidays or illness was unavoidable and compensated for as best as possible. One week after the completion of the training period, a post-measurement was performed (t2) consisting of the repeated measurement of 16 minutes of resting-state EEG and completion of the questionnaires. The same procedure was repeated approximately 3 months later after the first follow-up measurement was conducted (t3). In the final follow-up (t4), 6 months after the end of the training period, patients received a link by email and were asked for another completion of the set of questionnaires online. Subsequently, they were informed that they had fully completed the clinical study and were provided the opportunity to discuss their individual results with the study team.

2.3. Behavioral Measurements. The set of questionnaires consisted of a variety of forms according to the guidelines of the Tinnitus Research Initiative (TRI) [37, 38]. Specifically, an adjusted version of the Tinnitus Sample Case History Questionnaire (TSCHQ) was used to ask about demographics, tinnitus properties (e.g., origin, location, loudness, and type), prior treatment attempts, and other tinnitus-related issues. Two questionnaires were used to assess tinnitus distress: the Tinnitus Handicap Inventory (THI) (German version by [39]) and the Tinnitus Questionnaire (TQ) (German version by [40]). Sum scores can be calculated for both questionnaires ranging from 0 to 100 in the former and 0 to 84 in the latter case. In addition, the TQ score can be divided into the six subscores: "emotional distress," "cognitive distress," "intrusiveness," "auditory perceptual difficulties," "sleep disturbances," and "somatic complaints."

Additionally, participants completed German versions of Beck's Depression Inventory (BDI) [41], Beck's Anxiety Inventory (BAI) [42], the short form of the WHO Quality of Life scale (WHOQOL-BREF) [43], Symptom Check List (SCL-K-9) [44], and Short Form Health Questionnaire (SF-36) [45]. Completion of questionnaires took about 45 minutes in total and was done electronically on an iPad during the preparation of the EEG system at t1, t2, and t3 and online via an email link at t4.

The main behavioral outcome measures of this study are tinnitus loudness (rated from 1 "very low" to 100 "very

high"), sum score of the THI, and sum- as well as subscores of the TQ.

2.4. EEG Recording. A BrainAmp DC amplifier system in combination with 64 active channel actiCap electrode caps (Brain Products, Munich, Germany) were used to record the resting-state EEG at t1, t2, and t3. The array of silver/silver chloride electrodes corresponded with the 5/10 electrode position system [46]. Recording was referenced against the FCz electrode with a ground electrode positioned at the AFz position. A sampling rate of 1000 Hz was used. The electrodes were prepared with conductive paste for recording, and impedance was kept below 10 kΩ. Recordings were done in direct current (DC) mode with a high-cutoff filter of 1000 Hz with a slope of 12 dB/octave. Patients were asked to sit upright on a comfortable chair in a sound-proof and electromagnetically shielded room and to avoid excessive movements and muscle contractions in order to minimize artifacts. During recording, subjects were instructed by a prerecorded voice to open (EO) and close (EC) their eyes in regular intervals. For playback of these instructions, Presentation software (Neurobehavioral Systems Inc., 2010) was used and a fixation cross was presented during eyes-open segments.

Resting-state EEG was recorded twice over a time span of 8 minutes. While in the first 8 minutes of recording no additional instructions were given (EEG with no task: EEG-NT), in the second measurement, patients were asked to deliberately not suppress their tinnitus (EEG with task: EEG-WT). This was done to control for unwanted suppression effects that happen continuously in the brains of tinnitus sufferers (see also [31]). According to the recommendations of Working Group 3 of the European tinnitus research network, TINNET (http://www.tinnet.tinnitusresearch.net/), the resting-state activity of eyes-open segments was chosen as the main electrophysiological outcome measure.

2.5. Neurofeedback Training. EEG for neurofeedback training was registered with four silver/silver chloride electrodes, FC1, FC2, F3, and F4 combined with a NeuroAmp amplifier (BEE Medic GmbH, Singen, Germany). Electrodes at the earlobes served as reference electrodes and AFz as the ground electrode. The sampling rate was set at 250 Hz and impedance kept below 20 kΩ. The EEG signal was processed in real-time using the software Cygnet 2.0.3.34 (EEG Info, Kirchberg, Switzerland), and the feedback was implemented in the computer simulation Inner Tube (Somatic Vision, Encinitas, CA, USA). In this visualization, patients observed a space ship automatically navigating through a narrow tunnel. While increased power in the alpha band led to acceleration of the ship, delta as the defined inhibited band was linked to autopilot accuracy. It is important to note that automatic filtering is included in the Cygnet software so that excessive movement artifacts (blinking included) as well as system voltage (45-55 Hz) are automatically detected and excluded from feedback.

In the first neurofeedback training session, an individual alpha peak was determined for each participant by averaging alpha peaks over 30 seconds of resting-state EEG [35]. Subsequently, the reward frequency was set in the range of ±2 Hz around this peak frequency. As the undesired alternate, the frequency range of 3-4 Hz corresponding to the delta band was generally set to evoke negative feedback. Patients were asked to sit comfortably in a chair, avoid excessive muscle movement, and pay close attention to the feedback game. Following the custom of previous studies [29, 30], no further instruction was given as to how to influence the feedback or what strategy to use in order to allow for the highest amount of freedom possible. The training itself lasted 15 minutes and was repeated once a week, preferably on the same weekday at the same time.

2.6. Data Analysis

2.6.1. EEG Preprocessing. Preprocessing of EEG data was done with the BrainVision Analyzer 2 (Brain Products, Munich, Germany). Data was first band-pass filtered with Butterworth zero-phase filters between 0.1 Hz and 80 Hz with slopes of 24 dB/octave at the low and 48 dB/octave at the high cutoffs. In order to eliminate possible line noise, data was further filtered with a band-rejection filter with a central frequency of 50 Hz, a bandwidth of 1 Hz, and a slope of 24 dB/octave. The EEG signal was split into independent components in order to identify regular artifacts (e.g., eye blinks, pulse artifacts, noise). This was done by applying an independent component analysis (ICA) with a restricted Infomax algorithm implemented in BrainVision Analyzer 2. Bad channels (i.e., very noisy or dead channels, as well as electrodes with channel jumps) were temporarily excluded from this step. With the inverse ICA procedure, the resulting components indicative of artifacts were removed from the data. Subsequently, spline-type topographical interpolations [47] were performed for previously excluded channels and channels with remaining noise. On average, 5.4 components have been excluded and 1.9 channels interpolated per data set. A limit of ten bad channels (~15%) was priorly defined to lead to data set exclusion which was not the case for any of the data sets. A thorough visual inspection was performed in order to remove the remaining vertical artifacts (i.e., muscle movements and short drifts or jumps over single or multiple electrodes) from the signal. An average reference over all channels was calculated and applied whereby the implicit reference of data recording (FCz) was reincluded into the data and used for subsequent analysis. Finally, data was segmented into eyes-closed and eyes-open conditions and imported to MATLAB Statistics Toolbox Release 2017a (The MathWorks Inc., Natick, Massachusetts, United States) and EEGLAB 14.1.1b [48].

2.6.2. EEG Analysis. A hamming window with 2 s window length and 1 s overlap was first applied on the data of eyes-closed and eyes-open segments. Subsequently, Fast Fourier Transform (FFT) was computed for each 2 s segment, logarithmized, and then averaged over all segments for each patient. The resulting values provided power values in decibel (dB) for each electrode of each measurement (EEG-NT and EEG-WT). The frequency resolution was thus 0.5 Hz. Next, we calculated the alpha/delta ratio by dividing power

Table 1: Demographics, health, and tinnitus characteristics of the study sample.

	Mean	SD	Median	Min	Max
Age	46.29	12.22	44	24	71
Mean hearing loss (dB)	7.54	8.25	4.4	0	22.8
Tinnitus duration (months)	78.92	74.63	40	18	312
Age of onset	39.75	14.66	39	14	67
Tinnitus loudness	53.25	19.57	50	20	95
Tinnitus distress (THI)	29.33	14.7	27	4	56
Tinnitus distress (TQ)	23.75	11.63	23	6	45
BDI sum score[a]	6.29	4.34	7	0	13
BAI sum score[a]	7.12	5.77	6.5	0	21
WHOQOL-BREF domain 1: physical health[b]	76.49	14.48	79	43	100
WHOQOL-BREF domain 2: psychological health[b]	69.97	15.78	69	42	96
WHOQOL-BREF domain 3: social relationship[b]	66.32	19.73	67	25	100
WHOQOL-BREF domain 4: environment[b]	81.51	11.28	84	62	100
WHOQOL-BREF global value[b]	67.19	18.36	62	25	100
SCL-K-9[c]	0.72	0.71	1	0	3
SF-36: mental health[e]	45.79	9.46	47	22	60
SF-36: physical health[e]	53.38	6.76	55	35	60

Note: SD: standard deviation. [a]Sum scales (0-84) measuring severity of depressive/anxiety symptoms. [b]Scaled sum scores (0-100) indicating quality of life in specific domains or globally. [c]Mean over all items (0-4) measuring general psychological strain. [e]Normed sum scales ($M = 50$, $SD = 10$) indicating mental/physical disability; higher values indicate less disability.

values in the rewarded (individual) alpha range by those in the inhibited delta range (3-4 Hz). This ratio was finally averaged over the four electrodes used for training (FC1, FC2, F3, and F4) as well as over all 65 electrodes of the EEG system. In addition, power values in the standard frequency bands delta (0.5-4 Hz), theta (4.5-8 Hz), lower alpha (8.5-10 Hz), upper alpha (10.5-12 Hz), alpha (8.5-12 Hz), beta1 (12.5-15 Hz), beta2 (15.5-23 Hz), beta3 (23.5-35 Hz), and gamma (35.5-45 Hz) were calculated and analyzed.

2.6.3. Statistics. Data was analyzed using the software package R [49] including packages "ggplot2" [50], "ggsignif" [51], "Hmisc" [52], "jtools" [53], "multcomp" [54], "nlme" [55], and "xtable" [56]. Repeated-measure mixed model analysis of variance (ANOVA) was used to estimate time effects for behavioral (THI sum score, TQ sum- and subscores, and tinnitus loudness) and EEG-related data. A priori defined contrasts comparing t1 with all other time points (t2, t3, and t4 for behavioral measures; t2 and t3 for EEG data) were calculated to gain insight into training success and the stability of changes in the follow-up period. Since contrasts are not independent, Bonferroni correction was applied, and because the contrasts were set a priori, one-tailed p values are reported. Furthermore, effect size r for a priori defined contrasts is reported which was converted from respective t values according to Field et al. [57]. Cohen [58] suggests that $r = 0.1$ may be labelled a small, $r = 0.3$ a medium, and $r = 0.5$ a large effect. In addition, post hoc Tukey tests were performed comparing each of the four time points with each other in order to reveal other potential differences between time points. In order to test for relationships between changes in the behavioral and electrophysiological domain, Pearson product-moment correlation coefficients between difference scores (t2-t1) were calculated and tested for statistical significance. The alpha threshold was set at $p = .05$ for all statistical tests.

3. Results

3.1. Description of Study Sample. Two patients who completed the full study procedure had to be excluded prior to data analysis because their BDI scores at all four time points suggested clinically relevant depressive symptoms (i.e., a sum score of more than 18 points). The final sample size for data analysis was therefore reduced to 24 participants. Table 1 shows the demographic and clinical details of the participants included in the final analysis. The study sample had a mean age of 46.29 (SD = 12.22) and consisted of 19 males and 5 females. All participants were right-handed. The percept was described mostly as tonal ($n = 17$) with a pitch described as "very high" in 12 subjects. Almost all ($n = 21$) subjects perceived tinnitus in both ears; however, 9 subjects of this group indicated a left- while 6 specified a right-sided tendency. Stress was named as the primal cause of tinnitus by 6 participants, 4 indicated acoustic trauma or hearing loss to be responsible, while the majority ($n = 13$) could not name an unambiguous cause for the condition.

For the overall group on average, the mean distress value of 29.33 (SD = 14.7) suggested a "mild tinnitus" according to the THI, while the mean TQ value of 23.75 (SD = 11.63) is labelled a "slight tinnitus." It is important to note that all tinnitus distress and loudness measures were significantly positively correlated (THI and TQ: $r(22) = 0.8$, $p < .001$; THI and loudness: $r(22) = 0.47$, $p = .022$; TQ and loudness: $r(22) = 0.56$, $p = .004$).

Table 2: Pearson correlation between tinnitus and health questionnaires.

	THI	TQ	Loudness
BDI sum score	0.75***	0.79***	0.48
BAI sum score	0.34	0.41	-0.03
SCL-K-9	0.47	0.56*	0.30
WHOQOL-BREF domain 1: physical health	-0.65**	-0.42	-0.37
WHOQOL-BREF domain 2: psychological health	-0.63**	-0.55*	-0.52*
WHOQOL-BREF domain 3: social relationship	-0.30	-0.24	-0.19
WHOQOL-BREF domain 4: environment	-0.16	-0.11	-0.13
WHOQOL-BREF global value	-0.51*	-0.25	-0.20
SF-36 physical health	-0.43	-0.22	0.02
SF-36 mental health	-0.69**	-0.66**	-0.45

Note: Pearson correlation coefficient corrected for multiple comparisons with the method of Benjamini and Hochberg [59]. *$p < .05$; **$p < .01$; ***$p < .001$.

Table 3: Primary outcome variables of the study group.

	t1	t2	t3	t4
THI	29.33 (14.70)	23.92 (12.71)	24.83 (12.48)	24.75 (16.48)
TQ	23.75 (11.63)	21.62 (12.03)	21.54 (11.18)	20.58 (12.81)
Loudness	53.25 (19.57)	43.67 (22.42)	51.67 (22.00)	55.46 (17.28)
Ratio EEG-NT	0.955 (0.044)	0.959 (0.033)	0.965 (0.040)	
Ratio EEG-WT	0.961 (0.042)	0.978 (0.044)	0.968 (0.041)	

Note: values are mean (SD).

Pearson correlations between tinnitus- and health-related measures are summarized in Table 2. All correlations are corrected for multiple comparisons using the method of Benjamini and Hochberg [59]. Notably, depressive symptoms as measured with the BDI were positively correlated with THI, $r(22) = 0.75$, $p < .001$, as well as TQ sum scores, $r(22) = 0.79$, $p < .001$, but not loudness, $r(22) = 0.48$, $p = .052$. Furthermore, significant negative correlations were observed between quality of life as measured with the psychological health domain of the WHOQOL-BREF (domain 2) and all tinnitus measures (THI: $r(22) = -0.63$, $p = .004$; TQ: $r(22) = -0.55$, $p = .021$; loudness: $r(22) = -0.52$, $p = .029$). Moreover, significant negative correlations were found between the mental health score of SF-36 and THI, $r(22) = -0.69$, $p = .002$, and TQ sum scores, $r(22) = -0.66$, $p = .003$.

3.2. Effects of Neurofeedback Training

3.2.1. Main Outcomes. Primary outcome variables across the four time points are presented in Table 3, as well as Figures 1 and 2. Results of the repeated-measure mixed model ANOVA as well as a priori defined contrasts are summarized in Table 4.

The repeated-measure mixed model ANOVA suggested significant effects of the factor *time* on tinnitus-related distress measured with the THI, $\chi^2(3) = 9.18$, $p = .027$, and tinnitus loudness, $\chi^2(3) = 12.4$, $p = .006$. Results for the TQ, on the other hand, did not suggest significant differences over time, $\chi^2(3) = 5.24$, $p = .155$. However, an ANOVA performed on the subscores of TQ revealed significant time effects for "emotional distress," $\chi^2(3) = 8.94$, $p = .03$.

A priori defined contrasts for THI-measured distress showed significant decreases between t1 and the other 3 time points (see Table 4). A post hoc Tukey test corroborated these three significant results and revealed no further significant differences. It is important to note that, even though the main analysis for TQ did not reveal a significant effect, the sum score measured prior to the neurofeedback training at t1 ($M = 23.75$, SD = 11.63) was found to be significantly higher than the average over the three time points after neurofeedback ($M = 21.25$, SD = 12.01), $t(69) = -2.14$, $p = .018$ (one-tailed). In the case of TQ, no other significant differences were found with the Tukey post hoc test.

For rated tinnitus loudness, a priori-defined contrasts revealed a significant decline between t1 ($M = 53.25$, SD = 19.57) and t2 ($M = 43.67$, SD = 22.42), $t(69) = -2.74$, $p = .012$ (one-tailed). However, the Tukey test further revealed a significant increase between t2 and t4 ($M = 55.46$, SD = 17.28), $p = .003$, suggesting a recession of the rated tinnitus loudness to the baseline value, 6 months after the training.

Regarding EEG data, the repeated-measure mixed model ANOVA suggested a significant effect of the factor *time* for the EEG with the instruction to focus on the tinnitus percept (EEG-WT), $\chi^2(2) = 7.77$, $p = .021$. The alpha/delta ratio of the resting-state measurement without instruction (EEG-NT) did not vary significantly over time, $\chi^2(2) = 3.54$, $p = .17$. For EEG-WT, the alpha/delta ratio showed a significant increase between t1 ($M = 0.961$, SD = 0.0422) and t2 ($M = 0.9783$, SD = 0.0443), $t(46) = 2.83$, $p = .007$ (one-

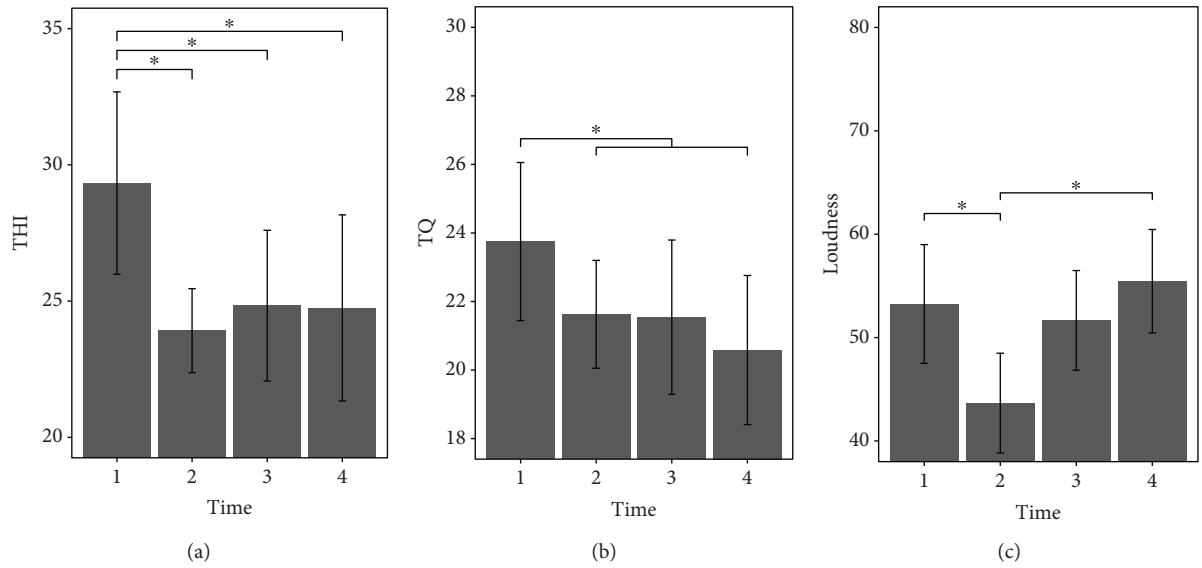

Figure 1: Barplots showing tinnitus-related symptoms before (t1), 1 week after (t2), 3 months after (t3), and 6 months after (t4) neurofeedback training. Error bars represent ±1 standard error for within-subject designs according to Morey [60]. THI scores (a) showed significant decreases from t1 to t2, and differences between t1 and the two follow-up time points were significant. TQ scores (b) were significantly higher before (t1) than after the neurofeedback intervention (t2-t4). For tinnitus loudness (c), a significant decrease between t1 and t2 was found followed by a significant increase to t4.

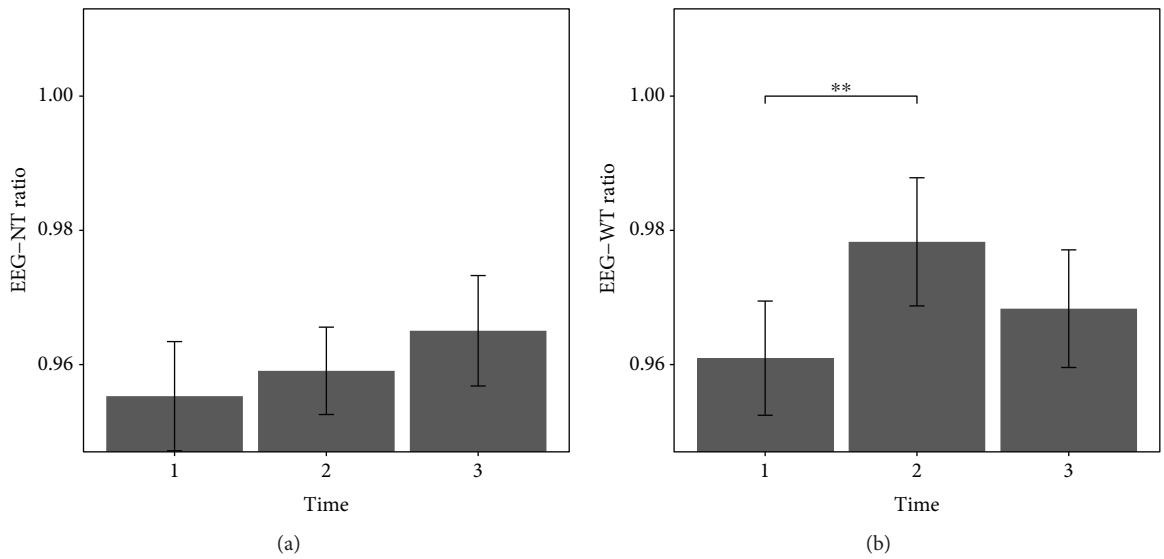

Figure 2: Barplots showing the alpha/delta power ratio over the four electrodes used for training in measurements before (t1), 1 week after (t2), and 3 months after (t3) the neurofeedback intervention. Error bars represent ±1 standard error for within-subject designs according to Morey [60]. The alpha/delta ratio of EEG-NT (a) did not vary significantly over time. The ratio of EEG-WT (b) increased significantly over the course of the training, between t1 and t2, followed by a nonsignificant decrease to t3.

tailed). This increase was followed by a slight decrease measured 3 months after the training, which was non-significant as Tukey tests, besides t1-t2, did not show any meaningful differences between time points. The contrast analysis for EEG-NT did not reveal any significant results.

When the individual alpha band as the reward frequency and the 3-4 Hz fixed delta band as the inhibit frequency of the neurofeedback training were compared separately across time, none of the repeated-measure ANOVAs suggested a significant time effect (see Table 4). Nonetheless, contrast analysis revealed a significant decrease in the trained delta band of EEG-WT over the course of the training between t1 ($M = 51.87$, $SD = 1.86$) and t2 ($M = 51.18$, $SD = 1.92$), $t(46) = -2.42$, $p = .02$ (one-tailed).

3.2.2. Control Comparisons. To control for band specificity of the neurofeedback training, separate analyses were performed for the other (non-trained) frequency bands: theta,

Table 4: Results of the repeated-measure mixed model ANOVA and a priori-defined contrasts for primary outcome variables.

	χ^2	t	df	p	Effect size r
THI					
ANOVA	9.18*		3	0.027	
t1-t2		-2.76*	69	0.011	0.32
t1-t3		-2.30*	69	0.037	0.27
t1-t4		-2.34*	69	0.033	0.27
TQ					
ANOVA	5.24		3	0.155	
t1-t2		-1.48	69	0.214	0.18
t1-t3		-1.54	69	0.192	0.18
t1-t4		-2.21*	69	0.046	0.26
Loudness					
ANOVA	12.4**		3	0.006	
t1-t2		-2.74*	69	0.012	0.31
t1-t3		-0.45	69	0.978	0.05
t1-t4		0.63	69	0.794	0.08
Ratio EEG-NT					
ANOVA	3.54		2	0.170	
t1-t2		0.72	46	0.475	0.11
t1-t3		1.86*	46	0.069	0.26
IAF EEG-NT					
ANOVA	0.99		2	0.610	
t1-t2		0.83	46	0.409	0.12
t1-t3		0.86	46	0.394	0.13
Delta EEG-NT					
ANOVA	1.24		2	0.539	
t1-t2		0.15	46	0.885	0.02
t1-t3		-0.87	46	0.390	0.13
Ratio EEG-WT					
ANOVA	7.77*		2	0.021	
t1-t2		2.83**	46	0.007	0.39
t1-t3		1.21	46	0.234	0.17
IAF EEG-WT					
ANOVA	0.51		2	0.776	
t1-t2		0.69	46	0.494	0.10
t1-t3		0.24	46	0.811	0.04
Delta EEG-WT					
ANOVA	5.74		2	0.057	
t1-t2		-2.42*	46	0.020	0.34
t1-t3		-1.13	46	0.263	0.16

Note: p values of contrast analysis are Bonferroni corrected and one-tailed. **$p < .01$; *$p < .05$.

beta1, beta2, beta3, and gamma. In addition, the standard bands delta and alpha were analyzed according to their traditional definitions of frequency boarders (see Section 2.6.2) instead of the ones used for neurofeedback in this study (3-4 Hz for delta and the individual range for alpha). The alpha band was further subdivided into a lower and an upper alpha band according to standard conventions.

Apart from the standard delta band, the ANOVAs for the two EEG conditions (EEG-NT and EEG-WT) did not suggest any significant effects of the factor *time* on these untrained frequency bands and none of the performed contrasts nor the Tukey post hoc tests showed significant differences between time points.

Secondly, topographical specificity of the neurofeedback protocol was investigated. In order to assess whether the effects described in the previous section were restricted to the four electrodes used in the training, time effects of the trained alpha/delta ratio averaged over all 65 electrodes of the EEG system were analyzed. Repeated-measure mixed model ANOVA suggested significant effects of the factor *time* for both EEG conditions (EEG-NT: $\chi^2(2) = 9.67$, $p = .008$; EEG-WT: $\chi^2(2) = 9.6$, $p = .008$). For the measurement without instruction (EEG-NT), contrasts only suggested a significant ratio increase between t1 ($M = 0.9636$, SD = 0.0433) and t3 ($M = 0.9786$, SD = 0.042), $t(46) = 3.2$, $p = .002$ (one-tailed). In the case of EEG-WT, both contrasts showed significant results and meaningful differences were found between t1 ($M = 0.9703$, SD = 0.0441) and t2 ($M = 0.9861$, SD = 0.0457), $t(46) = 3.1$, $p = .003$ (one-tailed), as well as between t1 and t3 ($M = 0.9815$, SD = 0.0443), $t(46) = 2.2$, $p = .033$ (one-tailed). Tukey post hoc tests confirmed these findings and suggested no further significant differences.

Finally, in order to determine whether the potential effects of the neurofeedback intervention are limited to a certain age group, a control analysis has been performed. The 24 tinnitus patients included in this study have been subdivided into two subgroups according to their age. This was done by means of a median split on the variable *age* (Mdn = 44). Accordingly, 13 patients have been assigned to a young and 11 cases to an old group. When including this control factor in the repeated-measure mixed model ANOVA as an interaction term, none of the models showed an increased fit on the data (see Table 5).

3.2.3. Correlations. To investigate the relationship between training-induced behavioral and electrophysiological changes, difference scores (t2-t1) in the two domains were calculated and compared. Pearson product-moment correlations are summarized in Table 6, as well as in Figures 3 and 4. Changes in the alpha/delta ratio correlated with THI differences with $r(22) = 0.12$ for EEG-NT and with $r(22) = -0.12$ for EEG-WT. None of these correlations reached statistical significance. Also, for TQ, the negative Pearson correlation coefficient for EEG-NT did not reach statistical significance, $r(22) = -0.03$, $p = .449$ (one-tailed). On the other hand, difference scores of the alpha/delta ratio of EEG-WT suggested a statistical trend for a negative correlation, $r(22) = -0.34$, $p = .053$ (one-tailed). Notably, when analyzed separately, a significant negative correlation was found between the changes in the trained individual alpha frequency band and TQ sum score differences, $r(22) = -0.4$, $p = .026$ (one-tailed). No significant relationships were found for the trained frequency bands and changes in tinnitus loudness.

Table 5: Results of the repeated-measure mixed model ANOVA for control comparisons.

	χ^2	df	p
Standard bands			
EEG-NT			
Delta	6.60*	2	0.037
Theta	1.20	2	0.549
L-Alpha	1.24	2	0.538
U-Alpha	1.05	2	0.591
Alpha	1.07	2	0.587
Beta1	0.17	2	0.917
Beta2	2.41	2	0.300
Beta3	1.82	2	0.402
Gamma	1.00	2	0.607
EEG-WT			
Delta	8.70*	2	0.013
Theta	1.49	2	0.474
L-Alpha	0.25	2	0.881
U-Alpha	0.17	2	0.916
Alpha	0.70	2	0.706
Beta1	0.36	2	0.836
Beta2	0.15	2	0.925
Beta3	3.11	2	0.211
Gamma	4.25	2	0.119
Ratio over all electrodes			
EEG-NT	9.67**	2	0.008
EEG-WT	9.60**	2	0.008
Control for age group			
THI	4.57	4	0.335
TQ	8.24	4	0.083
Loudness	1.39	4	0.846
Ratio EEG-NT	7.66	3	0.054
Ratio EEG-WT	1.52	3	0.677

Note: $^{**}p < .01$; $^{*}p < .05$.

Table 6: Pearson correlation between changes in tinnitus measures and trained EEG frequency band.

	THI	TQ	Loudness
EEG-NT			
Ratio	0.12	-0.03	0.08
IAF	0.25	-0.12	-0.25
Delta	0.10	-0.10	-0.28
EEG-WT			
Ratio	-0.12	-0.34+	-0.14
IAF	-0.06	-0.40*	-0.11
Delta	0.09	-0.10	0.06

Note: Pearson product-moment correlation coefficients of difference scores (t2-t1). $^{*}p < .05$ (one-tailed); $^{+}p < .1$ (one-tailed).

4. Discussion

The neurofeedback protocol used in this clinical study aimed at alpha-up, delta-down training with an individualized alpha reward frequency range determined for each patient. It is fair to say that the chronic tinnitus patients who participated in this study benefited greatly from the neurofeedback intervention as tinnitus-related distress measured with two different questionnaires (THI and TQ) decreased over the course of training. Furthermore, this decrease in distress was stable and remained on a lower level at both the 3- and 6-month follow-up evaluations. Tinnitus loudness was also found to be significantly decreased due to neurofeedback application. However, unlike tinnitus distress, loudness of the phantom percept increased again after the training was completed and returned to baseline levels in the follow-up period. It is important to note that patients did not report any severe and persisting side effects due to the neurofeedback application.

In line with these results, the two previous neurofeedback studies that worked with comparable protocols also reported improvements for tinnitus-related distress, as TQ values [30] as well as THI sum scores [29] were significantly diminished after the training and remained stable 6 months after completion of the training period. We were able to replicate these findings in our study. However, in both preceding studies, a stable recession for tinnitus loudness was also reported, which was not the case in our investigation since loudness was decreased only temporarily. A possible explanation for this inconsistency might be the higher frequency and length of neurofeedback sessions in these previous reports. While participants in our study underwent 15 minutes of neurofeedback training on a weekly basis, Dohrmann et al. [30] and Crocetti et al. [29] worked with 30 and 20 minutes, respectively, 2-3 times per week. Frequency and length of the training sessions might thus be considered a crucial factor for longer-lasting effects regarding tinnitus loudness.

In what follows, we discuss the most relevant implications that emerge from the comparison of our study with the previous reports. Included in the discussion will be the careful examination of whether data obtained within the scope of this project can support the hypothesis that our neurofeedback application led to specific training effects or whether these can be explained as the result of an unspecific placebo effect.

4.1. Analysis of Electrophysiological Data. Electrophysiological data has been analyzed in order to reveal whether the neurofeedback protocol indeed led to the establishment of the trained activity patterns in the brains of study participants. Regarding electrophysiological data, both the studies of Dohrmann et al. [30] and Crocetti et al. [29] did not include resting-state EEG measurements before and after the whole training period and did not obtain EEG data in the follow-up measurements. Instead, they focused their analysis on data obtained during the training phase (before and after each training) where they reported rather unspecific *increasing trends* of the alpha/delta ratio over the course of sessions. In contrast to these previous

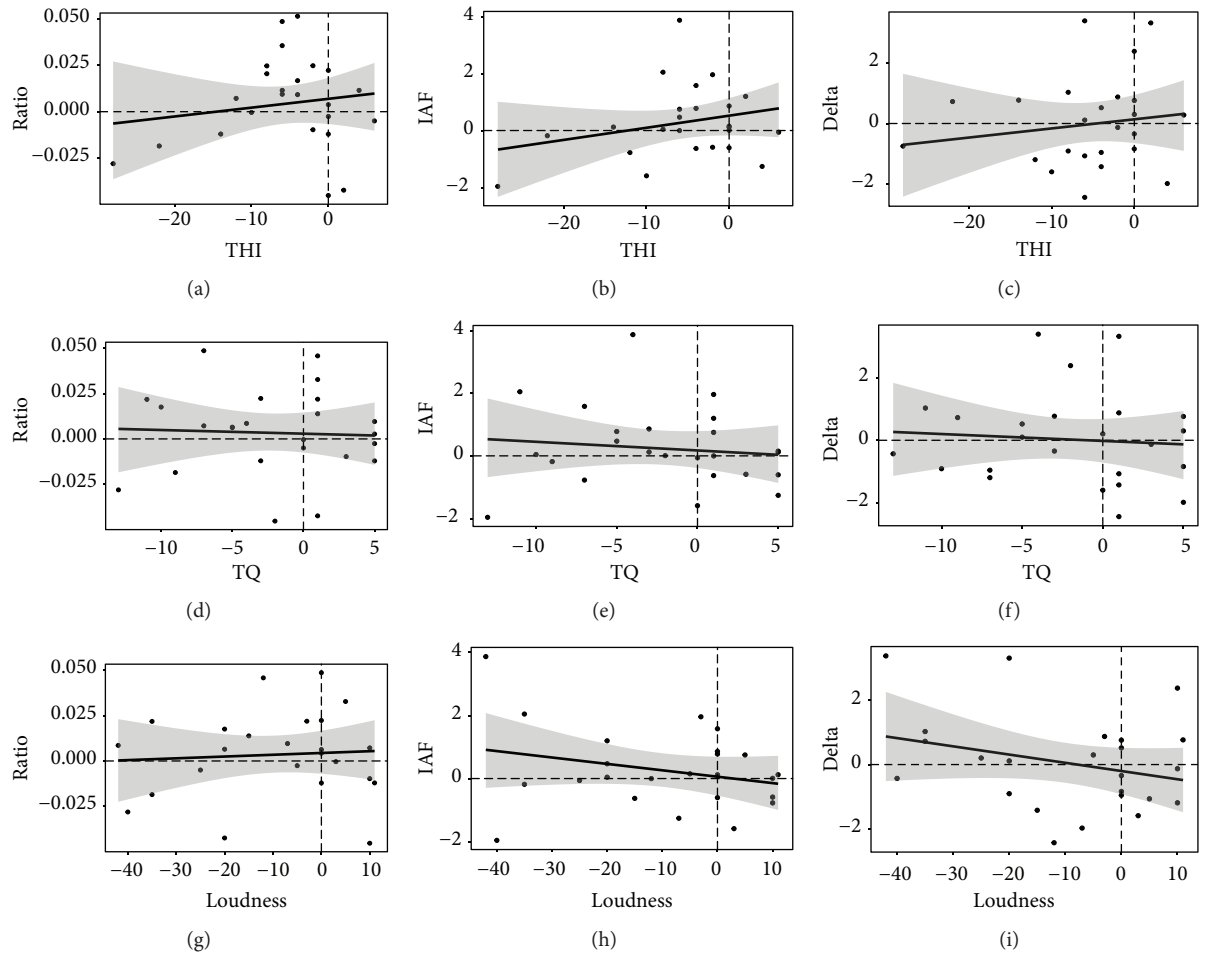

Figure 3: Scatterplots of difference scores (t2-t1) of EEG-NT resting-state data ((a, d, g) alpha/delta ratio; (b, e, h) rewarded individual alpha band power; (c, f, i) inhibited delta band power) and tinnitus-related symptoms ((a–c) THI; (d–f) TQ; (g–i) tinnitus loudness). The plots show the fitted regression lines with 95% confidence intervals. No correlations were found to be statistically significant.

reports, we considered resting-state EEG data obtained before and after the entire neurofeedback intervention to be more informative for objective changes in electrophysiological activity patterns as a long-term function of the treatment and thus to be more indicative of neurofeedback learning. Baseline resting-state EEG recording was thus performed in an environment essentially different from the training setting and some time before the actual start of the training period.

The comparison with the data obtained after all 15 sessions were completed showed that the trained alpha/delta ratio over the four training electrodes was higher after the training than before, suggesting a successful establishment of the desired frequency pattern. In this context, while a significant increase was found for EEG-WT, data from the EEG-NT condition did not show statistically significant effects in the anticipated direction (see Figure 2). A possible explanation for this inconsistency might be that, in the EEG-NT measurement, no clear and unambiguous instructions were given besides those to open and close the eyes and reduce muscle movements. During the 8 minutes of measurement, patients were thus free to contemplate whatever came to their minds which might have led to highly heterogeneous emotional reactions and evoked brain processes across measurements. In the other (EEG-WT) condition, however, an explicit instruction was given to the patients, asking them to focus on their tinnitus percept in order to control for unwanted tinnitus-suppressing activity, which has been found to occur continuously in the brains of chronic tinnitus patients (e.g., [31]). The enhanced focus on the tinnitus tone might have led to reduced heterogeneity of resting-state situations, thereby making them more comparable across the three measurement time points. Furthermore, the EEG used for neurofeedback training was also registered while a patient's tinnitus was clearly salient, thus making the altered EEG rhythms more likely to be reflected in this resting-state measurement condition. Taken together, we believe the significantly and stably increased alpha/delta ratio across the entire training period provides a valuable indication for the successful establishment of the trained frequency patterns.

4.2. Placebo Control. Despite the strong evidence for objective changes in brain activity, the lack of a placebo control group can certainly be considered a possible limitation of this study.

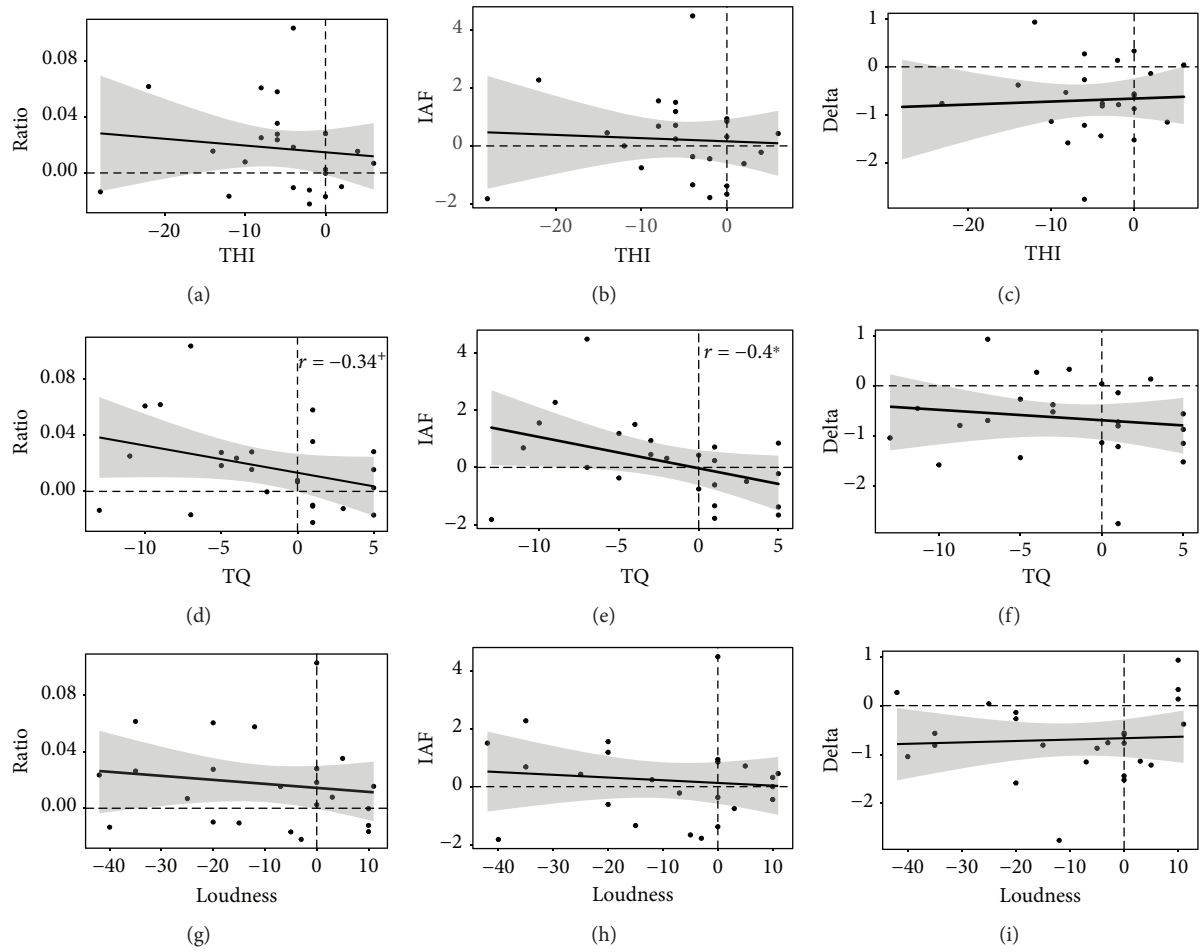

Figure 4: Scatterplots of difference scores (t2-t1) of EEG-WT resting-state data ((a, d, g) alpha/delta ratio; (b, e, h) rewarded individual alpha band power; (c, f, i) inhibited delta band power) and tinnitus-related symptoms ((a–c) THI; (d–f) TQ; (g–i) tinnitus loudness). The plots show the fitted regression lines with 95% confidence intervals. The correlation between IAF and TQ difference scores is statistically significant ($p > .05$).

We did not include a control group due to restrictions of time, infrastructure, and funding, as well as ethical reasons and other arguments discussed comprehensively in our previously published review [28]. To name the most important ones, we considered the investment on the part of the tinnitus patients, who received no monetary compensation for study participation, to be clearly out of proportion to justify placebo neurofeedback. Furthermore, we did not want to induce any form of expectation as to whether a subject believed themselves to be in the sham or verum neurofeedback group. Strehl et al. [27] have suggested that absent success after the first training sessions may automatically evoke misguided ideas on the part of patients to be assigned to the placebo group. This could negatively affect motivation and further treatment success regardless of what group the patients have in fact been allocated to. In a comparison with previously performed studies, the publication of Crocetti et al. [29] also does not mention the inclusion of a control group. Furthermore, even though Dohrmann et al. [30] reported the use of an active control group that worked with auditory frequency discrimination training, the legitimation of this group in the comparison to the rather specific neurofeedback setting remains unclear. In addition, the article of Hartmann et al. [61] should be mentioned in this context. This group performed an alpha neurofeedback training with chronic tinnitus patients and compared their results to a TMS and a sham-TMS condition. Without the use of a specific placebo neurofeedback control group, they could show that alpha power increased exclusively for the neurofeedback group.

However, especially in the field of tinnitus treatment, patients often enter a trial with moderately hopeful expectations as they have already endured a variety of disappointing treatment attempts on their own. This circumstance greatly increases the risk for placebo effects of any intervention, and unspecific effects of the training thus have to be considered and discussed [62]. Therefore, our data analysis attached great importance to minimizing the risk for these unspecific effects of neurofeedback training. In particular, our data analysis closely followed the considerations of Gruzelier [63] about specificity of neurofeedback treatments. The author suggested that three distinct forms of specificity have to be

fulfilled in order to label a neurofeedback intervention successful: frequency band specificity (effects in the trained frequency bands and only in these bands), topographical specificity (effects over the trained electrodes and only in these locations), and outcome specificity (correlations between changes in brain activity and analyzed behavioral outcomes) [63]. It will be discussed in the following section whether our data can support these three types of specificity.

4.3. Specificity of Effects. Regarding *frequency band specificity*, the data of this study indeed suggested specific effects in the trained frequency bands. As already discussed above, the alpha/delta ratio measured over the four training electrodes increased due to the intervention and remained on a stable high level in the follow-up period. Furthermore, we did not find any changes in other standard frequency bands which clearly speaks in favor of frequency band specificity for the applied neurofeedback protocol.

Topographical specificity, on the other hand, could not be confirmed with the data of this clinical study. The repeated-measure mixed model analysis of variance did suggest significant ratio effects over time not only for the four training electrodes but also over all 65 electrodes used for pre-, post-, and follow-up measurements. The neurofeedback protocol used in this study, therefore, did not only affect frequency band power in the vicinity to trained electrodes specifically but led to a global effect across the whole brain. This finding, however, is not unexpected since neurofeedback on the basis of activity measured with a limited number of electrodes on the scalp is generally considered to be unspecific, leading to widespread effects across the whole brain [64]. Unfortunately, neither Dohrmann et al. [30] nor Crocetti et al. [29] provided any information about possible activity changes on electrodes besides the trained ones. Furthermore, even Gruzelier [63] discusses the general possibility of topographically unspecific effects of surface-based neurofeedback. If the brain is seen as a holistic functional network rather than an aggregation of several strictly localized centers, topographically widespread effects of frequency band neurofeedback training should come as no surprise [63]. Also in the context of tinnitus, the view has recently shifted from the localized perspective to a more holistic concept with several proposed models aimed at describing the different (sub-)networks that contribute to the tinnitus percept (e.g., [33, 65]).

Finally, regarding *outcome specificity*, correlation analyses between difference scores of tinnitus and electrophysiological measures revealed an inconsistent picture. Meaningful negative correlations regarding the trained frequency bands could only be found with the changes in the Tinnitus Questionnaire. While a decrease of TQ scores was related to an increase of the alpha/delta ratio of EEG-WT on the trend level, the relation with increments in the rewarded individual alpha band was found to be statistically significant. It thus seems as if the increase in alpha was the driving force behind the improvements of tinnitus-related distress as measured with TQ. However, since also THI-measured distress as well as tinnitus loudness declined over the course of the training, we expected these changes to be related with electrophysiological measures as well, which was not the case.

Inconsistencies were also reported in the previous studies with comparable neurofeedback protocols as Dohrmann et al. [30] found electrophysiological measures to be correlated only with tinnitus loudness but not distress, while Crocetti et al. [29] reported findings to the exact opposite. In our study, Figures 3 and 4 provide a deeper look into the patterns of responder and nonresponder individuals in the study sample. In doing so, obvious neurofeedback responders can be identified as patients who were able to improve their alpha/delta ratio (increase their alpha, decrease their delta) and show reduced tinnitus symptoms (cases in the upper left quadrant for the ratio and IAF or in the lower left for delta). In contrast, obvious non-responders are also visible as cases unable to alter electrophysiological activity in the desired direction and not showing any changes or even increases in tinnitus symptoms (cases in the lower right quadrant for the ratio and IAF or the upper right for delta). There are, however, also examples of inconsistent cases. Several patients indicated having substantially benefited from the training and reported their tinnitus-related symptoms to be significantly lower, yet they did not show any EEG training effects (cases in the lower left quadrant for the ratio and IAF and in the upper left quadrant for delta). Others proved to be extremely successful in adjusting their brain activity in the intended direction over the course of training but did not report any or hardly any noticeable changes in tinnitus symptoms (cases in the upper right quadrant for the ratio and IAF and in the lower right for delta). Thus, even a superficial visual impression of our data already suggests a considerable amount of variability in the set. While the group in its entirety seems to have benefited from the neurofeedback application on average, a closer inspection of the results suggests a more complex picture in that we have identified a considerable amount of behavioral and/or electrophysiological non-responders. Therefore, a thorough future analysis of responder and non-responder groups would certainly prove fruitful in order to fathom the characteristics of certain subgroups and pave the way for better-suited neurofeedback protocols for each of them. These advanced analyses of data obtained in the scope of this study should also include considerations about the clinical relevance of observed difference scores (e.g., [66]) and will thus be discussed elsewhere.

5. Conclusion

To sum up, the neurofeedback protocol with individualized reward frequency bands discussed in this article can be considered a good option in the treatment of chronic tinnitus. We base this statement on the result that the distress of tinnitus sufferers was significantly and sustainably reduced and that a temporary effect for tinnitus loudness was also found. In order to influence the intensity of the percept in a sustainable way, a higher frequency (2-3 sessions a week) and longer training sessions (min 20 minutes) might be recommended. Even though unspecific effects are difficult to exclude due to the lack of a placebo control group, this study significantly extends current work in the field by carrying out data analysis

with utmost care. Compared to most neurofeedback studies to date that did not take the unspecific effects of this intervention into account, we were able to demonstrate the frequency band specificity of our protocol. Even though the training did not lead to topographically specific but rather global effects, this result speaks in favor of specific effects of the intervention. Neurofeedback-induced changes in tinnitus-related symptoms seem to be mainly driven by an increase in alpha rather than a decrease in delta power, and the relationship with the trained bands was strongest for distress measured with the TQ (see Figure 4). In the light of the TCD model and the SLIM, this finding suggests that tinnitus distress as well as loudness are closely related to inhibitory activity in auditory areas reflected in the alpha band. If activity in inhibitory neurons is fostered with neurofeedback training and thus the disturbed excitatory/inhibitory balance readjusted, the tinnitus percept seems to be softened and its distressing component weakened. However, as has been shown, individual reactions to the neurofeedback training are heterogeneous and thus do not speak in favor of outcome specificity on the whole. More comprehensive analysis of responder and non-responder data will prove to be crucial in future studies in order to establish individually based neurofeedback. These insights would contribute in the pursuit of the long-term goal of developing training protocols catering to the specific needs of each tinnitus patient.

Data Availability

The data used to support the findings of this study are available from the corresponding author upon request.

Conflicts of Interest

The authors declare that there are no conflicts of interest regarding the publication of this paper.

Authors' Contributions

Dominik Güntensperger and Christian Thüring shared first authorship. Contributions to this manuscript are as follows: DG and CT equally contributed to the conception, draft, and revision of the paper. MM, PN, and TK contributed to the conception, critically revision, and final approval of the manuscript.

Acknowledgments

The authors are indebted to the TINNET-COST Action BM1306 "Better Understanding the Heterogeneity of Tinnitus to Improve and Develop New Treatments" for providing a network, which allows exchange of knowledge among tinnitus researchers in Europe. During the work on his dissertation, DG was a predoctoral fellow of LIFE (International Max Planck Research School on the Life Course; participating institutions: MPI for Human Development, Humboldt-Universität zu Berlin, Freie Universität Berlin, University of Michigan, University of Virginia, and University of Zurich). The authors disclose the following financial support for research, authorship, and/or publication of this article: "Velux Stiftung," "Zürcher Stiftung für das Hören (ZSFH)," "Fonds zur Förderung des akademischen Nachwuchses (FAN) des Zürcher Universitätsvereins (ZUNIV)," and the University Research Priority Program "Dynamics of Healthy Aging" of the University of Zurich.

References

[1] J. A. Henry, K. C. Dennis, and M. A. Schechter, "General review of tinnitus: prevalence, mechanisms, effects, and management," *Journal of Speech, Language, and Hearing Research*, vol. 48, no. 5, pp. 1204–1235, 2005.

[2] R. A. Dobie, "Depression and tinnitus," *Otolaryngologic Clinics of North America*, vol. 36, no. 2, pp. 383–388, 2003.

[3] A. J. Heller, "Classification and epidemiology of tinnitus," *Otolaryngologic Clinics of North America*, vol. 36, no. 2, pp. 239–248, 2003.

[4] B. Langguth, M. Landgrebe, T. Kleinjung, G. P. Sand, and G. Hajak, "Tinnitus and depression," *The World Journal of Biological Psychiatry*, vol. 12, no. 7, pp. 489–500, 2011.

[5] S. Holmes and N. D. Padgham, "The incidence, management and consequence of tinnitus in older adults," *Reviews in Clinical Gerontology*, vol. 18, no. 4, p. 269, 2008.

[6] J. J. Eggermont, "On the pathophysiology of tinnitus; a review and a peripheral model," *Hearing Research*, vol. 48, no. 1-2, pp. 111–123, 1990.

[7] A. R. Møller, "Pathophysiology of tinnitus," *Otolaryngologic Clinics of North America*, vol. 36, no. 2, pp. 249–266, 1984.

[8] J. J. Eggermont and L. E. Roberts, "The neuroscience of tinnitus," *Trends in Neurosciences*, vol. 27, no. 11, pp. 676–682, 2004.

[9] A. B. Elgoyhen, B. Langguth, D. De Ridder, and S. Vanneste, "Tinnitus: perspectives from human neuroimaging," *Nature Reviews Neuroscience*, vol. 16, no. 10, pp. 632–642, 2015.

[10] B. Langguth, P. M. Kreuzer, T. Kleinjung, and D. De Ridder, "Tinnitus: causes and clinical management," *The Lancet Neurology*, vol. 12, no. 9, pp. 920–930, 2013.

[11] N. Weisz, K. Dohrmann, and T. Elbert, "The relevance of spontaneous activity for the coding of the tinnitus sensation," *Progress in Brain Research*, vol. 166, pp. 61–70, 2007.

[12] P. Adjamian, M. Sereda, and D. A. Hall, "The mechanisms of tinnitus: perspectives from human functional neuroimaging," *Hearing Research*, vol. 253, no. 1-2, pp. 15–31, 2009.

[13] H. Ashton, K. Reid, R. Marsh, I. Johnson, K. Alter, and T. Griffiths, "High frequency localised "hot spots" in temporal lobes of patients with intractable tinnitus: a quantitative electroencephalographic (QEEG) study," *Neuroscience Letters*, vol. 426, no. 1, pp. 23–28, 2007.

[14] N. Kahlbrock and N. Weisz, "Transient reduction of tinnitus intensity is marked by concomitant reductions of delta band power," *BMC Biology*, vol. 6, no. 1, p. 4, 2008.

[15] I. Lorenz, N. Müller, W. Schlee, T. Hartmann, and N. Weisz, "Loss of alpha power is related to increased gamma synchronization—a marker of reduced inhibition in tinnitus?," *Neuroscience Letters*, vol. 453, no. 3, pp. 225–228, 2009.

[16] W. Schlee, K. Dohrmann, T. Hartmann et al., "Assessment and modification of the tinnitus-related cortical network," *Seminars in Hearing*, vol. 29, no. 3, pp. 270–287, 2008.

[17] N. Weisz, S. Moratti, M. Meinzer, K. Dohrmann, and T. Elbert, "Tinnitus perception and distress is related to abnormal

spontaneous brain activity as measured by magnetoencephalography," *PLoS Medicine*, vol. 2, no. 6, article e153, 2005.

[18] N. Weisz, S. Müller, W. Schlee, K. Dohrmann, T. Hartmann, and T. Elbert, "The neural code of auditory phantom perception," *Journal of Neuroscience*, vol. 27, no. 6, pp. 1479–1484, 2007.

[19] R. R. Llinás, U. Ribary, D. Jeanmonod, E. Kronberg, and P. P. Mitra, "Thalamocortical dysrhythmia: a neurological and neuropsychiatric syndrome characterized by magnetoencephalography," *Proceedings of the National Academy of Sciences of the United States of America*, vol. 96, no. 26, pp. 15222–15227, 1999.

[20] D. De Ridder, S. Vanneste, B. Langguth, and R. R. Llinás, "Thalamocortical dysrhythmia: a theoretical update in tinnitus," *Frontiers in Neurology*, vol. 6, 2015.

[21] M. B. Sterman and L. Friar, "Suppression of seizures in an epileptic following sensorimotor EEG feedback training," *Electroencephalography and Clinical Neurophysiology*, vol. 33, no. 1, pp. 89–95, 1972.

[22] W. Wyrwicka and M. B. Sterman, "Instrumental conditioning of sensorimotor cortex EEG spindles in the waking cat," *Physiology & Behavior*, vol. 3, no. 5, pp. 703–707, 1968.

[23] M. Arns, S. De Ridder, U. Strehl, M. Breteler, and A. Coenen, "Efficacy of neurofeedback treatment in ADHD: the effects on inattention, impulsivity and hyperactivity: a meta-analysis," *Clinical EEG and Neuroscience*, vol. 40, no. 3, pp. 180–189, 2009.

[24] H. Gevensleben, B. Holl, B. Albrecht et al., "Is neurofeedback an efficacious treatment for ADHD? A randomised controlled clinical trial," *Journal of Child Psychology and Psychiatry, and Allied Disciplines*, vol. 50, no. 7, pp. 780–789, 2009.

[25] J. Lévesque, M. Beauregard, and B. Mensour, "Effect of neurofeedback training on the neural substrates of selective attention in children with attention-deficit/hyperactivity disorder: a functional magnetic resonance imaging study," *Neuroscience Letters*, vol. 394, no. 3, pp. 216–221, 2006.

[26] J. F. Lubar, M. O. Swartwood, J. N. Swartwood, and P. H. O'Donnell, "Evaluation of the effectiveness of EEG neurofeedback training for ADHD in a clinical setting as measured by changes in T.O.V.A. scores, behavioral ratings, and WISC-R performance," *Biofeedback and Self-Regulation*, vol. 20, no. 1, pp. 83–99, 1995.

[27] U. Strehl, P. Aggensteiner, D. Wachtlin et al., "Neurofeedback of slow cortical potentials in children with attention-deficit/hyperactivity disorder: a multicenter randomized trial controlling for unspecific effects," *Frontiers in Human Neuroscience*, vol. 11, article 135, 2017.

[28] D. Güntensperger, C. Thüring, M. Meyer, P. Neff, and T. Kleinjung, "Neurofeedback for tinnitus treatment-review and current concepts," *Frontiers in Aging Neuroscience*, vol. 9, article 386, 2017.

[29] A. Crocetti, S. Forti, and L. Del Bo, "Neurofeedback for subjective tinnitus patients," *Auris, Nasus, Larynx*, vol. 38, no. 6, pp. 735–738, 2011.

[30] K. Dohrmann, T. Elbert, W. Schlee, and N. Weisz, "Tuning the tinnitus percept by modification of synchronous brain activity," *Restorative Neurology and Neuroscience*, vol. 25, no. 3-4, pp. 371–378, 2007.

[31] W. Sedley and M. O. Cunningham, "Do cortical gamma oscillations promote or suppress perception? An under-asked question with an over-assumed answer," *Frontiers in Human Neuroscience*, vol. 7, article 595, 2013.

[32] W. Sedley, S. Teki, S. Kumar, G. R. Barnes, D.-E. Bamiou, and T. D. Griffiths, "Single-subject oscillatory gamma responses in tinnitus," *Brain*, vol. 135, no. 10, pp. 3089–3100, 2012.

[33] W. Sedley, K. J. Friston, P. E. Gander, S. Kumar, and T. D. Griffiths, "An integrative tinnitus model based on sensory precision," *Trends in Neurosciences*, vol. 39, no. 12, pp. 799–812, 2016.

[34] M. Landgrebe, F. Zeman, M. Koller et al., "The Tinnitus Research Initiative (TRI) database: a new approach for delineation of tinnitus subtypes and generation of predictors for treatment outcome," *BMC Medical Informatics and Decision Making*, vol. 10, no. 1, pp. 1–7, 2010.

[35] W. Klimesch, "EEG alpha and theta oscillations reflect cognitive and memory performance: a review and analysis," *Brain Research Reviews*, vol. 29, no. 2-3, pp. 169–195, 1999.

[36] W. Schlee, M. Schecklmann, A. Lehner et al., "Reduced variability of auditory alpha activity in chronic tinnitus," *Neural Plasticity*, vol. 2014, Article ID 436146, 9 pages, 2014.

[37] M. Landgrebe, A. Azevedo, D. Baguley et al., "Methodological aspects of clinical trials in tinnitus: a proposal for an international standard," *Journal of Psychosomatic Research*, vol. 73, no. 2, pp. 112–121, 2012.

[38] B. Langguth, R. Goodey, A. Azevedo et al., "Consensus for tinnitus patient assessment and treatment outcome measurement: Tinnitus Research Initiative meeting, Regensburg, July 2006," *Progress in Brain Research*, vol. 166, pp. 525–536, 2007.

[39] T. Kleinjung, B. Fischer, B. Langguth et al., "Validierung einer deutschsprachigen Version des "Tinnitus Handicap Inventory"," *Psychiatrische Praxis*, vol. 34, Supplement 1, pp. 140–142, 2007.

[40] G. Goebel and W. Hiller, "Tinnitus-Fragebogen (TF). Standardinstrument zur Graduierung des Tinnitusschweregrades. Ergebnisse einer Multicenterstudie mit dem Tinnitus-Fragebogen (TF)," *HNO*, vol. 42, no. 3, pp. 166–172, 1994.

[41] M. Hautzinger, M. Bailer, H. Worall, and F. Keller, *BDI Beck-Depressions-Inventar Testhandbuch*, Hans Huber, Bern, 1995.

[42] M. Prinz and F. Petermann, "Beck Angst-Inventar (BAI)," *Zeitschrift für Psychiatrie, Psychologie und Psychotherapie*, vol. 57, no. 1, pp. 63–66, 2009.

[43] M. C. Angermeyer, R. Kilian, and H. Matschinger, *WHO-QOL-100 und WHOQOL-BREF: Handbuch für die deutschsprachige Version der WHO Instrumente zur Erfassung von Lebensqualität*, Hogrefe, Göttingen, 2000.

[44] R. Klaghofer and E. Brähler, "Konstruktion und Teststatistische Prüfung einer Kurzform der SCL-90–R," *Zeitschrift für Klinische Psychologie, Psychiatrie und Psychotherapie*, vol. 49, no. 2, pp. 115–124, 2001.

[45] M. Bullinger, I. Kirchberger, and J. Ware, "Der deutsche SF-36 Health Survey Übersetzung und psychometrische Testung eines krankheitsübergreifenden Instruments zur Erfassung der gesundheitsbezogenen Lebensqualität," *Zeitschrift für Gesundheitswissenschaften = Journal of Public Health*, vol. 3, no. 1, pp. 21–36, 1995.

[46] R. Oostenveld and P. Praamstra, "The five percent electrode system for high-resolution EEG and ERP measurements," *Clinical Neurophysiology*, vol. 112, no. 4, pp. 713–719, 2001.

[47] F. Perrin, J. Pernier, O. Bertrand, and J. F. Echallier, "Spherical splines for scalp potential and current density mapping," *Electroencephalography and Clinical Neurophysiology*, vol. 72, no. 2, pp. 184–187, 1989.

[48] A. Delorme and S. Makeig, "EEGLAB: an open source toolbox for analysis of single-trial EEG dynamics including independent

component analysis," *Journal of Neuroscience Methods*, vol. 134, no. 1, pp. 9–21, 2004.

[49] R Core Team, *R: A Language and Environment for Statistical Computing*, R Foundation for Statistical Computing, Vienna, Austria, 2017, https://www.R-project.org/.

[50] H. Wickham, *Ggplot2: Elegant Graphics for Data Analysis*, Springer-Verlag, New York, 2009, http://ggplot2.org.

[51] C. Ahlmann-Eltze, *Ggsignif: Significance Brackets for'ggplot2'. R Package Version 0.4.0*, 2017, https://CRAN.R-project.org/package=ggsignif.

[52] F. E. Harrell Jr, *Hmisc: Harrell Miscellaneous. R Package Version 4.0-3*, 2017, https://CRAN.R-project.org/package=Hmisc.

[53] J. A. Long, *Jtools: analysis and presentation of social scientific data. R package version 0.5.0*, 2017, https://cran.r-project.org/package=jtools.

[54] T. Hothorn, F. Bretz, and P. Westfall, "Simultaneous inference in general parametric models," *Biometrical Journal*, vol. 50, no. 3, pp. 346–363, 2008.

[55] J. Pinheiro, D. Bates, S. DebRoy, D. Sarkar, and R Core Team, *nlme: linear and nonlinear mixed effects models. R package version 3.1-131*, 2017, https://CRAN.R-project.org/package=nlme.

[56] D. B. Dahl, *Xtable: export tables to latex or html. R package version 1.8-2*, 2016, https://CRAN.R-project.org/package=xtable.

[57] A. P. Field, J. Miles, and Z. Field, *Discovering Statistics using R*, Sage, London, 2012.

[58] J. Cohen, *Statistical Power Analysis for the Behavioral Sciences*, J. Cohen, Ed., Erlbaum, Hillsdale, NJ, USA, 2 edition, 1988.

[59] Y. Benjamini and Y. Hochberg, "Controlling the false discovery rate: a practical and powerful approach to multiple testing," *Journal of the Royal Statistical Society: Series B (Methodological)*, vol. 57, no. 1, pp. 289–300, 1995.

[60] R. D. Morey, "Confidence intervals from normalized data: a correction to Cousineau (2005)," *Tutorial in Quantitative Methods for Psychology*, vol. 4, no. 2, pp. 61–64, 2008.

[61] T. Hartmann, I. Lorenz, N. Müller, B. Langguth, and N. Weisz, "The effects of neurofeedback on oscillatory processes related to tinnitus," *Brain Topography*, vol. 27, no. 1, pp. 149–157, 2014.

[62] R. T. Thibault and A. Raz, "The psychology of neurofeedback: clinical intervention even if applied placebo," *The American Psychologist*, vol. 72, no. 7, pp. 679–688, 2017.

[63] J. H. Gruzelier, "EEG-neurofeedback for optimising performance. III: a review of methodological and theoretical considerations," *Neuroscience & Biobehavioral Reviews*, vol. 44, pp. 159–182, 2014.

[64] M. Congedo, J. F. Lubar, and D. Joffe, "Low-resolution electromagnetic tomography neurofeedback," *IEEE Transactions on Neural Systems and Rehabilitation Engineering*, vol. 12, no. 4, pp. 387–397, 2004.

[65] D. De Ridder, S. Vanneste, N. Weisz et al., "An integrative model of auditory phantom perception: tinnitus as a unified percept of interacting separable subnetworks," *Neuroscience & Biobehavioral Reviews*, vol. 44, pp. 16–32, 2014.

[66] D. A. Hall, R. L. Mehta, and H. Argstatter, "Interpreting the Tinnitus Questionnaire (German version): what individual differences are clinically important?," *International Journal of Audiology*, vol. 57, no. 7, pp. 553–557, 2018.